The heterogeneity of TRPV1 and its activation in nociceptive neurons

Dissertation

Zur Erlangung des akademischen Grades des Doktors
der Naturwissenschaften (Dr. rer. nat.)

eingereicht im Fachbereich Biologie, Chemie, Pharmazie
der Freien Universität Berlin

vorgelegt von

René Buschow
aus Friesack

Berlin 2014

Die experimentellen Arbeiten für diese Monographie wurden am Max-Planck-Institut für molekulare Genetik in Berlin, unter Betreuung von Prof. Dr. Tim Hucho, im Zeitraum Oktober 2009 bis April 2013 durchgeführt.

1. Gutachter Prof. Dr. Tim Hucho (Uniklinik Köln)
2. Gutachterin Prof. Dr. Petra Knaus (Freie Universität Berlin)

Termin der Disputation: 07. September 2015

Meinen Eltern

„Wenn jemand sucht, dann geschieht es leicht, dass sein Auge nur noch das Ding sieht, das er sucht, dass er nichts zu finden, nichts in sich einzulassen vermag, weil er nur an das Gesuchte denkt, weil er ein Ziel hat, weil er vom Ziel besessen ist. Finden aber heißt: frei sein, offen stehen, kein Ziel haben."

Hermann Hesse

Table of Contents

Table of figures

1. Summary

1.1 Summary

The question on the number of human senses in western societies is typically answered with five. Asking people anywhere in the world, what is most annoying feeling, the majority will answer emotional, physical, or diseases related pain. Whatever reason, the answer is mostly pain. But can the perception of pain be defined as sense? The answer is yes. Pain initiating stimuli activate specialized peripheral sensory neurons from the dorsal root ganglia - the so called nociceptive neurons.

One protein central for inflammatory temperature pain is the ion channel TRPV1. TRPV1 protein expression in sensory neurons is upregulated in situations of hightened pain sensitivity, suggesting a direct causal relationship between the TRPV1 expression levels and pain sensitivity. A number of processes have been identified describing the sensitization and desensitization of TRPV1 on a molecular level. But, to what extend the expression levels of TRPV1 correlates with its cellular activation kinetics on a population base has not been analyzed in detail so far. This is due to, a lack of suitable technical approaches to analyze the function and (TRPV1-) protein expression levels on a single cell base.

I quantified the heterogeneity of TRPV1 expression in nociceptive neurons, with confocal and “high content screening” microscopy approaches. Antibody based expression analysis and calcium imaging identified 60.4 ± 6.5 % (immune cytochemistry) and 58.2 ± 6.8 % (capsaicin responsive cells) sensory neurons, to be TRPV1 expressing. In depth analysis of the calcium imaging experiments revealed, that submaximal capsaicin concentrations do not result in lower responses but lower numbers of capsaicin sensitive cells. Further, a correlation between TRPV1 expression and the amplitude of capsaicin induced calcium influx was clearly detectable in exogenously expressed TRPV1 transfected cell lines, but was almost absent in endogenously expressing nociceptive neurons. Pretreatment with strong sensitization inducing substances (PMA and FSK) resulted in an improvement of the correlation – nevertheless, still not explaining all the heterogeneity between expression and response. Accordingly, a sensitization signaling protein, the regulatory subunit of PKA RIIβ, correlated better with the cellular capsaicin response than TRPV1 itself.

As the strong sensitization signaling did not result in a complete correlation between expression and capsaicin induced calcium influx, there must exist other mechanisms of regulation such as expression of modulators. To identify novel TRPV1 modulator and gain genetic insights into nociceptors, we developed a novel subgroup specific transcriptome analysis approach. The resulting list of up

regulated genes offers the opportunity to identify novel TRPV1 and pain modulators. Furthermore, the list presents the first complete transcriptome of a subpopulation of nociceptive neurons.

In collaboration with Steffen Waldherr, my results were analyzed by establishing a computational model for the cellular capsaicin sensitivity. From this model based on experimental data and literature derived values, a mechanism is suggested, which regulates the relative capsaicin sensitivity state inversely to the TRPV1 expression in sensory neurons. Thus, the TRPV1 response is surprisingly robust against changes in TRPV1 expression levels. My results question the conventional therapeutic use of TRPV1-channel blockers and suggest the need to define the cellular mechanisms how the TRPV1-mediated calcium influx-homeostasis is controlled.

1.2 Zusammenfassung

Die Frage nach der Anzahl menschlicher Sinne wird in westlichen Gesellschaften typischerweise mit fünf beantwortet. Fragt man Menschen irgendwo auf der Welt nach ihrem unangenehmsten Gefühl, wird die Mehrzahl entweder mit emotionalen, physischen oder krankheitsbedingten Schmerz antworten. Auf welcher Ursache auch immer die resultierende Antwort basiert, sie ist in den meisten Fällen Schmerz. Aber kann die Wahrnehmung von Schmerz als Sinn definiert werden? Die Antwort ist ja. Schmerz verursachende Stimuli aktivieren spezialisierte sensorische Neurone aus den dorsalen Hinterwurzel Ganglien, die sogenannten Nozizeptoren.

Ein zentrales Protein für entzündlichen Temperaturschmerz ist der Ionenkanal TRPV1. Unter Bedingungen erhöhter Schmerzsensitivität ist die TRPV1 Proteinexpression in nozizeptiven Neuronen erhöht. Dies deutet auf eine direkte kausale Beziehung zwischen TRPV1 Expressionsmengen und Schmerzsensitivität hin. Eine Reihe von Prozessen wurde bereits identifiziert, welche die Sensitivierung und Desensitiverung von TRPV1 auf molekularer Ebene beschreiben. In welchem Ausmaß jedoch die TRPV1 Expression mit zellulären Aktivierungskinetiken korrelieren, wurde noch nicht im Detail und auf Populationsebene untersucht. Dieser Umstand beruht vor allem auf fehlenden Untersuchungsmethoden, welche erlauben zelluläre Funktionen und endogene (TRPV1-) Proteinexpression in einzelnen Zelle zu untersuchen.

Mit konfokalen und “High Content Screening”- Mikroskopieverfahren quantifizierte ich die Heterogenität der TRPV1 Expression in nozizeptiven Neuronen. Antikörper basierte Expressionsanalysen als auch Calcium Imaging identifizierten 60.4 ± 6.5 % (Immunzytochemie) und 58.2 ± 6.8 % (Capsaicin sensitive Neurone) der sensorischen Neurone als TRPV1 exprimierend. Eine detaillierte Analyse der Calcium Imaging Experimente zeigte, dass submaximale Capsaicin-

Konzentrationen nicht in niedrigeren Calcium Antworten resultieren sondern weniger Capsaicin sensitive Zellen zeigten. Weiterhin wurde eine klare Korrelation zwischen exogener TRPV1 Expression und der Capsaicin induzierten Calcium Einstromamplitude in TRPV1 transfizierten Zelllinien detektiert, welche in endogen expremierenden nozizeptiven Neuronen fast nicht vorhanden war. Vorbehandlungen mit starken sensitivierungs-induzierenden Substanzen (PMA und FSK) zeigten eine Verbesserung, konnten jedoch nicht die Heterogenität zwischen Expression und Antwort erklären. Dementsprechend korrelierte ein Sensitivierungs-Signalwirkungsprotein, die regulatorische Untereinheit von PKA RIIβ, besser mit der zellulären Capsaicin-Antwort als TRPV1.

Da eine starke Sensitivierung nicht zu einer vollständigen Korrelation, zwischen Expression und Capsaicin induziertem Calcium Einstrom führten, müssen andere Regulationsmechanismen existieren wie beispielweise die Expression von Modulatoren. Um neue TRPV1-Modulatoren zu identifizieren und genetische Einblicke in Nozizeptoren zu erlangen, entwickelten wir subgruppen-spezifische Transkriptom-Analyseverfahren. Eine daraus resultierende Liste von hoch regulierten Genen eröffnet die Möglichkeit, neue TRPV1 und damit Schmerzmodulatoren zu identifizieren. Die Liste präsentiert weiterhin, das erste vollständige Transkriptom einer Subpopulation nozizeptiver sensorischer Neurone.

In Kollaboration mit Steffen Waldherr verwendete ich meine Ergebnisse um ein computergestütztes Modell für die zelluläre Capsaicin-Sensitivität zu entwickeln. In diesem, auf experimentellen Daten und Literatur basierten Modell, wird ein Mechanismus angedeutet, welcher die relative zelluläre Capsaicin Sensitivität invers zur TRPV1-Epression in sensorischen Neuronen reguliert. Daher ist die Capsaicin-Antwort überraschend robust gegenüber Veränderungen in der TRPV1-Expression. Wenn die TRPV1 vermittelte Calciumeinströme so unempfindlich gegenüber Veränderungen der TRPV1-Expression sind, hinterfragen meine Ergebnisse das konventionelle therapeutische Konzept von TRPV1-Kanalblockern. Sie zeigen den Bedarf auf, zelluläre Mechanismen zu definieren, welche die TRPV1 vermittelte Calcium-Einstrom-Homöostase kontrollieren.

2. Introduction

Sensations guide animals through their particular environments. The ability to sense its environment enables the individual animal to cope with the challenges of its habitat. Pain is a sensation crucial for survival allowing escaping and avoiding potentially dangerous substances and physical conditions such as strong pressure and extreme heat. The first introductory part gives an overview over the so far known senses of higher animals. In the following, I will focus on the sensation and differential subtypes of pain. Finally, I will delineate the need for cell biological research addressing the heterogeneity of the various sensory neurons for understanding regulation mechanisms of pain. I will focus one marker of nociceptive neurons, the Transient Receptor Potential Vanilloid 1 (TRPV1), its cellular expression, modulation, and functionality under normal and diseased conditions. I will delineate thereby the need to investigate TRPV1 not in a rather homogeneous cell line system but in large numbers of the highly heterogeneous nociceptive neurons.

2.1 The 5, the 12 the x senses…

Sensation allows the detection of a physical or chemical stimulus. The perceivable world is heterogeneous; its quantity remains a riddle since long. Thus, over 2000 years ago, Aristotle defined in *De anima* the five human senses touch, smell, see, taste, and hear (Osborne, 1983). This classical understanding is still broadly distributed in western societies when talking about the five senses. Often an enigmatic sixth sense is shining up allowing the forecasting of future developments. But depending on how one defines a sense there are many more senses known. In the late 19 century some anthroposophists even described up to 12 senses, which are further divided into three groups namely the social, the body, and the environmental senses (Steiner and Steiner, 1938). The correct number of senses, from a 2014 point of view, is still hard to name. Nowadays we are aware of at least 10 senses, that are experimentally measurable: the five named above by Aristotle plus proprioception, temperature sense, equilibrium sense, visceral sense and finally the nociception (Damann et al., 2008).

The complex processing structure of the brain is in principle able to sense even more types of sensory input, reminding the reader of the ability to sense magnetic (birds) or electric fields (some fishes), ultra-sonic waves or infrasound (elephants). Furthermore, some studies relate to more abstract entities such as fairness as sense (Knoch et al., 2006). In this thesis, I will focus on one particular sense, namely the nociception and some of the underlying molecular mechanisms on the cellular level.

2.2 Nociception and pain

With very few exceptions (Cox et al., 2006, Staud et al., 2011), every human being is able to sense pain. Pain is a subjective sense. Its quantities depend on the actual situation of the experiencing individual and take place predominantly in the central nervous system (brain). Nociception describes the process for the encoding of a stimulus which is damaging to normal tissues (also referred as noxious stimuli, latin noxa = damage) and aversive (Fields, 1989, Loeser and Treede, 2008). Nociception takes place in the periphery and transmits the incoming information over nociceptive neurons towards the brain. In the central nervous system the incoming information is emotionally interpreted and can be judged as pain. Nociception does not equal pain; a definition by the International Association for the Study of pain (IASP) states it as:

"A*n unpleasant sensory and emotional experience associated with actual or potential tissue damage, or described in terms of such damage.*" (Loeser and Treede, 2008).

Nociception by itself is the sense to detect damaging stimuli - pain is what the brain interprets. For example, chili spiced dishes enhance the taste. The same component, namely the hot ingredient in chili capsaicin, applied as skin patch produces a pleasant warm feeling and yet another application as tear gas results in severe pain in the eyes and nose. Thus, the same stimuli can either be tasty, comfortable, or painful if applied with certain intensity, to a sensitive tissue, or under diseased conditions. Taken together, pain by itself is neither a pure chemical or physical force, nor is it a distinct substance which could be quantified. Pain is always what the brain interprets and nociception is pain perception without the emotional interpretation of the brain (Sharif-Naeini and Basbaum, 2011). From this general introduction of nociception, I will present in the following part an overview of four different types of pain.

2.3 Four types of pain

Pain phenotypes are diverse and result from miscellaneous sources; while different definitions are given, I will follow the categorization of four pain types given by Costigan et. al. (Costigan et al., 2009).

2.3.1 Acute pain

The first and physiological most commonly occurring type of pain is the acute or nociceptive pain, which results from perception of an acute noxious stimulus. Typical examples of nociceptive pain are the step into nettles, a misguided hammer blow onto a body part, or the negligent touching of a hot dark colored car in the summer sun. This acute pain informs the organism to recognize and avoid conditions or objects which are potentially harmful.

Thinking about the above given examples, we can already spot three different types of pain causing stimuli which are chemical, mechanical, and temperature based. All those acute stimuli result in comparable reactions - the withdrawal of the affected body part to reduce the contact with the irritating condition or damaging object (Fields, 1989, Johansen and Fields, 2004).

2.3.2 Inflammatory pain

The second and possibly more hindering type of pain is the inflammatory pain which in contrast to the acute pain lasts for hours, days, weeks or even longer. An example is given with the swelled finger after an unfortunate hammer blow. This type of pain has an aversive and protective function. The sensation of pain promotes for example the immobilization of fractured bones or injured tissues, which in turn improves the healing of the affected body parts.

The main feature of inflammatory pain is that usually innocuous stimuli produce pain, a process termed allodynia (Loeser and Treede, 2008). A second feature, known from daily experience, is called hyperalgesia and represents the enhanced pain feeling after a noxious stimulus to inflamed/injured body parts (Kidd and Urban, 2001, Loeser and Treede, 2008). These hypersensitivities are typically the result of an auto- or paracrine sensitization event, after inflammatory mediators are released by damaged tissues and/or immune cells (Basbaum, 1999, Basbaum and Woolf, 1999, Julius and Basbaum, 2001, Hucho and Levine, 2007, Basbaum et al., 2009). The inflammatory mediators are thought to enhance the sensitivity of the sensory system and start a mechanism which subsequently amplifies the pain sensation. Some of the most important inflammatory mediators are prostaglandins (Ballou, 2000, Ballou et al., 2000), cytokines (Opree and Kress, 2000), tissue hormones and growth factors (Wood, 2010, Liu et al., 2011, Andres et al., 2013).

2.3.3 Neuropathic pain

The above described pain types serve as protective (nocifensive) mechanisms to prevent organisms from severe tissue damages and derive from external non-neuronal sources. The following two chronic pain types are both characterized by abnormal nervous system functions and a lack of physiological explanations for their occurrence.

The first subtype of this pathological pain is the so called neuropathic pain, which typically results from a damage of the peripheral nervous system. The causal basis for this pain class is a lesioned, damaged, or removed part of the somato-sensory pathways (Baron, 2006, Magrinelli et al., 2013). The most impressive example associated with neuropathic pain, is so called phantom pain. Phantom pain is associated with the painful sensation of a missing limb. A feature occurring as mal interpreted sensation of the blunted nerve endings by the brain (Manchikanti and Singh, 2004, Fieldsen and Wood, 2011, Flor et al., 2013).

2.3.4 Dysfunctional pain

Following Costigan et al. 2009, (Costigan et al., 2009) the fourth pain class supports neither an obvious protective nor a curative function. Nowadays it is expected, that the so called dysfunctional pain is based on a malfunction of the somato-sensory apparatus. This pain type occurs in situations, where no obvious pain causing or sensitizing stimuli or an obvious damage towards the nervous system can be detected. The dysfunctional pain can occur exemplary in the irritable bowel syndrome, tension type headaches, or fibromyalgia (Woolf, 2010, Klug et al., 2011). The molecular mechanisms resulting in this pain type are not well understood and remain under constant research. First studies suggest, that a central sensitization in the brain or spinal cord could amplify the incoming signal and over-interpret it as painful (Staud and Rodriguez, 2006, Nielsen et al., 2008).

2.4 The sensory neurons of the dorsal root ganglion

The first detector for pain causing stimuli in mammals is the peripheral nervous system, which are the nerves and ganglia that are not located in the central nervous system (brain and spinal cord). Within this network the dorsal root and trigeminal ganglia, locate the cell bodies of sensory neurons. The sensory peripheral termini from the trigeminal ganglia innervate the mouth, eyes, nose, and face surface. From here the sensory information is transmitted from the trigeminal ganglia directly into

the brain. This is different to the dorsal ganglia which transmit information first towards interneurons in the spinal cord and from here into the brain.

The dorsal root ganglia (DRG) positioned next to the spinal cord contains three branches. One innervates sensing tissues like the skin, inner organs as liver, intestines, or the stomach, a second branch targets the central nervous system in the spinal cord. The third branch is derived from axons of efferent motor neurons, which have their cell bodies in the spinal cord (Dubin and Patapoutian, 2010). Within the DRG specialized neurons are responsible for most detectable modalities. The neurons which perceive pain causing stimuli are termed nociceptors and were first anatomically described by Sir Charles Sherrington in 1906 and functionally specified by Burgess and Perl in 1967 (Sherrington, 1906, Burgess and Perl, 1967).

To spot those neuronal nociceptors they have to be identified, which can be achieved in different ways. I will focus in the following part on three major aspects to identify nociceptors: the anatomy, the physiology, and the molecular equipment.

2.4.1 Anatomic neuron categorization

The sensory neurons from the dorsal root ganglia can be sub grouped according to their axon and soma sizes, as well as by the degree of myelination. This categorization results in three major- classes (Julius and Basbaum, 2001). The first category is represented by the so called A α, β, γ, and δ-fibers and has the highest degree of myelination and largest axon diameter (2-20 µm). Functionally, this group mediates the sensation of proprioception, light mechanical stimuli and acute or first pain. The second group is represented by the so called B-fibers which are moderately myelinated and show medium axon diameters (1-3 µm). The B-fibers mainly coordinate visceral functions. The last group consists of so called c fibers which have the smallest diameter (0.5-1.5 µm) and are not myelinated. Within this group, the majority of cellular nociceptors are located, they account for the so called second pain that last for minutes to hours after an initial stimulus (Julius and Basbaum, 2001, Basbaum et al., 2009).

Furthermore, the spinal cord innervation by the peripheral sensory neurons is anatomically differentiated according to their functionalities. The central projection sides in the spinal cord for nociceptors are the lamina I, II and V. Other sensations are distinct as for example light touch which is conducted into lamina III, IV, and V (Snider and McMahon, 1998, Jessell, 2000).

Former studies extracted and correlated functional aspects from anatomical properties as the relation between axon width and conduction velocity or the neuronal projections. This functional

aspect is determined by the anatomy of the cell type, which is triggered by the interaction between glial and neuronal cells. Glial cells integrate the amount of expressed neuregulin by the neuron and apply a corresponding myelin sheath to the axon (Michailov et al., 2004). A fact which indicates that simple protein expression can determine the degree of myelination of an axon and in consequence its physiological properties.

2.4.2 Physiological neuron categorization

Classically peripheral sensory neurons are divided in two physiological categories, afferent and efferent, which refer to the direction of the signal flow. While the afferent neuron conducts signals from the periphery to the spinal cord, efferent or motor neurons transfer signals from the central nervous system into the periphery. The cells within the DRG reveal mostly afferent neurons, transferring information from organs and skin into the central nervous system. The peripheral nociceptive neurons seem to break out of this concept, where other neurons have clear input and output structure, dendrites and axons respectively, this is not the case for nociceptors. Hence, the polarity of nociceptive neurons is often described as pseudo-uni-polarity, the concrete information flow direction remains under constant research.

Following the fundamental biological concept, in which the form follows function and vice versa, the above described c-fiber nociceptive neurons vary from the rest of the DRG-neurons regarding the axon diameter and grade of myelination. As reviewed by Dubin and Pataputian 2010, large diameters and highly myelinated axons show faster conduction velocities, while the smaller, unmylelinated c-fibers the slowest. With a conduction velocity of 0.8-1 m/s a primate nociceptor conducts 11 times slower than A-fibers. While in smaller animals, as mice or rats, the overall signal velocities are lowered, this discrepancy holds also true for other species (Dubin and Patapoutian, 2010).

The physiology of a cell depends highly on its molecular instrumentation. This equipment, based mostly on proteins, enables the neuron to detect a certain stimulus range, transduce it, and give an appropriate response (depolarization, transmitter release, or transcription). Therefore, a sensory neuron detects a specific stimulus, as touch or temperature in a defined range. Examples in the DRG are the rapidly and slow adapting mechano-fibers, which are termed after the stimulus type and response quantity. These fibers are related to large diameter soma a-fibers, with high conduction velocities. The cell type which I will focus on in this study responds to noxious thermal and mechanical stimuli and is grouped into the slow conducting c-fiber class. These fibers sense a heterogeneous range of stimuli as bradykinin, prostaglandins, growth factors and capsaicin and are thought to contain the majority of nociceptors. While the quality of the stimulus response is defined by

the molecular instrumentation the quantity is defined by signal transduction machinery and will be specified here as cellular signaling state (Bessou and Perl, 1969, Lewin and Moshourab, 2004, Mandadi and Roufogalis, 2008).

2.4.3 Marker based neuron categorization

The requirements to sense an environment needs specialized sensors, which are represented by the peripheral nervous system. There is evidence that specific neuronal subpopulations are responsible for the sensation of specified stimuli as a distinct temperature range, the sensation of mechanical or itching stimuli (Mandadi and Roufogalis, 2008, Liu and Ji, 2013).

The specialized neurons, which sense pain, serve under physiological normal conditions as sensors for thermal, mechanical, or chemical stimuli. The determination what makes the cell a sensor for one of those stimuli, is made by unique molecular equipment (Lewin and Moshourab, 2004). How many different subpopulations in a DRG exists, is hard to estimate. A study from the year 2000 suggested more than 25 different, afferent, cellular subpopulations in the DRG (Petruska et al., 2000). This is just a binary attribute (marker positive or negative), which does neither take into account inhomogeneous expressed markers nor relates it to the cell size or the coexpression of other proteins. Nevertheless, the marker system is still a valid tool for the description and identification of neuronal cell population. Physiological relevant data can only be extracted from a simplified black box (= cell), which parameter are controlled as best as possible. These facts make the DRG an even more complex system to study a sensory physiology. The identification of markers for specialized neurons and the assignment of molecular function were for a long period the major goals in pain research (Julius and Basbaum, 2001). Thus, in this work I aim to develop tools that enable the field to investigate complex cellular features in its full complexity and heterogeneous appearance.

2.5 Molecular markers for nociceptive neurons

Neuronal specification depends on the expression of a specific repertoire of molecular receptors (e.g. receptor tyrosine kinase, or ion channels), modulators (e.g. small g-proteins or transcription factors), and effectors (e.g. ion channels, neurotransmitter or peptides).The following subchapter presents an introduction on some of the most prominent and later in the results section discussed markers for nociceptive neurons.

2.5.1 Peptidergic and non-peptidergic neurons

Lectins are glycoproteins that bind specifically to carbohydrates and are most predominantly present in plants but occur in animal beings as well. In their natural environment, lectins serve as antibiotics, cell surface proteins, and cell recognition elements. Nociceptors are classically divided into two subpopulations - the peptidergic population marked by the expression of the releasable peptide transmitters Calcitonin Gene Related Peptide (following CGRP) and Substance P and the segregating non-peptidergic cells which lack this peptides and express the glycoproteins of the versican family, which specifically binds the isolectin b4 derived from *Bandeira simplifolia*. (Sharon and Lis, 2004), (Julius and Basbaum, 2001, Bogen et al., 2005). The peptidergic and non-peptidergic subpopulation differ not only in their protein repertoire, but also in their functionality and growth factor dependencies (Stucky and Lewin, 1999, Hucho et al., 2005).

2.5.2 The tetrodotoxin resistant sodium channel NaV 1.8

Of high importance are voltage gated sodium channel. One can differentiate between the tetrodotoxin resistant and sensitive channels. An important marker for nociceptive neurons is the tetrodotoxin resistant voltage gated sodium channel 1.8 (following NaV 1.8). Beneath NaV 1.8 adult DRG neurons express different forms of voltage dependent sodium channels as the tetrodotoxin sensitive forms NaV 1.1, NaV 1.6 and the tetrodotoxin resistant NaV 1.5 and NaV 1.9 (Dib-Hajj et al., 2010). Following Djouhri et al 2003 (Djouhri et al., 2003) NaV 1.8 channels are mainly expressed in nociceptive neurons and are responsible for the major part of sodium influx, the depolarization of the neuron, and thereby the initiation and progression of action potentials (Blair and Bean, 2002). NaV 1.8 is believed to be a major contributor to the nociceptors excitability and thus takes a central role in the generation of pain. Nociceptors in various neuropathies and inflammatory pain show enhanced expression levels of NaV 1.8 protein, suggesting its influence on nociceptors hyper excitability during pain sensitized conditions (Yiangou et al., 2000, Black et al., 2004). The presence of NaV 1.8 in combination with other sodium channels is no one way direction. Hence, a publication by Rush et al. indicated that an enhanced activity of NaV 1.8 is not directly related to more neuronal activity. It is the cellular environment (cell type) and the coexistence of other channels that are responsible for the physiological outcome (Rush et al., 2006). A finding which indicates the need of novel methodologies to evaluate the coexistence of different ion channels among cell types and their impact on molecular functions.

2.5.3 TRP channels

One of the best understood receptors of nociception belongs to the Transient Receptor Potential family of ion channels (following TRP-channels). The first TRP-channel was discovered in 1969 in a Drosophila mutant, which showed a transient response to constant light exposures (Cosens and Manning, 1969). Nowadays, the TRPs present a large protein family which is sub-classified into seven protein subfamilies namely the ANKTM1 homologue TRP (TRPA), the canonical TRPs (TRPC), the mucolipin subfamily (TRPML), the melastin TRPs (TRPM), the NOMPC homologues TRPs (TRPN), the polycystin subfamily (TRPP), and the vanilloid TRPs (TRPV) (Clapham, 2003, Huang et al., 2006). A breakthrough in pain research was presented by Michael J. Caterina in 1997, whose group first cloned the Transient Receptor Potential subfamily member Vanilloid 1 (TRPV1). The discovery connected the first time pain with a protein, namely TRPV1. After its discovery, several studies showed the contribution of TRPV1 in different pain phenotypes. With two major impacts: a) the transmission of nociceptive signals and b) the change of protein and RNA turnover under diseased or inflamed conditions (Caterina et al., 1997, Caterina et al., 2000, Davis et al., 2000, Brederson et al., 2013). A detailed introduction to mechanistically subjects will be given in the following chapter.

The discovery of other mammalian TRP-channels enabled a major breakthrough for the determination of several sensations. For example, 9 out of the 28 mammalian TRP-genes are responsible for the sensation of warm (7 genes) or cold (2 genes) temperature. Together these nine “themoTRP” genes cover a detectable temperature range from 10 - 53 °C (Mandadi and Roufogalis, 2008, Tominaga, 2008). ThermoTRPs” share three major aspects a) steep temperature dependence, b) expression in relevant cell types, and finally c) be thermo sensitive in its physiological environment. Next to the sensation of temperature mammalian TRP proteins contribute to other sensations as photoreception in specialized retinal ganglion cells (Melyan et al., 2005), hearing/mechanosensation (Corey, 2003), chemical perception (as tatse and smell) (Lin et al., 2007, Huang et al., 2008), and osmo-sensation or -regulation (Corey, 2003).

Since the most prominent member of the TRP-protein family TRPV1 is the major focus of this work, I will give an extended introduction on TRPV1 functionality and pain association in the following chapter.

2.5.4 Further markers

Next to the mentioned cellular markers, for the transmission and balance of nociceptive signals, histamine-, cannabinoid - , metabotropic glutamate -, opiod- and purinergic receptors are of importance in the pain field but shall not be the focus of this work (for review see (Dray, 2003)).

The identification of novel markers, responsible for the modulation of nociceptive stimuli and pain under physiological normal or diseased condition, remain part of intense research (Basbaum et al., 2009). For the development of directed therapies, there is a need in the field to address the expression of markers towards nociceptive behavior. The impact of marker gene knockouts is already extensively described in the field, while pain cell biology is still in its infancy (Caterina et al., 2000, Hucho and Levine, 2007). Though, the concept of markers for specialized neuronal functionalities is not new, there is still a lack in objective description and identification of markers expressed by distinct cell types. Thus, one of the focuses of the first part of this work shall be the establishment of objective criteria and needs for the identification of nociceptive neurons by molecular markers.

2.6 TRPV1 as transducer of noxious pain

TRPV1 is one member out of 6 mammalian TRPV-channels. Since its discovery in 1997 the ion channel evolved as the most cited ion channels in science history (Ruth Isserlin, 2011). This is based on the attributed importance of the channel in its different physiological roles as temperature sensor (> 43 °C), vanilloid receptor (as capsaicin), lipid-sensor (endocannabinoids, anandamide), proton-receptor (pH < 5.2), and last but not least, as cellular marker for nociceptive neurons and as first protein directly linked to pain and pain transduction (Caterina et al., 1997, Caterina et al., 2000). The protein is considered as major transducer for noxious heat and heat hypersensitivity. A fact that is widely accepted, since TRPV1 is a) present in most heat sensitive, nociceptive neurons, b) show indistinguishable action potential between capsaicin and noxious heat, c) has enhanced responses under proalgesic or inflammatory conditions and d) knockout mice show reduced sensitivity towards noxious heat, while a basic heat sensation remains (Basbaum et al., 2009). The role as noxious heat transducer is actually discussed in the field. A study stated that TRPV1 is only connected to thermo effector pathways and TRPV1 activation initiates a cross reaction (Romanovsky et al., 2009). TRPV1 is a non-selective ligand gated ion channel with enhanced selectivity for calcium, which shows a nine fold higher permeability than sodium. A publication by Vriens and Nilius in 2009 defined the TRPV1 opening by capsaicin as a reduction of the channel open probability. Thus, Vriens et al postulated capsaicin as no classical TRPV1 agonist, but a modulator of the ion channels temperature threshold

(Vriens et al., 2009). TRPV1 protein shares important characteristics with other members of the mammalian TRPV family. Each functional TRPV1 channel consists of 4 individual homo- or heteromeric subunits. Each subunit contains 6 trans-membrane domains. A hydrophobic stretch in between domain 5 and 6 is predicted to form a functional pore (Kedei et al., 2001). For receptor activation each, of the four subunits, has its independent and energetically equivalent ligand binding site (Gees et al., 2013).

The opening of the channel in its physiological environment results in an ion influx consistent of mainly Na^+ and Ca^{2+} and some other divalent ions. As a consequence of the channel opening in nociceptors, the cell depolarizes and transmits action potentials. The recipient of this signal is an interneuron in the dorsal horn which transmits the information towards the brain. Growing evidence indicates that in mammals this incoming nociceptive signal is interpreted in the insular cortex of the brain (Starr et al., 2009, Eto et al., 2013).
Next to the depolarization of the cell is the TRPV1 induced calcium influx related with the release of neurotransmitters as CGRP or substance P and calcium based signal transduction events. The release of neurotransmitter sensitizes surrounding cells and is seen as initiator of an inflammatory process. The importance of neuropeptides as pain transmitter was shown in a knockout of CGRPα. Here, knockout mice showed an impaired sensitivity towards noxiuos heat and capsaicin, indicating its role as positive feedback for the pain transducer TRPV1 (Jeftinija et al., 1992, McCoy et al., 2013).

An opposite effect has the repeated stimulation with low doses of capsaicin in TRPV1 expressing cells. Herein, repeated stimuli with capsaicin show decreased cellular responses for subsequent capsaicin stimuli (Mohapatra and Nau, 2003). This tachyphylaxis called phenomenon is widely accepted and used for treatment of mild pain in warm-patches. Commercially available since the nineteen-thirties (by Hansaplast), is the expected underlying mechanism reported first about 80 years later, by Tamara Rosenbaum and Colleagues (Rosenbaum et al., 2004). The molecular explanation to this phenomenon and other TRPV1 modulators known today shall be illustrated in the next chapter.

High doses of TRPV1 ligands (as capsaicin or resiniferatoxin) have not only the potential to cause pain but to induce cell death of TRPV1 expressing neurons as well. This appears as consequence of either toxic ion overloads or through caspase signaling (Hiura et al., 2002, Jin et al., 2005).

Next to stimuli which open TRPV1 are inhibitory substances reported as the pseudo antagonist capsazepine and the unspecific calcium channel inhibitor ruthenium red (Maggi and Meli, 1988, Dickenson and Dray, 1991).

2.7 Modulation of the TRPV1 activatability

The ability of a receptor to sense a stimulus requires its activatability. In case of TRPV1 the sensitization can be modulated by several mechanisms, which apply to each single channel, consistent of 4 protein subunits, its individual sensitization state. In the following subchapter I will focus on the known modulators of single channel properties before referring to an overall cellular sensitization state in the next subchapter.

2.7.1 Voltage, protons and temperature modulate the TRPV1 open probability

Experiments conducted in artificial membrane bilayers suggest, that the temperature sensitivity in the prototypic "ThermoTRPs" is based on the lowering of the voltage sensitivity by increasing the channels open probability. Therefore, it is widely accepted that several TRP channels including TRPV1 are voltage dependent ion channels (Nilius et al., 2005).

While the overall mechanisms are not finally explained, it was possible to show, that temperature functions as graded modulator for the voltage sensitivity. As mechanism it is suggested, that lowering (e.g TRPM8) or elevating (e.g. TRPV1) the temperature affects the tertiary structure of the channels and thereby lower the voltage open threshold (Voets et al., 2004).

As already mentioned presents TRPV1 next to acid sensing ion channels II (ASIC2) one of the major pH sensors in the peripheral nervous system. Herein, protons have a dual effect on TRPV1 functionality. While high pH levels (6-7) lower the TRPV1 activatability by capsaicin or heat, lower pH levels do enhance the open probability (Jordt et al., 2000). Comparable to temperature, modulate protons from a certain pH (~ 6) gradually the TRPV1 open probability. It is mentionable that not the conductance of single channels for ions is enhanced as suggested by studies from (Tominaga et al., 1998, Baumann and Martenson, 2000), but the open probability. Newer studies suggest mechanisms, which modulate the open probability of the ion channel, respectively subunits, than changing the ion flux quantities (Aneiros et al., 2011).

2.7.2 Expression and localization influence the TRPV1 activatability

TRPV1 expression is not restricted to neuronal tissues, but sensory neurons show the highest concentrations. (Sanchez et al., 2001). As mentioned above was the expression of TRPV1 first described in a subpopulation of mainly afferent nociceptive fibers (Caterina et al., 1997).

Different lines of evidence suggest changes in the TRPV1 protein and RNA turn over under diseased and hyperalgesic conditions. The best accepted and cited example is the increase of TRPV1 protein and/or its localization towards cellular plasma membranes under pro-inflammatory conditions as a consequence of nerve growth factor release by injured tissues and/or immune responses. This process is thought to appear without gene transcriptional activity. Only translation and directed expression, as an antegrate transports to nerve endings, is expected to change cellular sensitivity for one or many targets of the neuron. As a consequence, it is suggested that these changes can turn an capsaicin insensitive silent cell into a functional nociceptor (Ji et al., 2002, Zhang et al., 2005, Adcock, 2009, Zhu and Oxford, 2011, Zhu et al., 2011).

Enhanced expression of the TRPV1 channels can be observed under many circumstances, for example after injury to peripheral nerves in patients suffering from endometriosis or as a response to sciatic nerve section. Enhanced TRPV1 protein kevels occurs interestingly not only at the affected tissue site, but in the associated vascularity and in the cell body of the DRG-neuron as well (Hudson et al., 2001, Stenholm et al., 2002, Orliac et al., 2007, Poli-Neto et al., 2009).

The reported differential TRPV1 expression in combination with decreased thresholds for noxious stimuli and enhanced responses towards noxious heat in animals, proposes that the amount of expressed ion channel directly affects the animals behavior. Meanwhile a relation between the ion channel expression and its cellular response is to my best knowledge never shown on a single cell level. To fill this gap, I aim in this work to establish a system which enables the parallel measurement of a) the endogenous native TRPV1 protein amount and b) associate it with a specific response in the very same cell.

2.7.3 TRPV1 and its posttranslational modifications

Phosphorylation by kinases and dephosphorylation by phosphatase are thought to be further important modulators of the TRPV1 activatability in sensory neurons (Zhang et al., 2005). In total, experimental evidence exists for four different kinases families. The most important one is given with the Protein Kinase C family (PKC), with a special focus on the ε isoform. Other studies suggest the involvement of the μ isoform as well (Wang et al., 2004). PKCs phosphorylate in total five different serine and threonine residues on the TRPV1 molecule while only S502 and S800 are thought to change the ion channel's performance. Phosphorylation of both residues is thought to enhance the open probability of TRPV1 and overall ion influx after channel activation (Vellani et al., 2001, Numazaki et al., 2002, Bhave et al., 2003, Studer and McNaughton, 2010).

The second most frequently occurring TRPV1 modulating kinases belong to the Protein Kinase A family (PKA). PKAs have with six serine and threonine residues more phosphorylation sides than PKCs while only S116, T144 and T 370 are thought to have a functional role. Even while some of PKCs and PKAs phosphorylation sites are overlapping (S502 and S800) phosphorylation by PKAs is thought to play a major role in the control of desensitization of TPRV1 instead of sensitization (Bhave et al., 2002).

Other works give evidence that the Calmodulin dependent Kinase II (CaMKII) phosphorylation at site S502 and S704 are mandatory for the binding of capsaicin to the ion channel. A study published by Jung and Cho et al. 2004 even reports a complete loss of capsaicin activated ion currents and abolishment to sense resiniferatoxin, indicating the importance of CaMKII dependent phosphorylation (Jung et al., 2004). The phosphorylation of a tyrosine residue at position 199 by the sarcoma kinases (src) is believed to play a crucial role in the trafficking of the channel from intracellular pools towards the plasma membranes (Zhang et al., 2005). For dephosphorylation of the ion channel several lines of evidence indicate a major involvement of the calmodulin dependent phosphatase protein phosphatase 2b (pp2b, also known as calcineurin). It is thought, that after calcium entry in the cell free Ca^{2+} ions binds calmodulin to form a complex, which is incorporated to form the full functional phosphatase (Mohapatra and Nau, 2003, Por et al., 2010). The mechanism of calcium based modulation of TRPV1 will be discussed later in this subchapter.

Next to the differential phosphorylation sites of TRPV1 other posttranslational modifications are reported. One is the glycosylation of TRPV1 at the asparagine residue 604, which is described to play a crucial role in the capsaicin induced calcium responses and desensitization of TRPV1 (Veldhuis et al., 2012). Another less prominent modification is the covalent coupling of 4-hydroxy-2-nonenal to TRPV1 (Kishimoto et al., 2011).

2.7.3 Calcium and calmodulin hinder the TRPV1 Ion permeability

There is broad acceptance in the field, that TRPV1-desensitization is triggered by the presence of cellular Ca^{2+}. Therein, the free ions are scavenged by calmodulin which either bind calcineurin and dephosphorylate mandatory phosphosites or, as proposed by Numazaki and Tominaga 2004, directly binds TRPV1 and decreases the ion permeability (Numazaki and Tominaga, 2004). An initial study by Rosenbaum et al. 2004 showed that the desensitization requires the presence of calmodulin and calcium (Rosenbaum et al., 2004). This last hypothesis gained further support by studies suggesting calmodulin affine ankyrin repeat on the TRPV1 N-terminus. It is hypothesized that both TRPV1 termini and calmodulin form a complex which blocks the pore (Lau et al., 2012). Taken together

there is a broad biochemical and cell biological evidence derived from heterologous expression systems indicating an indirect calcium and calmodulin based regulation of the channels ion permeability (Salazar et al., 2009), while an direct experiment in primary cells is still lacking. These experiments evaluate the appearance of calmodulin, calcium, TRPV1 and relate it with the TRPV1 activatability. An approach to fill this gap shall be later established and introduced in this study. Furthermore, the expression of calmodulin and the capsaicin activatability of TRPV1 in primary neurons shall be directly determined.

2.7.4 Protein coexpression affects the TRPV1 functionality

Expression of TRPV1 with endogenous modulators is one of the hot topics in current pain research. Opposing groups try to identify novel modulators of the TRPV activatability. One of the most prominent modulators is the calcium scavenger calmodulin, which inhibitory effect was already explained above.

Another modulator of TRPV1 channel activity was described with the A-kinase-Anchoring protein 79 (following AKAP 79). AKAP 79 is expected to build a molecular scaffold to associate PKAs and PKCs to TRPV1 and form a so called signalosome. Interruption of this interaction abolishes PKA and PKC based sensitization effects (Jeske et al., 2008, Schnizler et al., 2008, Zhang et al., 2008, Jeske et al., 2009, Jeske et al., 2011).

The identification of novel modulators of TRPV1, and therefore potential novel drug targets remains challenging since classical techniques as co-immuno precipitation are hard to handle in membranous proteins. In the here delivered work I aim to validate the impact of the most prominent protein modulators of TRPV1, namely AKAP and calmodulin in a) a quantitative approach and b) in primary dorsal root ganglia neurons. Thereby I want to validate results obtained from overexpression system in their physiological environment. Next to proof known candidates I aim to chase for novel modulators which will be tested in this system.

2.7.5 Other modifiers of TRPV1

Several other modulators are reported to depolarize cells throughout activation of TRPV1. This work cannot give a complete list, but I opt to mention the most important. TRPV1 is one of the primary targets for ginger derived gingerol (Iwasaki et al., 2006), allicine from garlic and onions (Macpherson et al., 2005), piperine from black pepper (McNamara et al., 2005), and alkylamides from sichuan

pepper (Menozzi-Smarrito et al., 2009). Next to the above introduced, spices developed several organisms' toxins which target the mammalian TRPV1. Within this, a large cohort of different peptide based venoms can be found in almost the complete spectra of the animal kingdom beginning at dinoflaggelates over jellyfish, snails, shellfish, snakes, spiders and scorpions. More detailed information is recently reviewed by Min et al. (Min et al., 2013). While most of the toxins cause TRPV1 channel activation and therefore severe pain for its recipient, more and more inhibitory substances (peptides) are found in animal venoms (Adams, 2004, Kitaguchi and Swartz, 2005).

For the sake of completeness, it is needful to mention the other regular cited TRPV1 modulators and activators, though these are not part of the present work. Membrane derived lipids as anandamide and oleoylethanolamide can directly activate TRPV1 (Zygmunt et al., 1999, Ahern, 2003). Ahern et al. 2003 reported, that several products of the endogenous lipooxygenase are able to activate TRPV1 in isolated membrane patches as well as heterologous expression system (Ahern, 2003). Therein, the reported enzymatic products showed high similarities to the capsaicin structure.

Other studies indicate a constitutive inhibitory binding of TRPV1 towards phosphatidylinositol 4,5 bisphosphate (following PIP_2). Upon activation of the phospholipase c the PIP_2 is cleaved from the membrane, resulting in diacylglycerol and inositol 1,4,5 triphosphate. The activation of the ion channel directly happens by the release of the channel inhibitor (Chuang et al., 2001, Prescott and Julius, 2003). The regulation of this mechanism is mapped to positively charged amino acid stretches, which contain also the PKC phosphorylation site S800. Thus, the proposed PLC mechanism could also be an upstream effect of PKC activation and a subsequent enhancement of channel open probability.

2.7.6 Outlook TRPV1 modification

Many targets for the modulation of TRPV1 are reported. But the chase for novel TRPV1 modulators/ligands, scaffold and modification is still one focus in pain research. Meanwhile, a major gap can be found in the validation of reported modulators in primary systems. Overexpression systems have high feasibilities for different techniques but fail to set up a close to physiology environment. In this work, I aim to fill this cap and validate known modulators with novel technical approaches in primary cells.

2.8 Sensitization states define the cellular response

The cellular sensitization state can be understood as the ability of a cell to react to a defined stimulus. A sensory neuron can respond to the very same stimulus in several ways. This discrepancy can be explained with the actual signaling state of a cell. In terms of pain research a phenomenon called hyperalgesic priming is described. Within, this concept a neuron exists in different states, a naive or unprimed state, a primed state and the hyperalgesic state (Ferrari et al., 2010, 2013, Hendrich et al., 2013). Depending on the animal model, the hyperalgesic state lasts for a few hours. Meanwhile the primed state, which is received after disappearance of the hyperalgesia, can last for weeks. (Hucho and Levine, 2007). Uncovering the mechanism of these states could deliver big steps into the understanding of pain perception and related diseases. But how can an individual cellular sensitization state be defined and identified?

2.8.1 Kinases as marker for cellular sensitization state

The identification of a cellular sensitization is challenging, since beneath functional readouts are markers for a particular cell state rare. Herein, the phosphorylation and localization of key kinases as ERK, CaMKII, PKA and PKC are thought to play major roles in sensitized or primed sensory neurons (Aley et al., 2001, Andres et al., 2010, Chaban et al., 2011, Ferrari et al., 2013). Since the field is rather new, further research on markers for the sensitization is yet to come. Especially is there a need to associate the potential marker with a pain relevant cellular function. Studies by our group just recently delivered evidence that the amount of expressed key kinases is directly correlated with its activity (Andres et al., 2010, Isensee et al., 2014). Therefore, I opt in this work to analyze those already identified markers and their ability to modulate the TRPV1 function.

2.8.2 TRPV1 activatability and the cellular sensitization state

The here delivered study is a majorly quantitative cell biological work. Therefore, I have to explain some basic hypothesis and concepts. In the previous chapter I introduced TRPV1 modulators which can impact the cellular TRPV1 responses.

Due to the composition of different protein states (e.g. phosphorylated, protonated, bound to modulators) within a single cell, each cell has the ability to fine tune its agonist/ligands sensitivity to an enormous grade. In the here delivered work I aim to validate the mechanisms which determine the nociceptors sensitivity against capsaicin.

Thus, a differentiation is made between the TRPV1 responses, which presents the open probability of a single ion channel, and the cellular response or sensitivity, which integrates the protein responses of some 100-10000 individual ion channels. Transferring these concepts towards a single cell, the cellular TRPV1 response represents an individual cell sensitization state. Concerning TRPV1 this is defined as the sum of open probabilities over all present TRPV1 molecules relative to the cell volume and the expression with molecular scaffolds or signaling components.

Herein, the hypothesis will be proven that the TRPV1-expression in individual primary sensory neurons impacts the channel response. Furthermore, shall the expression of main kinases and modulators be associated with the capsaicin sensitivity of DRG neurons. Thereby, literature suggested TRPV1-modulators shall be tested and a novel methodology established for the identification of modulators. Possible positive results could be used as novel markers for cellular sensitization state, and represent potential targets for pain treatments.

2.9 Aims

To study subpopulations of sensory neurons and the unraveling of regulatory mechanisms require a novel quantitative methodology. Within the here delivered work experiments shall be set up which allow a deeper understanding of nociceptors characteristics, functionality, and response regulation.

2.9.1 Setting up quantitative identification methods for nociceptive neurons

The analysis of pain relevant cell populations resulted so far in highly diverse reports. For example, based on differential techniques and quantification procedures the size of the TRPV1 positive cell population has been described to be between 40 and 100 % (Kobayashi et al., 2005, Price and Flores, 2007, Hoffman et al., 2010). Therefore, the first part of this study aims to establish objective tools for marker based, quantitative studies of heterogeneous subpopulation using microscopic techniques. Thereby I aim to set a standard for cellular pain studies, which can be applied for future studies on most cell types and tissues.

2.9.2 Population analysis of capsaicin sensitive DRG neurons

Beyond the quantification of marker expressions, the heterogeneity of functional single cell readouts such as calcium influx is enormous and has so far not been pursued. I aim to set up experimental

approaches which enable the large scale functional study of heterogeneous DRG neurons. This will give access to the heterogeneity of cellular capsaicin responses regarding qualitative and kinetic parameters.

2.9.3 Assessment of the relation between TRPV1 expression and cellular capsaicin sensitivity

The investigation of pain relevant ion channels on a cellular response is classically performed by fusing proteins of interest with fluorescent tags and subsequent expression in model systems. Drawback in these approaches is the crosstalk between tag and the channel functionality and the artificial cell systems. To save a physiological environment I aim to establish a system which enables the monitoring of protein contents and cellular functionalities in cultured sensory neurons. The generated multi-dimensional data shall be used to create a mathematical model which reproduces the heterogeneous TRPV1 mediated capsaicin responses in DRG neurons.

2.9.4 Evaluation of TRPV1 modulators in primary sensory DRG Neurons

Using newly established techniques to monitor cellular protein contents and functionalities, I opt to validate published TRPV1 modulators and validate the impact of the cellular sensitization state on the capsaicin sensitivity. Within these experiments the impact of signaling on the cellular heterogeneity concerning marker expression and response behavior shall be assessed. Furthermore, I will analyze published and potential TRPV1 modulators and markers for the cellular sensitization states.

2.9.5 Identification of novel TRPV1 modulators

Signaling might not explain the complex regulation of nociceptor sensitivities. The molecular composition including post translational modifiers, anchoring, and scavenging proteins determine the potential frame where signaling takes place. Hence, the identification of novel modulators for nociceptive neurons is one of the big issues in the current pain research. To get an in depth view on nociceptors I aim to perform a transcriptome analysis of the TRPV1 positive subpopulation in DRG neurons. The resulting data will be analyzed for novel insights into the molecular compositions of nociceptive neurons; reveal novel subgroup marker, and potentially allow the identification of novel TRPV1 modulators.

3. Materials and Methods

3.1 Materials

3.1.1 Antibodies

3.1.1.1 Primary antibodies

Antibody	Company	Cat #	Dilution
Chicken anti-UCHL1 antibody	Novus	NB110-58872	1:1000
Mouse anti-Calmodulin antibody	Sigma	C3545	1:1000
Mouse anti PGP 9.5 antibody	MorphoSys	7863-2004	1:500
Mouse anti-AKAP79 antibody	BD	610314	1:500
Mouse anti-CART antibody	R&D	MAB163	1:1000
Mouse anti-ERK antibody (pan),	BD	BD610124	1:1000
Mouse anti-KCNIP1 antibody	Abcam	ab99073	1:1000
Mouse anti-NaV1.8 antibody	NeuroMab	75-166	1:1000
Mouse anti-PKA RIIβ antibody	Abcam	ab32514	1:1000
Rabbit anti-CGRP antibody	Bachem	T-4032	1:1000
Rabbit anti-TRPV1 antibody	Alomone	ACC-030	1:500

3.1.1.2 Secondary antibodies

Antibody	Company	Cat #	Dilution
Chicken anti-mouse Alexa 488	Invitrogen	A11029	1:1000
Chicken anti-mouse Alexa 594	Invitrogen	A21201	1:1000
Chicken anti-rabbit Alexa 488	Invitrogen	A21441	1:1000
Chicken anti-rabbit Alexa 594	Invitrogen	A21442	1:1000
Donkey anti-mouse Alexa 647	Invitrogen	A-31571	1:1000
Goat anti-chicken Alexa 488	Invitrogen	A11039	1:1000
Goat anti-chicken Alexa 647	Invitrogen	A21449	1:1000
Goat anti-mouse Alexa 488	Invitrogen	A11029	1:1000
Goat anti-mouse Alexa 594	Invitrogen	A11032	1:1000

Goat anti-rabbit Alexa 488	Invitrogen	A11034	1:1000
Goat anti-rabbit Alexa 594	Invitrogen	A11037	1:1000

3.1.2 Media

Name	Company	Cat #
Dulbecco's Modified Eagle Medium (DMEM)	Lonza	BE12-707F
F-12 Ham Nutrient Mixture	Invitrogen	31765-027
Hank's Buffered Salt Solution	Invitrogen	14170-070
MEM	Invitrogen	42360-024
Neurobasal-A Medium	Invitrogen	12349-015

3.1.3 Buffers

Name	Composition
1x Blotting buffer	48 mM Tris, 39 mM Glycine, 0,04 % SDS, 20 % Methanol
5x Laemmli loading buffer	62.5 mM Tris-HCl pH 6.8, 5 % β-Mercaptoethanol, 50 % Glycerol, 2 % SDS, 0.1 % Bromphenol Blue
2x "Magic Mix"	8 M urea, 15 mM Tris-HCl pH 7.5, 8.7 % Glycerin, 1 % SDS 0.4 ‰ Bromphenol Blue, 143 mM β-Mercaptoethanol
TBS	137 mM NaCl, 26 mM KCl, 25 mM Tris
TBST	0.1 % Tween in TBS

3.1.4 Microscopy

Device	Company
ArrayScan VTI	Thermo Scientific
Axioskop (Objectives: 5x, 10x, 40x and 63x)	Zeiss
Axiowert 100 (Objectives: 5x, 10x, 20x and 40x)	Zeiss
LSM 510 (Objectives: 2.5x, 10x, 20x,40x,63x, and 100x)	Zeiss
LSM 700 (Objectives: 2.5x, 10x, 20x,40x,63x, and 100x)	Zeiss

3.1.5 Software

Software	Developer
Cellomics toolbox (Scan, View + iView)	Themo Scientific
ImageJ (MBF-Plugin package)	NIH, MacMaster Universty
LSM	Zeiss
Office 2003 + 2007	Microsoft
Prism (version 4 + 5)	GraphPad
R	University of Auckland
SDS Software v1.2.3	Applied Biosystems
Zen	Zeiss

3.1.6 Laboratory equipment

Equipment	Company
384-well Sensoplate	Greiner
96-well Microplate	BD Falcon
Centrifuge EBA 12	Hettich Centrifuges
Centrifuge EBA 12R	Hettich Centrifuges
Centrifuge Rotanta 4402	Techno Plastic Products
Cleanbench	Cleanair
Cover slips, Type 556	Fisher
Falcon tubes (15 ml , 50 ml)	Falcon
Filter paper	Whatmann International
Filter tips	Biozym
Fluid reservoirs	Roth
FUJI Film Super RX	Helmut Roesch Ltd
Garbage bag	Roth
Glass slides	Roth
Imaging Plate, 384 well (glassbottom)	Greiner
Imaging Plate, 96 well (µ-clear)	Greiner
Multichannel pipettes (0.5-10 µl, 5-100µl)	Eppendorf

ND-1000 spectrometer	Peqlab
PCR-Tubes	Fischer Scientific
pH Meter 763	Knick
Pipetboy acu classic	Integra Bioscience
Pipette tips (0-2 µl, 2-200µl, 100-1000 µl)	Gilson
Pipettes (0-2 µl, 2-20µl, 20-200µl, 100-1000 µl)	Gilson
Plastic cell Culture 24-well plate	Biochrom
Power supply	Biorad
Reaction tube 0.1 ml	Roth
Reaction tube 1.5 ml	Roth
Reaction tube 2 ml	Eppendorf
Rongeur	FST
Scalpel	FST
Scissors	FST
Serological pipettes (2.5 ml, 5 ml, 10 ml , 20 ml)	Corning
Steri-Cycle CO_2-Incubator	Thermo Scientific
Thermomixer 5436	Eppendorf
Tissues	Kimtech
Trans-Blot Semi-Dry Transfer Cell	Biorad
Vortex Genie 1	Scientific Industries
Tecan und Multiptobe II HT-Tips, 200µl,	Thermo Fisher / BioRobotics
Thermocycler ABI 7900HT	Applied Biosystems

3.1.7 Protein marker

The Page Ruler pre-stained protein ladder (Fermentas, # SM0671) was used as markers in SDS-PAGE and immune blots (Bands at: 170 kDa, 130 kDa, 100 kDa, 70 kDa, 55 kDa, 40 kDa, 35 kDa, 25 kDa, 15 kDa, and 10 kDa.

3.1.8 Kits

Name	Company
Qiashredder	Qiagen
High Capacity cDNA Reverse Transcription	Applied Biosystems
NucleoSpin RNA II	NucleoSpin RNA II
Power SYBR Green PCR Master Mix	Applied Biosystems

3.1.9 Drugs and chemicals

Drug/Chemical	Company	Cat#
Aceton, p.a.	Merck	1.000.142.500
4',6'-Diamidino-2-phenylindole dihydrochloride (DAPI)	Serva	18860.01
Ammonium persulfate	Biorad	161-0700
Azidohomoalanine	Invitrogen	C10102
B-27	Invitrogen	17504
Bovine serum albumine	Sigma	A3912
Calcium chloride	Merck	102392
Capsaicin	Sigma	12084
Casyton	Innovatis	43001
Chloroform, p.a.	Merck	1.024.452.500
Collagenase p	Roche	11 213 873 1
Complete protease inhibtior	Roche	1 697 498
Dimethylsulfoxid (DMSO)	Merck	1.02950:0500
DNase	Promega	M610A
Dulbecco's Phosphate Phosphate Buffered Saline	BioWhittaker	BE17-521
EDTA, p.a.	Merck	1.084.181.000
Ethanol, p.a.	Merck	1.009.832.500
Fetal Bovine serum	Sigma	F7524
Fluoromount-G	SouthernBiotech	0100-01
Forskolin	Sigma	F3917-10MG
FURA-2-AM	Invitrogen	F1201

Glycerin	Merck	104.095
Glycine, p.a.	Merck	1.042.011.000
HCS CellMask™ Deep Red stain	Invitrogen	H32721
Immersol	Zeiss	518F
Ionomycine	Sigma	I3909-1ML
Isopropanol, p.a.	Merck	1.096.342.500
Laminin	Invitrogen	23017-015
Isolectin B_4, FITC labeled	Sigma	L-2895
Isolectin B_4,TRITC labeled	Sigma	L-5264
L-Glutamate	Sigma	27647
L-Glutamine	Sigma	G6392
Methanol, p.a.	Merck	1.060.092.500
Murine nerve growth factor	Alomone Labs	450-02
N,N,N',N'-Tetramethylethylenediamine	Invitrogen	15524-010
Normal donkey serum	Dianova	017-000-121
Normal goat serum	Dianova	005-000-121
PageRuler prestained protein ladder	Fermentas	SM0671
Paraformaldehyde (PFA)	Sigma	158127
Penicillin/Streptomycin	Lonza	BE17-512F
Phorbol-12-myristat-13-acetate (PMA)	Sigma	P 8139
Poly-L-Ornithin Hydrochloride	Sigma	P2533
Potassium chloride, p.a.	Merck	104936
Rat Calcitonin gene related peptide	Sigma	C0292
Sigmacote	Sigma	SL2-100ML
Skim milk powder	TSI	
Sodium dodecyl sulfat	Roth	4360.1
ß-Mercaptoethanol	Merck	8.057.400.250
Staurosporine	Merck	569396-100UG
Sterile distilled water	Lonza	BE17-724F
SuperSignal West Femto	Pierce	34095

SuperSignal Wet Pico	Pierce	34080
Tris[(1-benzyl-1H-1,2,3-triazol-4-yl)methyl]amine	Sigma	678937
Triton X-100	Roth	3051.2
Trypsin	Worthington	LS 3703
Tween 20	Sigma	P9416

3.2 Methods

3.2.1 Cell culture

3.2.1.1 Animals

Adult male Sprague Dawley rats (*Rattus norvegicus*) were purchased from Harlan Winkelmann (Borchen, Germany). Adult black6 mice (*Mus musculus*) were bred in the animal facility of Max-Planck-Institute for Molecular Genetics in Berlin. Housing of animals was performed under controlled conditions with a 12 h dark-light cycle, food and water were available *ad libitum*. Care and use of animals were in accordance with the European Communities Council Directive of 24 November 1986 (86/609/EEC) and were approved by the LaGeSo, Berlin, Germany.

3.2.1.2 Cell culture surface treatment

For neuron culturing glass cover slips or multiwell plates were coated with a PBS-solution containing 0.1 mg / ml ornithine and 5 µg / ml laminin. Glass cover slips and multiwall plates for neuronal cultures were incubated for 90 min and air dried at room temperature for 30 min.

Surfaces for HEK- and F11-cells were pretreated using a 0.1 mg / ml poly-D-Lysine in PBS solution. Imaging plates were delivered in sterile batches, while glass cover slips were kept in an ethanol solution. Before use the ethanol was flamed with a bunsen burner.

3.2.1.3 Isolation and culturing of primary DRG neurons

Based on previously described methods cultures of dissociated Dorsal Root Ganglia Neurons (DRG) were prepared in 24- , 96- and 384- multiwell plates (Hucho et al., 2005). Before each dissection, supplemented Neurobasal media were prepared by adding 2 % B27, 0.25 % glutamate, 3.7 % glutamine and 1 % penicillin/streptomycin.

Adult male Sprague Dawley rats or black6 mice were sacrificed by constant CO_2 intoxication (20 % of the cage volume CO_2 per minute). The dorsal root ganglia L1-L6 were removed, pooled in Modified Eagle Media with GlutaMAX™ (MEM), cleaned from surrounding sheath with spring steel forceps, and placed into fully supplemented Neurobasal media. The isolated DRGs were digested with 0,125 % collagenase (0.2 U /ml) for 1 h at 37 °C and 5 % CO_2 to pre-separate the cells (neurons and glia). Following the dissection and digestion, the ganglia were separated by a mild trituration, using fire polished Pasteur pipettes. Throughout this process soft mechanical forces unify the individual cells, and remove glial cells and structures from neuronal surfaces. Tissue debris and dead cells were removed by placing the cell suspension on a gradient using 1,5 ml 15 % BSA / Neurobasal and a subsequent centrifugation for 8 min at 120 g (Hettich Centrifuge, EBA 12R) . The supernatant and BSA fractions were discarded. The remaining cell pellet was suspended in the appropriate volume of fully supplemented Neurobasal media to obtain 300-500 cells in 24- and 96-well and 1000 neurons in 384 well plates. The cultures were maintained in humidified atmosphere at 37 °C and 5 % CO_2. Experiments were performed on the next days to led cells attach to the surface and settle down.

3.2.1.4 Cell lines

The HEK-293 cell line was established by transformation of embryonic kidney cells with fragmented human Adenovirus DNA (Graham et al., 1977). Ancestors of those cells were kept at 37 ° C at 5 % CO_2 in Dulbecco's Modified Eagle media supplemented with 10 % fetal bovine serum and 1 % penicillin / streptomycin.

F11 cells are one of the sparse available neuronal cell lines made of embryonic rat DRG-neurons and mouse neuroblastoma cells. Due to the fusion of both cell types, a cell was generated that contains rat as well as mouse chromosomes. F11 cells are used because of neuronal features as action potentials and neurite like outgrowth (Platika et al., 1985, Jow et al., 2006). F11-cells were maintained in F12-Ham medium supplemented with 15 % FBS, 1 % Penicillin / Streptomycin, and 1.5 % glutamine. Either HEK as well as F11 cells were kept 384-well plates at 37 °C in a humidified atmosphere at 5 % CO_2.

HEK and F11 were passaged in a 2-2-3 day cycles into fresh media. For splitting, media was removed and cell debris and dead cells were discarded by PBS washing from the culture flasks. The remaining cells attached to the flask surface were washed 3 times with warmed PBS. Afterwards the attached cells were digested for 3 – 5 min with 0.025 % trypsin (~ 47 U / ml). The generated cell suspension was diluted 1:10 for passaging or adapted to a working concentration of 2000 cells 100 µl.

3.2.2 Immunocytochemistry and cell staining

3.2.2.1 Immunocytochemistry

For antibody based visualization of proteins the cultures were incubated with antibody solutions. Therein primary antibodies detect the proteins of interest. The primary antibodies were detected with secondary fluorophore coupled antibodies.

For immune cytochemistry cells were fixed using a 2 % or 4 % Formaldehyde / PBS solution (20 min or 10 min / RT). Following fixation, cells were washed, permeabilized, and blocked using a PBS-buffered solution containing 1 % BSA, 2 % Normal Donkey sera and 0.1 % Triton X 100 for 1 h at room temperature. After this step, the cells were washed 3 times with PBS. The primary antibodies were dissolved in 1 % BSA / PBS. Incubation of the primary antibodies was performed either for 1h at room temperature or for 16-18 h over night at 4° C. In a next step, the cells were washed for at least one hour with 1 % BSA in PBS. The secondary antibodies were also diluted in 1 % BSA / PBS and incubated for 1 hour at room temperature. Nuclear or membrane staining was performed in combination with the secondary antibody as described below. Following the secondary antibodies, the cells were washed 3 times with PBS for at least 1 hour. The 96- and 384-well plates were directly transferred to the image capturing procedure. Glass coverslips were sealed in Fluoromount on glass slides. All samples were stored at 4 °C in the dark. All pipetting steps in 96- or 384-well plates were performed using automated multichannel pipettes with exactly defined volumes and dispense velocities.

3.2.2.2 Nuclear staining

To perform nuclear stainings, 4,6-diamidino-2-phenylindole (following DAPI) was used. DAPI binds in two conformations to DNA: First, in AT rich regions in the minor groove of double stranded DNA and second, base independent but with lower affinities. Next to the ability to bind to DNA, DAPI intercalates with a certain lower degree (about five time lowered kD) to RNAs. Since the density and the amount of RNAs in the cytoplasm versus nuclear DNA is smaller, a DAPI staining shows sharp nuclei signals (Kubista et al., 1987). DAPI was used in a concentration of 0.005 µg / ml in either PBS (96- or 384-well plates) or Fluoromount (Cover slips).

3.2.2.3 IB4 staining

To label non-peptidergic nociceptive neurons of the rat, TRITC or FITC labelled Isolectin B4 was used in dilutions of 1:2500 to 1:10000. The binding of IB4 requires divalent ions. Therefore, the staining

solution was made of 1 % BSA in 1x PBS and contained 10 µM $CaCl_2$, 10 µM $MgCl_2$, and 10 µM $MnCl_2$. The IB4 staining was performed in combinations with the secondary antibodies.

3.2.2.1 Plasma membrane staining

For counterstaining of cell lines I used amphipathic cell mask dyes from Invitrogen. These dyes intercalate with lipophilic residues of cellular membranes and anchor themselves to the membrane via hydrophobic interactions. The plasma membrane dyes were typically used in dilution of 1:50000 and incubated with the nuclear staining for 60 min at room temperature.

3.2.3 Microscopy

3.2.3.1 High Content Microscopy

High content microscopy on living and formaldehyde fixed cells was performed using the cellomics ArrayScan VTI platform. Briefly, above the microscopes (Zeiss AxioVision) objective, an automated stage moves 24-, 96- , or 384- well-plates. For live-cell purposes this stage was temperature- and CO_2 controlled. Ahead of the live-cell chamber an automated pipettor was able to dispense liquids from a reservoir into the well.

Images were acquired using 5x, 10x, or 20x objectives, output images had a typical pixel resolution of 512 x 512 and depth of 12-bit (4096 grey levels). For the identification and quantification of neurons, the system associated software "Cellomics View" was used. Within this, an object detection algorithm identified cellular profiles according to their geometrical shape with circularity ($perimeter^2$ / 4π area) of 1-2 and length-to-width ratio of 1-2, fluorescence intensities typically in between 150-2000, and area of 150-4000 μm^2. The generated regions of interest were subsequently transferred to quantifiable images.

3.2.3.2 Confocal microscopy and sample preparation

Confocal microscopy was performed using the Zeiss LSM 700 or LSM 500 microscopes. For sample preparation, sterile 12 mm glass cover slips were placed in 24 well plates. The cleaned cell suspension was placed in a 100 µl droplet on top of the cover slip. To allow cells to settle down and attach to the surface, the cells were placed back to the 37 °C and 5 % CO_2. After 1 hour 400 µl Neurobasal A / B-27 media was added. On the next day, the immune cytochemistry procedure was

performed. The sample was placed in Fluoromount on glass slides and transferred to the microscope. For imaging the ZEN (LSM 700) or LSM (LSM 500) software were used. Exposure time and signal gain options were set to catch the optimal signal range without over exposition. Image analyses were performed in ImageJ-based customized (semi-) automatized pipelines established within the course of this thesis.

3.2.3.3 Calcium Imaging

Cellular calcium contents were elucidated with ratio metric measurements using FURA-2 coupled to acetoxymethyl esters (Grynkiewicz et al., 1985). To transfer FURA-2-AM into the DRG-neurons, F11 or HEK cell lines, the cells were loaded with 0.25 µg FURA-2-AM to 80 µl culture wells and incubated for 37 °C and 5 % CO_2. After 40 min, the wells were washed twice for 10 min with warmed MEM media for F11 or HEK cells, or supplemented Neurobasal A for neurons. Image capturing was performed after alternating excitations (340 and 380 nm) at 510 nm in the Cellomics ArrayScan VTI High Content Screening platform. Stimulation of cultures was handled by an integrated pipetting robot. A maximum of 8 wells was measured to reduce the measurement time and circumvent FURA based cell stress.

3.2.3.4 Combination of calcium imaging and immunocytochemistry

To analyze the relative protein expression of single cells and combine this with the functionality of the cell, a combined live cell imaging and immune fluorescence protocol was established. After a final stimulus in the live cell experiment, cells (HEK, F11 or DRG neurons) were fixated using 2 % PFA and immune cytochemistry protocols were performed. The cell preparation, FURA-2-AM loading, live cell imaging, and immune cytochemistry protocols were performed as described above. The plate was placed again to the ArrayScan VTI and identical view fields were imaged again.

3.2.4 Molecular Biology

3.2.4.1 Transfection of cell lines

F11 and HEK cells were cultured in a 384-well plates with a density of 1000 or 2000 cells per well. One day after seeding, Lipofectamine transfections were performed according to the provided guidelines (www.invitrogen.com). During the procedure, reaction tubes containing either, 0.25 µL

Lipofectamine reagent + 25 µl opti-MEM or DNA + 25 µl opti-MEM were incubated at room temperature for 5 min under sterile conditions. In the meantime, sera and antibiotics containing media were replaced by warmed opti-MEM. After the first incubation time, both reaction tubes were pooled and incubated at room temperature for another 20 min. The resulting 50 µl solution, made of DNA, Lipofectamine and opti-MEM, was added to the culture wells. The cultures were transferred to 37 ° C and 5 % CO_2 for 4 h. After transfection, procedure cells were placed into the appropriate media and maintained another 24 h until calcium or immune cytochemistry experiments were performed.

3.2.4.2 Isolation of RNA from tissue samples

Isolation of total RNA was performed using the commercial Machery Nagel Nucleospin kit RNA II. Cell pellets (~ 125 mg) were rinsed with 350 µl lysis buffer (Buffer RA1) and gently mixed by pipetting. Cell debris was removed by applying the solution to a NucleoSpin^{R} filter and a subsequent centrifugation. The flow through was collected and placed onto an ethanol equilibrated second silica column which binds nucleic acids. The column was washed with a desalting buffer, bound DNAs were digested with desoxyribonucleases followed by 3 washing steps (1xRA2, 2xRA3). Elution of RNAs was performed using 40-60 µl dH2O. For higher yields the eluation buffer was applied a second and third time to column.

3.2.4.3 Optical quantification of RNA in aqueous solutions

To determine RNA yields the NanoDrop 1000 (Thermo Scientific) spectroscopic RNA quantification was performed. Therefore, 1 µl of a diluted or undiluted RNA sample was placed on a sensor where the absorbance of 260 and 280 nm light is measured. The resulting concentrations were calculated following Lambert-Beers-Law, by the device. After analysis the nitrogen frozen RNAs were stored at -80 °C.

3.2.4.4 cDNA-libraries

To generate a library of RNA-transcripts for real time PCRs, RNA fragments were reversely transcribed to cDNA. Using high capacity cDNA reverse Transcription Kits by Applied Biosystems. Briefly a 2x reaction buffer was generated using the kit containing reagent. For one reaction this consisted of 2 µL 10 X Reaction buffer, 0.8 µl dNTP Mix random primers , 1 µl Multiscribe^{TM} Reverse Transcriptase, 1 µl RNA inhibitor and 3.2 µl sterile nuclease free water. Per reaction 100 µg of

isolated RNA were placed in a volume of 10 µl in a PCR reaction tube, and 10 µl of a 2 x PCR solution was added. Controls were prepared with sterile water instead cDNA. The reactions were placed into a thermocycler and incubated for 10 min at 25 ° C, 120 min at 37 °C, and 5 min at 85 °C. Following the three steps, the cylcer cooled down to 4 °C. The generated samples were directly used for validating PCR reaction or stored in dilution 1:10 in sterile water at -20 °C.

3.2.4.5 Quantitative polymerase chain reaction

For the relative quantification of RNA amounts, quantitative real time polymerase chain reaction (following q-PCR) was performed. Comparable to classical PCR approaches base the q-PCR based on three steps: DNA-denaturation, primer-annealing, and fragment-elongation. The here performed q-PCR used SYBR-green, which bind to double stranded DNA and forms a DNA-fluorophor complex. Quantification of transcripts was performed in the exponential amplification phase. The resulting cycle numbers were normalized and calculated against the house-keeping gene actin.

For each reaction, 10 µl reaction-mix was pipetted, containing 1 ng cDNA template, 5 pmol of each primer, 2 µl SYBR green PCR master-mix and nuclease free water. The reactions were placed into Taqman real-time PCR-machines. The polymerase was activated at 95 ° C, followed by 40 cycles of 15 s denaturation at 95 °C, primer annealing and elongation at 50 °C. Resulting data sets were analyzed using the SDS v2.4 software.

3.2.4.6 Transcriptome sequencing

The sample treatments for whole transcriptome sequencing were performed by the group of Prof. Andreas Kuss from the University Greifswald. Briefly, 2 µg of each RNA sample were cleaned from ribosomal RNA using the Ribo-Zero-Kit from life technologies. The single RNA molecules were fragmented, attached to beads, amplified with emulsion PCRs, and labeled using the life technology kit for total-RNA-Seq, bar coding EZ Bead, and the Emulsifier E80 Reagent kit. The prepared beads were placed onto solid 6-lanes flow chips and sequenced using the Solid 5500 Xl device. Sequencing was performed in a paired end manner, with a forward sequence length of 75 bp and reverse 35 bp, resulting in read lengths of 75 bp. The generated sequences were aligned to the reference rat genome rn_05 (NiH), read numbers per gene were normalized according to internal g-c contents.

3.2.4.7 Protein isolation from tissue samples

In order to reduce enzymatic digestion and protein breakdown all following steps were performed on ice. For the protein isolation from primary neurons, media was removed at best from the cell pellets and 100 µl of a cell Lysis buffer ("Magic Mix", 8 M Urea, 15 M Tris/HCl pH 7.5, 8.7 % Glycerin, 1 % SDS, 0.4 % bromphenol blue, 143 mM ß-mercaptoethanol) was added and slightly mixed to guaranty a proper cell extraction. The suspension was placed on Qiashredder column to separate cell debris, DNA, and proteins.

3.2.4.8 Optical quantification of proteins in aqueous solutions

Determination of protein concentration was performed on a NanoDrop 1000 (Thermo Scientific). Typically 2 µl undiluted solution was placed on top of the sensor of the spectroscope and measured against the empty solution at a wavelength of 280 nm. The concentration was calculated by the delivered software following Lambert-Beers-Law. Protein solutions were stored at – 80°C degree, after they were shock frozen in liquid nitrogen.

3.2.4.9 Protein separation using SDS-PAGE

Proteins were separated via electrophoresis in Sodium-Dodecyl-Sulfate Polyacrylamid gels (following SDS-PAGE). These gels consisted of two fractions: a stacking- and a separation gel with the following formulation.

Compound	stacking gel (25 ml)	resolving gel (5 ml)
H_2O	13.2 ml	3.4 ml
30 % acrylamide mix	5.0 ml	0.83 ml
1.5 M Tris (pH 8.8)	6.3 ml	-
1 M Tris (pH 6.8)	-	0.63 ml
10 % ammonium persulfate	0.25 ml	0.05 ml
10 % SDS	0.25 ml	0.05 ml
TEMED	0.016 ml	0.005 ml

Tab 3.1.: Formulation of SDS-PAGE stacking and resolving gels.

The stacking gel was set up with small pockets (later lanes) for the protein samples. Each pocket was loaded with 10 µg protein in a volume of 20 µl volume. A typical 10 % SDS-gel run was performed in running Buffer (25 mM Tris-HCl, 200 mM Glycine, 0.1 % SDS) with a current of 100 V (and ~ 10 mA) for 1 h or until the blue (leading phenol band) ran out of the chamber.

3.2.4.10 Protein detection with immuno western blot

To specifically detect individual proteins from SDS-pages, immuno western blots were performed. Herein, separated proteins on SDS-PAGEs were transferred to polyvinylidene difluoride (following PVDF-) membranes. The PVDF-membranes were activated in 100 % methanol for 5 min at RT, rinsed with sterile water, and incubated in 1x blotting buffer (48 mM Tris, 39 mM glycine, 0.04 % SDS, 20 % methanol). The blot was set up with 3 layers of whatman filter papers wetted with blotting buffer, second with the activated PVDF-membrane, third the SDS-gel, and finally another three layers of Whatman filter papers. This stack was placed in a semi-dry blotting apparatus (Biorad, Trans-Blot SD). Proteins were transferred in an electric field with strength of 2.5 mA / cm^2 for 40 min to a PVDF-membrane. To prevent unspecific bindings of the subsequent antibodies and to saturate the charged surface, the membranes were blocked for 1 h at RT in TBST containing 5 % skim milk. In a following step primary antibodies were applied in 1 x TBST over night at 4 °C and constant mild shaking. After 14-16 h the membranes were rinsed 3 x 15 min with 1x TBST. Secondary antibodies coupled to Horse radish peroxidase were chosen in accordance to the primary antibodies. In a final step the blots were rinsed with “Super signal west femto” and developed on a FUJI medical x-ray film. The exposure times were adjusted to guaranty optimal signals.

3.2.5 Data processing

3.2.5.1 Statistics and presentation

The data analysis was performed using prism software version 4 and 5, Microsoft Excel version 2003 and 2007, or the statistics software “R”. To circumvent variations, based on animals or transfection efficiency, each experiment was performed, if not otherwise identified, at least on three independent days with not less than three replicates per condition. For analysis of repeated measures or repeated experiments, one way analysis of variance was performed. If more than two measurements are compared to each other, a post turkey test was performed. Analysis of sample population with differing cell numbers were performed using the student t test.

The analysis of two dimensional data sets was performed using the spearmans rank correlation test. Significance values are displayed with the following abbreviation: ns for not significant, * for $p < 0.05$, ** $p < 0.01$, and *** $p < 0.001$.

The large data sets were analyzed using customer scripts in R. To visualize multi-dimensional data set the smooth scatter plot function in R was used.

3.2.5.2 Random sampling

While performing quantitative analysis of cell populations, it is beneficial to be aware of the number of cells needed to detect a certain population feature. Thus, random sampling scripts in "R" were developed. Typically those scripts sampled a defined number of events from over sampled datasets. This very large dataset is assumed to represent the "real" distribution. The computational sampling of smaller datasets out of this large one identifies the number of cells required for the full population representation.

3.2.5.3 Image analysis

More than 3.000.000 images were analyzed during the course of this thesis. Image quantification was performed, using the ImageJ plugin compilation, supported by the McMaster Biophotonics facility (Ontario, Canada). The cell identification in life cell experiments was based on fluorescence intensities after high potassium stimulation or the appropriate counter staining. To identify regions of interest (ROIs) single images were chosen and set to binary images by applying a Li algorithm. After this procedure, the image consisted of a binary matrix with values of 1 or 0 (black or white). The resulting image underwent a watershed algorithm to segment close by objects. In the next step cells were identified by circularity (= 4π (area/perimeter^2)) of 0.5 to 1 (perfect circle) and size in between 150 and 4000 μm^2 (neurons). Cells located at edges of images were excluded to prevent incomplete objects to be analyzed. Following the object identification fluorescence intensities were measured using the Ratio ROI manager plugin in ImageJ.

3.2.5.4 Ramp fitting of calcium traces

To extract kinetic information from measured cellular calcium responses, Steffen Waldherr (Uni Magdeburg) developed in close collaboration a ramp fitting analysis. Herein, an equation system fits an idealized curve to measure calcium traces and extracts kinetic parameters of the response as the response amplitude, baseline and response time. Mathematically the curve is described by the differential equation system shown in the results part chapter 4.2.

3.2.5.5 Gene annotation with “DAVID”

The “Database for Annotation, Visualization and Integrated Discovery” allows on three analyzable levels a functional classification of genes, respectively gene lists. In detail these levels are i) the biological process, ii) the gene occurrence in its particular cell compartment, and iii) the molecular function the gene associates with. In the DAVID annotation tool each gene is classified with an open number of so called terms. These terms integrate the appearance of a gene in association with a physiological function. In a result, regularly appearing functions are grouped and compared to a background, here the complete genome, and an enrichment score was calculated. This score ranks the probability of incidental appearance compared to a genome wide background and defines specific enrichments of functional groups. The background chosen was the latest rat genome available namely rn5 (also known as Rnor_5.0). DAVID was used as online tool (source: david.abcc.ncifcrf.gov)

4. Results

4.1 Quantitative identification and description of cellular subpopulations

To study the physiology of peripheral nociceptive neurons, the neuron of interest has to be identified first. Therefore, immune cytochemical experiments were performed in combination with confocal laser scanning and a quantitative automated fluorescence microscopy technique which was recently established for DRG neurons (Andres et al., 2010, Andres et al., 2013). This first results chapter describes the identification of nociceptive neurons by the expression of markers as TRPV1, NaV 1.8, CGRP, and IB4. For this puprose a methodology will be stated that ensures a quantitative identification and objective description of nociceptive neurons.

4.1.1 Heterogeneous expression of TRPV1, CGRP and the IB4 binding Versican in DRG neurons

In this first results part nociceptive neurons were detected with a confocal microscopy approach. Therefore, DRG-neurons were cultured and stained for the nociceptive markers TRPV1, CGRP and IB4. Image capturing was accomplished with the confocal Zeiss LSM 700. For identification of neuronal cells, in the glial neuron mix cultures, antibodies against the Ubiquitin carboxyl-terminal hydrolase L1 (UCHL1) also known as Protein Gene Product 9.5 (PGP 9.5) were used. The identification of nuclei was achieved with the DNA staining DAPI.

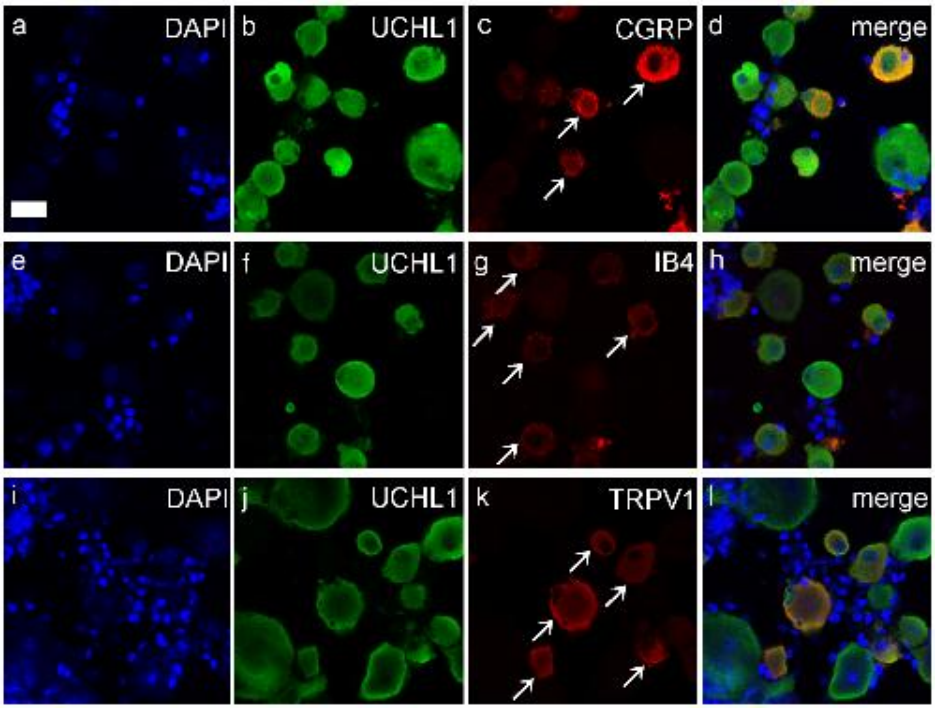

Figure 4.1.1.1 Subgroup positive neurons are in-homogenous in rat DRG neurons (a, e, i) Nuclear staining with DAPI stains glial (light blue) and neuronal (faint blue) nuclei,. **(b, f, j)** Overall neuronal staining with UCHL1 shows a cytoplasmic pattern and clear signal. **(c, g, k)** Staining for the neuronal subgroup markers CGRP, IB4 and TRPV1 show marker positive (arrows) and negative neurons. **(d, h, l)** False color image with merged channels. The scale bar indicates 25 µm.

The experiment illustrated in figure 4.1.1.1 shows the expected signal pattern. The neuronal overall marker UCHL1 (see images 4.1.1.1a, e, + f) shows a distribution all over the cell with slightly enhanced signals at cell edges. The subgroup marker CGRP (image 4.1.1.1b) shows a vesicular localization next to the plasma membrane in a vesicle typical manner. The IB4-signal shows a ring surrounding the cell surface image and slightly enhanced dots in the soma (image 4.1.1.1. f). Both findings are in line with former studies on CGRP and IB4 positive cells (Price and Flores, 2007, Jimenez-Andrade et al., 2010). The TRPV1 protein expression does not show a specific pattern in the image sets (image 4.1.1.1j), since the signal is distributed all over the cell soma.

The assignment of marker positive or negative is hardly possible in an unbiased manner. Hence, the decision between positive or negative needs a reference object. Thus, a judgment of individual fluorescence intensities has to be performed in a relative manner to all other cells. To achieve this I applied a quantitative microscopy technique. I cultured primary DRG-neurons in 96-well imaging plates. The individual cellular marker protein content was detected with usual immune fluorescence protocols, as described in the methods part (compare 3.2.2.1). The automated microscopy approach quantified cellular protein levels by adding up the fluorescence intensity of each single pixel within a cell and divided it by the number of pixels. Thereby, I expected to observe a two peaked distributions of fluorescence intensities, illustrating the amount of marker expressing (positive) and none expressing (negative) cells.

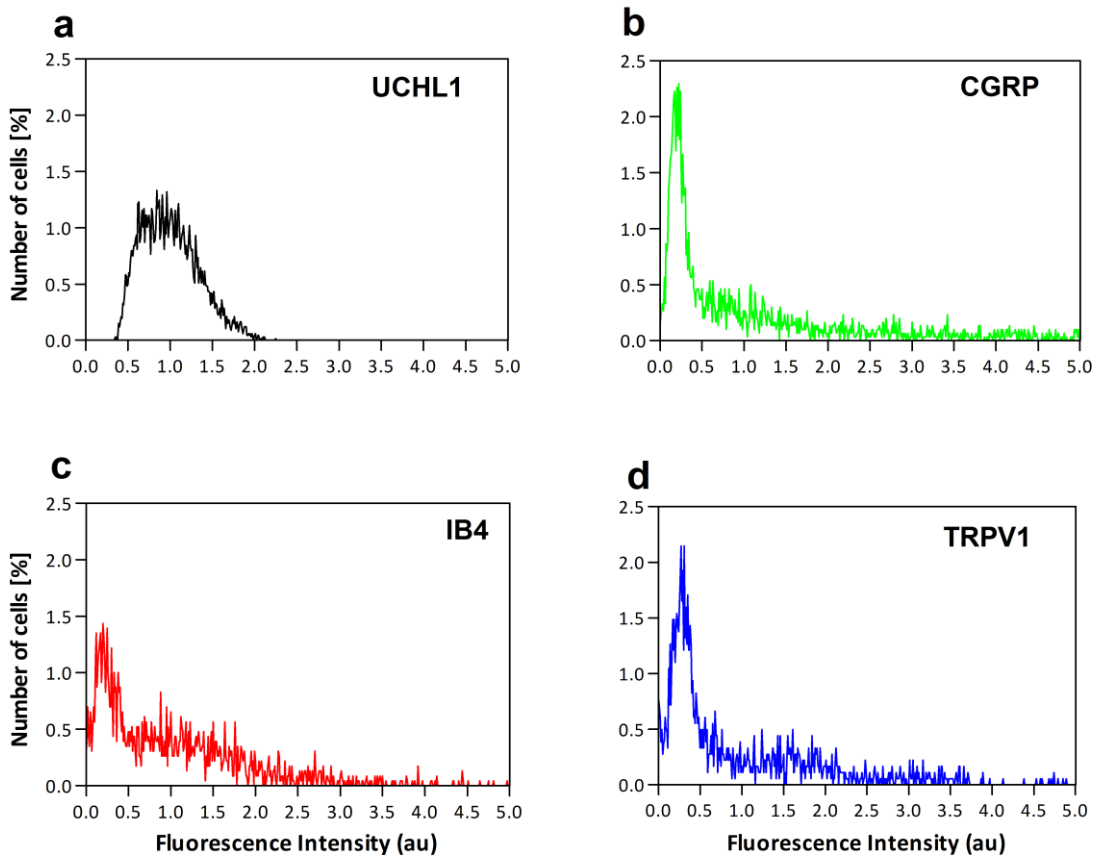

Figure 4.1.1.2 Heterogeneous expression of CGRP, IB4, and TRPV1 in rat DRG neurons The data shown here are normalized relative fluorescence intensities (au) of individual neurons. The shown data is normalized and binned to reduced inter experimental variances in the fluorescence signals (au). **(a)** The distribution of UCHL1 is close to a normal distribution (data generated from 7143 neurons out of 9 independent animals). **(b)** The distribution of the CGRP shows a peak on left hand side, with weak fluorescence intensities, and a broad shoulder of high fluorescence signals. The Data was generated from 3007 neurons in 9 replicates and 3 independent animals. **(c)** The distribution of the isolectin B4 binding subpopulation shows a background peak and one higher intensity shoulder. The data generated from 2300 neurons and 3 independent animals. **(d)** The TRPV1 positive subpopulation shows also a broad distribution of cellular expression levels. Data generated from 1836 neurons and 3 independent animals.

None of the subpopulations (CGRP, IB4, and TRPV1) showed a distribution which easily separates marker positive and negative neurons. The distributions rather present broadly spread protein expression levels. Within this the first peak indicates marker negative or low expressing cells, and the shoulder the heterogeneous protein levels per neuron (see figure 4.1.1.2b-d). This observation makes the evaluation of neuronal subpopulation by eye error-prone.

To clarify if the heterogeneous protein expression levels are restricted to rat tissue the above shown experiment, was repeated, in a second widely used model system for cellular pain research, namely

mouse dorsal root ganglia neurons. Comparable to the rat experiments primary mouse DRG-neurons were cultured in 96-well plates, followed by immune cytochemistry and automated fluorescence microscopy.

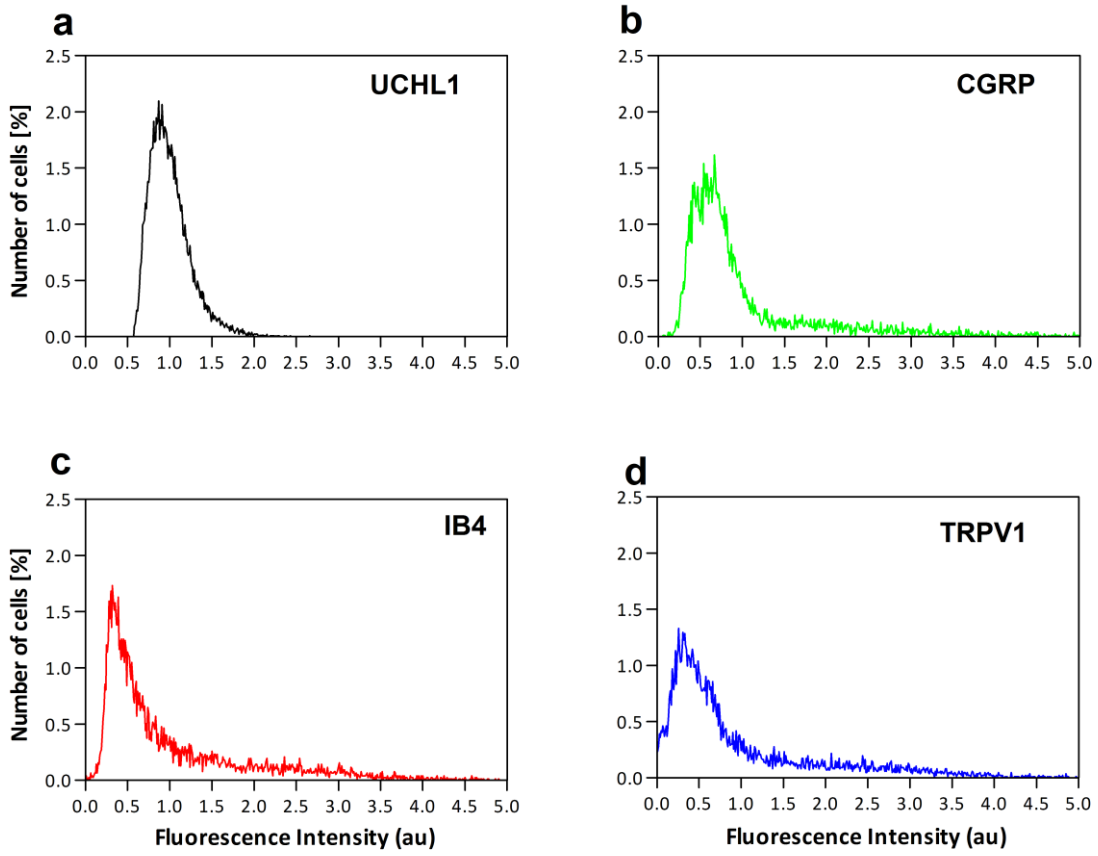

Figure 4.1.1.3 Heterogeneous expression of CGRP, IB4, and TRPV1 in mouse DRG neurons Data is normalized and binned to reduced inter experimental variances in the fluorescence signals (au). **(a)** The distribution of UCHL1 shows a dense distribution with a small shoulder (24277 neurons and 6 independent animals). **(b)** CGRP expression levels show broad expression pattern of fluorescence signals (7826 neurons and 2 independent animals). **(c)** The isolectin B4 signals show differentially to the rat tissue a more flatten distribution (7738 neurons and 2 independent animals). **(d)** The TRPV1 expression is long tailed indicating a wide range of possible protein expression levels (data was generated from 8713 neurons and 2 independent animals).

The signal distribution for the nociceptive subgroup markers CGRP, IB4 and TRPV1 (4.1.1.3 b-d) showed in mouse DRG neurons an equally heterogeneous distribution as in rat DRG. The distribution of the overall neuronal marker UCHL1 remained almost indistinguishable from the rat results (compare 4.1.1.2.b). Thus, the observed heterogeneity of protein expression levels is not restricted to the rat and appears in mouse sensory neurons as well.

But still, it is necessary to determine cells as marker positive or negative to quantify the portion of an investigated cell type or assign certain attributes as functionality, signaling events, or morphological phenotypes. This problem illustrates the need of objective quantification techniques, to assign phenotypes from protein expression levels.

4.1.2 Subgroup identification based on protein expression needs threshold decisions

As shown in the part 4.1.1 are protein expression levels highly heterogeneous among individual DRG neurons. Nevertheless, commonly nociceptive subgroups are assigned based on marker expression. One way to achieve this is to set an intensity threshold, defining the cells with lower fluorescence signals as marker negative and the ones with higher signals as marker positive. In quantitative cell biology this is typically set by an x-fold of the standard deviation of an image background. Other experimenters just cut a subjective threshold that distinct positive and negative cell (Kashiba and Senba, 1999, Price and Flores, 2007, Hoffman et al., 2010). In the following figure I will apply commonly used thresholds on complex distribution of protein expression levels and introduce a novel threshold based method to separate marker positive and negative cells.

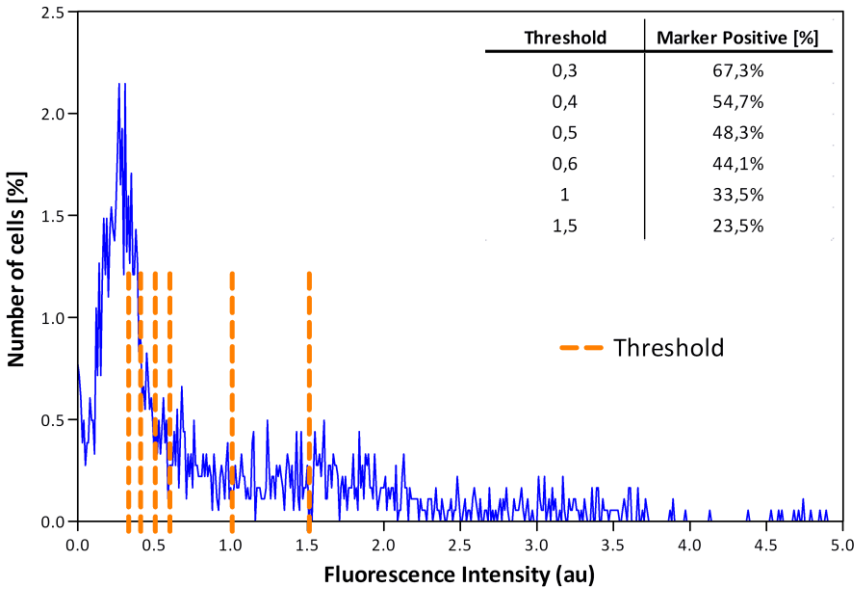

Figure 4.1.2.1 Thresholds determine the size of a cellular subgroup Thresholds (orange lines) are applied concerning 3x (0.3), 4x (0.4) and 5x (0.5) times the standard deviation of the background. One experimenter based subjective threshold (0.6), which interpolates the background peak of proposed marker negative cells, the mean of the distribution (1) and the standard deviation of all objects (1.5). The discrepancy in the number of positive cells is striking, with population sizes in between 23.5-67.3 %. The here exampled inconsistency is obviously based on technical and not biological reasons.

I applied commonly used thresholds (orange dotted lines) as the 3-5 fold standard deviation of the background, a subjective threshold, the mean, and the standard deviation of the total distribution. The subsequent number of marker positive cells differed in this example from 23.5 % for the standard deviation up to 67.3 % for 3 times the standard deviation of the background. While all methods will find a rational explanation the outcome (ranging from 23.5 % - 67.3 % positive cells) remains inconsistent. Thus, other workable methods become necessary to determine marker expressing cells. Thereby, a standard shall be set to determine reliable judgments on biological data sets as the here shown protein expression levels from high content screenings.

4.1.3 Marker positive and negative cells can be distinguished with competition assays

Next to the observed heterogeneity among protein expression levels, immune fluorescence based microscopy approaches often face background fluorescence, recognitions of the wrong epitope by the paratope (specific, false positive), or false antibody bindings via protein-protein interaction (unspecific, false positive). To define those false positive signals, a practicable threshold assay was used, which is accessible without high end technology or complex knowledge in statistics. Within this assay the antigen recognition site of polyclonal antibodies is blocked with specific antigens (peptide epitopes). Thereby, the antibodies are disabled to detect their cellular antigens; potentially remaining signals are derived from false positive binding. For the isolectin B4, melibiose was introduced which contains an alpha-1,6 glycoside linkage which specifically binds the B subunit and N-acetyl-D-galactosamine that is preferentially bound by the lectins A (Fullmer et al., 2007, Verderio et al., 2012). The remaining fluorescence signal was used as threshold.

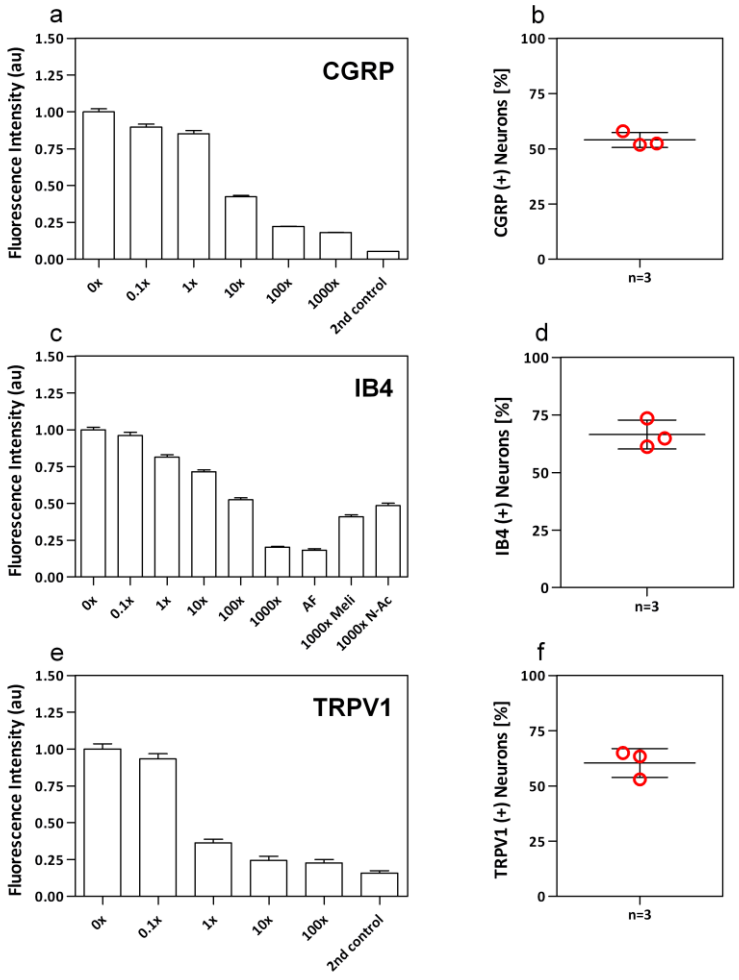

Figure 4.1.3.1 Competition assays produce reliable population sizes The data sets for each marker are pooled from 3 individual animals. Shown are the mean values of all replicates and the standard error of the mean. **(a)** CGRP competition assay, the averaged intensities are reduced proportional to the applied antigen (CGRP) concentration. The shown data is pooled from 31861 neurons from 12 replicates per condition and 3 animals. **(b)** The size of the CGRP expressing population is 54 ± 3.4 %. **(c)** The IB4 signal is reduced accordingly to the sugar residues excess. The shown data is pooled from 15371 neurons from 9 replicates per condition and 3 animals. **(d)** The size of the IB4 positive subpopulation is 66.5 ± 6.3 %. **(e)** Also the TRPV1 signal distribution is reduced in accordance to the antigen amount. **(f)** The here evaluated TRPV1 population size was 60.4 ± 6.5 %. The shown data is pooled from 11792 neurons from 9 replicates per condition and 3 animals.

The competition assay showed in all case the expected result, wherein fluorescence signals are reduced in accordance to the amount of competing antigens. The remaining averaged fluorescence signals under maximal blocking conditions were slightly higher than the secondary (without the primary antibody) or auto fluorescence (without primary and secondary antibodies) controls (Fig. 1.3.1 a, c, d). The resulting intensities were used as threshold and identified populations sizes of 54 ± 3.4 % for CGRP (+), 66.5 ± 6.3 % for IB4(+), and 60.4 ± 6.5 % for TRPV1(+) sensory neurons (Fig. 1.3.1

b,d,f). The low variance in between experiments indicates the competition assay as valid tool for the differentiation between marker positive and negative neurons.

4.1.4 Antibody signals can be defined with dilution series

Several antibodies, as the monoclonal NaV 1.8, are not supplied with adequate blocking peptides, and are therefore not suitable for the introduced competition assay. For those antibodies, dilution series can be used to determine the unspecific antibody signal. If an antibody has a certain unspecific affinity to a tissue the unspecific signals shall be enhanced by higher antibody concentrations. Thus, dilution series can be conducted to determine the grade of unspecific signals, a saturating point and subsequently a threshold.

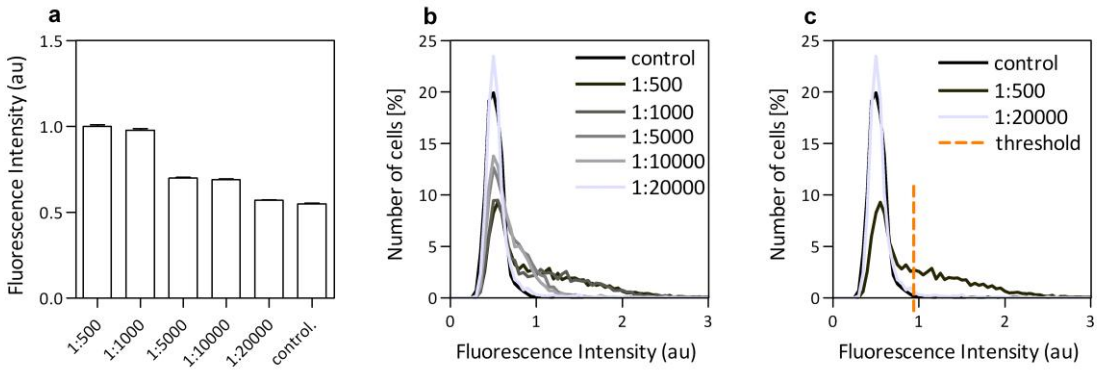

Figure 4.1.4.1 Quantification of the NaV 1.8(+) population with antibody dilution series (a) The panel shows the mean values of all replicates and the standard error of the mean. According to the antibodies concentration decreases the averaged fluorescence signals. **(b)** Distribution of cellular NaV 1.8 fluorescence signals. The background peak is not shifted to higher signals indicating low unspecific antibody bindings. Also, higher signals stagnate at the antibody dilution 1:2000. Thus, it is presumable that saturating conditions are reached. **(c)** A threshold (at 0.75 (au)), generated from 95 % signal of the lowest dilution (1:20000), identified the NaV 1.8 (+) neuronal population with 54.2 ± 8.9 %. The shown data is pooled from 3 individual animals with a total of 5962 DRG neurons.

The NaV 1.8 expression profile showed a long broad shoulder, comparable to the above described subgroup markers (Fig. 4.1.2). According to the antibody concentration the averaged NaV 1.8 fluorescence signals decreased with lower concentration (Fig. 4.1.4.1 a). The dilution series showed that low fluorescence signals (background peak – negative cells) are not shifted to higher intensities. Thereby, the conclusion can be drawn that enhanced antibody concentrations will not raise unspecific bindings but true positive signals. The definition of the saturated condition offers the

advantages that the dynamic range of signals is best (maximal) and an optimal working concentration can be defined. Meanwhile, the highest dilution can be understood as the antibodies background. Both together background and saturated condition were used to determine thresholds which generate here a population size of 54.2 ± 8.9 %. An outcome in line with former reported functional results were 60 % of DRG neurons are reported to express NaV 1.8 (Garrison et al., 2014).

4.1.5 Subpopulation analysis requires a sufficient sample size

In the former part of this chapter I introduced neuronal subpopulation as heterogeneous cohort of protein expression levels. This cohort is diverse and individual cells need to be judged as positive or negative in comparison to all other cells. Thus, a sample number is necessary which ensures the coverage of all cell phenotypes and allows the ranking of single cells to all others.

A random sampling was established to determine the minimal cell number. Herein, the feature of interest was the protein expression levels of TRPV1. Therefore, 2622 TRPV1 fluorescence intensities measured from primary neurons out of 3 independent experiments were pooled. From this pool cells were randomly depicted and the number of positive cells (counts) calculated. This procedure was repeated for 100 times at different sample sizes ranging from 20 until 2200 with an increment of 10.

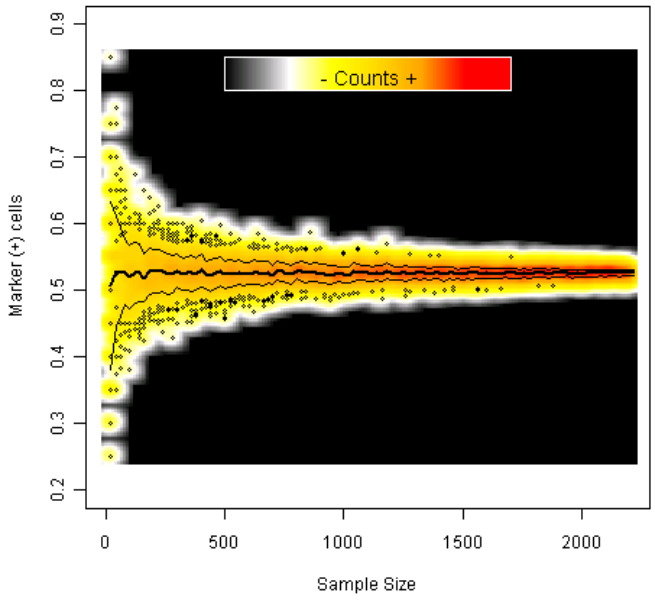

Figure 4.1.5.1 Definition of minimal number of cells For the estimation how many cells are needed to show a reliable numbers of cellular attributes, sub pools were sampled and the number of positive objects quantified. The count density shown (scale bar) indicates the results obtained by the *in silico* experiment. The thick black

line represents the average number of positive cells after 100 repeats. The thin black line is the standard deviation in two directions. The shown data is pooled from 3 independent rats.

The *in silico* experiments showed that the higher the number of sampled cells / objects is, the closer the expected result fits to the "reality" (here 54.2 %). To reach a result which is with 100 % probability in the range of less than 5 % deviation it is necessary to analyze at least 560 objects. Another sample size independent method would be the frequent repetition of experiments. While small repetition (with a cell number around 10-20) require independent samples (animals), which causes ethical problems (Lazic, 2010). The optimal solution is a medium sample size in between 50-100 cell analyzed per animal and 3 or more replicates. The here performed *in silco* experiments indicate another time the need of quantitative techniques while analyzing population effects in neurons and other heterogeneous cell types.

4.1.6 Thresholds on fluorescence signals have to be relative to its distribution

The sizes of neuronal subpopulations are still extensively discussed. A study by Hoffman et al. 2010 concluded that the number of positive cells for several markers, including TRPV1, has to be reanalyzed under optimized staining conditions. Hoffman and colleagues showed that changes in the fixative composition results in severe shifts of fluorescence signals. In detail, the amount of fixative decreased the marker signal in an anti-proportional manner. To validate Hoffmans results the competition assay was performed under differential fixative protocols. Therefore, formaldehyde dilution series were conducted, changing the concentrations from 1 %, over 2 % till 4 %, followed by identical immune fluorescence protocols. After image acquisition, with the Cellomics ArrayScan VTI platform, the cellular fluorescence intensities were quantified to determine population sizes.

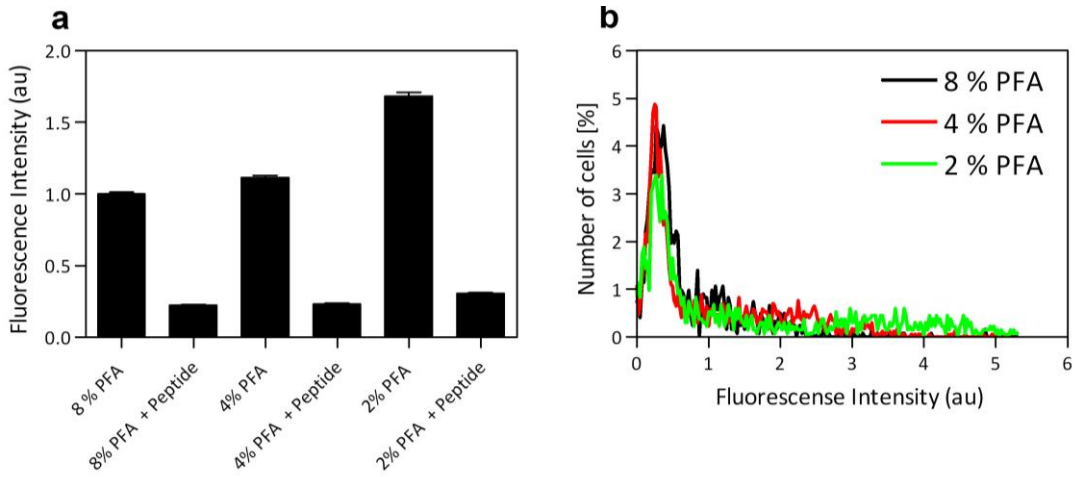

Figure 4.1.6.1 TRPV1 expression profiles after differential fixation protocols (a) Shows the meanTRPV1 fluorescence intensities (au) of all replicates plus standard error of the mean. Blocking conditions were treated with the TRPV1 antigen peptides and show the expected signal decrements. **(b)** Distribution of TRPV1 signals after differential fixative compositions. Reduction of formaldehyde led to a broader fluorescence distribution. The shown data is pooled from 3 rats with a total of 26263 neurons.

The experimental series reproduced the results published by Hoffman and colleagues in 2010 (Hoffman et al., 2010). The fact that lower concentrations of fixative compounds enhance fluorescence signals (Fig. 4.1.5.1 a + b) is based, most probably, on higher crosslink grades of reactive residues (predominantly primary amines). As consequence, steric hindrance prevents the antibody from diffusing deep into a tissue to find its epitope (Fox et al., 1985). Another explanation is that crosslinking masks potential epitopes by changing their molecular structure. A quantification of positive and negative cells is given by the following table.

Condition	total cells	(+) cells	TRPV1 (+) [%]
8 % PFA	4018	2496	62,1
8 % PFA + peptide	3991	200	5
4 % PFA	5296	2999	56,6
4 % PFA + peptide	4678	236	5
2 % PFA	4350	2149	49,4
2 % PFA + peptide	3930	197	5

Tab 4.1.6.1 Number of TRPV1 positive neurons after fixation series

While observing the same effect, as described by Hoffman et al, remained the number of positive neurons in the here conducted experimental series in a comparable range (49.4 – 62.1 % TRPV1(+) (tab. 4.1.6.1)). The threshold placed relative to the fluorescence distributions delivered results that show constant population sizes.

4.1.7 Summary Part 1: Identification of cellular subpopulations requires quantitative tools

To assign a single cell as marker positive or negative it is obligate to integrate differential expression levels. With quantitative fluorescence microscopy thousands of neurons were imaged to define marker expression profiles. Thus, I identified the protein expression pattern of the pain relevant neuronal markers TRPV1, CGRP, IB4, and NaV1.8 as highly heterogeneous populations in rat and mice dorsal root ganglia neurons (Fig. 4.1.1.2).

Discrimination of positive and negative cells was performed with competition assays. This assay enables the assignment of specific (protein of interest based) and unspecific (background or cross reactivity based) signals to complex distributions (compare Fig. 4.1.3.1). The competitive approach is

also valid under changed fluorescence distribution as shown with fixative changes in the immune cytochemistry protocols (Fig. 4.1.6.1). Cellular studies handling with protein expression levels have to take into account that each cell type of the studied system (e.g. high or low protein expressing) is represented according to its physiological appearance. This finding requires for a quantitative study, as shown for the TRPV1 positive population in DRG neurons, a minimal sample size of 560 cells for a single experiment or around 3 times a hundred cells for multiple replicates (compare Fig. 4.1.5.1).

Taken together the field of cellular nociceptor research has a need for quantitative techniques. These techniques revealed a high grade of heterogeneity for TRPV1 and other nociceptive subpopulations. But, what is the impact of this heterogeneity? What is the physiological outcome of these heterogeneous systems? Is the differential expression directly linked to the nociceptors functionality? Thus, in case of TRPV1 depicts an enhanced expression a stronger response? To proof this, the following chapters 4.2-4.4 will focus on the capsaicin sensitivity of the TRPV1 expressing neurons.

4.2 The capsaicin sensitivity of DRG neurons

As described in the first chapter (4.1) of this results part, is the protein expression of nociceptive markers highly heterogeneous in DRG neurons. I hypothesized that this heterogeneity shall result in an inhomogeneous functionality of individual TRPV1 expressing neurons. Thus, the aim of the following part is to unroll the capsaicin sensitivity in all sensory neurons. The evaluation of the capsaicin sensitive subpopulation will focus on the percentage of responsive neurons as well as the quantities of individual neuronal calcium responses.

4.2.1 High throughput calcium imaging

It is necessary to measure more than 500 sensory neurons to ensure the full coverage of a heterogeneous feature as protein expression levels. To compare my expression results with a functional read out a large scale calcium imaging set up was developed and shall be introduced within this first subchapter. To perform quantitative live cell imaging experiments, cells were seeded into 384-well plates. Using the Cellomics ArrayScan VTI platform, I handled a system were a drug once applied stayed on top of the cells. Thus, I failed to show transient responses but was able to describe a close to physiology setting. For example, a substance rests "*in vivo"* until its degradation or dilution throughout the normal tissue turnover (Kessler et al., 1992, Nathan, 2002).

The following figure illustrates the typical outcome of a single view field. The stimuli applied to the DRG neurons are media to control for mechano-responsive cells, capsaicin as TRPV1-activator and finally potassium (30 mM KCl) to ensure for neurons vitality. The figure illustrates the behavior of seven marked and traced cells during a typical experimental protocol.

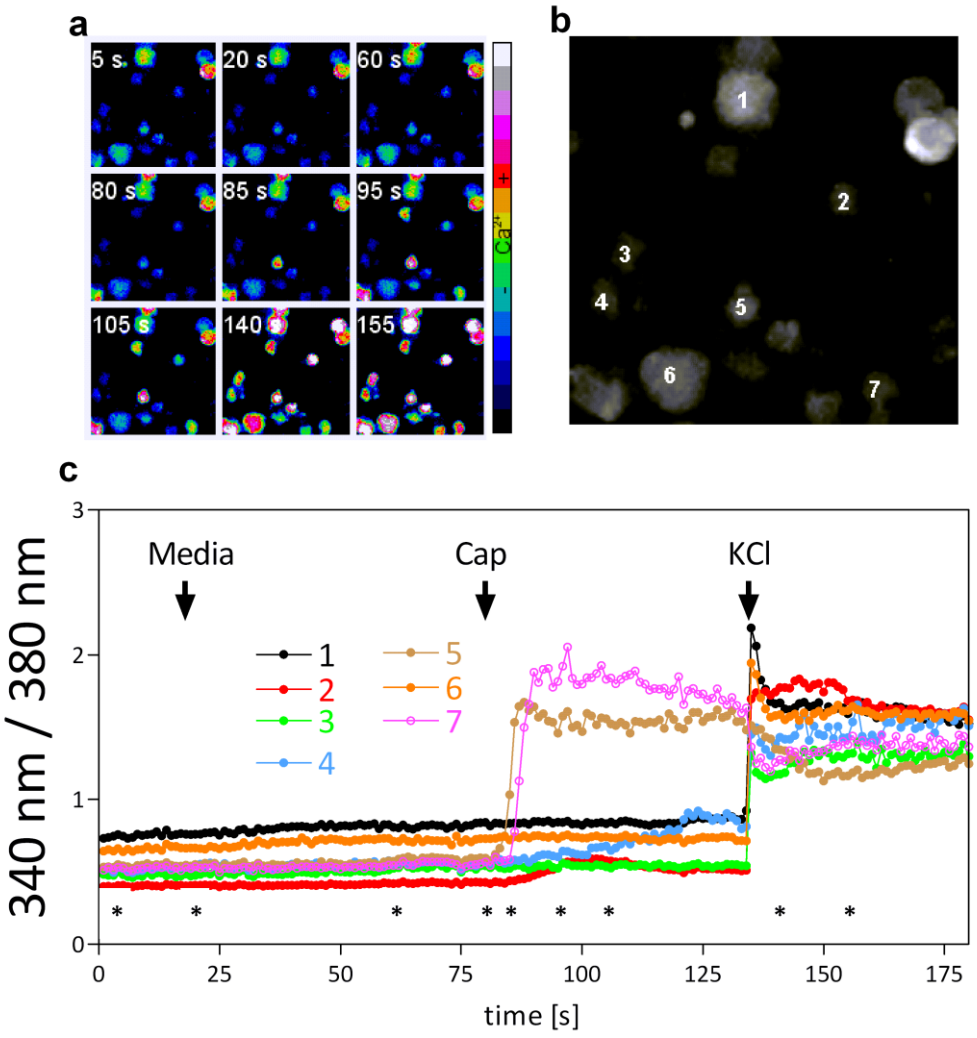

Figure 4.2.1.1 Capsaicin calcium imaging on primary DRG neurons (a) FURA-2-AM ratio images of rat DRG-neurons captured at different time points (compare * in (c)). The panel illustrates the relative calcium amounts (see color scale bar at the right). Media, 250 nM capsaicin and 30 mM KCl were applied in this order at time points 15 s, 75 s and 135 s. **(b)** Gray scale image of the exemplary view field. Seven neurons are marked with numbers, which are traced in the next panel. **(c)** Calcium traces of 7 sensory neurons. The black arrows indicate time points of stimuli application. None of the neurons shows a response towards media, 4 out of 7 neurons responded towards 250 nM capsaicin, all neurons showed enhanced calcium levels upon 30 mM KCl.

The figure shows an exemplary view field cut out of cultured primary DRG-neurons. The panel 4.2.1.1a illustrates color coded cellular calcium levels, panel 4.2.1.1c shows calcium changes of the

seven in panel 4.2.1.1b marked neurons. None of the seven followed calcium traces showed a response upon media treatment, while all cells showed an enhanced calcium level after high potassium (30 mM KCl). A total of four out of seven neurons reacted upon 250 nM capsaicin treatment while two (4.2.1.1b, cell 5 + 7) react strong and two showed a mild response (4.2.1.1b, cell 2 + 4). This simple experiment indicated three different types of reaction none, small, and strong capsaicin responses.

4.2.2 Quantitative calcium imaging obliges automated data processing

For the achievement of the required sample size of about 100 neurons per condition and replicate, I established processing pipelines which enabled the parallel quantification of 50-200 neurons. The preparation of one rat delivered under optimal conditions around 30.000 sensory neurons. Those neurons were scattered into 32 wells on four 384-well plates (4 times 8 wells) to obtain a density of roughly 800-1000 neurons per well in an 80 µl volume.

Usually a live cell experiment performed on the HCS platform had at least three protocols (stimulus 1, 2, and 3) per well. Typically each protocol consisted of 60 single frames with a temporal distance of 1 or 4 seconds, each frame included two images one excited at 340 nm another at 380 nm. Thereby, at least 11520 images (32 wells x 3 protocols x 60 frames x 2 images) were captured per experimental day. To handle these huge data sets I developed automated image analysis pipelines. Accordingly, the established working routine automatically imported image data sets of single wells, identified regions of interest (cells), analyzed the fluorescence intensities (FURA-2-AM signal), and stored the generated data-files and masks. This whole procedure shall be illustrated in the following figure.

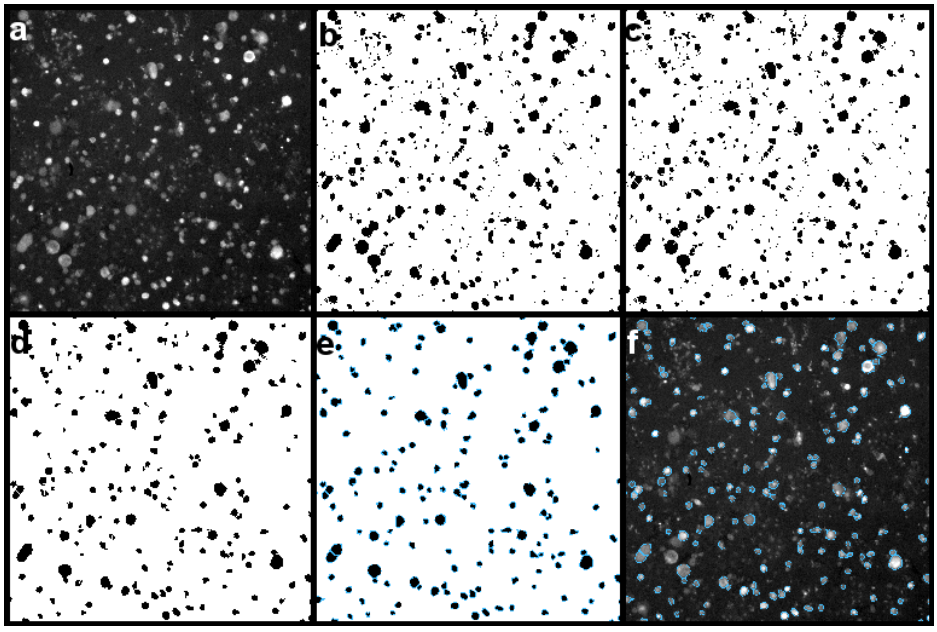

Figure 4.2.1.2 Automated cell identification for large scale live cell imaging (a) Ratio image of rat dorsal root ganglia neurons. **(b)** A Li-algorithm assigns each pixel as positive (black) or zero value (white) and reconstituted a binary image. **(c)** The binary image is segmented using a watershed algorithm. **(d)** Incomplete, too small, or wrong shaped objects are removed from the image. **(e)** Objects matching the size of 150 - 4000 μm^2 and circularity between 0.5-1 are identified and marked as "Region of Interest" (masks, displayed with blue borders). **(f)** The regions of interest are applied to the initial images and used to quantify the fluorescence signals.

Briefly the figure illustrates an object recognition method based on fluorescence signals. To identity an object, ratio images after the final stimulus are used to ensure maximal image contrasts. To these images a Li-algorithm is applied which discriminates each pixel as positive (black) or negative (white) value, followed by watershed algorithms to segment close by objects. Too small or misshaped objects are removed while those matching the identification parameters circularity of 0.5-1 and an area in between 150 μm^2- 4000 μm^2 were defined as neurons. The so generated "Region of interest" are marked with borders and stored for later (re-)analysis.

4.2.3 Large scale calcium imaging in DRG neurons

Most of the functional TRPV1 studies conducted so far used set ups which displace the measuring system from the natural physiological TRPV1 appearance. One major difference, to the here conducted experiments is the use of transfected cell lines instead of primary neurons. While the feasibility of such system is much easier, the physiological relevance remains questionable (Puntambekar et al., 2004, Neelands et al., 2005, Lizanecz et al., 2006, Veldhuis et al., 2012). The central aim behind this experimental series was to figure out if the capsaicin sensitivity of DRG neurons can be related to the heterogeneous appearance of TRPV1. To unroll the capsaicin sensitivity in a natural environment and display cellular responses in their complete spectrum, a large scale calcium imaging set up was used. Furthermore, this first experimental series aimed to quantify the number of false positive (mechano sensitive) and false negative (dead or depolarized neurons) calcium responses.

The established set up enabled quantitative and functional live cell imaging in between 50-200 primary neurons per individual measurement, at physiological 37 °C, a pH in between 7.3-7.4, in a complete supplemented media (compare method section 3.2.3.3). For each individual neuron a complete calcium time trace was calculated and plotted in a graph of relative calcium changes signal (340 nm / 380 nm) over time. Trace irregularities as missing time points, under-, or overexposed images, were excluded by an experimenter control.

The following graph presents pooled data from 18 wells and 6 independent animals. In the graph displayed are the mechano-sensitivity and vitality of cultured primary dorsal root ganglia neurons.

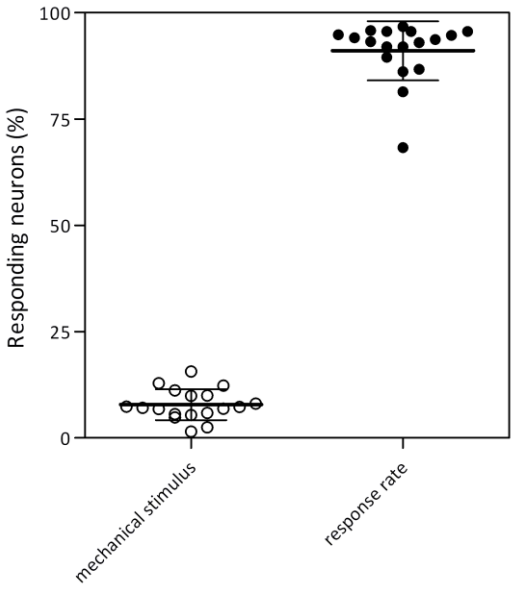

Figure 4.2.2.1 8 % of cultured DRG neurons are mechano sensitive The graph shows the number of mechano-responsive (media stimulus) neurons with a mean of 7.8 ± 3.6 %. The overall response rate is 91.0 ± 7.0 % neurons responding to any stimulus. Wells showing less than 80 % responding cells were excluded from the analysis. The shown data is pooled from 18 wells out of 6 independent animals.

Wells or single measurements showing a cell response rate lower than 80 % towards any stimulus (including 30 mM KCl) were excluded from the later analysis. Neurons responding with a calcium elevation after media stimuli were declared as mechano-sensitive and excluded in order to eliminate false positive capsaicin responses. In total, 7.8 ± 3.6 % neurons showed calcium responses towards mechanical stimulation. This is, to my best knowledge, the first reported quantification of calcium responses in cultured DRG neurons after a mechanical stimulus (media). An average of 91.0 ± 7.0 of all identified objects showed responses to any stimulus. A finding that demonstrates that the here used culture system contained about 9 % of depolarized or dead objects per well. Those unresponsive neurons were excluded from the subsequent analysis to eliminate false negative responses. The remaining traces were used to study the capsaicin induced calcium responses. The following figure of capsaicin dose response experiments presents an overview on the experimental outcome after eliminating false positive and negative results.

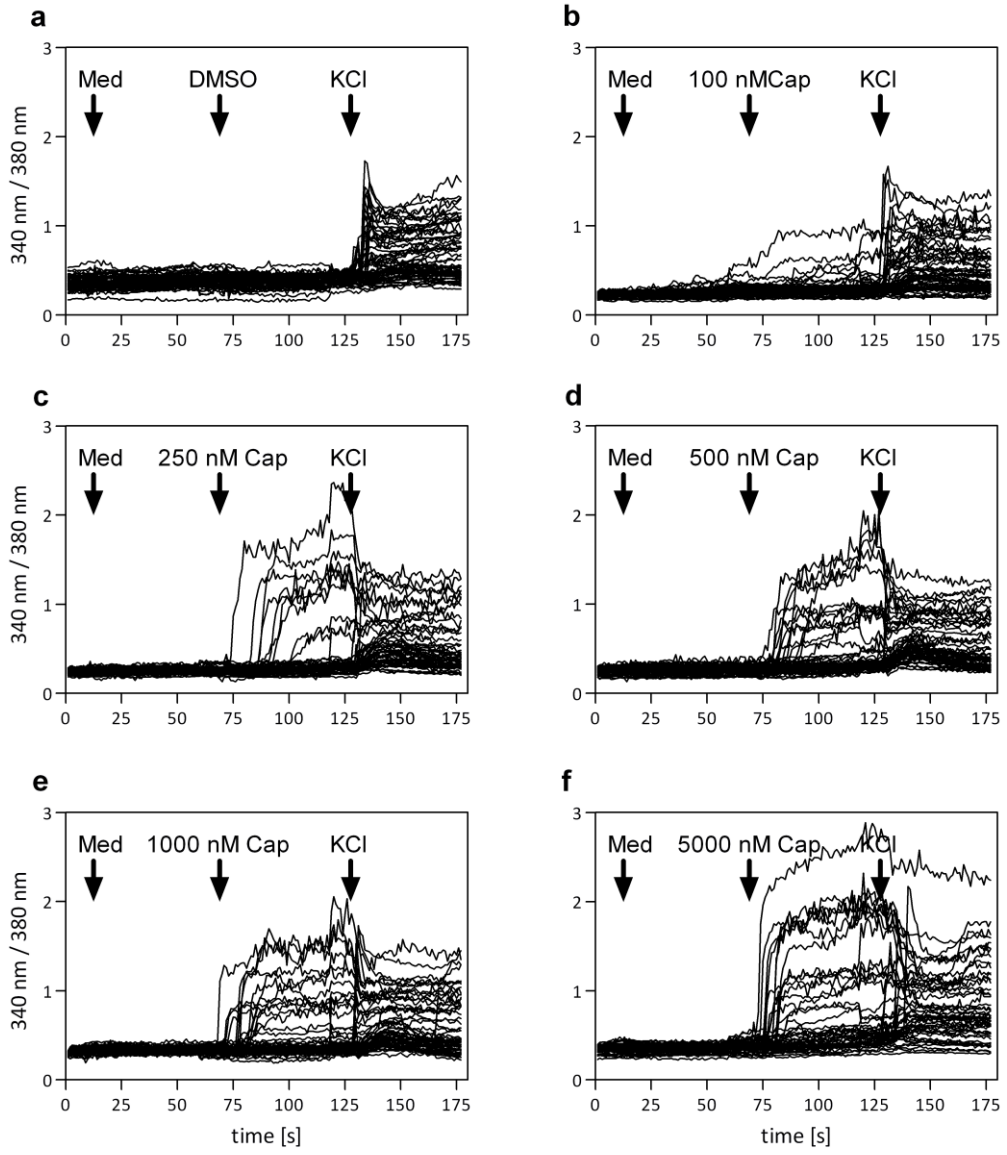

Figure 4.2.3.2 Calcium responses after capsaicin stimulation Shown for each condition (f.c. 0-5000 nM capsaicin) are 50 random calcium traces from rat DRG neurons. **(a)** Treatment with 5 µl media, 0.2 % DMSO (solvent control), and 30 mM KCL. **(b)** Treatment with media, 100 nM cap in 0.2 % DMSO/media, and 30 mM KCL/media.**(c)** Treatment with media, 250 nM cap in 0.2 % DMSO/media, and 30 mM KCL/media. **(d)** Treatment with media, 500 nM cap in 0.2 % DMSO/media, and 30 mM KCL/media. **(e)** Treatment with media, 1000 nM cap in 0.2 % DMSO/media, and 30 mM KCL/media. **(f)** Treatment with media, 5000 nM cap in 0.2 % DMSO/media, and 30 mM KCL/media. Data in each data set is randomly depicted from a total of 6 rats.

Analyzing 2786 sensory neurons from 6 independent rats, capsaicin responses of cultured primary DRG neurons were identified as highly variable (4.2.3.2b-f). The capsaicin treated neurons show broad differences in the number of responding cells as well as the amplitude and response time (4.2.3.1b-f). The change of intercellular calcium concentrations (relative $\Delta[Ca^{2+}]_I$) was calculated by

subtracting baseline values from those 10 s after capsaicin application. The obtained results represent the relative calcium changes and an overview on the heterogeneous response amplitudes.

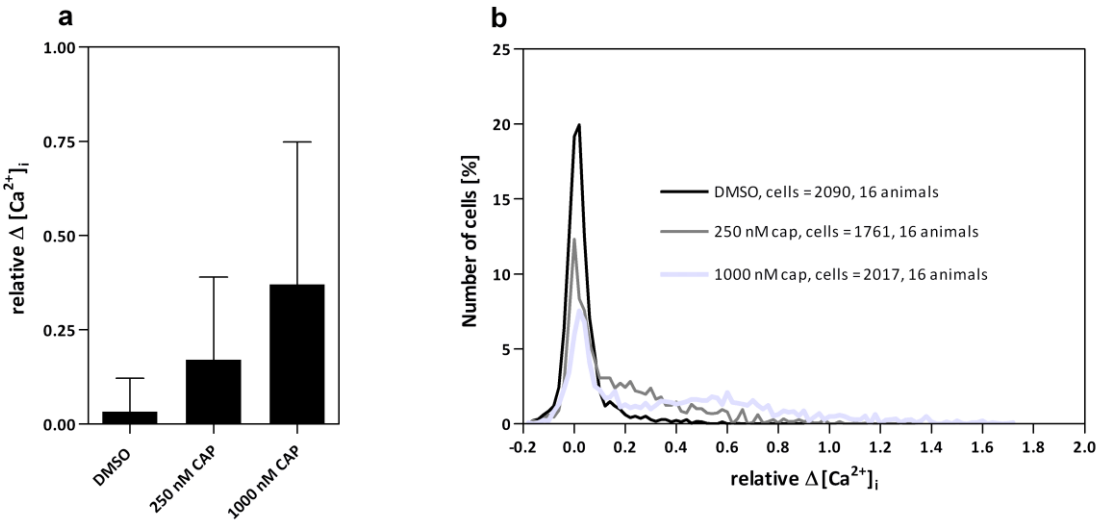

Figure 4.2.3.3 Heterogeneous capsaicin responses in DRG neurons (a) The graph shows the averaged relative $\Delta[Ca^{2+}]_i$ values and standard deviation after 0.2 % DMSO, 250 nM cap, and 1000 nM cap treatments. **(b)** Both capsaicin treated conditions show long shoulders, while 1000 nM (light grey) indicates already a second peak. The shown data is pooled from a total of 16 rats and 5868 primary sensory neurons.

The bars of averaged calcium responses in Fig. 4.2.3.3a show the expected pattern of increasing means with higher capsaicin concentration. Meanwhile, the standard deviation hints towards a higher diversity behind the mean, which is presented in the calcium response distribution in 4.2.3.3b. The capsaicin responses show a broad distribution of calcium responses upon capsaicin treatments. A finding, in line and expected with the data generated in immune fluorescence experiments (compare 4.1.1.2d). Both distributions for capsaicin responses and protein expression (see chapter 4.1.1) supported the hypothesis where the TRPV1 expression defines the cellular capsaicin sensitivity.

In the following section, the results obtained from primary neurons shall be compared with commonly used cell systems. Therefore, I seeded 2000 cells per 384-well let them distress overnight and performed Lipofectamine transfection with a native rat TRPV1 DNA construct (namely pcDNA3.1-TRPV1 full length). The transfected HEK and F11 cells were stimulated with capsaicin concentrations of 1 nM, 10 nM, 100 nM, 250 nM and 1000 nM. To ensure the cell viability I applied 10 µM ionomycin.

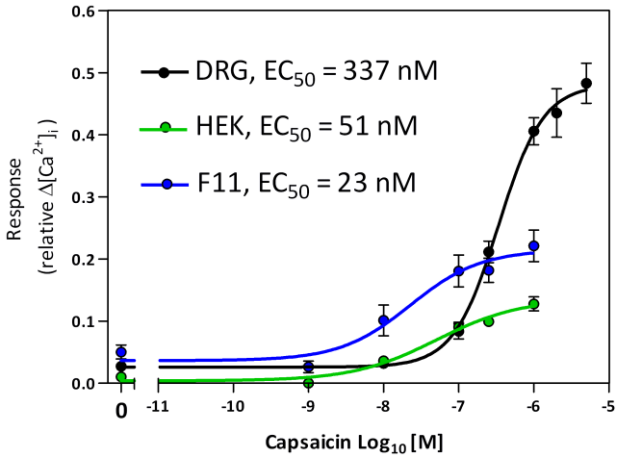

Figure 4.2.3.4 Capsaicin dose response curves of DRG neurons, HEK, and F11 cells The illustrated data summarizes the averaged changes in intracellular calcium levels (relative $\Delta[Ca^{2+}]_i$), 10 s after capsaicin application. All three compared cell systems show typical sigmoid dose response behaviors. Apparently, DRG neurons exhibit the strongest calcium responses, followed by F11 and HEK cells. The capsaicin-EC_{50} of DRG neurons is with 337 nM 6.6 times higher than in HEK-cells, and 14.7 times higher than in F11 cells. The data is pooled from independent experiments, respectively 2786 DRG neurons from 6 rats; 1390 HEK cells from 5 transfections; and 1117 F11 cell from 3 transfections.

Cells receiving only the lipofectamine reagent without DNA constructs, showed no capsaicin induced response, indicating no functional TRPV1 presence (data not shown here). The capsaicin response of DRG neurons showed larger calcium amplitudes, than HEK and F11 cells, while the extra cellular free calcium concentration was with 1.8 mM identical in all systems. Furthermore, with 337 nM the EC_{50} in neurons was about 6.6 times higher than in HEK (51 nM) and 14.7 times higher than F11 cell (23 nM). The calculated capsaicin EC_{50} of 336 nM in DRG neurons are in line with other studies (244 nM (Studer and McNaughton, 2010) to 390 nM (Kim et al., 2006)). Averaging the response of thousands of neurons or transfected cells resulted in all three systems in typical sigmoid dose response behaviors. While the results showed the expected performance, averaging individual cells offers the drawback, that individual cell responses are masked. Beyond the typical dose response trend (in figure 4.2.3.4) are many different cells showing diverse responses as visible in the figures 4.2.3.2 and 4.2.3.3. The viewer neither knows whether cells react stronger or faster nor can he identify if the number of responsive cells is changed. To fill this gap and to extract characteristic information from neuronal responses a novel method became obligate.

4.2.4 Ramp fitting of calcium response reveal kinetic parameters

The above introduced analysis using the $\Delta[Ca^{2+}]_I$ quantifies the calcium response concerning a single time point and reduces the calcium trace to a single number. To unmask the heterogeneity and extract kinetic parameter of large cohorts of calcium responses a novel analysis approach was necessary. I started collaborating with Professor Steffen Waldherr (Uni Magdeburg), to establish a novel tool to extract kinetic cell response features. The tool fits an idealized trace to the measured calcium trace and extracts specific kinetics for each calcium response in the following order. The ideal calcium trace is flat at the beginning, corresponding to the baseline (given as B). From this baseline the trace describes a ramp to the next static level with the maximal calcium per cell (plateau). The time to reach this plateau is defined as the response time (given as T_r). The difference between the baseline and static plateau is defined as the response amplitude (given as R).

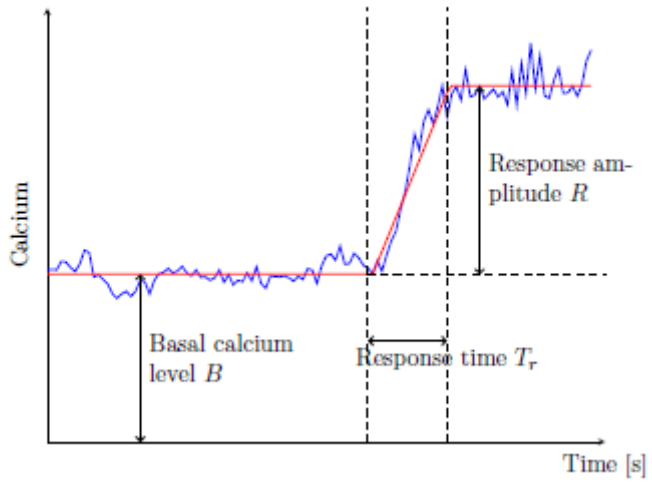

Figure 4.2.4.1 Ramp fitting for calcium traces In the illustration shown is a typical calcium trace of DRG neurons (blue line) and fitted response (red line).

Mathematically the curve is given by the following formula.

$$y_{ramp}(t) = \begin{cases} B, & t < T_s \\ B + \frac{R}{T_r}(t - T_s), & T_s \leq t \leq T_s + T_r \\ B + R, & t > T_s + T_r \end{cases} \qquad \textbf{[Formula 1]}$$

Where B is the basal calcium level under not stimulated conditions, t is the general time, T_s the time point when the stimulus (here capsaicin) is applied, T_r is the response time after a stimulus is applied,

and R stands for the response amplitude. To determine the parameters from real data, a least square optimization problem is solved as illustrated in the following formula.

$$B, T_r, R = argmin_{B,T_r,R} \int_0^{T_{end}} (y_{meas}(t) - y_{ramp}(t))^2 dt \qquad \textbf{[Formula 2]}$$

In this optimization paradigm the basal calcium levels are determined by averaging the relative calcium value from time 0 to T_s (stimulus application). The parameters T_r and R were computed via the optimize.leastsq function from Python "scypy" package.

Using the newly established ramp fitting method, the capsaicin dose response data for DRG neurons were reanalyzed. This time, the analysis focused on response amplitudes, -time, and the number of responding cells.

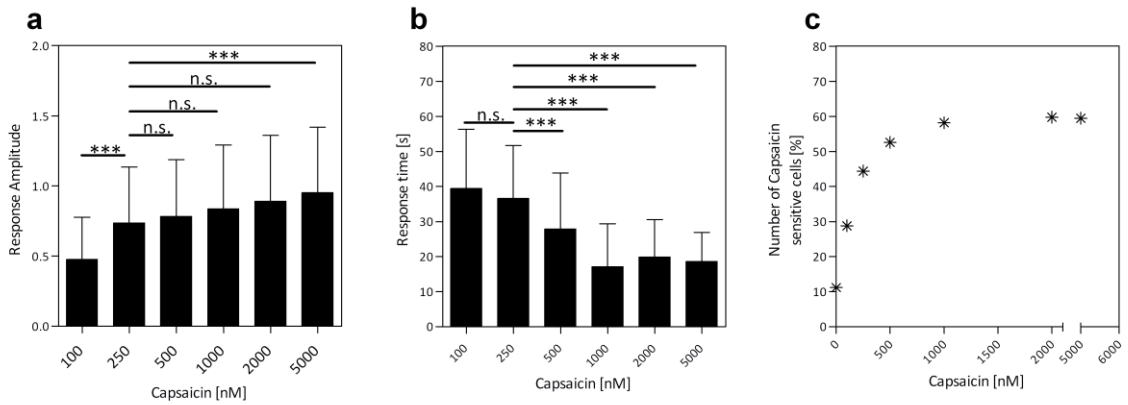

Figure 4.2.4.2 Capsaicin response kinetics in primary DRG neurons (a) Calcium response amplitudes after capsaicin stimulation in DRG neurons. Shown are the averaged responses of capsaicin sensitive neurons. The averaged calcium responses differ at 250 nM capsaicin only between 100 nM and 5000 nM (both $p > 0.001$). There is no significant ($p > 0.05$) difference between 250 nM and higher concentrations. **(b)** Shows the averaged response times [s] of capsaicin sensitive neurons. In contrast to the response amplitudes, show only high capsaicin concentration (500 nM and higher) significant changes from 250 nM. **(c)** Number of capsaicin sensitive neurons upon capsaicin dose response experiments. The number of capsaicin sensitive cells increases with the capsaicin concentration. The analyzed data is pooled from six independent rats with a total of 2786 DRG neurons.

The number of capsaicin sensitive cells increases with the capsaicin concentration (Fig. 4.2.5c), while the portion TRPV1 expressing neurons should be identical in all measurements. The finding indicates that low capsaicin concentrations show a significant number of neurons insensitive towards

capsaicin. In contrast the maximal capsaicin concentration (5000 nM) shows with 58.2 % of capsaicin sensitive neurons a number in the range of TRPV1 expressing neurons as quantified in section 4.1. While expecting that lower capsaicin concentrations result in lowered amplitudes, already half maximal capsaicin concentration (250 nM) shows no significant difference ($p > 0.05$) to higher concentrations (1000 nM and higher, Fig. 4.2.5a). Controversially decreases the response time with increasing concentration. Therein, only concentration between 500 nM – 5000 nM showed significant ($p < 0.001$) response differences (Fig. 4.2.5 b). The here introduced ramp fitting, revealed novel features of the capsaicin response kinetics in DRG neurons as the quantification of response time and the similarities in overall response amplitudes.

4.2.5 Sensitization enhance the number of capsaicin sensitive neurons and response amplitudes

In the dose response experiments silent, capsaicin insensitive DRG-neurons are activated under high capsaicin concentration. It was shown that each TRPV1 expressing neuron is able to respond if the capsaicin concentration is high enough. Therefore, the cellular explanation for this silencing mechanism is probably not based on expression levels but the TRPV1 activatability. This in turn is regulated within the cellular sensitization state (see introduction part 2.7). Hence, the following experiments aimed to proof if sensitization over distinct regulatory pathways can modulate the number of capsaicin sensitive cells. For sensitization DRG-neurons were pretreated with Phorbol 12-myristate 13-acetate (following PMA) (Zhou et al., 2001). PMA is able to resensitize cells, a process which recovers the desensitization and furthermore sensitizes a neuron (Mandadi et al., 2006). To reproduce this result I conducted in collaboration with Marian Brackmann (Charite Berlin), calcium imaging experiments in a flow chamber to ensure transient stimuli. The aim was to desensitize DRG-neurons by repeated pulses of capsaicin, and test if PMA restores the capsaicin sensitivity in the used culture system.

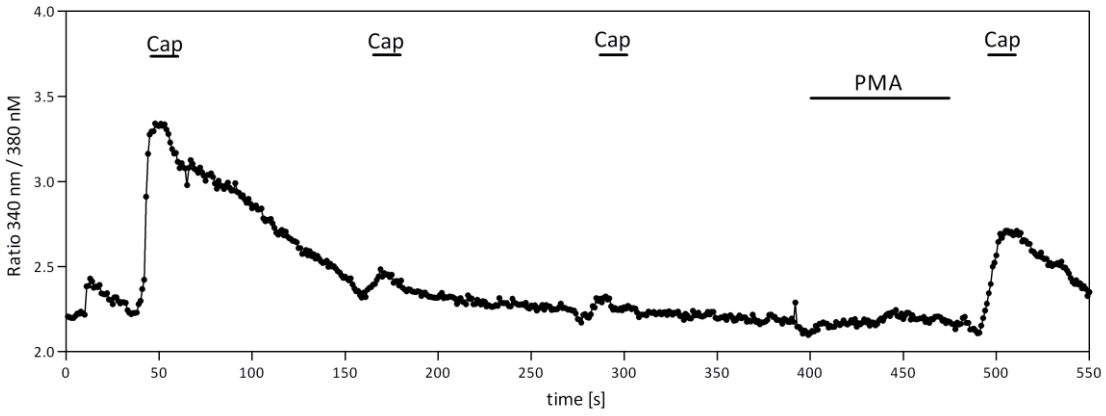

Figure 4.2.5.1 PMA restores the capsaicin sensitivity in DRG neurons The graph shows a representative calcium trace of a single rat DRG neuron loaded with FURA-2-AM. Capsaicin pulses were applied for 10 s with a final concentration of 250 nM capsaicin. After the first pulse (at 40 s) a peak is visible which sustains for around 120 s until a baseline is reached again. The second and third pulses (at 160 s and 240 s) generate smaller calcium amplitudes which return after 20 s to the baseline. The lowered calcium response is recovered in the fourth capsaicin pulse after application of 100 nM PMA (at time point 400).

Figure 4.2.5.1 shows a rat DRG neuron with a strong calcium peak after a 250 nM capsaicin pulse. The following pulses (at 160 s and 280 s) show reduced calcium amplitudes. This phenomenon is the cellular equivalent of tachyplaxie, the adaptation of a system towards a stimulus. After stimulation with 100 nM PMA the capsaicin induced calcium response recovers. Thereby, the experiment shows the ability of PMA to resensitize neurons. To quantify the impact of desensitization I went back to the HCS platform ArrayScan VTI.

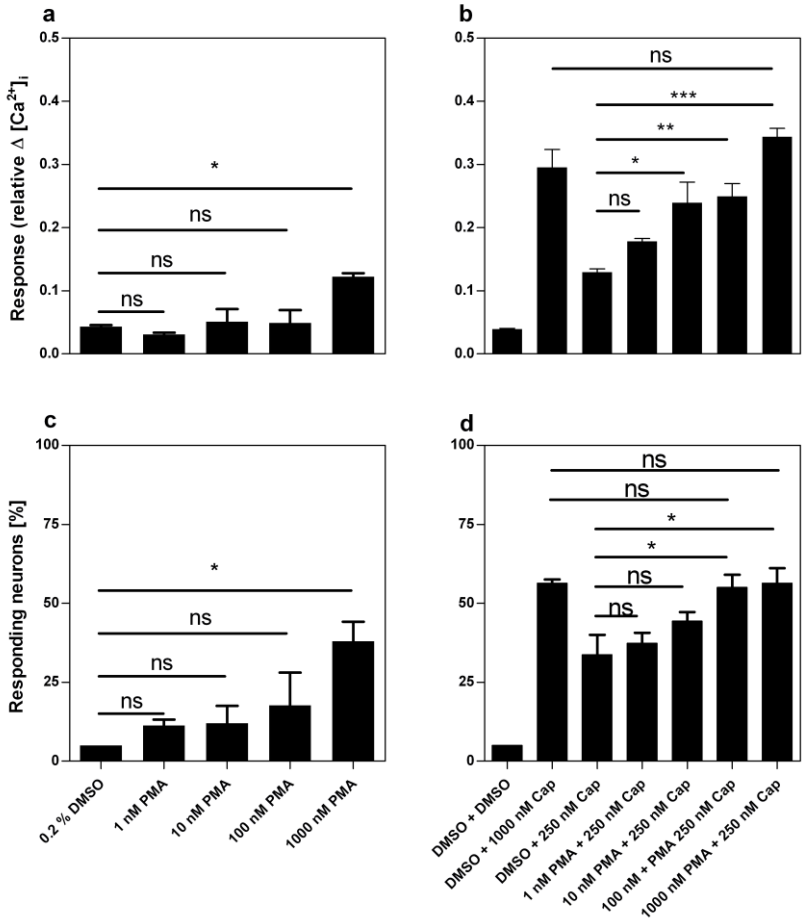

Figure 4.2.5.2 PMA restores the number of capsaicin sensitive DRG neurons (a) Shows the calcium response of DMSO and different PMA concentrations (dose response). Only 1000 nM PMA shows a significant enhancement in the calcium response. **(b)** Calcium responses upon differential PMA application followed by a stimulus of 250 nM capsaicin. Significant changes are visible in the 10 nM – 1000 nM capsaicin condition. The

100 nM and 1000 nM PMA pretreated samples differ not significantly from those achieved by 1000 nM capsaicin without pretreatment. **(c)** The panel indicates the portion of cells responding with a calcium influx after PMA treatments. The 1000 nM PMA condition shows a significant increase in the number of calcium responses from 5 % (DMSO treatment) to 38 % (for 1000 nM PMA). **(d)** The panel shows the number of capsaicin responsive neurons after PMA treatments. Again pretreatment with PMA concentration of 100 nM and 1000 nM showed significant distinctions from the 250 nM capsaicin ($p < 0.05$) and similarities to 1000 nM capsaicin ($p > 0.05$). The data is plotted as mean plus standard error of three rats and 9 replicates per condition with a total of 1965 neurons.

The PMA dose response experiments show the ability of the PKC activator to restore the capsaicin sensitivity in DRG neurons. After 100 nM and 1000 nM PMA priory to capsaicin the number of responding cells is comparable to high doses of capsaicin (compare Fig. 4.2.6.2d). Furthermore, induce high PMA concentrations (from 1000 nM) a calcium response by itself (Fig. 4.2.6.2a). The PMA could cause a shift of the TRPV1 (and other channels) open probability and a subsequent calcium influx (compare introduction part 2.7.3). Taken together, restored the sensitization with PMA the expected number of capsaicin sensitive cells and thereby showed a signaling dependency of the silencing mechanism.

Within this experimental set I was able to show that the discrepancy of capsaicin sensitive neurons in low and high capsaicin doses, as observed in chapter 4.2.5, is based on the different cell sensitization states. A change in this state restores the number of responding cells to comparable ranges as achieved with high doses of capsaicin.

4.2.6 Summary Part 2: Quantitative approaches give novel insights to cellular functionalities

I conducted a quantitative population analysis of primary DRG neurons and cell lines. Analyzing dose response curves of DRG neurons and two cell lines, I found typical sigmoid shapes for all investigated cell systems. The calculated EC_{50} was with 336 nM for DRG neurons comparable to former results by other groups (Kim et al., 2006, Studer and McNaughton, 2010). Mentionable here is that the calcium responses in DRG are higher than in two cell lines (HEK and F11 cells). Also capsaicin evoked calcium responses in DRG neurons showed a broad distribution (Fig. 4.2.3.3).

For in depth population analysis the existing data analysis tools were expended with a ramp fitting algorithm that extracts kinetic parameters from individual calcium traces. Within this approach I found that the response time decreases with increasing capsaicin concentrations. Upon application of high doses capsaicin (1000-5000 nM) the maximal cellular calcium levels were reached after 17.1 – 19.9 s. The calcium response amplitude of capsaicin sensitive cells shows no significant

enhancement from 250 nM capsaicin and higher concentration. While the number of capsaicin responding cells dropped down at low concentrations, indicating TRPV1(+) neurons to stay insensitive against capsaicin. The introduction of the pharmacological sensitizer PMA restored the number of capsaicin sensitive cells, indicating cellular sensitization states as potential silencing mechanism (Fig. 4.2.5). As further results, it was possible to quantify the number of mechano-sensitive cultured DRG neurons to 7.8 %.

But again, a striking heterogeneity in the capsaicin response distribution was found (Fig. 4.2.3.3). If the heterogeneous TRPV1 expression is reasonable remains open and required a direct experiment analyzing both parameters in a single cell. Therefore, a new technical approach became obligate which enables the investigation of protein contents and functionalities in the very same cell. This approach and its outcome shall be the focus of the following chapter 4.3.

4.3 Relation between TRPV1 expression and cellular capsaicin sensitivity

Observing two times broad distribution concerning the functionality and appearance of TRPV1 (Fig. 4.1.1.2d and Fig. 4.2.3.3b), I hypothesized, that the differential TRPV1 expression levels would explain the response heterogeneity. I established techniques, which monitor the protein expression and cellular calcium responses in the very same cell. To judge the outcome of this experimental approach, spearmans correlation coefficient was used. This test delivers a correlation coefficient ρ (rho) which represents the correlation grade, ranging from – 1 (perfect negative correlation), over 0 (no correlation), to + 1 (perfect positive correlation). The advantage of Spearmans correlations test is a rank based correlative testing which offer the opportunity, to be free of inter-experimental signal variations and thereby data manipulation as normalization procedures.

4.3.1 Analyzing protein contents and functionalities in single cells

To circumvent the impact of fluorescence tags as GFP or RFP on the channels functionality, I performed a two stepped experiment. In a first step, neurons were seeded in 384-well plates followed by calcium imaging, subsequent formaldehyde fixation and finally immune cytochemistry protocols. The cultures were imaged twice, first during the live cell imaging process and a second time after immune cytochemistry.

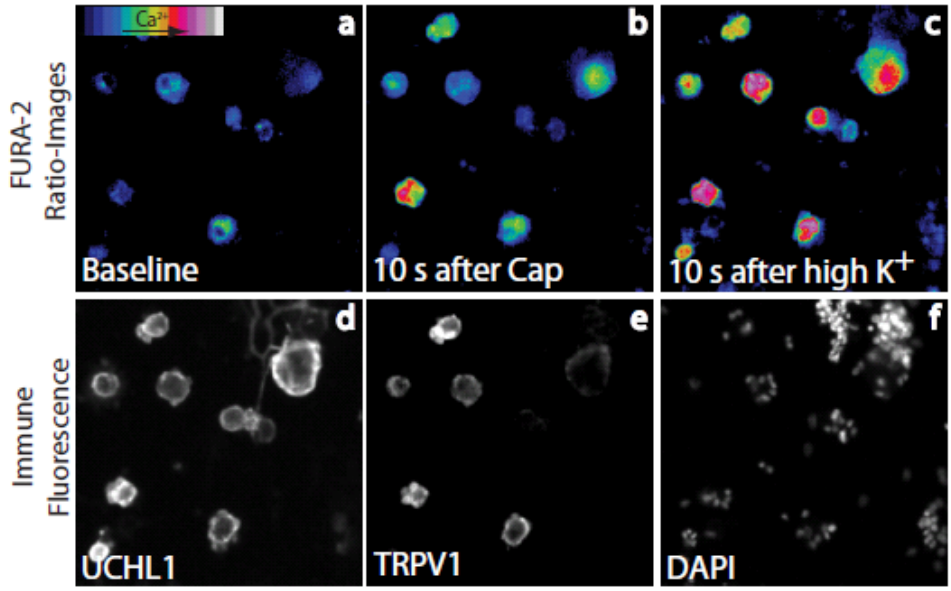

Figure 4.3.1.1 Combination of calcium imaging and immune cytochemistry (a-c) Fura-2-AM ratio images (a) Relative calcium levels (340 nm / 380 nm, upper left scale bar) before stimulus addition (baseline). **(b)** Relative calcium levels, 10 seconds after a 250 nM capsaicin stimulus. A subpopulation of 4 out of 10 neurons show elevated calcium levels. **(c)** Calcium contents 10 s after 30 mM KCl. **(d-f)** F**luorescence images of DRG neurons (d)** UCHL1, as overall neuronal marker identifies neuronal cell bodies. **(e)** Subgroup marker for TRPV1 detects a subgroup of all neurons (6 out of 10). **(f)** Nuclear staining with DAPI indicates the neuronal and glial nuclei (scale bar = 25 µm).

Due to the use of imaging plates and a fixed stage in the ArrayScan VTI platform, the imaged view fields were regained with an accuracy of about 0-7.2 µM in x (vertical) and y (horizontal) position. The resulting gap of non-overlapping images was closed with a self-made image processing pipeline (ImageJ), which adjusted horizontal and vertical aberrations. Image sets were quantified using a customer ImageJ-analysis approach. Briefly, cells were defined according to their shape, circularity and fluorescence signal in the ratio image after potassium chloride (DRG neurons) or ionomycin (cell lines) treatments. The resulting image masks were used to quantify the UCHL1, TRPV1, DAPI, and FURA-2 signals.

4.3.2 TRPV1 expression predicts the capsaicin response in HEK and F11 cells

I aimed to proof the correlative approach in cell lines. Therefore, HEK cells were transfected with pcDNA 3.1 TRPV1 full length constructs followed by calcium imaging and immune cytochemistry protocols. Again, neither the untransfected HEK, nor later F11 cells, showed a calcium response upon

capsaicin application (data not shown here). Also, there was no detectable TRPV1 fluorescence signal in untransfected cells.

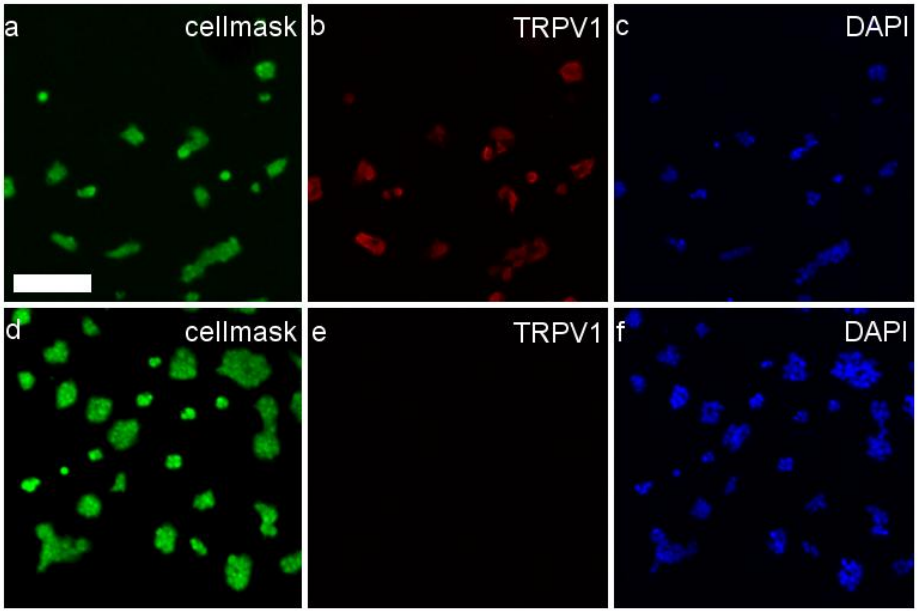

Figure 4.3.2.1 TRPV1 expression in transfected HEK cells (a-c) TRPV1 transfected HEK cells (a) The cell mask dye shows a bright signal in all cells. **(b)** TRPV1 fluorescence is restricted to a portion of all cells, as a result of incomplete transfection efficiency. **(c)** Nuclear staining with DAPI. **(d-f) Control HEK cells (d)** Cell mask dye shows again a bright signal in all cells. **(e)** No detectable TRPV1 signal in the untransfected control. **(f)** DAPI nuclei staining of untransfected HEK cells. Scale bar = 25 µm

The immune fluorescence images show the expected result. A clear TRPV1 signal is found in HEK cells transfected with pcDNA 3.1 TRPV1 full length DNA-constructs and no detectable signal in the untransfected control. For functional experiments, a capsaicin concentration was chosen in the range of the half maximal dose (see chapter 4.2.3, EC_{50} transfected HEK cell = 51 nM).

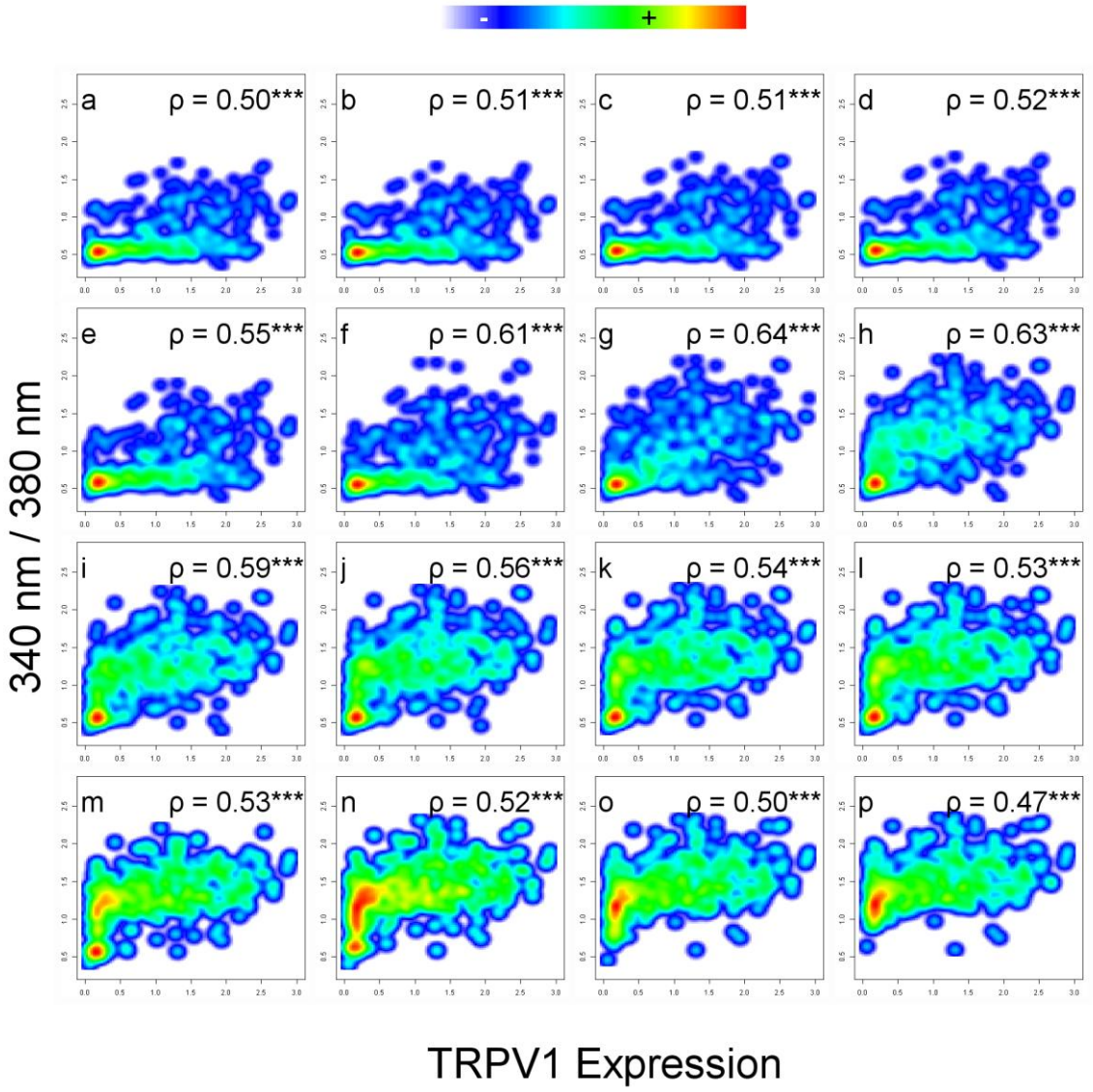

Figure 4.3.2.2 TRPV1 expression predicts the capsaicin response in transfected HEK cells Shown are 2 dimensional cell density plots. The abscissa indicates the relative expression of TRPV1 (fluorescence intensities in au), the ordinate the relative intracellular calcium levels (340 nm / 380 nm). The letter ρ (rho) presents spearmans rank correlation with its significance values (ns - ***). **(a)** Before any stimulus is added, the baseline shows already a good correlation ρ = 0.50 ***. **(b)** The correlation was slightly enhanced after media stimulus ρ = 0.51 ***. **(c)** HEK cells 10 s after media stimulus ρ = 0.51 ***. **(d)** HEK cells 20 s after media stimulus ρ = 0.52 ***. **(e)** The correlation increased during 50 nM capsaicin application to ρ = 0.55 ***. **(f)** 10 s after 50 nM capsaicin the correlation reaches ρ = 0.61 ***. **(g)** The highest correlation was achieved 15 s after 50 nM capsaicin ρ = 0.64 ***. **(h)** The correlation started to decrease 20 s after 50 nM capsaicin with ρ = 0.63 ***. **(i)** Later time points, 25 s after 50 nM capsaicin, the correlation sinks to ρ = 0.59 ***. **(j)** HEK cells 30 s after 50 nM capsaicin ρ = 0.56 ***. **(k)** 40 s after 50 nM capsaicin ρ = 0.54 ***. **(l)** 45 s after 50 nM capsaicin ρ = 0.53 ***. **(m)** 5 s after stimulation with 10 µM ionomycin the correlation declines to baseline values ρ = 0.53 ***. **(n)** 10 s after 10 µM ionomycin stimulus ρ = 0.52 ***. **(o)** HEK cells 15 s after 10 µM ionomycin application ρ = 0.50 ***.

(p) The correlation even underwent baseline condition 20 s after ionomycin stimulation ρ = 0.47 ***. The data shown here was generated from 2 representative experiments with a total of 8 replicates and 781 cells.

In HEK cells a significant correlation between basal calcium levels and TRPV1 is reached already under baseline conditions (ρ = 0.50, p < 0.0001). This observation is interpreted best with the channel leakiness. Thereby, the expressed single ion channel has a certain open state probability which allows ions to pass passively. (Voets et al., 2004, Nilius et al., 2005, Vriens et al., 2009). After applying media controls, this association remains unchanged with ρ = 0.50 (p < 0.001). After stimulation with 50 nM capsaicin the correlation is enhanced with ρ = 0.61 (p < 0.0001). After stimulation with 50 nM capsaicin, the density plots in figure 4.3.2.2h-m show a hyperbolic shape. Accordingly, cells on the left-hand side with a low or no TRPV1 expression level show low calcium levels, meanwhile the right hand side show high TRPV1 levels and elevated calcium levels. After stimulation with 10 µM ionomycin the correlation remains significantly high in between ρ = 0.47 and ρ = 0.53 (with p < 0.0001). The hyperbolic shape was diminished, since none or low TRPV1 expressing cells now react with ion influxes.

To proof the assay in a second system and approximate a neuronal environment, I performed the correlation assay in the neurons derived F11 cell line (see chapter 3.1.2.4).

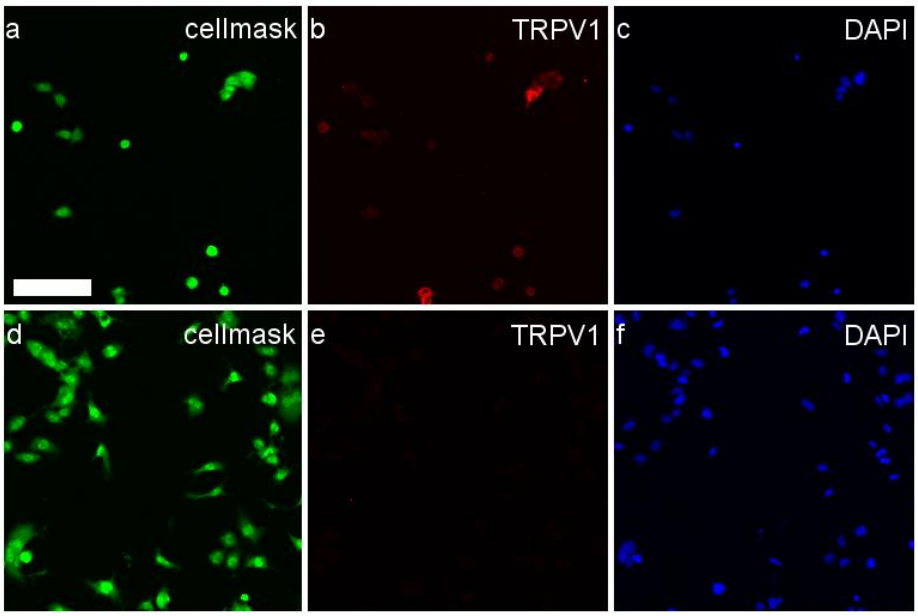

Figure 4.3.2.3 TRPV1 expression in transfected F11 cells (a-c) TRPV1 transfected F11 cells (a) The Cell mask dye shows a clear signal in all cells. **(b)** TRPV1 signal is in almost all cells visible with differential intensities. **(c)** Nuclear staining with DAPI. **(d-f) Control F11 cells (d)** The cell mask dye shows a bride signal. **(e)** No obvious TRPV1 signal is found in the untransfected control. **(f)** Nuclear staining with DAPI. Scale bar = 25 µm

The TRPV1 fluorescence signals are detectable only in transfected F11 cells. This shows that TRPV1 is not expressed endogenously in F11 cells. After transfection with rat pcDNA 3.1 TRPV1 constructs I found a strong signal, indicating the specificity of the antibody and the working transfection. The chosen capsaicin concentration for the correlation experiment was with 20 nM in the range of the half maximal dose (EC_{50} = 23 nM, see 4.2.3.4).

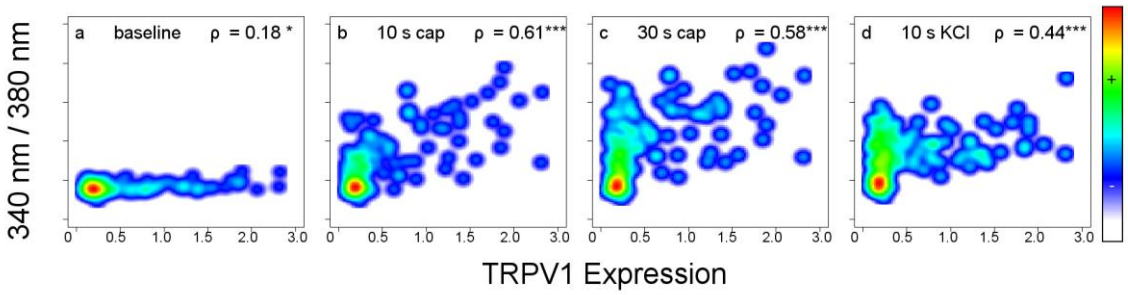

Figure 4.3.2.4 TRPV1 expression predicts the capsaicin response in transfected F11 cells Shown are 2-dimensional density plots, representing the expressed TRPV1 protein and relative calcium levels (340 nm / 380 nm) at a given time point. **(a)** Before any stimulus is applied, the correlation between TRPV1 and calcium is lower compared to HEK cells with ρ = 0.18 *. **(b)** The second panel shows the F11 cells 10 s after 20 nM capsaicin treatment with a high correlation of ρ = 0.61 ***. **(c)** 30 s after 20 nM capsaicin the correlation slightly decreases to ρ = 0.58 ***. **(d)** After ionomycin stimulation the correlation decreases further to ρ = 0.44***. Shown are data sets from 3 independent experiments (transfections), with a total of 9 replicates and 166 cells.

The correlation between basal calcium levels is with ρ = 0.18 ($p < 0.05$) lower compared to HEK cells (ρ = 0.18, $p < 0.05$ see Fig. 4.3.2.2). A finding most probably based on the neuronal characteristics of the F11 cell line and the presence of functional ion pumps. Again the correlation between TRPV1 expression and cellular calcium response is quite high (ρ = 0.61 and ρ = 0.58, both with $p < 0.001$).

Taken together, both tested cell lines show a good correlation between capsaicin stimulation and the expressed TRPV1 protein levels. Thereby, the conducted experiments in HEK and F11 cells technically approved the approach to study the influence of TRPV1 expression on the capsaicin response in primary neurons.

4.3.3 TRPV1 expression in DRG neurons does not predict the capsaicin response

To test the hypothesis that the heterogeneous TRPV1 amounts in DRG neurons could be reasonable for the heterogeneous calcium responses in DRG neuron, the combined calcium imaging and immune fluorescence experiment was performed. The capsaicin concentration used was 250 nM close to the half maximal concentration (DRG neuron capsaicin EC_{50} = 330 nM).

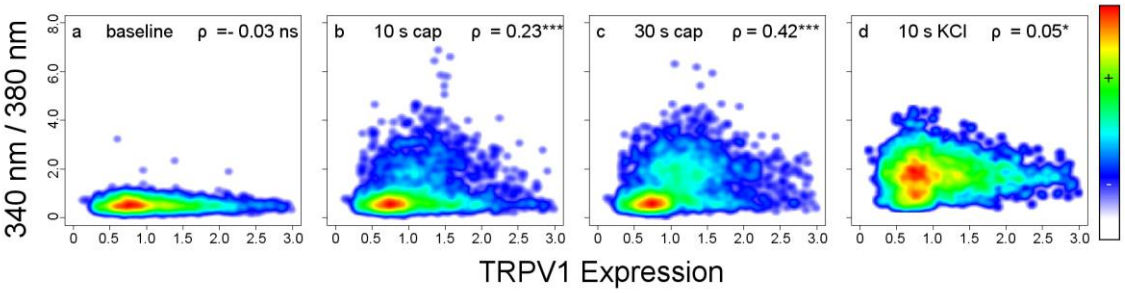

Figure 4.3.3.1 TRPV1 expression fails to predict the capsaicin response in primary DRG neurons (a) Shows no significant dependency between the TRPV1 expression and the basal calcium contents with ρ = -0.03 ns. **(b**) The correlation 10 s after 250 nM capsaicin is enhanced towards a correlation of ρ = 0.23***. Obviously, a portion of TRPV1 expressing neurons are insensitive towards the capsaicin stimulus. **(c)** Shows the correlation with ρ = 0.42*** 30 s after 250 nM capsaicin. While the correlation increases, remains a portion of TRPV1 expressing neurons unresponsive. **(d)** After the final stimulus with 30 mM KCl the correlation brakes down towards ρ = 0.05**. The data shown here is pooled from 6 independent rats with a total of 18 replicates and 3190 primary sensory neurons.

In comparison to HEK and F11 cells show DRG neurons no significant correlation between response and TRPV1 expression under baseline conditions (with ρ = -0.03 not significant, compare to ρ = 0.50*** in HEK-cells and ρ = 0.18 F11-cells). After application of 250 nm capsaicin the correlation slightly increased with ρ = 0.23 ($p < 0.001$). Thirty seconds after a 250 nM stimulus the correlation reached ρ = 0.42 ($p < 0.001$). The number of capsaicin sensitive cells was 41.5 % a total of 1325 neurons of 3190 showed a calcium response towards a 250 nM capsaicin stimulus. Of special interest is the in panel 4.3.3.1b+c shown cell population which expresses TRPV1 and is insensitive towards capsaicin. The total portion of TRPV1 expressing and potential capsaicin sensitive neurons lays around 60 % of all cells (compare 4.1.3.1 and 4.2.4.2), but only 58.5 % of all TRPV1 expressing neurons (1123 out of 1917) responded towards capsaicin. These cells are alive as indicated in the panel 4.3.3.1 d, since potassium induces a calcium response.

The conducted experiments negotiated the hypothesized model and the TRPV1 expression failed to predict the capsaicin induced calcium response in DRG neurons. To ensure a proper experimental

design, I aimed to test if the performed assay has a sufficient sample number to generate statements on the dependencies in between two parameters.

4.3.4 1200 neurons are necessary to quantify two independent parameters

Of central importance is the knowledge on the minimal number of cells to display a combined feature as protein expression and functionality. If the sample number is to low and fails to cover the whole population inconsistent results are produced, while oversampling causes ethical and funding problems. Hence, a random sampling approach was used to estimate the minimal number of cells needed for two dimensional data. Therefore, data from the relative cellular calcium at the time point 10 seconds after 250 nM capsaicin and the measured TRPV1 expression were pooled (in total 4200 neurons from 9 rats). From this pool random samples were depicted with a sample size ranging from 10-4200, subsequently the spearmans correlation coefficients were calculated.

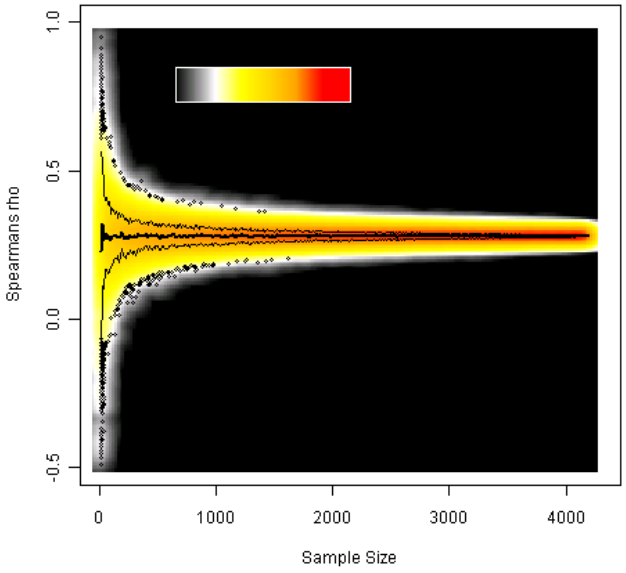

Figure 4.3.4.1 Minimal number of cells for the analysis of two parameters In the graphic shown are *in silico* results to estimate how many cells are necessary to display a combined cellular attribute (TRPV1 expression and cellular calcium response). Sub pools are sampled from a main pool to estimate how close a random experiment hits the "reality". This reality was a correlation coefficient of ρ = 0.279. The count density (see scale bar) indicates the dispersion of results obtained by *in silico* experiments. The thick black line indicates the average correlation coefficients after 800 repeats. The thin black line represents the standard deviation. The total number of correlation tests was 336000.

An expected outcome which varies less than 10 percent from the "reality" is expected earliest around a sample size of 1200 measurement (= cells). Thus, a typical later shown combined live cell and immune fluorescence experiment consisted of three individual experiments. Each one with an outcome of 300-600 cells, where both parameters are measured. Since the expected variation of this sample sizes is very high (compare Figure 4.3.1.2), three independent experiments were pooled and Spearmans correlation coefficient is calculated.

4.3.5 Sensitization impacts the dependencies between TRPV1 and capsaicin sensitivity

I hypothesized, that the neurons of the here used culture system represent different cellular sensitization states. In between both extremes, silent and hypersensitive, neurons can adapt all possible states. Thus, the capsaicin sensitivity is not an all or none mechanism but a continuous system, with as many steps as individual TRPV1 molecules are present. To proof this, a sensitizing stimuli was introduced, which synchronizes TRPV1 molecule states and shall enhance the correlation.

A widely used sensitizing stimulus is the nerve growth factor (NGF) (Ji et al., 2002, Zhang et al., 2005, Zhu et al., 2011). Since, NGF targets only NGF-receptor (p75 or TrkA) expressing neurons and those are not completely overlapping with the TRPV1 positive population (Winter et al., 1988, Kobayashi et al., 2005) pharmacological substances were chosen. In a first attempt, the PKC activator PMA and PKA activator Forskolin were chosen (Castagna et al., 1982) to prevent complex subgrouping effects. At a later point in this chapter (subchapter 4.3.7) NGF will be tested as endogenous substance. The depicted PMA concentration (100 nM) and incubation time, was in accordance with other studies (Studer and McNaughton, 2010) and the performed dose response experiments in chapter 4.2.5.1.

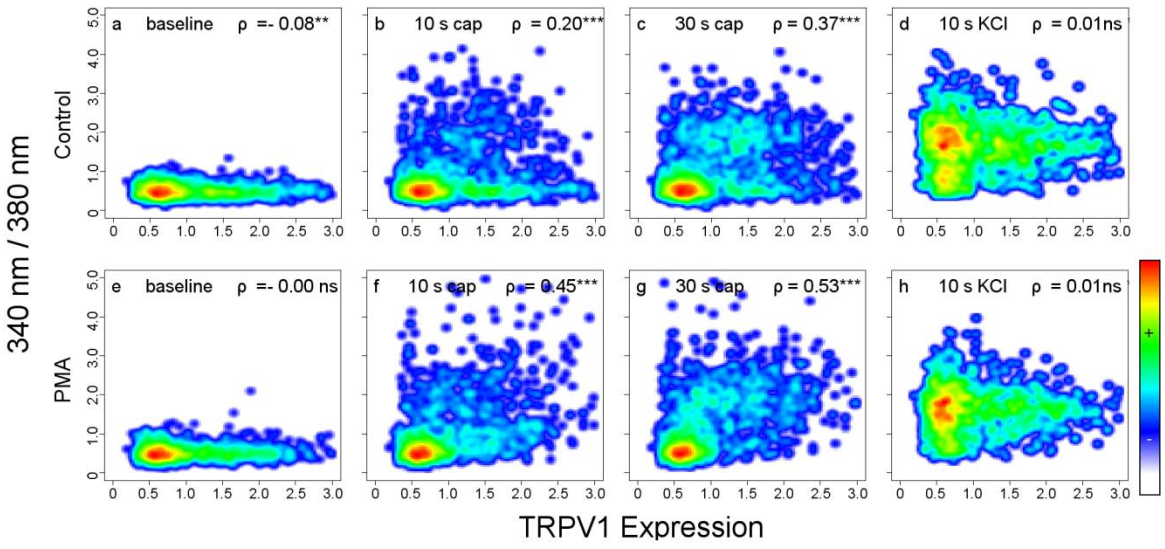

Figure 4.3.5.1 Sensitization with PMA enhances the correlation between TRPV1 and the capsaicin response (a-d) Native DRG neurons solvent controls. (a) After stimulation, with 0.2 % DMSO in complete Neurobasal media, TRPV1 and the basal calcium level show no correlation ρ = -0.08**. **(b)** 10 seconds after 250 nM capsaicin a weak correlation is achieved with ρ = 0.20***. **(c)** Correlation 30 seconds after 250 nM capsaicin, ρ = 0.37***. **(d)** After the potassium control (30 mM KCl) the rho decreased to ρ = -0.01 ns. In total, 46.9 ± 14.8 % of neurons show a calcium response after stimulation with 250 nM capsaicin. **(e-f) DRG neurons sensitized with 100 nM PMA**. **(e)** Correlation after addition of 100 nM PMA with ρ = -0.00 ns shows no change compared to the solvent control (DMSO). **(f)** After treatment with 100 nM PMA and 250 nM Capsaicin the correlation increases to ρ = 0.45 ***. **(g)** 30 seconds after capsaicin the correlation is further enhanced with ρ = 0.53***. **(h)** After 30 mM KCl the correlation decreased to no significant value of ρ = 0.01 ns. 60.6 ± 6.1 % of all neurons show a calcium response after 250 nM capsaicin. The data shown is pooled from three rats, with a total of 9 replicates per condition and 1526 neurons for DMSO and 1399 neurons for the PMA treated condition.

The sensitization with PMA clearly enhanced the dependencies between TRPV1 expression and capsaicin induced calcium amounts. The treatment with 100 nM PMA showed no correlation change under baseline condition (Fig. 4.3.5.1a + e). After 250 nM capsaicin the correlation between TRPV1 and cellular calcium levels increases with a 2.3 fold (comparing Fig. 4.3.5.1b+f). Thirty seconds after 250 nM capsaicin, the correlation in the PMA treated neuros was still elevated but with 1.4 fold to a milder degree than earlier time points (Fig. 4.3.5.1 c and g).

The experimental set shows, that pharmacological activation of PKC signaling enhances the correlation between TRPV1 and the capsaicin responses. Furthermore, DRG neurons treated with 100 nM PMA before capsaicin showed an elevated capsaicin response rate (46.9 ± 14.8 for control and 60.6 ± 6.1 for PMA treatments). To study the PKA mediated TRPV1 sensitization pathway, I chose the adenylyl cyclase activator forskolin. Forskolin (following g FSK) activates PKA signaling via the building of cyclic adenosine monophosphate (following cAMP). The chosen stimulation time point was with 90 seconds in line with earlier studies (Bhave et al., 2002, Bhave et al., 2003).

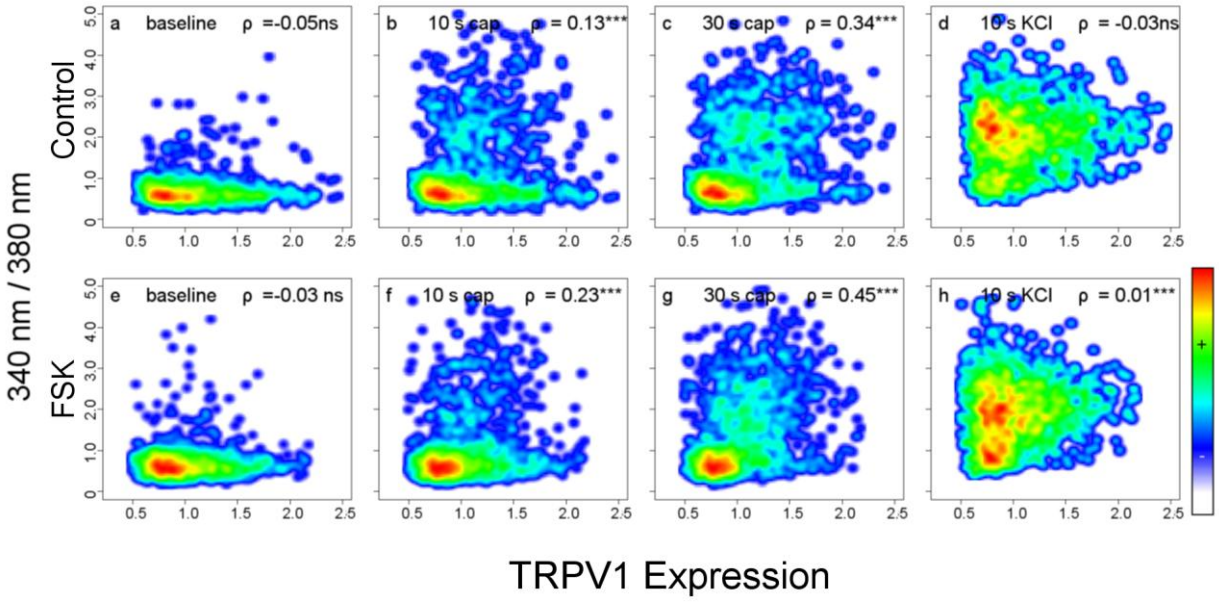

Figure 4.3.5.2 Sensitization with FSK enhances the correlation between TRPV1 and capsaicin response (a-d) DMSO controls (a) TRPV1 and cellular calcium level show no correlation after the solvent (0.2 % DMSO in Neurobasal media) control ρ = -0.05 ns. **(b)** 10 seconds after stimulation with 250 nM capsaicin the dependency increased to ρ = 0.13***. **(c)** The correlation increase 30 seconds after stimulation with 250 nM capsaicin, ρ = 0.34***. **(d)** After 30 mM KCl the correlation decreases to ρ = 0.03 ns. In total 49.1 ± 12.3 % of all neurons showed a calcium response after 250 nM capsaicin. **(e-f) 10 µM FSK treated DRG neurons**. **(e)** Treatment with 10 µM FSK does not change the rho, with ρ = -0.03 ns. **(f)** After sensitization with FSK and stimulation with 250 nM capsaicin the rho increased to ρ = 0.23***. **(g)** 30 seconds after 250 nM capsaicin the correlation increases to ρ = 0.45*** **(h)** Stimulation with 30 mM KCl resulted in no dependencies ρ = 0.01***. In total 45.3 ± 8.4 % of DRG neurons showed a calcium response after 250 nM capsaicin. The data shown is pooled from three rats with a total of 9 replicates per condition and 1207 neurons for DMSO and 1649 neurons for the FSK conditions.

Under baseline conditions appear no correlations between calcium levels and TRPV1 expression in FSK and DMSO treated neurons (Fig. 4.3.5.2a+d). 10 s after capsaicin stimulation the FSK treated neurons show a 1.8 fold correlation improvement (compare 4.3.5.2b+f). At the later time point 30 s after capsaicin the enhancement remained at 1.3 fold higher, comparable to the late capsaicin time point in the PMA treated condition (compare Fig. 4.3.5.1c+g). In contrast to the PMA treated neurons showed stimulation with 250 nM capsaicin following 10 µM FSK a lower correlation enhancement, compared to the solvent control (DMSO). Also the capsaicin response rate was unchanged after FSK treatments (49.1 ± 12.3 % for DMSO and 45.3 ± 8.4 for FSK treatments).

If kinase (PKA and PKC) activity mediated TRPV1 sensitization enhances the correlation, than inhibition of kinases activity shall decrease the correlation. To test this hypothesis, the broad range kinase inhibitor staurosporine (following stauro) was included in the experimental series. Stauro

blocks, the catalytic activity of several kinases, including PKAs, PKCs, PKGs, and S6 kinase (Ward and O'Brian, 1992, Meggio et al., 1995, Tee and Proud, 2001). The chosen concentrations and treatment times were in accordance to priory published data by (Studer and McNaughton, 2010).

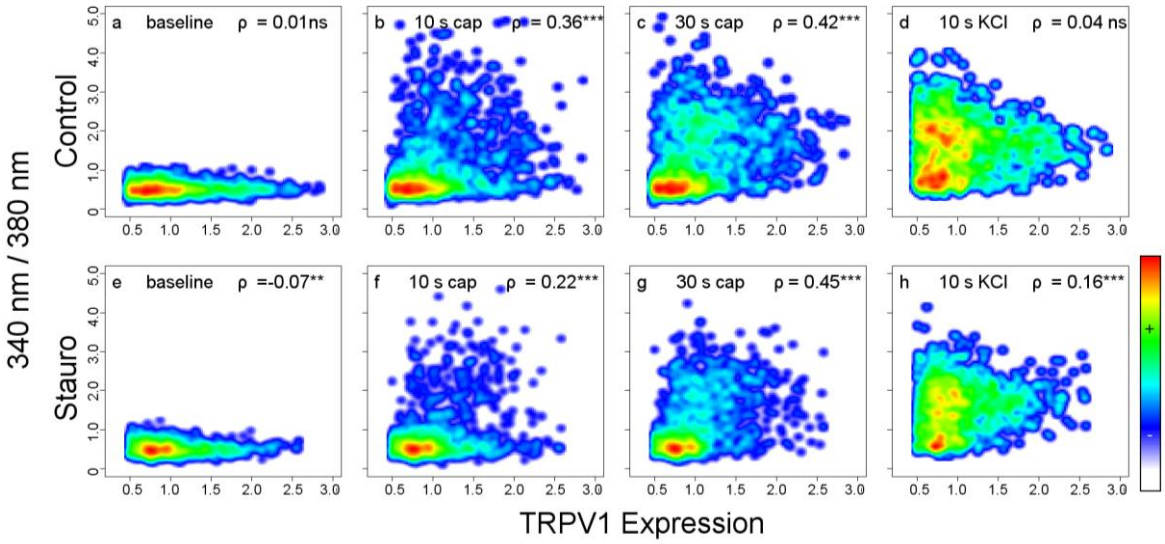

Figure 4.3.5.3 Staurosporine decreases the correlation between TRPV1 and capsaicin response (a-d) DRG neurons treated with DMSO (solvent controls). (a) The solvent (DMSO) control shows no correlation, ρ = 0.01 ns. **(b)** 10 seconds after 250 nM capsaicin a high correlation is achieved with ρ = 0.36***. **(c)** The correlation remains high 30 seconds after 250 nM capsaicin, ρ = 0.42***. **(d)** After the potassium control (30 mM KCl) the rho decreased to ρ = 0.04 ns. In total 48.4 ± 8.6 % of DRG neurons showed a response upon 250 nM capsaicin. **(e-f)** 200 nM **Staurosporine treated neurons. (e)** The correlation slightly decreased after addition of 200 nM stauro with ρ = -0.07**. **(f)** After kinase inhibition, the correlation decreases to ρ = 0.22***. **(g)** Thirty seconds after capsaicin the correlation increases to ρ = 0.45*** **(h)** 30 mM KCl results in a correlation of ρ = 0.16***. In total 44.6 ± 8.4 % of DRG neurons showed a response upon 250 nM capsaicin. The data shown is pooled from three rats with a total of 9 replicates per condition and 1529 neurons for DMSO and 1407 neurons for staurosporine treated conditions.

The treatment with the kinase inhibitor showed no impact on the baseline correlation between the relative calcium levels and TRPV1 expression (Fig. 4.3.5.3a+e). The correlation of the native neurons was with ρ = 0.36 ($p < 0.001$, 10 s after 250 nM capsaicin) and ρ = 0.42 ($p < 0.001$, 30 s after 30 s 250 nM capsaicin) already high. Treatments with staurosporine decreased the high correlation to a 0.6 fold (10 s after 250 nM capsaicin, Fig. 4.3.5.3b + c) and remained almost identical at later time points with a 1.1 fold (30 s after 250 nM Capsaicin). Within this experimental set it becomes clear that kinase inhibition reduces the correlation between TRPV1 and the capsaicin responses in rat primary DRG neurons.

Taken together the here performed experimental series proofed the initially proposed hypothesis that the synchronization of sensitization states using sensitizing (PMA and FSK) or desensitizing substances (Stauro) changed the dependencies between TRPV1 and the cellular calcium response.

4.3.6 High capsaicin concentrations predict the calcium response

I hypothesized already after the dose response experiment (part 4.2.3), that the silencing mechanisms which keep the neuron silent upon low doses of capsaicin (less than 1000 nM) can be overcome by high doses of capsaicin. This would denote the capsaicin regulatory mechanism takes place on the TRPV1 sensitivity state and not cellular localization. Hence, the dependencies between receptor expression and capsaicin response should be better for high capsaicin concentration. To test this hypothesis DRG neuron were treated with 5000 nM capsaicin, followed by immune fluorescence protocols.

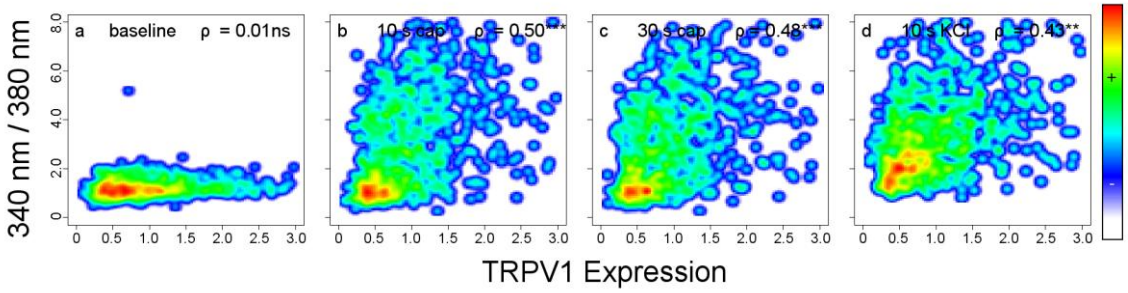

Figure 4.3.6.1 High capsaicin enhance the correlation between TRPV1 and capsaicin response (a) Under baseline conditions no correlation after media treatments are observed with ρ = 0.01 ns. **(b)** 10 seconds after high capsaicin (5000 nM) appears a significant correlation with ρ = 0.50 ***. **(c)** The later time point 30 s after 5000 nM capsaicin shows a resting high correlation with ρ = 0.48 *** **(d)** After 30 mM KCl the correlation remains high with a ρ = 0.43***. In total 64.3 ± 3.3 % of all DRG neurons reacted towards capsaicin. The shown data is generated from 3 independent experiments with a total of 12 replicates and 836 neurons.

The correlation between TRPV1 and cellular calcium levels is clearly increased for high capsaicin concentration with ρ = 0.50 ($p < 0.001$, 10 seconds after 5000 nM cap) and ρ = 0.48 ($p < 0.001$, 30 seconds after 5000 nM cap) compared to the 250 nM condition (see Fig. 4.3.5.1-3, panels b + c). The baseline relation between TRPV1 expression and cellular calcium contents are almost unchanged. Differentially to former experiments remains the correlation high after the final potassium stimulus (30 mM KCl) with ρ = 0.43 ($p < 0.001$, 10 s after 30 mM KCL).

4.3.7 Short term NGF enhances the correlation between TRPV1 and capsaicin sensitivity

The nerve growth factor (NGF) is an endogenous TRPV1 modulator used by a broad range of studies to sensitize DRG neurons and especially capsaicin responses (Winter et al., 1988, Lewin and Mendell, 1993, Lewin et al., 1993, Zhang et al., 2005, Andres et al., 2010, Zhu et al., 2011). Enhanced levels of NGF are found as oncogenic consequence, after tissues damage, or under inflammatory conditions as shown in the early 90ies by Gary Lewin and colleagues (Lewin and Mendell, 1993, Lewin et al., 1993). The release, respectively the injection, of NGF causes mechanical as well as thermal hyperalgesia. Lewin and Colleagues showed that subcutaneous application of NGF reduced the heat withdrawal latencies significantly already after 15 minutes, an effect which lasts up to 3 days in rats. Thus, NGF was chosen as endogenous substance to be tested in the correlation assay. Therefore, cultures of primary sensory neurons were treated for 3 h with 100 ng / ml NGF (f.c. NGF 2 nM) before proceeding with calcium imaging and immune fluorescence experiments.

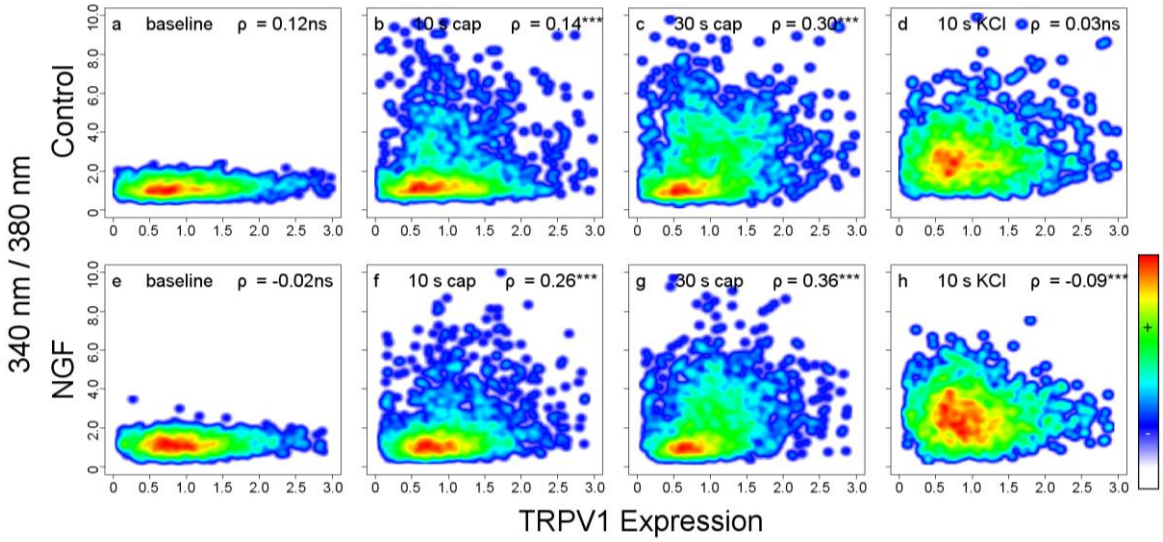

Figure 4.3.7.1 NGF treatment increase the correlation between TRPV1 and the capsaicin response (a-d) Native primary DRG neurons (a) As observed before, under baseline conditions exists no significant correlation, ρ = 0.12 ns. **(b)** 10 s after 250 nM capsaicin stimulation the correlation slightly increases towards ρ = 0.14 ***. **(c)** 30 s after capsaicin the correlation increases further to ρ = 0.30 ***. **(d)** After 30 mM KCl the correlation declines to ρ = 0.03 ns. A total of 45.8 ± 8.0 cells show a calcium response upon treatment with 250 nM capsaicin. **(e-f) Primary DRG neurons treated for 3 h with 2 nM NGF (e)** Under baseline conditions no correlation is observable ρ = 0.02 ns. **(f)** 10 s after 250 nM capsaicin the correlation increases compared to the control with ρ = 0.26***. **(g)** The same setting 30 s after 250 nM capsaicin, the correlation remained enhanced with ρ = 0.36 ***. **(h)** After stimulation with 30 mM KCl the spearman coefficient rests on an insignificant level with ρ = -0.09 ns, but shows no dependencies. 48.8 ± 4.1 % of DRG neurons show a calcium response after stimulation with 2 nM NGF followed by 250 nM capsaicin. The data shown is pooled from 3 rats in 12 replicates with 1749 neurons for control and 1903 for the NGF treated condition.

The endogenous stimulus NGF enhances the correlation between the capsaicin response and the TRPV1 expression by 1.8 fold (10 s after 250 nM cap, Fig. 4.3.7.1b + f) and 1.2 changes (30 s after 250 nM capsaicin Fig. 4.3.7.1c + g). This enhancement is lower than in pharmacological experiments using PMA but in a comparable range with forskolin (with 1.8 and 1.3). The experiment shows that also endogenous stimuli modulate the correlations. To validate if the enhancement is affected by the protein turnover, the TRPV1 expression is analyzed in the next figure. Therefore, the already measured TRPV1 fluorescence intensities of the above shown experiments were averaged over all replicates and compared.

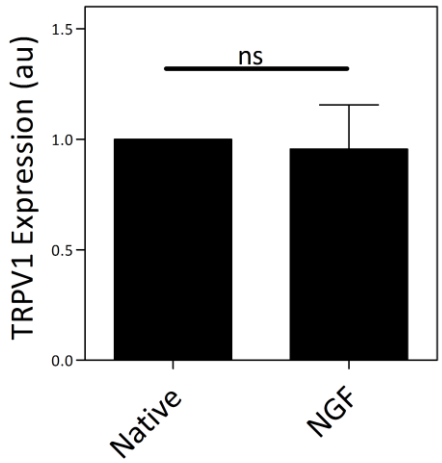

Figure 4.3.7.2 TRPV1 expression is not changed after NGF stimulation Shown is the mean TRPV1 expression (fluorescence intensity (au)) after 3 hours with 2 nM NGF. The treatment marks no significant change in the TRPV1 fluorescence signal. The data shown presents normalized experiments, from 3 rats in 12 replicates per condition, with a total of 1749 analyzed native DRG neurons and 1903 treated with NGF.

The stimulation for 3 h with 2 nM NGF results in no change in the TRPV1 expression in cultured primary DRG neurons. Thus, the observed correlation increment is based on signaling events, or protein translocation instead of enhanced TRPV1 expression.

4.3.8 Summary part 3: Sensitization modulate the correlation between TRPV1 and cellular capsaicin sensitivity

I established an experimental set up to study the impact of protein expression on calcium responses in three cellular environments (HEK, F11, and DRG-neurons, chapter 4.3.1). The introduced new technique offers the opportunity for the analysis of two dimensional data sets. To receive a certain degree of invariance within the assay up to 1200 neurons have to be analyzed as elucidated in figure 4.3.4.1.

Within the experimental sets it became clear that the amount of TRPV1 in HEK and F11 cells is a valid predictor of the calcium response evoked by capsaicin concentrations in the EC_{50} range (compare part 4.3.2.2 and 4.3.2.4).

The same experiments, performed in cultured primary DRG neurons, found deviating results. In DRG neurons the expressed TRPV1 amounts do not predict the calcium response. Even more there was a tendency in 850 out of 1973 TRPV1(+) neurons to stay silent after stimulation with half maximal capsaicin dose. This discrepancy was hypothesized to rely on differential neuronal sensitization states. Hence, I treated the neurons with the PKC-activator PMA and PKA-activator FSK to synchronize the sensitization states. Both treatments resulted in an enhancement of the correlation coefficient compared to control conditions (compare Fig. 4.3.5.1 and 4.3.5.2). Desensitization of DRG neurons using the kinase inhibitor staurosporine resulted in a decrease of the correlation compared to control conditions (compare Fig. 4.3.5.3).

As already mentioned in the dose response experiments, conducted in part 4.2.4, show low capsaicin concentration a sub maximal number of capsaicin responding neurons. Thus, the correlation was improved for high capsaicin concentration (5000 nM cap) and former capsaicin insensitive neurons become reactive (Fig. 4.3.6.1). This result indicates that the regulation of the capsaicin sensitivity take place at the TRPV1 molecule within the plasma membrane. Since the enhanced correlation was achieved without priory sensitization, the neurons had no opportunity to relocate the receptor. Treatments with the endogenous stimulus NGF enhanced the correlation, while the TRPV1 protein expression remained unchanged (compare Fig. 4.3.7.1 and 4.3.7.2).

Taken together I showed that the TRPV1 expression fails to predict the capsaicin response in native DRG neurons. This discrepancy can be pharmacologically reduced using PKA and PKC activators, and increased using the kinase inhibitor staurosporine. Also high dose of capsaicin are able to partially solve the discrepancy. These facts together suggest a mechanism which regulates the capsaicin sensitivity on the TRPV1 receptor sensitization state instead of cellular localization. To extract further details on the cellular capsaicin sensitivity the here obtained data sets were used to set up a mathematical model mimicking the neuronal environment.

4.4 A Mathematical model mimics the cellular capsaicin sensitivity

In the previous part, I described the discrepancy between the TRPV1 expression and the capsaicin evoked calcium response in rat dorsal root ganglia neurons. No correlation between both parameters was observed under native conditions. Following pharmacological treatments, the dependencies

between capsaicin receptor and the cellular capsaicin sensitivity transformed, in accordance to the sensitizing or desensitizing nature of the applied stimulus. The expected correlation after pharmacological treatments remained still far beyond the control experiments conducted in cell lines. To receive further insights on the TRPV1 depended regulation of the capsaicin sensitivity a mathematical model shall be developed based on the previously measured multi-dimensional data sets. For this purpose I collaborated again with Dr. Steffen Waldherr (Universität Magdeburg). The model was designed to cover the heterogeneity of DRG neurons regarding the TRPV1 expression and capsaicin sensitivity in the complete heterogeneous spectrum. Herein, the neuronal capsaicin sensitivity is defined as the sum of present activatable TRPV1 molecules, disregarding any cellular localization than the plasma membrane. The previously measured data for calcium kinetics and TRPV1 expression are integrated into a reaction network of possible TRPV1 activity states. In a consequence the pool sizes of TRPV1 states shall be extracted and originate for the interpretation of the cellular capsaicin sensitivity.

4.4.1 Reaction network of TRPV1 sensitization states

The assembly of a reaction model needs some previous information how the TRPV1 functionality in cells is modulated. It was assumed that cellular capsaicin sensitivity states are based on the combination of individual TRPV1 states. Therein, the sizes of the sensitized or desensitized TRPV1 pools determine the overall cellular capsaicin sensitivity as suggested by Publication of Bautista, Julius, Studer and McNaughton (Bautista and Julius, 2008, Studer and McNaughton, 2010).

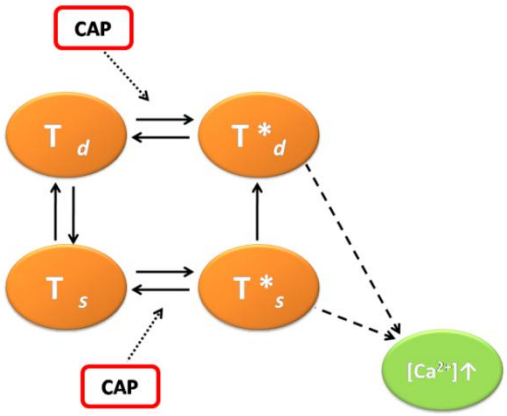

Figure 4.4.1.1 Reaction model for TRPV1 activity states TRPV1 Ion channel (T) open states are marked with asterisk (*) under sensitized (T_s) and desensitized (T_d) conditions. Each state can be transformed into its neighboring state. With one exception given from T_d* to T_s* to achieve this state 3 individual steps are required.

Within this system each single TRPV1 molecule (T) can adopt a sensitized (T_s) or desensitized (T_d) confirmation in an open (T_d* or T_s*) or closed (T_d or T_s) conformation. Calcium fluxes can appear in the open desensitized and open sensitized state. Based on the work of (Studer and McNaughton, 2010), the system was designed in a way, that each individual state can be achieved by transforming a neighboring one. Herein all states can be adopted, excepting the desensitized open to the sensitized open. This state has to underwent a closing sensitization and opening before adapting to the sensitized open state (T_d* > T_d > T_s > T_s*). This phenomenon can be explained as resensitization and requires the activity of determined sets of signaling and scaffolding components, as describe by Bhave et al. (Bhave et al., 2002).

A TRPV1(+) neuron comprises a mixture of all four molecular states determining the individual cellular sensitivity towards capsaicin. Thereby, the sum of all molecular TRPV1 states (open probabilities) can be understood as cellular capsaicin sensitivity.

4.4.2 An equation system describes TRPV1 transmitted calcium fluxes

To realize a reaction network several parameters had to be defined which describe cellular calcium in- and efflux rates, capsaicin binding, sensitization, and desensitization rates, all together are summarized in the following table.

Parameter	Description	Value
k_{on}	Capsaicin binding to TRPV1	0.12 s^{-1}
k_{off}	Capsaicin unbinding TRPV1	0.14 s^{-1}
k_{in}	Calcium influx rate through opened TRPV1, computed from P_{ca}^{2+}	485 $\mu M^{-1}s^{-1}$
k_{out}	Calcium efflux rate through opened TRPV1, computed from P_{ca}^{2+}	2.2 $\mu M^{-1}s^{-1}$
k_{in0}	Calcium influx rate through closed TRPV1, computed from P_{ca}^{2+}	0.016 μMs^{-1}
k_{ex}	Calcium efflux rate through closed TRPV1, computed from P_{ca}^{2+}	0.16 μMs^{-1}
k_s	TRPV1 sensitization rate	$1.2*10^{-3}s^{1-}$
k_d	TRPV1 desensitization rate	$1.2*10^{-2}s^{1-}$
H	Hill coefficient (from capsaicin dose response experiments)	1.7
[Ca](0)	Basal cellular calcium concentration	0.1 µM
P_{Ca}	TRPV1 calcium permeability	$2.55*10^{-19}m^3s^{-1}$
$K_{cap,d}$	Maximal capsaicin sensitivity of desensitized TRPV1 molecule	70 µM
K_{cap}	Half time capsaicin sensitivity of native TRPV1 molecule	0.115 µM
$[T_s](0)$	Amount of sensitized TRPV1, fitted to experimental data	0.135 nM
$[T_d](0)$	Amount of desensitized TRPV1, fitted to experimental data	1.35 nM
$[T^*_s](0)$	Amount of open sensitized TRPV1 under basal conditions	0 nM
$[T^*_d](0)$	Amount of open desensitized TRPV1 under basal conditions	0 nM

Tab 4.4.2.1 Parameters for TRPV1 reaction network

The parameters shown in tab 4.2.1 were used to set up the differential equation system describing the response behavior and sensitization of the TRPV1 channel. The equation system was described by the following equation. The data points used in the model were extracted from publications by (Caterina et al., 1997, Zeilhofer et al., 1997, Voets et al., 2004, Bautista and Julius, 2008, Studer and McNaughton, 2010, Hasenauer et al., 2011, Voets, 2012)

$$\frac{d[T_s]}{dt} = -k_{on}[T_s]\frac{[cap]^h}{K_{cap}^h+[cap]^h} + k_{off}[T_s^*] + k_s[T_d] - k_d[T_s] \quad \textbf{[Formula 3]}$$

$$\frac{d[T_s^*]}{dt} = k_{on}[T_s]\frac{[cap]^h}{K_{cap}^h+[caps]^h} + k_{off}[T_s^*] - k_d[T_s^*] \quad \textbf{[Formula 4]}$$

$$\frac{d[T_d]}{dt} = -k_{on}[T_d]\frac{[cap]^h}{K_{cap,d}^h+[caps]^h} + k_{off}[T_d^*] - k_s[T_d] + k_d[T_s] \quad \textbf{[Formula 5]}$$

$$\frac{d[T_d^*]}{dt} = k_{on}[T_d]\frac{[cap]^h}{K_{cap,d}^h+[caps]^h} + k_{off}[T_d^*] + k_d[T_s^*] \quad \textbf{[Formula 6]}$$

$$\frac{d[Ca]}{dt} = (k_{in} - k_{out}[Ca])([T_s^*] + [T_d^*]) + k_{in0} - k_{ex}[Ca] \quad \textbf{[Formula 7]}$$

Formula 4.4.2.1 Differential equation system for the extraction of cellular sensitization states

The proposed model of differential equations includes as variables the intracellular calcium concentration [Ca^{2+}], cellular appearance of sensitized [T_s], and desensitized [T_d] TRPV1 molecules. Both TRPV1 states appear in the closed (none marked) and open confirmation (marked with *), resulting in a total of four different states for TRPV1 (written [T_s], [T_s^*], [T_d] and [T_d^*]). Remarkably opens the desensitized receptor only under high capsaicin concentration. As indicated by the experimental sets in Fig. 4.2.4.1 and 4.3.6.1. The nominal parameters for sensitization are computed and calculated from an estimated sensitization half-time of ten minutes as suggested by the work of Cholewinski and colleagues (Cholewinski et al., 1993), as well as presumed 10 % sensitized TRPV1 molecules per neuron. We expected a portion of cells as insensitive towards capsaicin, even after high capsaicin concentration as 5 µM, to capture this assumption we set the parameter describing the sensitivity of TRPV1 towards capsaicin to 70 µM.

4.4.3 TRPV1 expression correlates negative with the amount of sensitized TRPV1 molecules

To display the heterogeneous and apparently uncoordinated response vs. expression relation (compare Fig. 4.3.3.1) the TRPV1 pool sizes were allowed to vary among individual neurons. For each cell the initial condition (0) for sensitized [T_s] and desensitized [T_d] receptors were adjusted to the measured TRPV1 fluorescence signals. The basal TRPV1 desensitization rate (k_d), which together with the resensitization rate (k_s) determines the percentage of desensitized TRPV1 channels, is considered as heterogeneous parameter for individual cells. Since no independent measurement of desensitization rate were feasible, the values were estimated from the calcium response by solving a least square optimization problem for each individual cell with k_d, [T_s](0), and [T_d] as determined from experimental results

$$k_d^* = argmin_{k_d} \int_0^{T_{end}} (y_{meas}(t) - y_{sim}(t \,|\, k_d, [T_{(s,d)}](0), k_{in0}))^2 \, dt \qquad \textbf{[Formula 8]}$$

The fitted responses were compared to the experimental data. The resulting pool sizes of TRPV1-states are compared with the cellular amount of TRPV1 and a Pearson correlation was calculated.

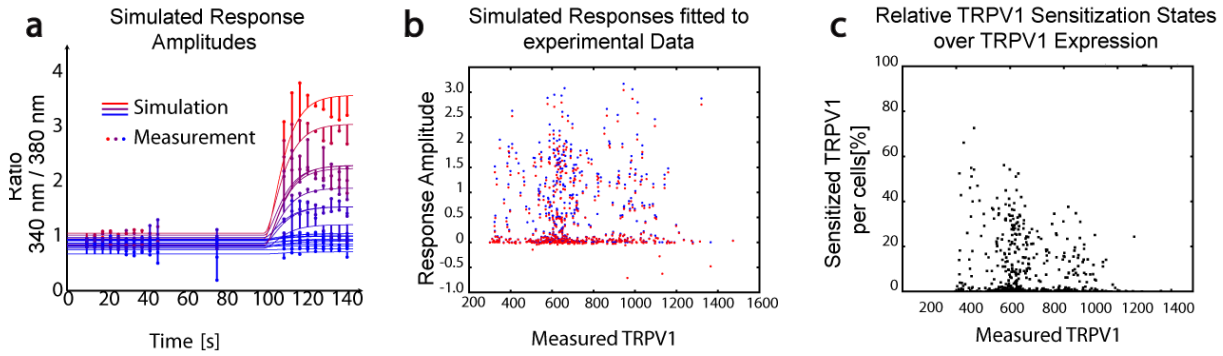

Figure 4.4.3.1 TRPV1 expression correlates negative with the pool of sensitized TRPV1 (a) Simulated response amplitudes (lines) fitted to experimental data (dots). **(b)** Response amplitude of experimental traces (blue dots) and simulated traces (red dots) versus measured TRPV1 expression. The graphic shows almost perfect overlaps between computed amplitudes and measurements and thereby validated the simulation. **(c)** The plot shows the predicted sensitized TRPV1 pool versus the measured total TRPV1 expression. A Pearson correlation test results in a mild negative correlation ρ = -0.27***.

The mathematical model reproduces the experimental data obtained by a wet experiment (Fig. 4.4.3.1a and b). The free parameters obtained from the model [T_d] fitted to experimental data suggested divorced populations. Herein, some TRPV1 positive neurons are completely desensitized

(silent), and a second group of neurons are partially sensitized cells. Focusing on this second cell population, it was figured out that the portion of sensitized TRPV1 pools declines when the total measured expression of TRPV1 increases. Quantifying this effect a negative correlation between the TRPV1 expression and the sensitized TRPV1 pool results with Pearson $\rho = -0.27$.

4.4.4 Summary part 4: Inverse relation between capsaicin sensitivity and TRPV1 expression

In close collaboration with Steffen Waldherr a model was established that enables to *in silico* reproduce experimental results (Figure 4.4.3.1b). This model captured transitions between sensitized and desensitized receptor species. By adjusting the transition parameters (k_d and k_s, tab. 4.4.2.1) the model simulates experimental data and quantifies the sizes of sensitized and desensitized TRPV1 pools.

The measured data and computational analysis indicated that the TRPV1 expression level affects cellular capsaicin sensitivity. But in contrast to the expected mechanism, high TRPV1 expressing neurons showed relatively lower capsaicin sensitivities than those expressing low levels. This proposed mechanism would enable a neuron to react independently of the expressed ion channel quantity.

An explanation of this unforeseen mechanism might be based on the leakiness of the ion channel. Downstream of the leaky ion pore, calcium scavenger as calmodulin may regulate the channel permeability as suggested in *Xenopous* oocytes experiments by Rosenbaum et al 2004 (Rosenbaum et al., 2004). A functional proof of this hypothesis in a primary system needs further experimental evidence and will be one of the foci in the following chapter.

4.5 Evaluation of TRPV1 modulators in primary neurons with novel approaches

I searched for mechanistically explanation of the phenomenon observed in chapter 4.4, where the amount of TRPV1 negatively correlated with the capsaicin sensitivity of sensory DRG neurons. With the recently established approach for quantification of endogenous protein contents in combination with live cell imaging technique (compare chapter 4.3.1), it was possible to directly proof the impact of potential modulator coexpression on the calcium response in a primary cell system. For this purpose I chose in the following chapter prominent examples of TRPV1 modulators namely the coexpression with the A Kinase Anchoring protein 79 / (AKAP) (Jeske et al., 2008, Schnizler et al.,

2008, Zhang et al., 2008, Jeske et al., 2009, Jeske et al., 2011), calmodulin (Rosenbaum et al., 2004, Lau et al., 2012) and basal calcium levels .

Next to the established ones novel potential TRPV1 modulators are tested as the voltage dependent ion channel NaV 1.8 and the markers for cell sensitization ERK and the PKA-regulatory subunit RIIβ.

4.5.1 Intracellular calcium levels do not impact the capsaicin response

The model in chapter 4.4 suggested that the TRPV1 expression inversely regulates the cellular capsaicin sensitivity. TRP-channels also show in closed conformation open probabilities, which allows ion fluxes into the neuron (Voets et al., 2004, Voets, 2012). Thus, the more channels expressed denote more passively diffusing ions throughout the membrane and thereby more calcium based TRPV1 desensitization.

As suggested by the relatively high TRPV1 open probability at physiological temperatures shown by Voets et al 2004, I hypothesized that the leakiness of the ion channel is the same in all here studied systems (rat primary DRG-neurons, transfected HEK and F11 cells). While, HEK and to a lower degree F11 cell showed a high basal correlation between calcium levels and TRPV1 expression (part 4.3.2), neurons invented mechanisms that help them to prevent potentially toxic ion overloads with a diverse set of ion pumps and scavenger, working against a toxic overload and tightly control transmitter release, transcription and the most important the membrane currents (Berridge, 1998).

Thus, I first analyzed if the basal calcium levels could predict the capsaicin sensitivity in primary neurons. As suggested by the publication of Vaughn and Gold (Vaughn and Gold, 2010), which concluded that the basal calcium levels could be an indicator for cellular sensitization states. I tested this hypothesis by evaluating the capsaicin induced calcium responses against the basal calcium levels.

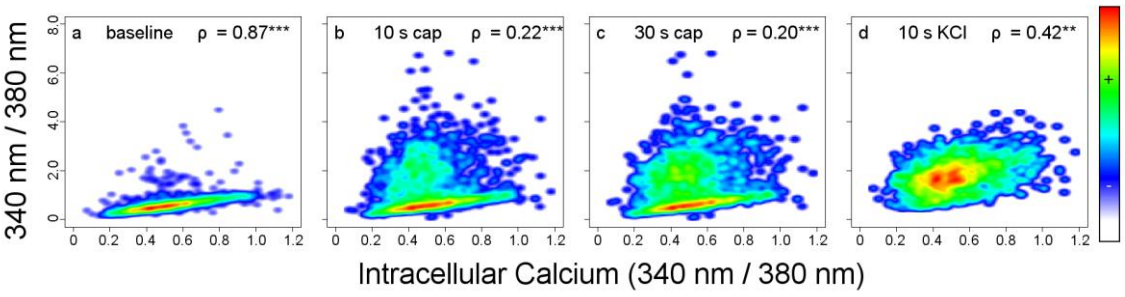

Figure 4.5.1.1 Basal calcium levels do not influence the capsaicin responses Illustrated in the figure are 2 dimensional plots between the basal calcium levels (time point 1), before any stimulus was added and the three test stimuli media, 250 nM capsaicin, and 30 mM KCl. Shown are only TRPV1 expressing neurons to circumvent cross analysis. **(a)** The first panel shows a correlation between basal calcium levels and the cellular calcium amounts 30 s after media stimulus ρ = 0.87 ***. **(b)** After addition of 250 nM capsaicin the correlation decreases to ρ = 0.22***. **(c)** After 30 s of 250 nM capsaicin the rho slightly decreases to ρ = 0.20***. **(d)** The last panel indicates the correlation 10 seconds after a final potassium stimulus ρ = 0.42***. The data shown here is pooled from six independent animals with a total of 18 replicates and 1916 primary sensory neurons.

As expected was the correlation between basal calcium levels and the cellular calcium contents after media high ($\rho = 0.87$, $p < 0.001$). This can be interpreted by correlating mainly neurons with each other which show no response to medium. After capsaicin application this correlation brakes down to spearmans rho of $\rho = 0.22$ (10 s after 250 nM capsaicin) and $\rho = 0.20$ (30 s after 250 nM capsaicin) (both with $p < 0.001$). There is no obvious relation found between the analyzed basal calcium levels and the capsaicin induced calcium responses. After addition of high potassium stimulation (30 mM) the dependency raised towards $\rho = 0.42$ ($p < 0.001$).

The here shown data suggests that the basal free calcium do not impact the capsaicin response. Furthermore, as suggested by the two dimensional plots the lower the basal calcium levels are the higher the number of responding cells became. A virtual threshold, that divides the cells into low and high basal calcium levels at the ratio value of 0.7 (x-axes). The number of capsaicin (250 nM) responses in TRPV1 positive neurons at high basal calcium levels was 43.8 % (123 out of 281 cells) for low calcium levels (< 0.7) the response rate was 61.1 % (999 out of 1635 cells). Taken together the basal calcium levels do not impact the capsaicin sensitivity neither in the amplitude (correlation test) nor in the relative number of responsive cells. Meanwhile the calcium levels have a certain predictive power for the potassium response.

4.5.2 Calmodulin and TRPV1 occur rarely in identical DRG neurons

The part 4.5.1 shows that basal free calcium level has no impact on the capsaicin response. There are a couple of studies suggesting the calcium binding protein calmodulin to be an important TRPV1 modulator. Herein a study published by Rosenbaum et al. 2004 (Rosenbaum et al., 2004) and further studies as introduced in chapter 2.7.3 indicated that TRPV1 expressing cells treated with calmodulin and Ca^{2+}, show lowered capsaicin induced ion fluxes. Following this, in combination with the hypothesis that the leakiness of TRPV1 could result in a calmodulin mediated decoy of the capsaicin

response, the impact of calmodulin expression on the capsaicin response was directly tested in DRG neurons. Therefore an anti-calmodulin was introduced to detect the calmodulin expression.

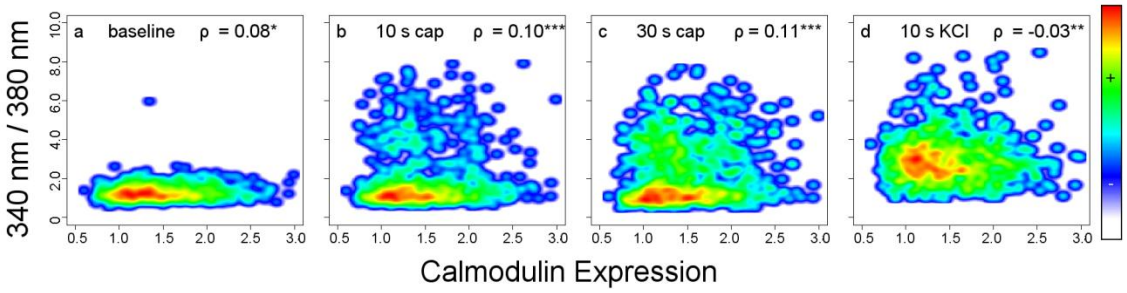

Figure 4.5.2.1 High calmodulin expression shows no correlation with the capsaicin response Shown are two dimensional density plots between cellular calcium levels and the calmodulin expression. **(a)** The basal calcium levels and calmodulin expression are not correlated ρ = 0.08 *. **(b)** Ten seconds after stimulation with 250 nM cap the correlation is slightly enhanced to ρ = 0.10 **. **(c)** Twenty seconds later spearmans rho remains unchanged with ρ = 0.11 **. **(d)** After high potassium stimulus (30 mM KCl) the correlation declines to ρ = -0.03 ns. The data shown here is pooled from 3 individual rats with a total of 12 replicates and 927 cells.

In the here conducted experimental series it was possible to partially proof the hypothesis established by Rosenbaum et al 2004, describing the presence of calcium bound calmodulin as negative regulator of the capsaicin response. The grade of dependencies under baseline conditions was ρ = 0.08 ($p < 0.05$) and showed therewith, no significant relation between basal free cellular calcium levels and calmodulin expression. In the shown data is the correlation between calmodulin expression and capsaicin induced calcium response very mild with a ρ = 0.10 (10 seconds after 250 nM cap, $p < 0.01$) and ρ = 0.11 (30 s after 250 nM cap, $p < 0.001$) (compare 4.5.2.1b + c). Expecting the calmodulin to be equally distributed over the TRPV1 positive cells (data not shown here) a negative correlation was supposed. Again, cells were dissected virtually into a calmodulin positive and negative population (threshold at 1.0) in calmodulin(-) cells a total of 227 out of 545 (41.7 %) neurons were sensitive against capsaicin and 178 out of 382 (46.6 %) for the calmodulin(+). To verify if calmodulin and TRPV1 do truly occur in identical primary neurons I conducted a second experimental series which targeted the coexpression of both markers.

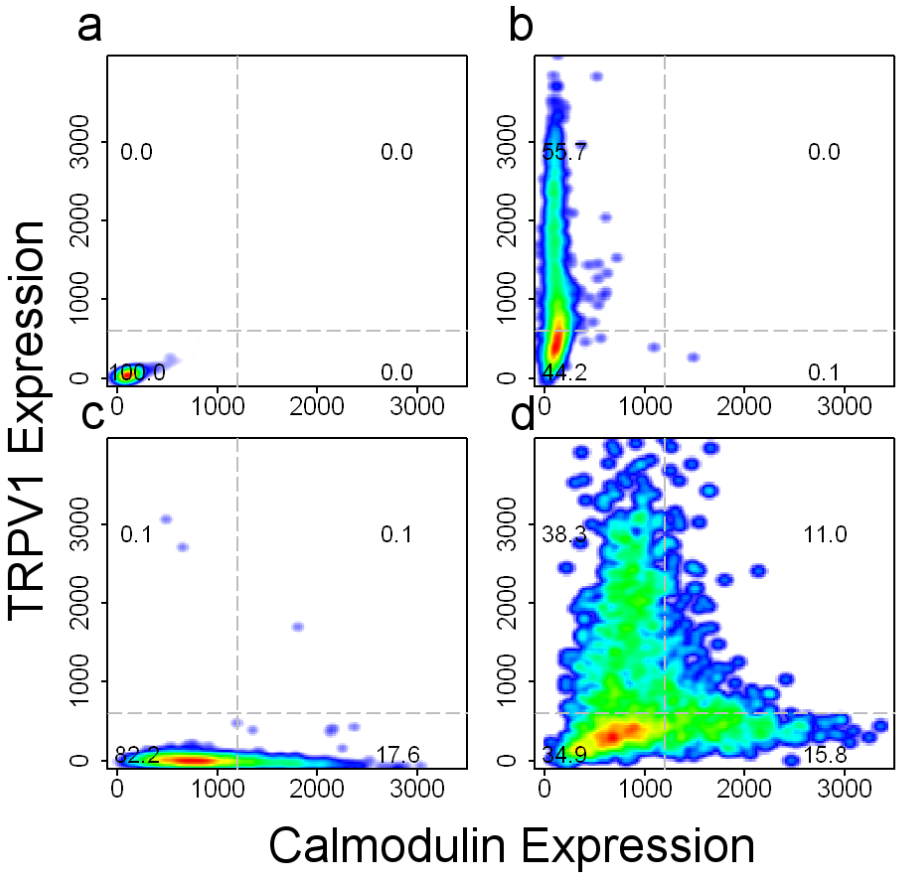

Figure 4.5.2.2 Segregating expression of Calmodulin and TRPV1 Shown are two dimensional plots of immune fluorescence data analyzing the coexpression of calmodulin and TRPV1. The numbers in the panels illustrate the relative population sizes. **(a)** Double control without primary antibodies against TRPV1 or Calmodulin. **(b)** Primary control, without the antibody against calmodulin. **(c)** Second primary control skipping the primary antibody against TRPV1. **(d)** Within the plot the TRPV1 and Calmodulin protein expression seem to segregate. Shown is one representative experiment with a total of 7769 primary neurons.

The here used anti calmodulin antibody resulted in a weak calmodulin signal, which was eliminated in the primary control (Figure 4.5.2.2 a + b). This calmodulin signal almost segregates with the TRPV1 signal as indicated in Figure 4.5.2.2d, only 11.0 % of all neurons express both proteins.

Taken together the results obtained in the Rosenbaum 2004 publication were not validated within the here conducted experimental series on primary sensory neurons. Furthermore, the used antibody pair results in segregating signals. While, calmodulin shall be present in almost each cell the data set requires further experimental proof.

4.5.3 TRPV1 coexpression with AKAP79 does not influence the cellular capsaicin response

Another well studied modulator for the TRPV1 activity is the A Kinase Anchoring Protein 79 formally known as AKAP 79. While calmodulin (and calcium) decrease the TRPV1 activity, AKAP 79 is reported to set up a functional signalosome, consisting of AKAP, kinases (PKA and/or PKCs) and the functional TRPV1 channel. The three components together are thought to build a hyper reactive module (Jeske et al., 2008, Jeske et al., 2009). Hence, the following experimental analyzes the relation between AKAP 79 expression and the capsaicin response in primary sensory neurons.

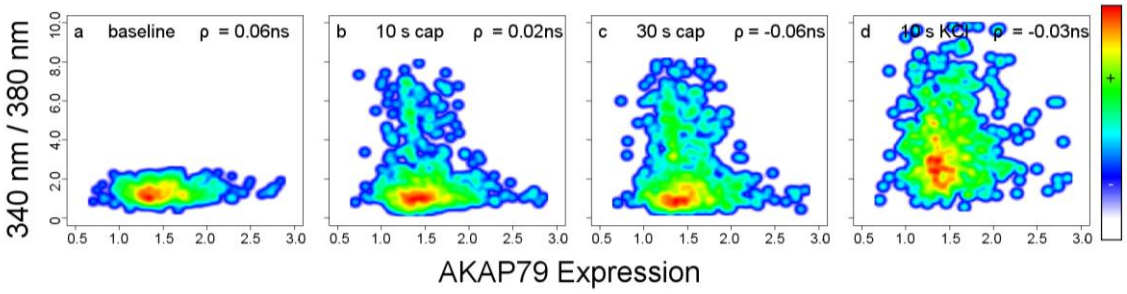

Figure 4.5.3.1 AKAP79 expression does not influence the capsaicin responses in DRG neurons Analyzed here is the influence of AKAP79 on capsaicin induced calcium levels in primary DRG neurons. **(a)** The baseline calcium levels are not influenced by the expression of AKAP79 with a correlation of ρ = 0.06 ns. **(b)** After a stimulus with 250 nM capsaicin the correlation was not significant with ρ = -0.02 ns. **(c)** The later time point 30 s after 250 nM capsaicin shows a not significant correlation with ρ = -0.06 ns. **(d)** After 30 mM KCl no significant result is achieved with ρ = -0.03 ns. The data shown is pooled from 3 individual experiments with a total of 9 replicates and 449 primary sensory neurons.

The depicted time points, after media, capsaicin, and potassium stimulation, resulted in no dependencies. Furthermore, did none of the correlation test result in any significance, all p-values were larger than 0.5. Thus, a coherent statement of the AKAP79 influence on the capsaicin response cannot be drawn. The number of capsaicin sensitive cells was for AKAP(+) neurons with 46.9 % (76 out of 162) lower than for AKAP(-) cells with 63.7 % (183 out of 287). Taken together no relation was found between the capsaicin response and the AKAP79 expression in sensory neurons.

4.5.4 NaV 1.8 expression does not modulate the capsaicin response

NaV 1.8 specifically occurs in small sensory neurons. It is generally assumed, that NaV 1.8 expressing neurons predominantly mark nociceptive neurons. A study by Laird and colleagues (Laird et al., 2002) identified in genetically NaV 1.8 knockout mice a reduced behavior in the acute sensitivity towards abdominal capsaicin stimulation compared to wild type animals. This indicated, but not shown, that coexpression of the voltage gated sodium channel subunit 1.8 and TRPV1 in sensory neurons result in

a synergistic response. Following this hypothesis an opening of the TRPV1 ion channel, causes a local decrease in the voltage over the membrane, which downstream induces an ongoing depolarization, over voltage gated channels as NaV 1.8, and further enhancements of ion influxes. To proof this hypothesis on a cellular level TRPV1 and NaV 1.8 expression were detected after functional calcium imaging.

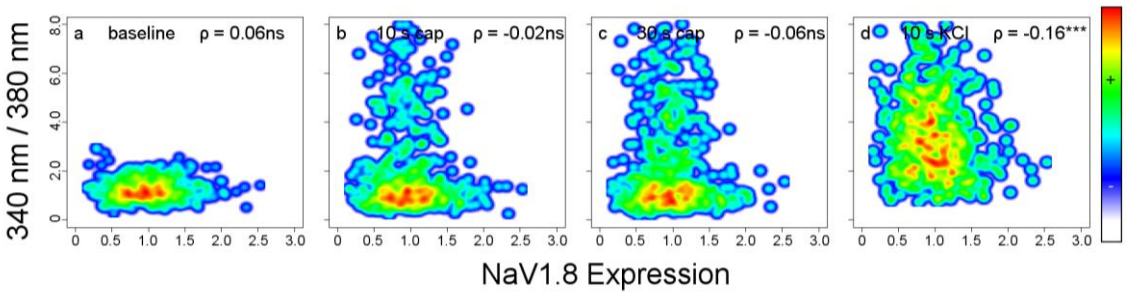

Figure 4.5.4.1 NaV 1.8 expression does not influence the capsaicin response in DRG neurons Shown are two dimensional density plots between the expression of NaV 1.8 and the cellular calcium levels after media, capsaicin and potassium stimuli. **(a)** After a media stimulus no measurable correlation is observed with ρ = 0.06 ns. **(b)** Ten seconds after stimulation with 250 nM capsaicin the spearmans rho stays not significant with ρ = -0.02 ns. **(c)** Also, no significant difference is reached after 30 s 250 nM capsaicin ρ = -0.06 ns. **(d)** The final stimulus of 30 mM KCl resulted in the only significant correlation of this experimental set with ρ = -0.16 ***. The data shown here was pooled from 3 individual experiments with a total of 12 replicates and 589 primary sensory neurons.

Analyzing the influence of the NaV 1.8 expression on the cellular calcium levels after TRPV1 activation with 250 nM capsaicin there is no detectable correlation (compare Fig. 4.5.4.1b + c). Hence, the cellular calcium response of DRG neurons is not affected by the expression of NaV 1.8. The number of NaV 1.8 positive cells that are sensitive against capsaicin is with 46.1 % (158 out of 343) in the same range as the capsaicin insensitive neurons with 43.5 % (107 out of 246).

4.5.5 ERK expression does not impact the capsaicin response

So far, the signaling state of sensory neurons is defined best by dynamics of post translational modification as phosphorylation of ERK, s6, RIIβ, or CREB (Latremoliere and Woolf, 2009, Andres et al., 2010, Knight et al., 2012, Isensee et al., 2014). Others are differences in membrane potentials or the expression of fast proteins as c-fos (Gao and Ji, 2009, Vaughn and Gold, 2010). A drawback within the here used sequential experimental approach (live cell imaging followed by immune fluorescence) was that phospho-specific antibodies are not suitable for this set up. Since,

the stimulation during live cell imaging causes phosphorylations by itself (Dai et al., 2002). On this background and a shown positive correlation between the basal ERK-levels and the ERK-phosphorylation states (Andres et al., 2010), a pan-ERK antibody was used to correlate it with the capsaicin response.

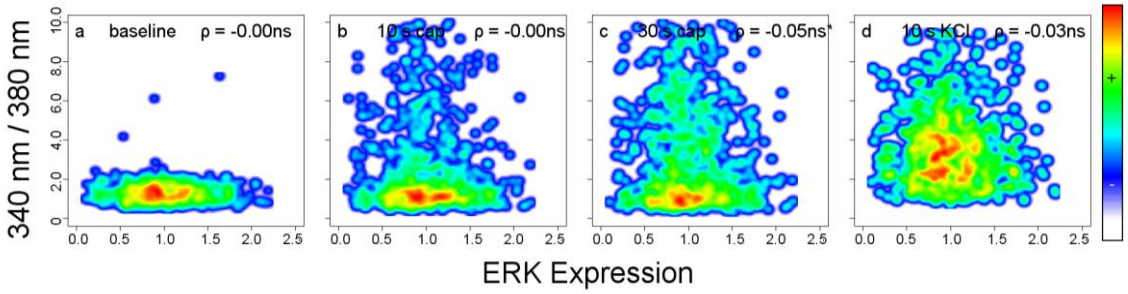

Figure 4.5.5.1 ERK expression does not influence the capsaicin response in DRG neurons Shown are two dimensional plots of ERK expression and calcium levels after different stimuli. **(a)** Under baseline condition there is no dependency between the ERK expression and cellular calcium levels with ρ = -0.00 ns. **(b)** Shortly (10 seconds) after a stimulus of 250 nM capsaicin the correlation remains unchanged with ρ = -0.00 ns. **(c)** Medium time (30 seconds) after 250 nM capsaicin the correlation is not significant changed with ρ = -0.05 ns. **(d)** Ten second after a 30 mM KCl the correlation between ERK and calcium reaches no significant levels with a ρ = -0.03 ns. The shown data is pooled from three independent experiments with 9 replicates per condition and 1025 neurons.

The ERK expression does not influence the calcium levels under baseline condition. Neither does the expression of ERK influence the calcium levels after a 250 nM capsaicin stimulus (ρ = -0.02 and -0.05 both not significant), nor after the 30 mM (ρ = -0.02 ns). The results obtained here show no significant impact of ERK-expression on the capsaicin response. Furthermore, a division into an ERK positive and negative subgroup was impossible since the expression pattern followed a Gaussian distribution.

4.5.6 Expression of the PKA regulatory subunit RIIβ marks capsaicin responsive cells

The next protein that shall be tested in this part is the regulatory subunit RIIβ which marks mostly nociceptive neurons (Isensee et al., 2014). The expression of the catalytic RIIβ subunit shows large overlaps with the nociceptive markers TRPV1 and NaV 1.8. The phosphorylation of RIIβ is crucial for the release of the activated catalytic PKA subunit. Furthermore, a correlation was shown between the overall RIIβ expression and its phosphorylation state (Isensee et al., 2014). This and the observation that PKA-signaling impacts the TRPV1-capsaicin-response correlation qualified the RIIβ expression as candidate to test its influence on the capsaicin response.

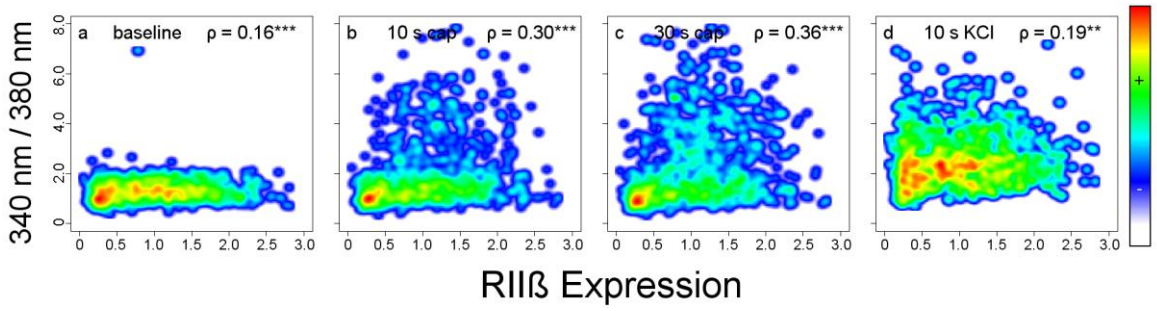

Figure 4.5.6.1 RIIβ expression predicts the capsaicin response in DRG neurons Two-dimensional representation of RIIβ expression and calcium responses. **(a)** Under baseline conditions there is already a mild correlation with basal calcium levels with ρ = 0.16 ***. **(b)** After a 250 nM capsaicin stimulus (10 seconds) the spearmans rho reaches ρ = 0.30 ***. A significant enhancement was achieved compared to former here studied markers (AKAP 79, ERK and calmodulin). **(c)** The correlation remains high 30 s after 250 nM capsaicin with a rho of ρ = 0.36***. **(d)** After the control with high potassium stimuli (30 mM KCl) the correlation decreases, but still shows a significant dependency with ρ = 0.19***. The shown data is pooled from 3 individual rats and 12 replicates with a total of 942 DRG neurons.

From all analyzed markers showed the RIIβ-subunit the highest correlation coefficients, with ρ = 0.30 ($p<0.001$, 10 s after 250 nM capsaicin) and ρ = ($p<0.001$, 30 s after 250 nM capsaicin). Although under baseline condition there was a mild correlation between cellular calcium contents and the RIIβ -expression levels. In a next step the coexpression pattern between TRPV1 and an RIIβ was analyzed and the response behavior of 4 resulting subgroups were quantified (namely the RIIβ (-) / TRPV1(-),RIIβ (-) / TRPV1(+), RIIβ (+) / TRPV1(-), and RIIβ (+) / TRPV1(+).

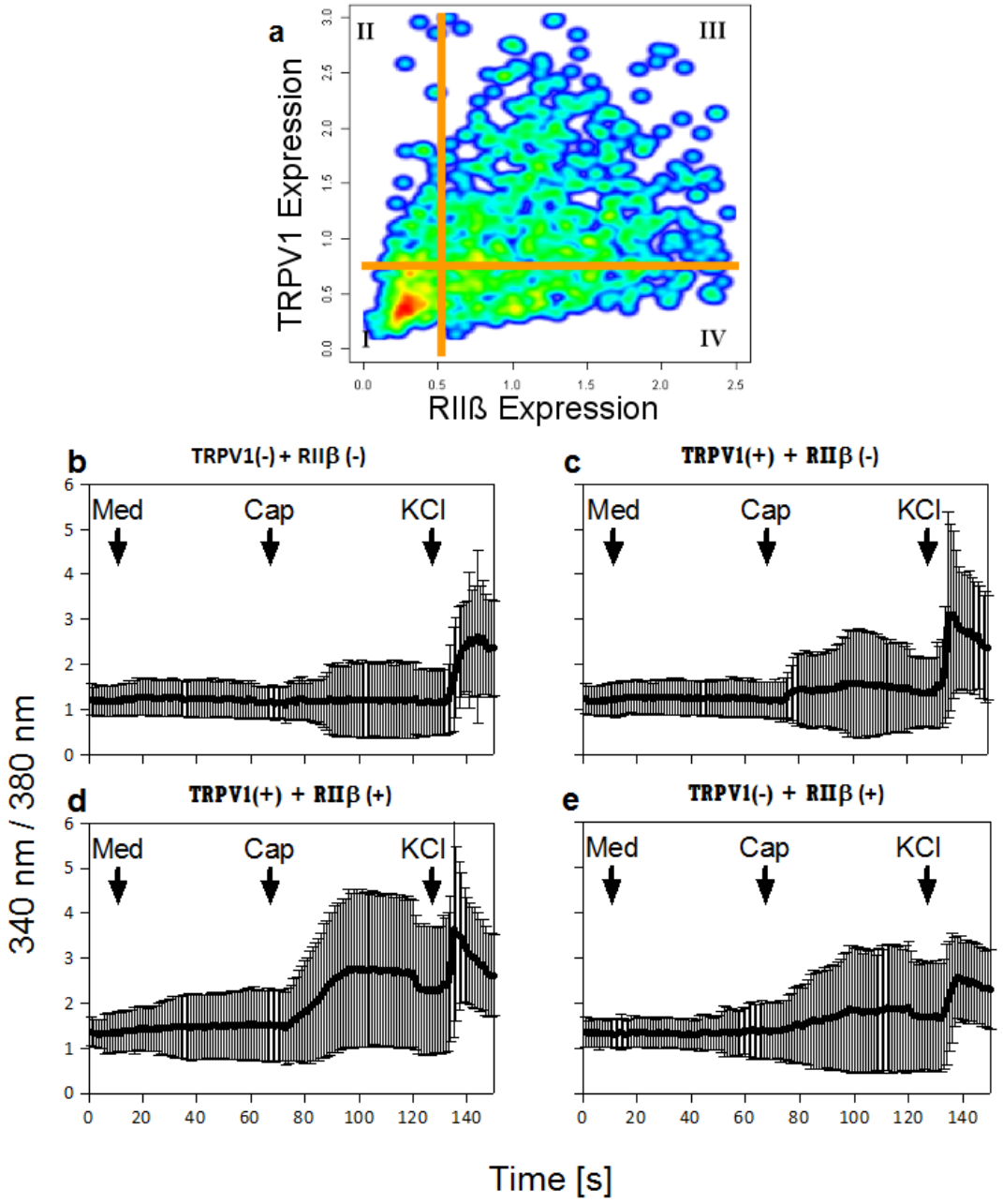

Figure 4.5.6.2 Coexpression of TRPV1 and RIIß in DRG neurons show enhanced capsaicin responses Shown in the figure are the coexpression between RIIβ and TRPV1 and the capsaicin response behavior of four resulting subpopulations. **(a)** Coexpression plot of TRPV1 and RIIß subunit of PKA in rat DRG neurons. Orange lines indicate the thresholds between the four subpopulations. **(b)** The RIIß (-) and TRPV1(-) negative population shows almost no capsaicin response. In total 9.8 % of neurons (20 out of 204) respond toward 250 nM capsaicin. **(c)** The RIIß (-) and TRPV1(+) population show with 21.6 % (21 out of 97) neurons a stronger capsaicin response. **(d)** The RIIß (+) and TRPV1(+) subpopulation showed the highest number with 55.2 % capsaicin sensitive neurons (257 of 466), while the amplitude was even higher than in the RIIß (-) and TRPV1(+) population **(e)** A total of 24.6 % of RIIβ (+) and TRPV1(-) showed a calcium response after 250 nM capsaicin stimulation. The shown data is pooled from three individual experiments with a total of 12 replicates and 942 neurons.

In the figure above shows RIIβ a huge overlap with the TRPV1 expression in cultured rat DRG neurons (4.5.6.2 a). The RIIβ positive cell population (here 68.0 % of all neurons) covered 79.2 % of all TRPV1 expressing neurons (Figure 4.5.6.2 a). The TRPV1(+) and RIIβ (-) negative population showed only in 21.6 % of all neurons a capsaicin response comparable to the TRPV1(-) and RIIβ (+) population with 24.6 % (Fig. 4.5.6.2c + e). Furthermore, the RIIβ and TRPV1 coexpressing population exhibited with 55.2 % the highest amount of capsaicin sensitive cells and the highest cellular calcium responses (see averaged traces in 4.5.6.2d). These results highlight that the PKA regulatory subunit RIIβ marks capsaicin sensitive and thereby nociceptive neurons.

4.5.7 Summary part 5: Signaling components modify the capsaicin response

In this chapter I tried to pinpoint the mechanism underlying the negative regulation of TRPV1 on the capsaicin sensitivity towards known and novel potential TRPV1 modulators. Therefore, literature supported cofactors of the capsaicin sensitivity namely the AKAP79 and calmodulin expression and basal calcium were tested. None of the mentioned modulators, or NaV 1.8 showed any significant influence towards the calcium response after capsaicin stimulation.

Next to the TRPV1-modulators the signaling components ERK and RIIβ were tested, which are known to be effectors of the cell sensitization state. ERK- and RIIβ expression are valid predictors for the amounts of their activated phosphoforms and thereby the neuronal sensitization state. Nevertheless, the expression of ERK showed no influence on the capsaicin sensitivity in DRG neurons. The RIIβ experimental series resulted in a significant correlation between TRPV1 expression and the calcium levels after capsaicin stimulations. In depth analysis of this phenomenon revealed that RIIβ expression shows a huge overlap with the TRPV1 subpopulation in DRG neurons. Furthermore, displayed the RIIβ and TRPV1 expressing subpopulation higher calcium signals than the TRPV1 only expressing population.

Taken together the expression of calmodulin and AKAP 79 or basal calcium levels failed to modify the capsaicin response in accordance to their published function. The literally extracted candidate and nociceptive marker NaV 1.8 showed no association to capsaicin evoked calcium levels. The only significant dependency was observed with the PKA-RIIβ subunit, while the common modulator ERK shows no impact. After 5 fails, one potential modulator for the capsaicin sensitivity was identified within this chapter.

To bypass the laborious approach performed on empirical candidates for the modulation of TRPV1, I aimed for a top-down approach to identify genes which are over proportionally active in TRPV1 expressing DRG-neurons.

4.6 Extracting the transcriptome of the TRPV1(+) subpopulation

After most of the in chapter 5 tested TRPV1 modulators failed to result in a clear cut candidate for the regulation of the capsaicin sensitivity of sensory neurons. The strategy was changed; instead of proofing published data with new approaches (empirical hypothesis) a data based hypothesis became necessary. Together, in a close internal collaboration with Dr. Jörg Isensee and external with the Group of Prof. Dr. Andreas Kuss from the Molecular Human Genetics department of the University in Greifswald, namely Dr. Lars Jensen, Robert Weißmann, and Christian Sperling we aimed to identify the transcriptome of TRPV1 expressing sensory neurons. Thereby we opt to identify potential novel modulators based on “State of the Art” RNA-sequencing-data. For this purpose we followed a protocol established in out lab to deplete the TRPV1(+) population of sensory neurons. Since, the isolation of TRPV1 positive neurons delivered to less material specifically expressed genes should be identified by the difference of a TRPV1 depleted cell pool versus the complete DRG.

4.6.1 Depletion of TRPV1(+) DRG neurons using resiniferatoxin

For the depletion of a certain cell type, as TRPV1(+) neurons, an approach is necessary that specifically targets the cells of interest. The background: Studies reported that high doses of TRPV1 activators directly injected into an animal eliminate TRPV1 expressing sensory neurons. The underlying mechanism is still discussed. One explanation is based on a toxic ion-overload into the TRPV1 expressing neurons (Jin et al., 2005), another one is driven by activation of mitochondrial apoptosis pathway via caspase 3 signaling (Song et al., 2013).

Nevertheless, the elimination phenomenon is existent and was used as basis to eliminate TRPV1 expressing neurons in cell suspensions by a stimulus overload with resiniferatoxin (RTX). RTX is a naturally occurring substance in the Moroccan spurge *Euphorbia resinifera*. The compound RTX is expected so far as the most potent TRPV1 activator. The affinity of RTX towards the rat TRPV1 protein is more than 40000 times higher than capsaicin (Chou et al., 2004). The following protocol gives a brief overview of the method established in the diploma thesis by Carsten Wenzel.

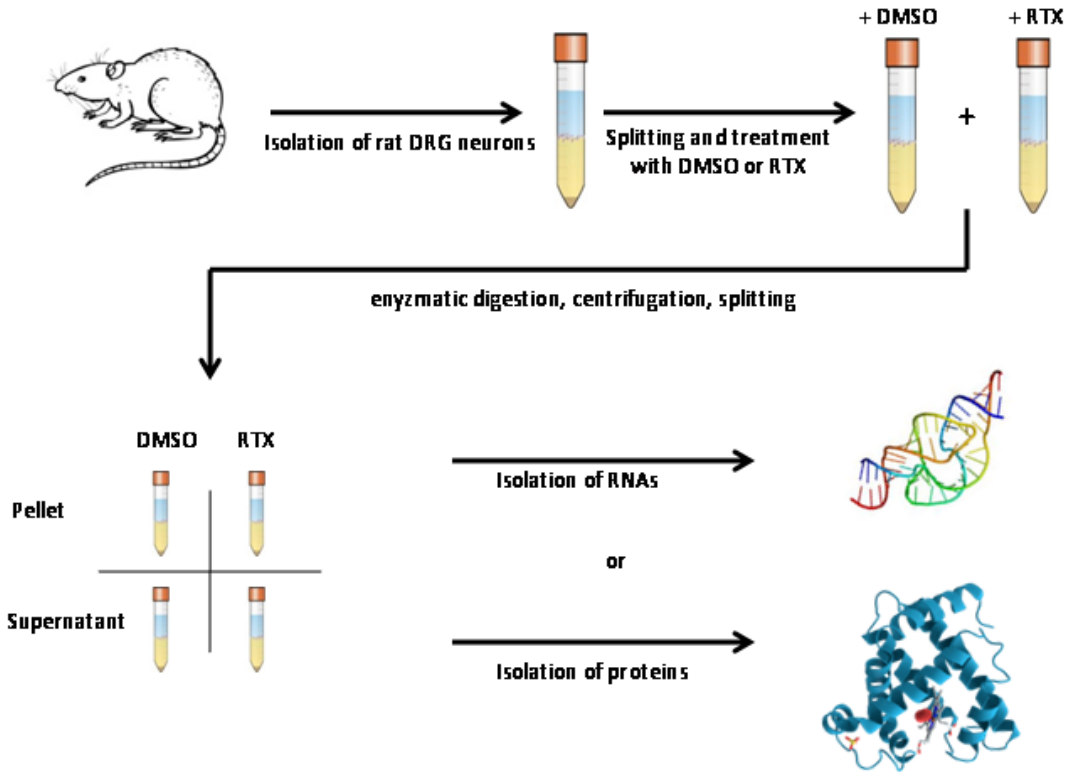

Figure 4.6.1.1 Depletion of TRPV1(+) DRG neurons DRG neurons were isolated following standard procedures. Cell suspensions are treated using either the TRPV1 activator RTX or DMSO as solvent control. Following an enzymatic digestion, the suspensions were centrifuged over a BSA gradient. Due to an increased volume (decreased cell density), TRPV1(+) neurons shall rest in the supernatant and TRPV1(-) in the pellet fraction after centrifugation. In a final step, the pellet and supernatant fractions were separated, resulting in a total of 4 samples.

12 dorsal root ganglia neurons were separated, cell debris were removed by a first BSA gradient. In a next step the neurons were treated with 100 nM RTX or 0.02 % DMSO (solvent control) for 40 min at 37° C and 5 % CO_2. The cell suspensions were spun down, followed by incubation with trypsin to further dissociate probably attached cells. Both samples (DMSO and RTX treatments) were placed on a second BSA gradient followed by a centrifugation. After these procedures the RTX-sensitive (TRPV1(+) neurons) were found in the upper part of the gradient, intact cells (TRPV1(-) neurons) settled down to the pellet. The upper cell fractions were diluted again and pelleted with 10000 xg for 10 min and 4 ° C to isolate TRPV1(+) neurons. This procedure resulted in 4 samples **(a-d)**, the RTX treated samples with its **a)** pellet presenting all neurons without TRPV1(+) cells and its **b)** supernatant with the TRPV1(+) neurons only. The DMSO treated cells were given with **c)** the pellet as the overall cell pool, and the DMSO stimulated supernatant **d)** DMSO sensitive cells (if existent).

4.6.2 TRPV1 protein decreases after RTX depletion

To evaluate if the protocol was valid to extract the TRPV1(+) DRG neurons from the overall cellular population, immune western blot analysis were performed. The protein purification of three animals and the optical quantification was performed as describe in the methods parts. The immune blots were performed using the rabbit-anti-TRPV1 and a mouse anti-tubulin as loading control.

a

Sample	Total protein yield
DMSO – pellet	1484 µg
RTX – pellet	1106 µg
DMSO – supernatant	501 µg
RTX – Supernatant	452 µg

b

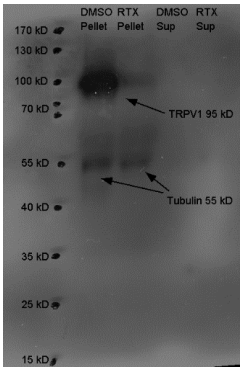

Figure 4.6.2.1 Western blots confirm TRPV1 depletion (a) Total protein yields after TRPV1 subgroup depletion from rat primary sensory neurons. Both pellet samples show (2-3 folds) higher yields than the supernatant samples. **(b)** Immune blot with TRPV1 and tubulin in 4 fractions after DMSO or RTX treatments. Each lane contained 10 µg proteins in a volume of 20 µl. The detected TRPV1 signal (91 kD) is clearly reduced in the pellet of the RTX treated neurons compared to the DMSO treated pellet (compare lane 2 and 3). The supernatant fractions showed only very weak signals, which made an objective ranking impossible.

Three rats delivered approximately 300 mg DRG tissue material (36 DRGs) and yielded in a total of 3543 µg protein (Figure 4.6.1.2a). Important to note is, that based on the cell isolation protocol a not negotiable BSA-backlog is expected in all fractions. Nevertheless, RTX treatments clearly showed a reduced protein yield compared to the DMSO controls (1484 µg for DMSO and 1105 µg for RTX treated cells), indicating already a condensed number of input cells. The performed immune western blot analysis (Figure 4.6.1.2b) confirmed the depletion of the TRPV1 positive cells. The DMSO treated condition (Figure 4.6.1.2b, lane 2) showed a broad band in the range of 90-100 kD, which presents the 91 kD TRPV1 protein. This band fades out in the RTX treated sample (Figure 4.6.1.2b lane 3). The tubulin control at 55 kD showed that the protein input was comparable in lane 2 and 3 while the supernatant conditions shows no signal here. The protein fraction analyzed in the supernatant samples, are most probably restricted to the BSA backlogs. The western blot experiment confirmed the elimination of the TRPV1 positive subpopulation of DRG neurons, but shows a constraint enrichment of the TRPV1(+) neurons.

4.6.3 TRPV1 RNA transcripts decrease after depletion protocols

The depletion of TRPV1(+) neurons was confirmed on the RNA-transcript level using real time PCRs. Consequently, RNA contents were extracted from DMSO and RTX treated supernatants and pellets, cDNA-libraries were synthesized, followed by real time PCR reactions. The exon spanning primer pairs used for TRPV1_forward: AGGGAGAAACTGGAAGAACTTTG and TRPV1_reverse: GCTGGGTGGCATGTCTATCT, resulted in amplicon lengths of 77 base pairs. The q-PCR extracted RNA amounts were normalized against a control reaction for cytoplasmatic actin b, with the primer pairs: actinb_forward GGGAAATCGTGCGTGACATT and actinb_reverse: GCGGCAGTGGCCATCTC, which generated an amplicon of 76 base pairs.

a

Sample	Mean RNA yields
DMSO – pellet	15.97 ± 3.39 µg
RTX – pellet	13.45 ± 0.57 µg
DMSO – supernatant	0.33 ± 0.16 µg
RTX – supernatant	0.58 ± 3.7 µg

b

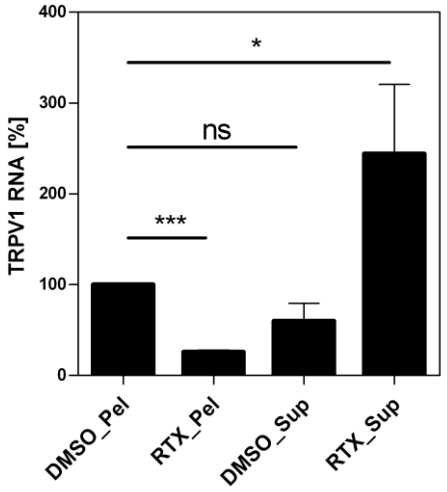

Figure 4.6.3.1 TRPV1 RNA transcripts decrease after RTX treatments (a) Tabular result of RNA yields after three experimental repetitions. The DMSO and RTX pellets have the highest RNA yields, while the DMSO treatment show slightly enhanced amounts (+ 2.53 µg). The supernatant fractions yield in significantly less material. (**b**) The shown bar diagram represents three replicated experiments each based on three real time PCR reactions. Shown are the normalized mean and standard error. The TRPV1 transcripts are significantly ($p < 0.001$) reduced in the RTX treated pellet. The averaged RNA-transcript amounts are not changed in the DMSO supernatant. While the RTX treated supernatant showed an enrichment of TRPV1-transcript.

The data shown in figure 6.1.3 indicates that from all samples RNAs were isolated; according to the expected result that TRPV1 expressing neurons are depleted after RTX treatments decrease the RNA yields (Fig. 4.6.1.3a). The RTX-supernatant fraction displays the RNA decay from the RTX versus DMSO treated fraction, which is about 2.5 µg, but yielded in only 0.6 µg. The major reason could be a) the lower amount of neurons in the depleted control and b) not optimized cell filtration protocols. Nevertheless, the transcribed cDNA showed the expected result in all fractions (Fig. 4.6.1.3b). The RTX treated pellet, which should have a reduced number of TRPV1 positive cells, had a significant

reduction of TRPV1 transcripts with 25.75 ± 2.32 % of the DMSO control ($p < 0.001$). The DMSO treated supernatant was not significantly changed regarding the TRPV1 transcript amounts. While the RTX supernatant, which represents the TRPV1 positive fraction, showed a clear enhancement of transcripts with 244.10 ± 76.36 % compared to the DMSO control ($p < 0.05$).

Taken together, the depletion of the TRPV1(+) neurons worked on protein (see Fig 4.6.1.2) and RNA (see chapter 4.6.1.3) levels. Furthermore, indicated the quantitative RNA results enrichments of TRPV1 transcripts in the RTX treated supernatant (Fig. 4.6.1.3b). Since the absolute RNA yields of supernatant fractions were too low for a downstream analysis, only DMSO and RTX treated pellets were used for the following transcriptome sequencing.

4.6.4 Subgroup sequencing reveals novel TRPV1 modulation candidates

In collaboration with the group of Prof Andreas Kuss I performed a whole transcriptome analysis of the depleted versus all DRG neurons. Therefore, the protocols shown in chapter 4.6.1.1 were repeated three times, each time with 3 rats (littermates). The procedure resulted in 6 biological samples (3 x DMSO and 3 x RTX) with the annotated transcripts and individual read numbers. The read numbers of both groups were compared, followed by calculations of a fold change and its statistical significance. A threshold at $p < 0.05$, between individual read-number-changes, resulted in a list with 209 candidates which are potentially overrepresented in TRPV1 expressing primary DRG neurons. Representative for this list is here an extract of the top 25 targets. A complete version of the list consisting of 210 individual genes can be found in appendix 8.2.

Rank	Symbol	Description	DMSO	RTX	FC	p-value
1	Cartpt	CART prepropeptide	702	78	8.94	3.72E-38
2	Iapp	islet amyloid polypeptide	449	60	7.54	4.64E-26
3	Crh	corticotropin releasing hormone	394	53	7.46	1.03E-23
4	Hal	histidine ammonia lyase	198	29	6.73	6.19E-13
5	Ptgdr	prostaglandin D receptor	291	59	4.98	1.98E-13
6	Ptgdrl	prostaglandin D receptor-like	396	81	4.87	2.73E-16
7	Nos1	nitric oxide synthase 1	677	147	4.61	3.28E-21
8	Slc16a12	solute carrier family 16, member 12	1269	275	4.61	7.39E-28
9	Mrgprd	MAS-related GPR, member D	2299	527	4.36	3.15E-31
10	Trpv1	transient receptor potential cation channel, subfamily V, member 1	14013	3446	4.07	1.40E-35
11	Mrgprx3	MAS-related GPR, member, X3	1919	499	3.84	1.65E-25
12	Lmx1a	LIM homeobox transcription factor 1 alpha	342	89	3.84	3.91E-11

13	Cldn16	claudin 16	80	21	3.77	4.14E-03
14	Gfra3	GDNF family receptor alpha 3	5060	1403	3.61	8.32E-28
15	Vom2r43	vomeronasal 2 receptor, 43; similar to putative pheromone receptor (Go-VN3); vomeronasal 2 receptor, 40; vomeronasal 2 receptor, 41; vomeronasal 2 receptor, 42	73	20	3.59	1.07E-02
16	Lpar3	lysophosphatidic acid receptor 3	1746	487	3.58	1.38E-22
17	Hprt1	hypoxanthine phosphoribosyltransferase 1	230	66	3.50	3.28E-07
18	Trpc4	transient receptor potential cation channel, subfamily C, member 4	210	62	3.37	2.07E-06
19	Pnmal1	paraneoplastic Ma antigen family-like 1	149	44	3.35	1.05E-04
20	Vwa5a	von Willebrand factor A domain containing 5A	920	280	3.29	1.01E-15
21	Tcf15	transcription factor 15	319	97	3.28	1.87E-08
22	Tac1	tachykinin 1	28731	8838	3.25	2.87E-26
23	Ewsr1	Ewing sarcoma breakpoint region 1	163	51	3.19	1.03E-04
24	Slc51a	solute carrier family 51, (orphan transporter)	789	247	3.19	4.98E-14
25	Zic5	Zic family member 5	1365	430	3.17	3.30E-17

Tab 4.6.4.1 Top 25 genes coexpressed in TRPV1(+) DRG neurons Shown in the table are the enrichment rank, the gene name, a brief gene description, the average transcript read number from three technical replicates in the columns DMSO and RTX, a fold change (FC), and significance value from single replicates. The data shown is generated from three independent technical experiments each based on 3 rats.

The table 4.6.2.1 presents the 25 top target genes of the conducted depletion experiments. Next to the official gene symbol a brief description of the gene can be found. In the second column is the averaged read number, calculated from 3 replicates. This average presents a relative RNA level estimation of the here studied genes and were used to calculate a fold change with significance values in the final column.

The ranking in the list was performed in accordance to the maximal fold change between DMSO and RTX treated cells. The TRPV1 transcripts appeared at rank 10 with a fold change value of 4.07 (compare figure 4.6.2.1). Thus, the transcriptome analysis revealed that the RTX treatments reduce the TRPV1-transcripts to 24.6 % TRPV1; this is comparable with the 25.6 % obtained by quantitative real time PCR in chapter 4.6.2

4.6.5 Functional gene annotation validates the sequencing results

After generating a list of 210 genes which are potentially active in TRPV1 expressing nociceptive neurons, the diversity of candidates increased. I aimed to systematically classify the outcome of the candidates using bio-informatic and gain a deeper understanding of the TRPV1(+) population of

nociceptive neurons. For this purpose, an open source gene ontology tool was used named "Database for Annotation, Visualization and Integrated Discovery"

The following part presents an overview of the results by DAVID gene ontology analysis and will be further discussed in chapter 5. The pie diagrams shown in this section are generated by grouping the 210 candidate genes in accordance to specific functions. The clockwise occurrence (starting at 12) of functional groups, illustrates a fold enrichment against the whole rat genome. The percentage and areas of single pie diagram slices represent the relative number of genes occurring in the specific group. A detailed overview on numerical enrichment score and the genes appearing in the specified group is listed in the appendix section 8.2.

Biological Process

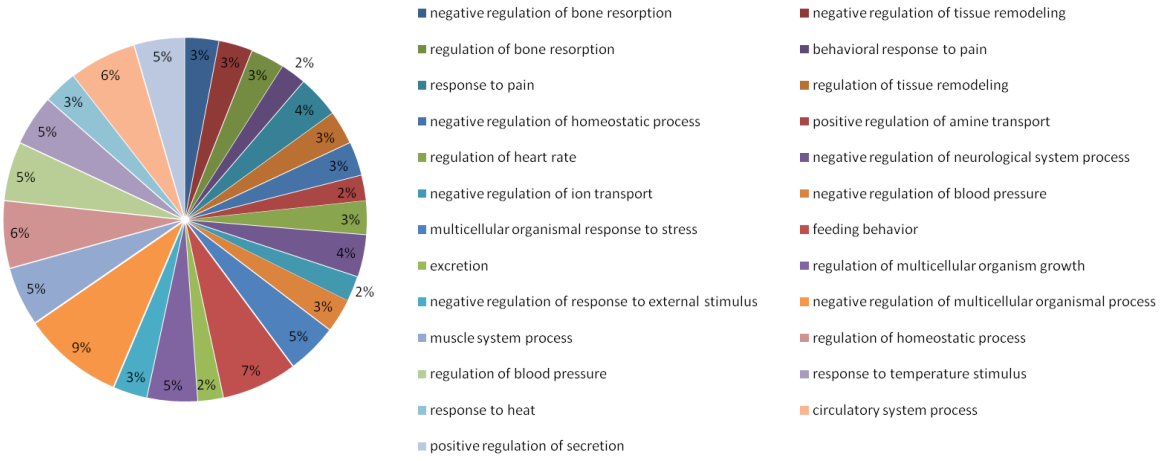

Figure 4.6.5.1 Gene annotation: Biological process Shown are the top 25 groups, a complete and detailed list can be found in the appendix section 8.2. The pie diagram shows that the top three groups are related to tissue homeostasis. At enrichment position 4 and 5 appear two pain related groups; approving that here a pain associated cell population was analyzed. Further important findings, which validate the coherent information of the here analyzed gene set, are heat associated functions and those related to ion transport, both typical features of thermo sensory neurons. A total of 141 out of 210 genes have been grouped by DAVID.

The introduced DAVID analysis of the depletion list revealed under the top 25 groups 2 directly related to pain responses, 2 for heat and temperature responses, and 2 related to ion transport and stress response. Ahead of these groups the top three enriched groups related to tissue remodeling and bone resorption. A finding that is mainly based on the occurrence of the Calca genes, which is the coding gene for the above introduced peptide CGRP.

The next gene ontology level depicted here is the cellular compartment. Again the pie diagram presents the gene grouping following their enrichment score and group size, starting at virtually 12 o'clock.

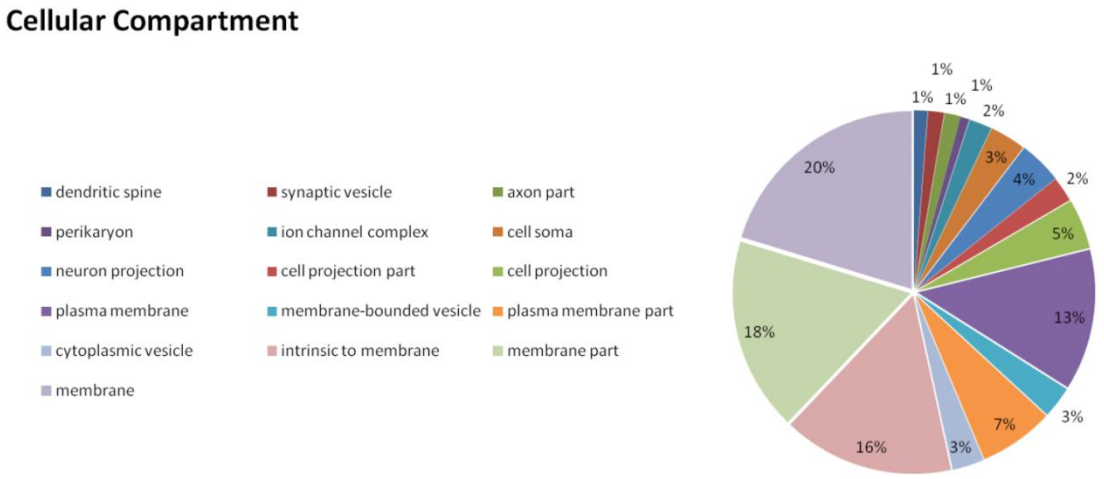

Figure 4.6.5.2 Gene annotation: Cellular compartment The input material is derived from sensory DRG neurons, since 4 groups directly represent major neuronal compartments. This approves another time the validity of the list. The fifth group display ion channel complexes. Another mentionable group here was the cell/neuron projection associated groups. A total of 150 out of 210 genes were annotated by DAVID.

The cellular compartment analysis resembled enrichments for mainly neuronal tissues, associated to dendritic spines, vesicles, the axon, and the complete perikaryon. Unexpected here was the identification of three groups associated to cell projections. In total 19, 11 and 22 genes grouped in one of the three projections related groups. The projection groups hints towards innervations phenomena that are rarely reported in the pain literature and the DRG field so far (Goswami, 2010). The last here illustrated ontology level was the molecular function.

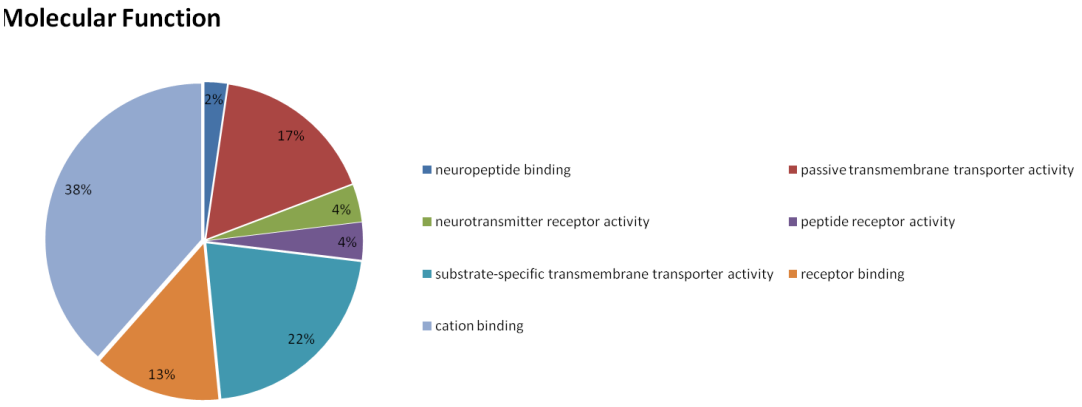

Figure 4.6.5.3 Gene annotation: Molecular function Shown are 7 groups which are significantly enriched against the control pool (rn5). The highest enriched group with a total of 3 genes was the neuropeptide binding group. The largest group shown are the cation binding with 35 % off all genes (50 genes), followed by substrate specific transmembrane transporter activity 20 % (28 genes) and passive transmembrane transporter activity 16 % (22 genes). In this run 141 out of 210 genes were successfully annotated by DAVID.

The molecular function of the studied genes revealed mainly neuro-peptide related functions and ion channel properties. This indicates another time the neuronal characteristics of the input materials. The enrichment of peptides is in line with several older publications indicating the endocrine characteristics of capsaicin sensitive neurons (Yaksh et al., 1979, Saria et al., 1987).

Taken together the DAVID gene ontology results assembled characteristics of pain relevant neurons in all three categories. The most surprising finding is the enrichment in the DAVID annotation for cellular compartments (compare figure 4.6.3.2). Herein, the projection and tissue remodeling sections show the highest scores. This finding potentially delivers novel targets for the control of innervation phenomena associated with pain chronification.

4.6.6 Summary part 6: Unraveling the genetic equipment of TRPV1(+) sensory neurons

Within the experimental series it was possible to directly deplete the TRPV1(+) population of isolated rat primary sensory neurons. In a first attempt immune western blots showed a significant reduction of TRPV1 protein contents after RTX treatments. In a second step the same phenomenon was validated on mRNA levels using quantitative real time PCRs on sample derived cDNA libraries (compare chapter 4.6.2 + 4.6.3). The depletion was validated by whole transcriptome sequencing experiments performed in close collaboration with the University of Greifswald.

The transcriptome sequencing revealed a list with 209 genes which are significantly enriched in the TRPV1(+) population of DRG neurons. To gain a deeper understanding of the gene candidates I performed a DAVID annotation, which categorized the candidate list into functional groups. The molecular function and cellular compartment sections present typical neuronal features as ion homeostasis and neuronal cell compartments. Furthermore, indicated the biological process an enrichment of thermo sensitive and pain relevant neuronal tissues (compare chapter 4.6.5). A novelty in the DAVID analysis was the enrichment for tissue remodeling and cell projection genes which can guide the field towards pain chronification associated genes.

Thus, the end of this study presents the beginning of a novel which validates a) the coexpression of candidate gene products in nociceptive neurons and b) tests the impact on the capsaicin sensitivity and thereby its relation towards nociception and/or pain sensation.

4.7 Validation of potential modulators for the cellular capsaicin sensitivity

The final chapter investigates the expression and functional impact of gene candidates derived from the transcriptome analysis in the previous part 4.6. Therefore, antibodies were ordered against candidates as ion channels, ion channel modulators, and signaling associated proteins. More than 20 antibodies were tested against protein products of selected candidates. Two of those antibodies showed clear signals in immune fluorescence experiments (data not shown). These were the cocaine and amphetamine regulated transcript pre-propeptide (following CARTPT) and the potassium channel interacting protein 1 (following KCNIP1). Both candidates shall be validated in the next chapter, for protein coexpression with TRPV1 and its influence on the capsaicin induced calcium response in primary DRG neurons.

4.7.1 CARTPT expression marks a small subpopulation of DRG neurons

The first here depicted candidate was CARTPT, which showed with a 8.94 fold change the highest enrichment score. The relative low RNA read number with 701.52 in the DMSO pool proposed either a low CARTPT-RNA expression or a very small population of CARTPT expressing sensory neurons. The coexpression of CARTPT and TRPV1 was quantified with the ArrayScan VTI platform after immune fluorescence experiments.

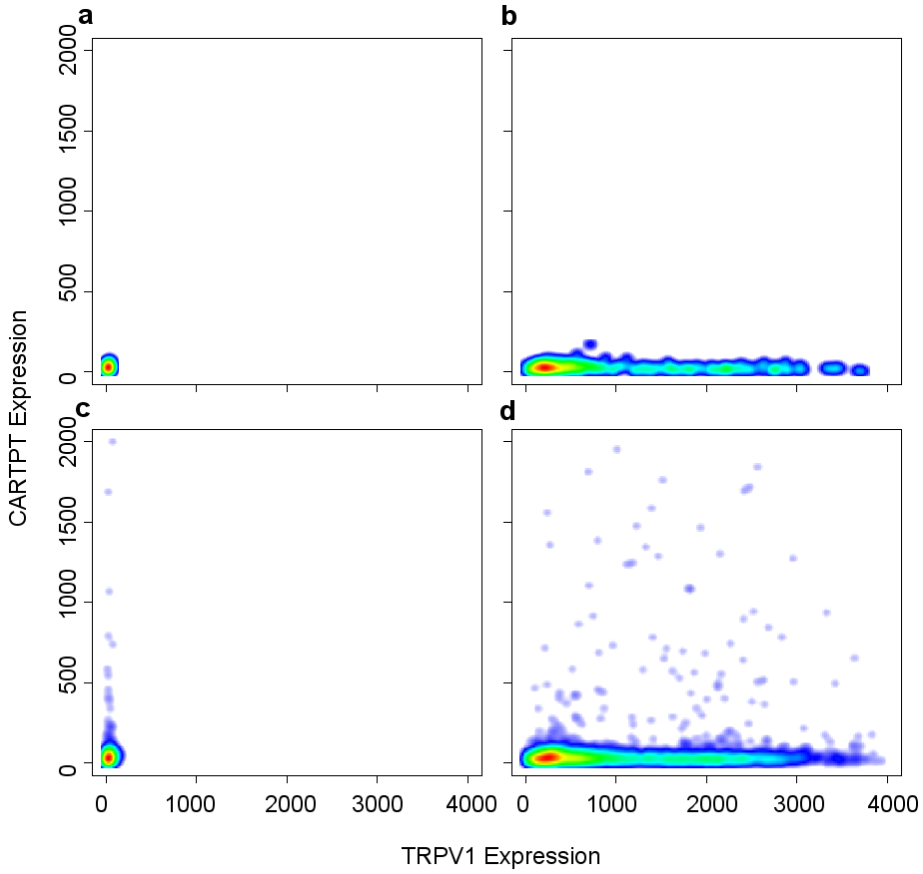

Figure 4.7.1.1 The CARTPT(+) is part of TRPV1(+) subpopulation in primary sensory neurons A representative experiment is shown out of two replicates. **(a)** Double control without the primary antibodies against CARTPT and TRPV1, with 1001 neurons. **(b)** Control for CARTPT staining, with 1153 neurons, shows no detectable fluorescence signal for CARTPT. **(c)** The control for TRPV1 staining shows no fluorescence signal for TRPV1. **(d)** Coexpression of CARTPT and TRPV1 in 5083 sensory neurons. The CARTPT signal appeared within 6.8 ± 0.9 % of DRG neurons. Quantification of the shown experiment and one additional replicate resulted in population sizes of 49.0 ± 0.9 % TRPV1(-) / CARTPT (-), 44.3 ± 0.1% for TRPV1(+) / CARTPT (-), 2.2 ± 0.2% for TRPV1(-) / CARTPT (+), 4.6 ± 1.0% for TRPV1(+) / CARTPT (+). A total number of 11091 neurons are analyzed from two animals.

The results obtained in the CARTPT experiment illustrate the need for quantitative approaches for the evaluation of neuronal subpopulations. With a population size of 6.8 ± 0.9 %, appears CARTPT in a relative small fraction of sensory neurons. The impact of CARTPT expression on the cellular capsaicin sensitivity was evaluated using the combined immune fluorescence and calcium imaging approach. To ensure a proper number of CARTPT positive cells the culture density was enhanced by 50 %.

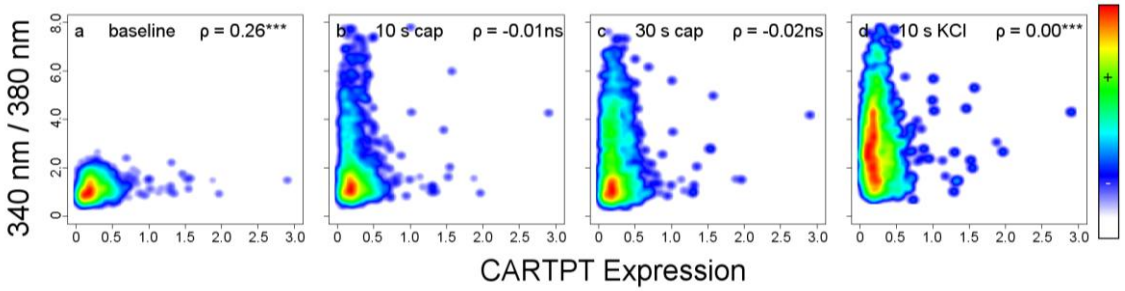

Figure 4.7.1.2 CARTPT-expression has no impact on the capsaicin response (a) During baseline conditions there is a mild correlation between the CARTPT levels and calcium levels with ρ = 0.26***. **(b)** Following the application of 250 nM capsaicin this baseline correlation disappears to ρ = -0.01 ns. **(c)** 30 s after 250 nM capsaicin no significant dependencies are found with ρ = 0.02 ns. **(d)** After 30 mM KCl the correlation remains almost unchanged and reaches significant independency with ρ = 0.00***. The data shown here is pooled from three independent experimental days and animals with a total of 12 replicates and 3061 cells.

Analyzing the correlation between a small subpopulation (6.8 ± 0.9 % of DRG neurons) has the disadvantage that low cell numbers could be handled as out layers in the correlation test. However, significant correlation results were obtained for baseline- and potassium-treatments. A total of 222 DRG neurons expressed the CARTPT peptide. From those DRG-neurons 205 co expressed TRPV1 and 100 responded to sub maximal capsaicin concentrations (45.0 %, of CARTPT positive cells). Taken together, the expression of CARTPT peptide shows no influence or mark high capsaicin responses in primary neurons. Nevertheless, the here shown population analysis is the first quantification of CARTPT(+) neurons in rat sensory neurons.

4.7.2 KCNIP1 is expressed in a subpopulation of TRPV1 positive neurons

The second here analyzed candidate was the Kv channel interacting protein 1 KCNIP1. KCNIP1 appeared in the depletion list (chapter 4.6.3) at position 32. The reasons to choose this protein for further validation was the high mRNA transcript levels resulting from the depletion list with an averaged read number of 3731 from the overall pool, and 1305 reads in the remaining pool without TRPV1 positive cells and last but not least a clear antibody signal. I hypothesized that the coexpression of a Kv-channel modulating protein could also enhance the calcium response on the same reason as introduced for NaV 1.8. The coexpression of this channel modulating protein could enhance the activatability of voltage operated potassium channels. This in turn would positively feedback the depolarization, and thereby ion fluxes over the membrane and downstream affect the calcium fluxes after capsaicin treatments. In a first attempt the coexpression between TRPV1 and KCNIP1 was analyzed using double immune fluorescence protocols on cultured rat DRG neurons.

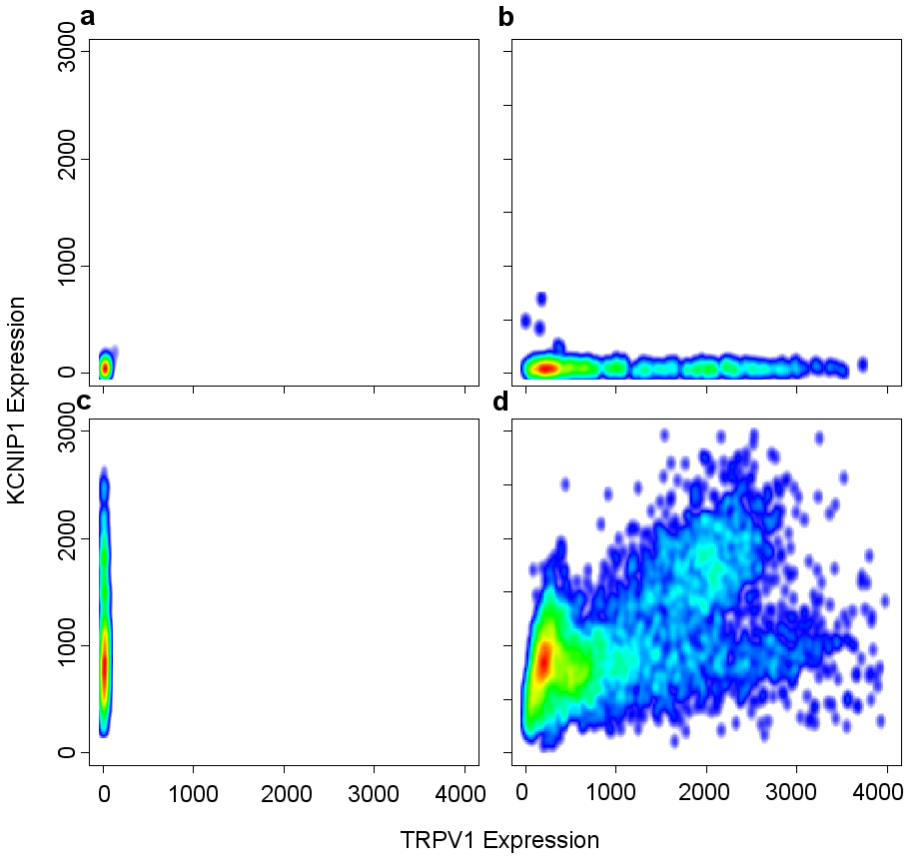

Figure 4.7.2.1 KCNIP1(+) neurons overlap with the TRPV1(+) population in DRG neurons Shown in the figure is a representative experiment out of three independent replicates. **(a)** Double negative control shows a background signal in the lower signal range for both channels. The panel displays 774 rat DRG neurons. **(b)** Control for KCNIP1 staining, with 946 DRG neurons. The graph shows in the abscissa direction the broad distribution of the TRPV1 signal while the ordinate has no signal for KCNIP1. **(c)** Control for TRPV1 staining, KCNIP1 shows a broad distribution; meanwhile a TRPV1 signal is not present. In the graph shown are 927 primary neurons. **(d)** The last panel illustrates the coexpression of KCNIP1 and TRPV1 in 6914 neurons. A subpopulation of 41.6 % expressed KCNIP1 at detectable levels. Pooling three replicated experiments together resulted in the following population sizes: 34.4 ± 3.2% for TRPV1 (-) / KCNIP1 (-), 27.0 ± 3.4 % for TRPV1(+) / KCNIP1 (-), 11.2 ± 1.4 % for TRPV1(-) / KCNIP1 (+), 27.7 ± 1.6 % for TRPV1(+) / KCNIP1 (+). A total number of 17404 neurons were analyzed here from three individual rats.

As expected from the high read numbers (compare Fig. 4.6.2) shows a relatively large population of sensory neurons a KCNIP1 signal in immune fluorescence experiments. Three independent replicated experiments resulted in a total of 38.9 ± 2.2 % KCNIP1 positive DRG neurons. Furthermore, 71.2 % of KCNIP1 positive cells expressed TRPV1. The final step evaluated the influence of KCNIP1 expression on capsaicin responses in DRG neurons.

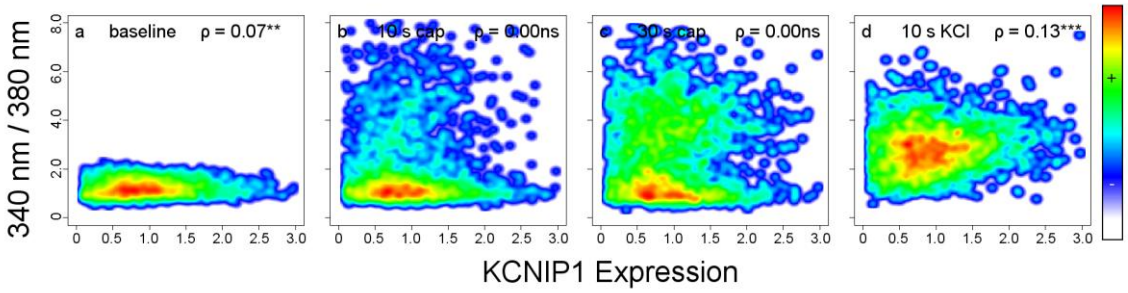

Figure 4.7.2.2 KCNIP1 does not influence the capsaicin response in DRG neurons (a) At baseline conditions there is no correlation between KCNIP1 and basal calcium levels with ρ = 0.07**. **(b)** 10 s after 250 nM capsaicin no significant correlation is observed with ρ = 0.00 ns. **(c)** 30 seconds after stimulation with 250 nM capsaicin the correlation remains not present with ρ = 0.00 ns. **(d)** After stimulation with 30 mM KCl stimulus the correlation increased to ρ = 0.13***. The data shown here is pooled from a total of four independent animals and 12 replicated wells in 2198 primary neurons.

Analyzing KCNIP1 positive cells there is no significant correlation between the protein expression and cellular calcium levels. The number of capsaicin responsive cells was with 57.0 % in a comparable range for TRPV1 (+) / KCNIP1 (+) and 50.7 % for TRPV1 (+) / KCNIP1 (-).

4.7.3 Summary part 7: Two novel neuronal subpopulations, no TRPV1 modulator

In accordance to the read numbers, obtained by transcriptome sequencing, was the portion of CARTPT expressing neurons with 6.8 ± 0.9 very small. Nevertheless, the automated immune fluorescence microscopy approach enabled a quantification of this small cell population. Moreover, was the quantification of the KCNIP1 positive population with 38.9 ± 1.5 % in the range of the so far analyzed markers for nociceptive neurons (compare chapter 4.1). Both here analyzed candidates KCNIP1 and CARTPT, extracted from the depletion list in chapter 4.6, are partially coexpressed within the TRPV1 positive subpopulation of rat dorsal root ganglia neurons. A fact which indicates another time the complexity of the here studied system and the need of quantitative approaches to face it. However, both described markers display novel subgroups in sensory neurons. No obvious relation between KCNIP1 or CARTPT expression was found on the capsaicin induced calcium responses (Fig. 4.7.1.2. and 4.7.2.2). Testing for the remaining 207 candidates following the above mentioned terms was not possible within this work and will be discussed in following chapter.

5. Discussion

I set out to investigate the characteristics of pain relevant neuronal subpopulations and perceived novel insights to their functionality. The idea that more TRPV1 proteins denote more pain response is accepted widely, but has never been shown on a cellular level. Hence, the major aim was to analyze the heterogeneous protein expression of TRPV1 in dorsal root ganglia neurons, its effect on the cellular capsaicin sensitivity, the identification of novel, and evaluation of known modulatory cofactors.

My results corroborate that pain relevant sensory neurons are highly heterogeneous concerning the expression and functionality of marker proteins as CGRP, IB4, Nav 1.8, and especially TRPV1. Many mechanisms are described modulating the neuronal sensitivity towards the TRPV1 activator capsaicin. Most of these mechanisms are characterized in cell lines. But which of the described and mostly counterbalancing mechanisms such as the regulation of the receptor expression level, capsaicin induced calcium response and thereby calcium dependent desensitization, as well as the individual cellular (re)sensitization processes is most defining for the capsaicin induced responses in the diverse population of primary nociceptive neurons remained mostly unclear. Accordingly, one broadly accepted notion is that more TRPV1 protein per cell results in more TRPV1 mediated calcium influx (Orliac et al., 2007, Poli-Neto et al., 2009, Zhu and Oxford, 2011). While this is true, when the sensitization state is brought to the same baseline level by e.g. multiple consecutive TRVP1 stimulations and by testing for very acute responses, it has not been investigated for long term responses allowing the counterbalancing mechanisms to reach equilibrium. To fill this gap, I pursued two approaches: 1) I analyzed TRPV1 in its endogenous expression environment, the nociceptive neuron, on a true population basis taking snapshots of the single cell established equilibria. 2) Based on experimental stimulus paradigms I established a first quantitative and dynamic TRPV1 model for analysis.

The results are surprising: the capsaicin sensitivity of DRG neurons is regulated anti proportionally to the expression levels of TRPV1-protein under native conditions. Thereby, a single cell robustness can be achieved which applies a stimulus sensitivity independent of protein / receptor expression levels. Subsequent experiments conducted within this work tried to pinpoint the modulation of the observed regulatory effects towards known and novel modulators. Thereby, the regulatory subunit of PKA, RIIß was identified to mark capsaicin sensitive neurons, and consequently could display a novel target in pain research. In a final experiment a whole transcriptome analysis was performed to elucidate genes which are predominantly active in TRPV1 expressing nociceptive neurons. Thereby, the field of cellular nociceptors research receives another opening, since within the here presented

list more than 200 novel gene candidates are delivered which have the potential for novel targets in pain research.

5.1 Basic research on pain requires primary cell systems

Research on TRP channel is often performed in cell lines. While allowing wide ranging control over these systems and thus a very precise investigation of focused mechanistic aspects, the relevance of the investigated mechanism in neurons remains to be shown in primary cells (Lev et al., 2012). Outstanding cell line studies have been conducted figuring out the open and closed probabilities (Studer and McNaughton, 2010), oligomerisation (Garcia-Sanz et al., 2004, Storti et al., 2012), or modulations of TRPV1 (Rosenbaum et al., 2004). Those studies from cell lines are helpful for single channel/protein characterization. But the molecular context of the primary neuron might result in different outcomes. For example, TRPV1 can be sensitized by ligands which result in activation of PKCe and thus subsequent TRPV1 phosphorylation (Vellani et al., 2001, Bhave et al., 2002, Numazaki et al., 2002, Bhave et al., 2003). This is true for cell lines as well as for neurons. Nevertheless, it is unclear in the baseline situation in neurons endogenously expressing TRPV1 if TRPV1 is phosphorylated by PKCe or not.

My study shows a counterintuitive result of such potential discrepancy. The dose response experiments in over expressed cell lines and DRG neurons showed typical sigmoidal dose responses behaviors upon capsaicin stimulation. Nevertheless, primary sensory neurons if compared to over expressed systems showed lower sensitivities towards capsaicin than cell lines. Also the correlation experiments between TRPV1 expression and capsaicin responses differ strongly in regard to relation of the calcium response and number of capsaicin sensitive cells. This indicated diverging action modes of TRPV1 in the analyzed cellular systems.

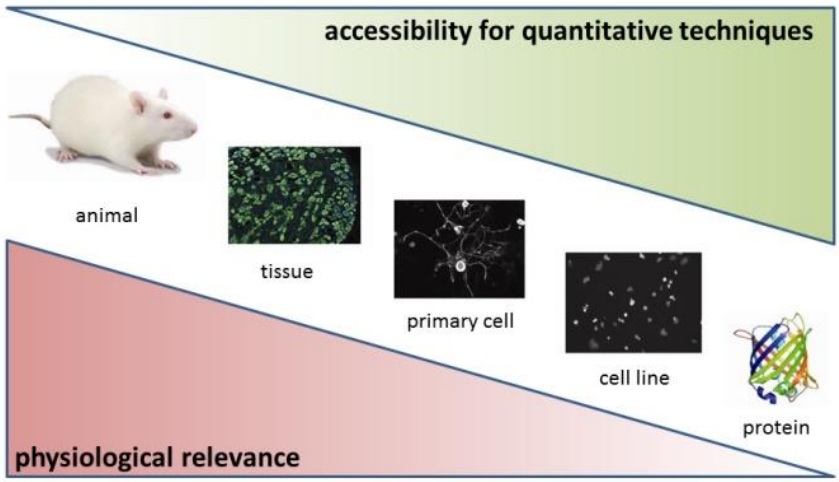

Figure 5.1.1 Relation between the reference system and physiological outcome The figure illustrates the increasing accessibility for quantitative techniques from an animal over primary cells to proteins, while the physiological relevance of the obtained results is decreasing. The approaches within in this work focused on primary cells and thereby the optimal yields of both parameters in terms of quantification and transferability to animal behavior.

Figure 5.1.1 gives an overview of the discrepancy between the physiological relevance and accessibility for quantitative techniques in 5 different experimental systems. While for sure experiments conducted in animals result in the most relevant physiological outcome the level of mechanistic detail is small. For the analysis of proteins the opposite is the case: The level of mechanistic detail can be very high, while the relevance for a physiological process could be very limited.

To study pain and nociception related processes as the expression, sensitization, resensitization, and calcium fluxes of and throughout TRPV1 cell lines are useful systems that discovered many regulatory mechanism (Rosenbaum et al., 2004, Jeske et al., 2009, Salazar et al., 2009, Por et al., 2010). Anyway, the next step to relate TRPV1 functionalities to nociception requires the description and quantification of the interplay between the four mentioned processes. This can only be achieved in a cell system which comprises the ion channel in its endogenous environment. This system integrates the heterogeneous TRPV1 expression, the possible activation states, and the existence of the complete range of modulators. As closer the chosen cell system hits the reality the more relevance has the drawn physiological conclusion. Because, cell lines fail to recreate the heterogeneous environment of nociceptors, primary sensory neurons are the system of choice for nociception related questions.

So far, this was hardly possible based on the sensory neurons heterogeneity. New quantitative microscopy approaches allow access to this complexity and enable for the first time the integration of expression and sensitization processes which can be related to functionalities in sensory neurons and nociception. The within this work performed quantitative microscopy approach on cultured primary sensory neurons delivered up to 32 individual measurements per animal. Furthermore, the used high content microscopy platform offers access to cell populations in their heterogeneous appearance and fills the gap in between classical pain cell biology and behavioral experiments. Thus, experiments using screening platforms have a predictive power for behavioral responses and thereby can reduce animal testing, as shown for phosphorylated ERK in recent publications (Andres et al., 2010, Andres et al., 2013).

5.2 Why cellular pain research need quantitative approaches

One aim central to cellular pain research is the assignment of functionalities to nociceptive cell populations (Julius and Basbaum, 2001, Basbaum et al., 2009). As shown in the first chapter of the results section (see part 4.1) describes the subgrouping of sensory neurons nociceptive subpopulations (CGRP, IB4, TRPV1, NaV 1.8). My data corroborates studies showing that indeed the peripheral sensory neurons are highly heterogeneous (Stucky and Lewin, 1999, Lewin and Moshourab, 2004, Andres et al., 2010). The quantitative single cell based approach shows even the degree of heterogeneity also for the individual TRPV1(+) neuron and subgroup with a variation span of ± 6.8 %. This heterogeneity is a great challenge. One approach to bypass this diversity is, to focus either on one/few exactly defined cell types or draw assumptions from an individual neuron to a physiological phenomenon (inductive strategy). Another way to overcome the heterogeneity is to measure it and analyze the population diversity/heterogeneity in its whole spectrum and draw ideas extracted from the complete population behavior on the individual cell (deductive strategy). I chose the second strategy.

Crucial for population analysis is to perform power analysis to evaluate the number of cells required for a full representation of a heterogeneous population or attribute. Such analyses are occasionally performed in pain research. To my knowledge the study by Andres et al 2010 (Andres et al., 2010) from our group was the first one to analyze this aspect. For my objective the analysis of 500 neurons for a single cell feature (e.g. protein expression) and around 1200 for combined features (e.g. expression and functionality) are necessary for a full coverage of chosen attributes.

The point that the analyzed sensory neurons appeared as highly heterogeneous within their subpopulation is rarely reported in the past, but gains more acceptance in the common pain literature (Kobayashi et al., 2005, Andres et al., 2010, Andres et al., 2012). Each nociceptor displays an individual repertoire on features as protein expression (compare part 4.1.1 and 4.1.2 and (Price and Flores, 2007, Isensee et al., 2014)), functionality (compare part 4.2.3 and (Stucky and Lewin, 1999, Lewin and Moshourab, 2004)) or size response-relationship (Andres et al., 2010) and thereby offers a hardly feasible research system. On the other hand, offers the heterogeneity of DRG neurons especially in case of TRPV1 one major benefit, which is the appearance of the receptor in various sensitization states and expression quantities. Thus, quantitative techniques that enable a single cell immune fluorescence resolution plus the possibility to add functional read outs allow the coverage of the complete physiological spectrum of expression-response-relation. Thereby, cell regulatory mechanisms can be extracted in a deductive manner and novel insights obtained, as the inverse relation between TRPV1 expression and capsaicin sensitivity.

5.3 Quantitative microscopy approaches deliver novel insights into sensory neurons

Using quantitative microscopy approaches I was able to quantify the number nociceptors based on fluorescence markers, without huge variation as suggested from the common literature (compare part 4.1). An extreme case varying was published in a technical paper by Hoffmann et al. (Hoffman et al., 2010). The most striking reason for the discrepancy between the results presented by Hoffman et al. 2010, where the number of TRPV1(+) DRG-neurons was quantified in between 30-100 %, and mine is the used threshold. I used a cut off, for separation of positive and negative cells, based on the blockage of specific signals Hoffman and colleagues used "*For each comparison a relative IR* [Fluorescence Intensity here referred as Immune Reactivity] *threshold was determined that best distinguished labeled from unlabeled cells.*" While comparing differential fixative composition they applied the same threshold for each condition, disregarding the distribution of fluorescence signals. The here used relative threshold based on the blockage of specific signals and a quantitative microscopy approach resulted in a reliable population quantification, which was conformed for TRPV1 with functional calcium imaging.

I present within this work for the first time the comparability of cellular calcium responses following different capsaicin concentration in primary DRG-neurons. Within this experimental series, calcium amplitudes of capsaicin sensitive neurons, show no significant difference ($p > 0.05$) between medium (250 nM) and high doses capsaicin (1000 nM and higher) (Fig. 4.2.4.2a). The finding was unexpected since several publication showed response amplitudes proportionally to the applied capsaicin stimulus in averaged dose response traces (Kim et al., 2006, Studer and McNaughton, 2010). Whereas no changes in the calcium amplitudes were identified, significant ones were observed in the calcium response time, which decreased from 40 s to below 20 s at concentrations above 1 µM capsaicin. This effect of the calcium response is not described so far and could provide a new directive, concerning cellular behavior and its physiological effect.

My calcium imaging experiments identified 6.8 % of cultured dorsal root ganglia neurons as calcium responsive for a mechanical stimulus, which was presented with a media stimulus. The assignment of the underlying sensory cell type as categorized by Lewin et al. 2004 is with the calcium response impossible (Lewin and Moshourab, 2004). Nevertheless, the obtained results indicate the existence of a neuronal population sensitive towards mechanical stimuli without any additional mechano-receptive cell structure as the so far supposed keratinocytes, follicle or merkel cells (Damann et al., 2008, Romanovsky et al., 2009). The machinery detecting this mechanical stimulus is still under research, proposed so far is the presence of force transmission throughout matrix components (Rush et al., 2006, Riol-Blanco et al., 2014), the detection of mechanical strain via membrane curvature (Damann et al., 2008), or the detection of minimal osmotic changes via TRP-channels (Sanz-Salvador

et al., 2012). Whatever the underlying receptor system is based on, if a calcium channel can be identified appearing in about 7 % of sensory neurons associated to the extracellular matrix or membrane compartments, is enriched at axotomized nerve endings (Jiang and Chen, 2009), as well as in cultured DRG neurons, could be a reasonable candidate as future mechano-receptor discovery.

5.4 Signaling regulates the conversion from silent to functional nociceptors

The activity of a particular part of nociceptive neurons increases under diseased or inflamed conditions from silent towards active. This concept of silent or sleeping nociceptors is rather old, neurons ranging in this particular (in-) activity state are thought to play an outstanding role regarding inflammatory and hyperalgesic pain phenotypes (Handwerker et al., 1991, Kessler et al., 1992, Wang et al., 2004). Nevertheless, a quantification of their population size in cultures of primary neurons was not existent so far. As a result of my immune cytochemistry experiments, I expected about 60 % of DRG neurons as capsaicin sensitive (see part 4.1.3). While performing dose response experiments I found that the amounts of capsaicin sensitive cells were below the number of expected TRPV1(+) neurons. Herein, I found that low capsaicin concentration caused only in 28.8 % (100 nM Cap) or 44.4 % (250 nM Cap) of DRG neurons a measurable calcium response, indicating a mechanism which silences the neuron under not sensitized conditions. The here presented quantification extracted the portion of TRPV1 expressing capsaicin insensitive rat sensory neurons to lay around 30 % at half maximal capsaicin concentration (250 nM capsaicin). To my best knowledge, this number represents for the first time a determination of silenced nociceptors in cultured DRG neurons. Comparable results were obtained by Handwerker et al. 1991 (Handwerker et al., 1991) with single fiber stimulations in animals, and in the results part 4.2.5 where repeated capsaicin stimuli resulted in a lowering of calcium response until no measureable effect of a capsaicin stimuli was observed and the neuron reached a silent state. This phenomenon is already extensively studied and differential mechanisms are proposed as signaling pathways, scaffolds, internalization and modulators (Jung et al., 2004, Rosenbaum et al., 2004, Mohapatra and Nau, 2005, Mandadi et al., 2006, Schnizler et al., 2008, Veldhuis et al., 2012). I set out to directly proof published and new modulators of the capsaicin sensitivity with a novel methodology on primary neurons.

The pharmacological sensitization using PKA and PKC activators resulted in both cases in enhanced correlations between TRPV1 and the capsaicin induced calcium responses. Though, activation of the PKC pathway with PMA showed a higher correlation enhancement than the PKA pathway. Furthermore, enhanced PMA the number of capsaicin sensitive cells from 46.9 ± 14.8 % towards 60.6 ± 6.1 %, while the PKA activator forskolin did not. A finding that supports the hypothesis in which PKA and its phosphorylation targets Ser-116 and Thr-37 are mainly involved in an attenuation of the

receptor desensitization (Mohapatra and Nau, 2003, Wang et al., 2010), whereas PKC is able to sensitize the cell (Vellani et al., 2001, Zhou et al., 2001). Although, both kinases have consensus phosphorylation sites at the TRPV1-molecule is the functional cellular outcome diverging and hints towards additional factors and modulators involved in the modulation of the cellular capsaicin response. The exact mechanism remains unclear so far, and will be topic of downstream studies unraveling the signaling mesh in between TRPV1 sensitization and resensitization.

The silencing mechanism was successfully bypassed by sensitizing neurons using the PKC-activator PMA (compare Fig. 4.2.5.2). A molecular explanation to that phenomenon could be the model proposed by Studer and McNaughton in 2010 (Studer and McNaughton, 2010). Herein, TRPV1 ion channels can exist in a completely desensitized (dephosphorylated) state. Thereby, the ion channels open probability is reduced to a degree that the neurons become insensitive towards any outer stimuli. A follow up work by Aneiros et al. 2011 specified this TRPV1 channel activity is based on three factors i) the number of channels in the membrane versus vesicular pools, ii) unitary channel conductance, and the iii) individual open probability (Aneiros et al., 2011). Nevertheless, my results indicate that the silencing mechanism can be overcome with high capsaicin doses, which show a clearly enhanced correlation and almost no TRPV1(+) capsaicin insensitive cell. Thus, the first statement by Aneiros et al 2011, that the TRPV1-activity is restricted to the channel appearance in the membrane cannot be held for cultured sensory neurons, since neurons keeping the channel at internal pools should be insensitive towards capsaicin or at least show a weaker correlation between TRPV1 expression and capsaicin response (compare in chapter 4.3.6). Or the high capsaicin concentration results in an immediate insertion of internalized (vesicular) TRPV1 into the membrane. This hypothesis should be tested by comparing TRPV1(+) pool in vesicles versus those in plasma membranes.

5.5 The capsaicin sensitivity is negatively regulated by the TRPV1 expression

In close collaboration with Steffen Waldherr and we developed a computational model which is to my best knowledge the first system computational model describing the cellular capsaicin sensitivity. The underlying data sets are based on measurements of thousands of individual sensory neurons in combination with single molecule kinetics extracted from the latest TRPV1 research. The model indicates that the TRPV1 expression levels contribute to the regulation of the cellular capsaicin sensitivity. But, in contrast to the expected mechanism that the TRPV1 amounts predict the capsaicin response, neurons expressing TRPV1 at low levels showed relatively higher capsaicin sensitivity than neurons expressing high TRPV1 levels and vice versa. Such a mechanism would enable neurons to sense the intensity of a stimulus independently of its ion channels quantity. The observation suggests

that independent tissue regions, with e.g. unequal TRPV1 pools, could sense a specific capsaicin stimulus with a comparable response. This proposed sensitivity regulation could provide robustness against stochastic variations in gene expression and protein levels (Rao et al., 2002, Steuer et al.). Thereby, a detection system is established which ensures the sensitivity of the receptor system independent of the intercellular heterogeneity.

A molecular explanation of this unforeseen mechanism might be based on the leakiness of the ion channel in combination with receptor internalization. Herein the leakiness of the TRPV1 channel regulates its own plasma membrane expression. The more channel expressed in the plasma membrane the higher is the passive calcium influx. This feedbacks a rarely known calcium depended (TRPV1-) internalization mechanism based on free cytosolic calcium and small g-protein as suggested by recent publications (Jiang and Chen, 2009, Sanz-Salvador et al., 2012). Different to the agonist dependent mechanism postulated by Sanz-Salvador et al. 2012 is the here assumed mechanism agonist independent but directly related to the passive calcium fluxes throughout TRPV1. Nevertheless, not sensitized sensory neurons showed a high correlation between TRPV1 expression and the capsaicin induced calcium response. How this finding fits into the above proposed capsaicin sensitivity regulation remains questionable and hints the capsaicin sensitivity regulation towards signaling instead of receptor localization. To proof the idea, primary neurons should be held in media containing differential calcium concentration. Thereby, the passive calcium influx shall be reduced and the correlation accordingly enhanced.

I hypothesized that the observed leakiness is comparable in all here analyzed systems (primary neurons or cell lines) as suggested by the relatively low TRPV1 open probability at physiological temperatures (at ~ 37° C) shown by Voets et al 2004 (Voets et al., 2004). Neurons developed mechanisms to balance this TRPV1-leakiness by a receptor internalization mechanism which lack in and HEK or F11 cells, and explains the here found high baseline correlation between TRPV1 and basal calcium levels. Furthermore, show the experiments conducted with F11 and HEK cells the general possibility to correlate the capsaicin response and TRPV1 expression.

Another explanation is that downstream of the leaky ion channel, calcium scavenger may regulate the channel permeability as suggested in calcium and calmodulin experiments conducted in *Xenopous* oocytes by Rosenbaum et al. (Rosenbaum et al., 2004). In their raised hypothesis a calcium-calmodulin-complex binds TRPV1 close to the pore and physically blocks the ion permeability. Within this work conducted experiments, proofing the impact of the calmodulin expression in rat primary neurons and correlate it with the capsaicin sensitivity resulted in no obvious contribution of the calcium scavenger.

While there was no correlation between TRPV1 and the capsaicin response in native primary neurons, a significant one was obtained in transfected cell systems. The identification of this

molecular brake, separating the TRPV1 functionality in cell lines and primary cells, will be of central interest in different pain models related to the hypersensitivity of TRPV1. Those causalities or effectors might be targets for future pain drugs which target the modulators instead of blocking ion channels or stores.

5.6 A signaling related protein predicts the capsaicin sensitivities

In the initial experiments I set out to correlate the TRPV1 expression levels with the observed capsaicin induced calcium influx. As described, this correlation is very low. My analysis indicates that activation of sensitization signaling is one of the factors improving the correlation. This raised the question, if I could find other single-cell specific parameters such as signaling activity to allow a better correlation with the observed calcium responses. The first candidate tested was the basal cellular calcium level which is thought to be interconnected with the sensitization state under hyperalgesic and neuropathic pain conditions (Vaughn and Gold, 2010). Studies reporting the calcium connection used calcium channel and store blockers to reduce behavioral pain responses. So far, no direct relation between cellular functionalities and altered calcium levels were presented (Ohsawa and Kamei, 1999, Li et al., 2005, Vaughn and Gold, 2010). Hence, I correlated neuronal calcium levels under native and sensitized condition (PMA, FSK, and NGF) with capsaicin evoked calcium responses and found no direct correlation. A possible explanation could base on the used calcium dye, because free calcium was scavenged with higher affinity to FURA-2 (Kd = 0.140 (μMs^{-1}) (source www.lifetechnologies.com) than endogenous calcium binding proteins as calmodulin (Kd = 1 - 10 (μMs^{-1}) (Yang et al., 2003). Nevertheless, a study by Ohsawa et al. 1999 observed a significant reduction in pain responses in behavioral experiments using calcium store blockers and thereby reduced cytosolic calcium levels (Ohsawa and Kamei, 1999). The cellular explanation for the reduced physiological response could base in a reduced calcium induced calcium release (CICR) and thereby lowered subsequent action potential (Miller, 1991, Shmigol et al., 1995).

Validating further known modulators as calmodulin showed no obvious relation. The finding that calmodulin and TRPV1 are not expressed in the same neuronal population is surprising (compare Fig. 4.5.2.2) as the coinfluence has been proposed in previous publications (Rosenbaum et al., 2004, Lau et al., 2012). One possible reason for the contradictory expression results is that the here used pan anti-calmodulin antibody detects an unspecific epitope in the isolated neurons or the detected signal results from an over represented isoform in the TRPV1(-) population. Indeed, the transcriptome sequencing experiments revealed different calmodulin isoforms within the list. To give a final proof on the calmodulin impact on the capsaicin response another experimental set is necessary, which

uses low affinity calcium dyes in combination with specificity approved or isoform specific calmodulin antibodies in primary neurons.

Also, the voltage gated sodium channel NaV 1.8 showed no correlation on capsaicin responses. A novel study reported a direct link between the TRPV1(+) and NaV 1.8(+) population of DRG neurons under interleukin driven inflammatory conditions (Riol-Blanco et al., 2014). Mentionable, the here conducted experiments investigated the coexpression in not sensitized DRG neurons. Hence, an influence of the coexpression between TRPV1 and NaV 1.8 is still rather possible under sensitized conditions.

In the light of the many non-existent correlations between classical markers of nociceptors and capsaicin induced calcium influx, I switched strategies and started to evaluate for correlation with signaling components instead. This approach was also indicated by the results, showing that strong signaling activation results in an improved correlation of TRPV1 expression and capsaicin induced calcium influx. The first candidate was the extracellular-signal related kinase (ERK1 and ERK2) which is known to enhance sensitivity of nociceptive neurons in response to inflammatory conditions (Dai et al., 2002, Andres et al., 2013). Unfortunately, it was impossible to correlate the capsaicin response with activated, phosphorylated ERK, since the calcium imaging and capsaicin treatment induce an ERK phosphorylation by itself (Dai et al., 2002). Earlier, our group could show that the ERK expression has a positive correlation with the phosphorylation levels of ERK (Andres, 2011). Thus, I was able to take ERK measurements as a surrogate measurement of basal phospho-ERK levels. But no influence was found on the capsaicin sensitivity.

The only molecule which showed a significant correlation with the calcium response after 250 nM capsaicin was the regulatory subunit of PKA, RIIβ. The expression of RIIβ was the better predictor of the capsaicin response than the TRPV1 expression. Not only that there was a significant correlation, between RIIβ and the capsaicin response, also coexpression with TRPV1 showed an enhancement in the calcium levels after capsaicin treatments (see results part 4.5.6). We recently published the relation between RIIβ and its appearance in pain relevant subpopulations, such as TRPV1(+) and its activation after treatments with diverse inflammatory mediators (Isensee et al., 2014). That RIIβ(+) and TRPV1(+) neuronal population showed the highest calcium amplitudes upon capsaicin stimulation hints to a functional relation between PKA-RIIβ signaling and TRPV1 which is determined by the additive quantities of protein level in this subgroup. Thereby, the RIIβ displays a potential novel target in the treatment of TRPV1 associated pain types. A finding which illustrates another time the need of quantitative techniques in pain, and in general cell biological research, plus a rethinking of signaling impacts instead of simple Ion channel functionalities. However a functional link connecting RIIβ and TRPV1 remains to be shown.

5.7 Transcriptome sequencing of TRPV1(+) neurons

I could show that indeed activation of sensitizing signal increases the correlation between TRPV1 expression and capsaicin induced calcium influx. Nevertheless, the correlation was still far from high. Thus, apparently other factors play a role as well. This could mean the involvement of other sensitization signaling, which I did not test for so far. But also, coexpression of modulators could change the response magnitude as well. Thus, I attempted to identify which proteins are specifically expressed in TRPV1(+)nociceptive neurons. A transcriptome analysis of a subgroup of sensory neurons had so far never been attempted. With a creative approach developed in our group, I present within this work the first complete transcriptome of a nociceptive subpopulation derived from rat dorsal root ganglia neurons. I identified a set of 209 genes to be especially enriched in nociceptive neurons. The transcriptome result offers two possibilities: on the one hand already known coexpressed proteins can be approved by the list, on the other hand the results can hint to novel candidates related to the perception of pain causing stimuli. One of those candidates is the gene Calca encoding for the propeptide CGRP, which is reported to appear in TRPV1(+) neurons and are functionally related (Jeftinija et al., 1992, Price and Flores, 2007, Meng et al., 2009). Contradictory to published data appeared the Mas-related G-protein coupled receptor member D (following MRGPD) as one of the top candidates of coexpressed genes. While, Cavanaugh and colleagues reported MRGPRD as possible marker for mechano-sensitive nociceptors in mice, appeared the gene in rats enriched within the TRPV1(+) subpopulation (Cavanaugh et al., 2009). The sequencing result presents for sure no final evidence for the coexpression of TRPV1 and MRGPRD but highlights the need of quantification and evaluation of nociceptive subgroups. Under the 209 candidates appearing to be enriched in TRPV1(+) neurons results one gene product namely the nitric oxide synthase 1 (NOS1) which was already described as modulator of TRPV1 related functions. (Ito et al., 2013). Interesting candidates for pain related studies supplies the candidate list from the DAVID alignment which identifies a set of cell projection associated genes that predominantly occur in the TRPV1(+) subpopulation. These finding supports TRPV1 related pain research, since the number of known genes related to tissue organization, and directed projection (also known as neuronal sprouting), is low (Jimenez-Andrade et al., 2010, Liu et al., 2012). The need for novel inputs in this field is obvious, since even the extensively studied ability of NGF to induce neuronal sprouting is controversially discussed in the latest literature (Hirth et al., 2013, Petrie et al., 2013). A first validation of potential TRPV1 modulators was started using KCNIP1 and CARTPT which both showed no significant impact on the capsaicin evoked calcium responses in DRG neurons. Nonetheless, these final experimental sets identified and quantified to novel subgroups of sensory neurons. Thereby, the complexity of the sensory system was reduced by another small step.

5.8 Outlook

The introduced quantitative techniques for the analysis of nociceptive neurons are just a first step in future TRPV1 research. The heterogeneity observed in the CGRP(+), IB4(+), NaV 1.8(+), and TRPV1(+) indicates the need to investigate neuronal subpopulations in a quantitative manner using a methodology that allows the coverage of attributes in there complex spectrum. Especially the coexpression between individual cellular markers and there functional characterization will remain in the focus of pain research, with an opening towards components which are directly related to signaling events. (Andres et al., 2013, Isensee et al., 2014). The molecular components influencing the interplay between sensitization, resensitization, and calcium fluxes deliver potential therapeutic targets for TRPV1 mediated pain phenomena. Herein, future drugs could target the TRPV1 modulators instead blocking calcium channels or stores.

It will be of interest if the discovered discrepancy between (TRPV1-) receptor and capsaicin sensitivity holds also true for comparable pain relevant ion channels or is unique to TRPV1. And if the mechanism described is a general robustness feature of neurons (and other cell types) to ensure its stimulus sensitivity. Hence, multidimensional analysis as the protein coexpression, of two or more proteins, and the association to cellular and physiological functions will stay in the focus of TRPV1 research. Especially the influence of calcium and calmodulin on the activatability of TRPV1 has to be reevaluated in primary sensory neurons. Another direction that arises within this work was the striking influence on signaling components. Thus, future projects in the TRPV1 field shall predominantly focus on the signaling status and appearance of modulators or activated kinases instead of simple TRPV1 expression.

Therefore, a gene-list was presented within this work which allows the identification of potential novel modulators of TRPV1, related cell functions, as well as pain impacts and signaling components. The here identified targets with the key aspect of cell projection could be the starting point for several novel studies, which targets innervation phenomena in neuropathic and chronic pain diseases.

6. Conclusions

The major aim of this work was to investigate the heterogeneity in nociceptive subgroups and its influence on cellular functionalities. Within this study I demonstrated the heterogeneity of pain relevant dorsal root ganglia neurons using microcopy based high content approaches. I established quantitative approaches which enable researchers to identify pain relevant sensory neurons over descriptive analysis of expression profiles and a subsequent assignment of positive and negative signals as well as functional calcium imaging methods. The performance of in depth analysis of the heterogeneity of the TRPV1 positive neuronal population revealed a severe discrepancy between the channel expression and cellular functionality. A mathematical model of the generated multidimensional data sets revealed an inverse relation between sensitized receptor pools and the amount of expressed TRPV1 protein. Thus, in combination with dose responses experiments a robustness mechanism can be proposed which applies each neuron independent of the TRPV1 expression comparable capsaicin sensitivity. This in turn enables the sensory system to react towards a capsaicin stimulus without integrating the receptor amount of the individual sensory neuron.

The lacking correlation between TRPV1 expression and the capsaicin response was partially solved by pharmacological treatments activating the PKA, PKC and NGF pathways, indicating a fundamental signaling role instead of protein expression. Hence, the results suggest that the TRPV1 expression sets the general framework while the sensitivity is determined by the actual signaling state of the cell and a maximal response is determined by the appearance of functional TRPV1 protein. A hint into this direction was shown with the additive effect of the coexpression between the PKA regulatory subunit RIIβ and TRPV1 on the cellular capsaicin sensitivity.

Finally a transcriptome analysis of the TRPV1 positive subpopulation was performed to identify novel TRPV1 modulator candidates. The so successfully identified genes, which are significantly enriched in nociceptive neurons, will be of interest for upcoming pain research.

The presented data sets are a starting point for future studies which will pin point the signaling mechanisms that impact the TRPV1 activatability under inflammatory and pain condition. The supported gene candidates have the potential to contain this novel target for the modulation of TRPV1 and consequential novel target for pain therapeutics. The combination between subgroup functionalities and quantitative modeling will allow a very sensitive further delineation of the complexity of TRPV1-modulation in its natural heterogeneous environment, the primary nociceptive neurons.

7. Literature

Adams ME (2004) Agatoxins: ion channel specific toxins from the American funnel web spider, Agelenopsis aperta. Toxicon : official journal of the International Society on Toxinology 43:509-525.

Adcock JJ (2009) TRPV1 receptors in sensitisation of cough and pain reflexes. Pulmonary pharmacology & therapeutics 22:65-70.

Ahern GP (2003) Activation of TRPV1 by the satiety factor oleoylethanolamide. J Biol Chem 278:30429-30434.

Aley KO, Martin A, McMahon T, Mok J, Levine JD, Messing RO (2001) Nociceptor sensitization by extracellular signal-regulated kinases. J Neurosci 21:6933-6939.

Andres C (2011) Growth factor induced subgroup specific signaling in nociceptive neurons. pp VI, 119 S. München: Dr. Hut.

Andres C, Hasenauer J, Ahn HS, Joseph EK, Isensee J, Theis FJ, Allgower F, Levine JD, Dib-Hajj SD, Waxman SG, Hucho T (2013) Wound healing growth factor, basic FGF, induces Erk1/2 dependent mechanical hyperalgesia. Pain.

Andres C, Hasenauer J, Allgower F, Hucho T (2012) Threshold-free population analysis identifies larger DRG neurons to respond stronger to NGF stimulation. PloS one 7:e34257.

Andres C, Meyer S, Dina OA, Levine JD, Hucho T (2010) Quantitative automated microscopy (QuAM) elucidates growth factor specific signalling in pain sensitization. Molecular pain 6:98.

Aneiros E, Cao L, Papakosta M, Stevens EB, Phillips S, Grimm C (2011) The biophysical and molecular basis of TRPV1 proton gating. The EMBO journal 30:994-1002.

Ballou LR (2000) The regulation of cyclooxygenase-1 and -2 in knockout cells and cyclooxygenase and fever in knockout mice. Ernst Schering Research Foundation workshop 97-124.

Ballou LR, Botting RM, Goorha S, Zhang J, Vane JR (2000) Nociception in cyclooxygenase isozyme-deficient mice. Proc Natl Acad Sci U S A 97:10272-10276.

Baron R (2006) Mechanisms of disease: neuropathic pain--a clinical perspective. Nature clinical practice Neurology 2:95-106.

Basbaum AI (1999) Spinal mechanisms of acute and persistent pain. Regional anesthesia and pain medicine 24:59-67.

Basbaum AI, Bautista DM, Scherrer G, Julius D (2009) Cellular and molecular mechanisms of pain. Cell 139:267-284.

Basbaum AI, Woolf CJ (1999) Pain. Current biology : CB 9:R429-431.

Baumann TK, Martenson ME (2000) Extracellular protons both increase the activity and reduce the conductance of capsaicin- gated channels. J Neurosci 20:RC80.

Bautista D, Julius D (2008) Fire in the hole: pore dilation of the capsaicin receptor TRPV1. Nature neuroscience 11:528-529.

Berridge MJ (1998) Neuronal calcium signaling. Neuron 21:13-26.

Bessou P, Perl ER (1969) Response of cutaneous sensory units with unmyelinated fibers to noxious stimuli. Journal of neurophysiology 32:1025-1043.

Bhave G, Hu HJ, Glauner KS, Zhu W, Wang H, Brasier DJ, Oxford GS, Gereau RWt (2003) Protein kinase C phosphorylation sensitizes but does not activate the capsaicin receptor transient receptor potential vanilloid 1 (TRPV1). Proc Natl Acad Sci U S A 100:12480-12485.

Bhave G, Zhu W, Wang H, Brasier DJ, Oxford GS, Gereau RWt (2002) cAMP-dependent protein kinase regulates desensitization of the capsaicin receptor (VR1) by direct phosphorylation. Neuron 35:721-731.

Black JA, Liu S, Tanaka M, Cummins TR, Waxman SG (2004) Changes in the expression of tetrodotoxin-sensitive sodium channels within dorsal root ganglia neurons in inflammatory pain. Pain 108:237-247.

Blair NT, Bean BP (2002) Roles of tetrodotoxin (TTX)-sensitive Na+ current, TTX-resistant Na+ current, and Ca2+ current in the action potentials of nociceptive sensory neurons. J Neurosci 22:10277-10290.

Bogen O, Dreger M, Gillen C, Schroder W, Hucho F (2005) Identification of versican as an isolectin B4-binding glycoprotein from mammalian spinal cord tissue. FEBS J 272:1090-1102.

Brederson JD, Kym PR, Szallasi A (2013) Targeting TRP channels for pain relief. European journal of pharmacology.

Burgess PR, Perl ER (1967) Myelinated afferent fibres responding specifically to noxious stimulation of the skin. The Journal of physiology 190:541-562.

Castagna M, Takai Y, Kaibuchi K, Sano K, Kikkawa U, Nishizuka Y (1982) Direct activation of calcium-activated, phospholipid-dependent protein kinase by tumor-promoting phorbol esters. J Biol Chem 257:7847-7851.

Caterina MJ, Leffler A, Malmberg AB, Martin WJ, Trafton J, Petersen-Zeitz KR, Koltzenburg M, Basbaum AI, Julius D (2000) Impaired nociception and pain sensation in mice lacking the capsaicin receptor. Science 288:306-313.

Caterina MJ, Schumacher MA, Tominaga M, Rosen TA, Levine JD, Julius D (1997) The capsaicin receptor: a heat-activated ion channel in the pain pathway. Nature 389:816-824.

Cavanaugh DJ, Lee H, Lo L, Shields SD, Zylka MJ, Basbaum AI, Anderson DJ (2009) Distinct subsets of unmyelinated primary sensory fibers mediate behavioral responses to noxious thermal and mechanical stimuli. Proc Natl Acad Sci U S A 106:9075-9080.

Chaban V, Li J, McDonald JS, Rapkin A, Micevych P (2011) Estradiol attenuates the adenosine triphosphate-induced increase of intracellular calcium through group II metabotropic glutamate receptors in rat dorsal root ganglion neurons. Journal of neuroscience research 89:1707-1710.

Cholewinski A, Burgess GM, Bevan S (1993) The role of calcium in capsaicin-induced desensitization in rat cultured dorsal root ganglion neurons. Neuroscience 55:1015-1023.

Chou MZ, Mtui T, Gao YD, Kohler M, Middleton RE (2004) Resiniferatoxin binds to the capsaicin receptor (TRPV1) near the extracellular side of the S4 transmembrane domain. Biochemistry 43:2501-2511.

Chuang HH, Prescott ED, Kong H, Shields S, Jordt SE, Basbaum AI, Chao MV, Julius D (2001) Bradykinin and nerve growth factor release the capsaicin receptor from PtdIns(4,5)P2-mediated inhibition. Nature 411:957-962.

Clapham DE (2003) TRP channels as cellular sensors. Nature 426:517-524.

Corey DP (2003) New TRP channels in hearing and mechanosensation. Neuron 39:585-588.

Cosens DJ, Manning A (1969) Abnormal electroretinogram from a Drosophila mutant. Nature 224:285-287.

Costigan M, Scholz J, Woolf CJ (2009) Neuropathic pain: a maladaptive response of the nervous system to damage. Annual review of neuroscience 32:1-32.

Cox JJ, Reimann F, Nicholas AK, Thornton G, Roberts E, Springell K, Karbani G, Jafri H, Mannan J, Raashid Y, Al-Gazali L, Hamamy H, Valente EM, Gorman S, Williams R, McHale DP, Wood JN, Gribble FM, Woods CG (2006) An SCN9A channelopathy causes congenital inability to experience pain. Nature 444:894-898.

Dai Y, Iwata K, Fukuoka T, Kondo E, Tokunaga A, Yamanaka H, Tachibana T, Liu Y, Noguchi K (2002) Phosphorylation of extracellular signal-regulated kinase in primary afferent neurons by noxious stimuli and its involvement in peripheral sensitization. J Neurosci 22:7737-7745.

Damann N, Voets T, Nilius B (2008) TRPs in our senses. Current biology : CB 18:R880-889.

Davis JB, Gray J, Gunthorpe MJ, Hatcher JP, Davey PT, Overend P, Harries MH, Latcham J, Clapham C, Atkinson K, Hughes SA, Rance K, Grau E, Harper AJ, Pugh PL, Rogers DC, Bingham S, Randall A, Sheardown SA (2000) Vanilloid receptor-1 is essential for inflammatory thermal hyperalgesia. Nature 405:183-187.

Dib-Hajj SD, Cummins TR, Black JA, Waxman SG (2010) Sodium channels in normal and pathological pain. Annual review of neuroscience 33:325-347.

Dickenson AH, Dray A (1991) Selective antagonism of capsaicin by capsazepine: evidence for a spinal receptor site in capsaicin-induced antinociception. British journal of pharmacology 104:1045-1049.

Djouhri L, Fang X, Okuse K, Wood JN, Berry CM, Lawson SN (2003) The TTX-resistant sodium channel Nav1.8 (SNS/PN3): expression and correlation with membrane properties in rat nociceptive primary afferent neurons. The Journal of physiology 550:739-752.

Dray A (2003) Novel molecular targets in pain control. Current opinion in anaesthesiology 16:521-525.

Dubin AE, Patapoutian A (2010) Nociceptors: the sensors of the pain pathway. The Journal of clinical investigation 120:3760-3772.

Eto K, Ishikawa T, Sun Kwang K, Nabekura J (2013) [Mechanisms of neural circuit remodeling in the primary somatosensory cortex in mouse models of chronic pain]. Brain and nerve = Shinkei kenkyu no shinpo 65:623-633.

Ferrari LF, Bogen O, Levine JD (2010) Nociceptor subpopulations involved in hyperalgesic priming. Neuroscience 165:896-901.

Ferrari LF, Bogen O, Levine JD (2013) Role of Nociceptor alphaCaMKII in Transition from Acute to Chronic Pain (Hyperalgesic Priming) in Male and Female Rats. J Neurosci 33:11002-11011.

Fields HL (1989) Pain modulation: opiates and chronic pain. NIDA research monograph 95:92-101.

Fieldsen D, Wood S (2011) Dealing with phantom limb pain after amputation. Nursing times 107:21-23.

Flor H, Diers M, Andoh J (2013) The neural basis of phantom limb pain. Trends in cognitive sciences 17:307-308.

Fox CH, Johnson FB, Whiting J, Roller PP (1985) Formaldehyde fixation. J Histochem Cytochem 33:845-853.

Fullmer JM, Riedl M, Williams FG, Sandrin M, Elde R (2007) Enzymes that synthesize the IB4 epitope are not sufficient to impart IB4 binding in dorsal root ganglia of rat. The Journal of comparative neurology 501:70-82.

Gao YJ, Ji RR (2009) c-Fos and pERK, which is a better marker for neuronal activation and central sensitization after noxious stimulation and tissue injury? The open pain journal 2:11-17.

Garcia-Sanz N, Fernandez-Carvajal A, Morenilla-Palao C, Planells-Cases R, Fajardo-Sanchez E, Fernandez-Ballester G, Ferrer-Montiel A (2004) Identification of a tetramerization domain in the C terminus of the vanilloid receptor. J Neurosci 24:5307-5314.

Garrison SR, Weyer AD, Barabas ME, Beutler BA, Stucky CL (2014) A gain-of-function voltage-gated sodium channel 1.8 mutation drives intense hyperexcitability of A- and C-fiber neurons. Pain 155:896-905.

Gees M, Alpizar YA, Boonen B, Sanchez A, Everaerts W, Segal A, Xue F, Janssens A, Owsianik G, Nilius B, Voets T, Talavera K (2013) Mechanisms of TRPV1 Activation and Sensitization by Allyl Isothiocyanate. Molecular pharmacology.

Goswami C (2010) Structural and functional regulation of growth cone, filopodia and synaptic sites by TRPV1. Communicative & integrative biology 3:614-618.

Graham FL, Smiley J, Russell WC, Nairn R (1977) Characteristics of a human cell line transformed by DNA from human adenovirus type 5. J Gen Virol 36:59-74.

Grynkiewicz G, Poenie M, Tsien RY (1985) A new generation of Ca2+ indicators with greatly improved fluorescence properties. J Biol Chem 260:3440-3450.

Handwerker HO, Kilo S, Reeh PW (1991) Unresponsive afferent nerve fibres in the sural nerve of the rat. The Journal of physiology 435:229-242.

Hasenauer J, Waldherr S, Doszczak M, Radde N, Scheurich P, Allgower F (2011) Identification of models of heterogeneous cell populations from population snapshot data. BMC bioinformatics 12:125.

Hendrich J, Alvarez P, Joseph EK, Chen X, Bogen O, Levine JD (2013) Electrophysiological correlates of hyperalgesic priming in vitro and in vivo. Pain 154:2207-2215.

Hirth M, Rukwied R, Gromann A, Turnquist B, Weinkauf B, Francke K, Albrecht P, Rice F, Hagglof B, Ringkamp M, Engelhardt M, Schultz C, Schmelz M, Obreja O (2013) Nerve growth factor induces sensitization of nociceptors without evidence for increased intraepidermal nerve fiber density. Pain 154:2500-2511.

Hiura A, Nakae Y, Nakagawa H (2002) Cell death of primary afferent nerve cells in neonatal mice treated with capsaicin. Anatomical science international 77:47-50.

Hoffman EM, Schechter R, Miller KE (2010) Fixative Composition Alters Distributions of Immunoreactivity for Glutaminase and Two Markers of Nociceptive Neurons, Na(v)1.8 and TRPV1, in the Rat Dorsal Root Ganglion. J Histochem Cytochem 58:329-344.

Huang J, Zhang X, McNaughton PA (2006) Modulation of temperature-sensitive TRP channels. Seminars in cell & developmental biology 17:638-645.

Huang YA, Maruyama Y, Stimac R, Roper SD (2008) Presynaptic (Type III) cells in mouse taste buds sense sour (acid) taste. The Journal of physiology 586:2903-2912.

Hucho T, Levine JD (2007) Signaling pathways in sensitization: toward a nociceptor cell biology. Neuron 55:365-376.

Hucho TB, Dina OA, Levine JD (2005) Epac mediates a cAMP-to-PKC signaling in inflammatory pain: an isolectin B4(+) neuron-specific mechanism. J Neurosci 25:6119-6126.

Hudson LJ, Bevan S, Wotherspoon G, Gentry C, Fox A, Winter J (2001) VR1 protein expression increases in undamaged DRG neurons after partial nerve injury. The European journal of neuroscience 13:2105-2114.

Isensee J, Diskar M, Waldherr S, Buschow R, Hasenauer J, Prinz A, Allgower F, Herberg FW, Hucho T (2014) Pain modulators regulate the dynamics of PKA-RII phosphorylation in subgroups of sensory neurons. Journal of cell science 127:216-229.

Ito N, Ruegg UT, Kudo A, Miyagoe-Suzuki Y, Takeda S (2013) Activation of calcium signaling through Trpv1 by nNOS and peroxynitrite as a key trigger of skeletal muscle hypertrophy. Nature medicine 19:101-106.

Iwasaki Y, Morita A, Iwasawa T, Kobata K, Sekiwa Y, Morimitsu Y, Kubota K, Watanabe T (2006) A nonpungent component of steamed ginger--[10]-shogaol--increases adrenaline secretion via the activation of TRPV1. Nutritional neuroscience 9:169-178.

Jeftinija S, Liu F, Jeftinija K, Urban L (1992) Effect of capsaicin and resiniferatoxin on peptidergic neurons in cultured dorsal root ganglion. Regulatory peptides 39:123-135.

Jeske NA, Diogenes A, Ruparel NB, Fehrenbacher JC, Henry M, Akopian AN, Hargreaves KM (2008) A-kinase anchoring protein mediates TRPV1 thermal hyperalgesia through PKA phosphorylation of TRPV1. Pain 138:604-616.

Jeske NA, Patwardhan AM, Ruparel NB, Akopian AN, Shapiro MS, Henry MA (2009) A-kinase anchoring protein 150 controls protein kinase C-mediated phosphorylation and sensitization of TRPV1. Pain 146:301-307.

Jeske NA, Por ED, Belugin S, Chaudhury S, Berg KA, Akopian AN, Henry MA, Gomez R (2011) A-kinase anchoring protein 150 mediates transient receptor potential family V type 1 sensitivity to phosphatidylinositol-4,5-bisphosphate. J Neurosci 31:8681-8688.

Jessell TM (2000) Neuronal specification in the spinal cord: inductive signals and transcriptional codes. Nature reviews Genetics 1:20-29.

Ji RR, Samad TA, Jin SX, Schmoll R, Woolf CJ (2002) p38 MAPK activation by NGF in primary sensory neurons after inflammation increases TRPV1 levels and maintains heat hyperalgesia. Neuron 36:57-68.

Jiang M, Chen G (2009) Ca2+ regulation of dynamin-independent endocytosis in cortical astrocytes. J Neurosci 29:8063-8074.

Jimenez-Andrade JM, Bloom AP, Stake JI, Mantyh WG, Taylor RN, Freeman KT, Ghilardi JR, Kuskowski MA, Mantyh PW (2010) Pathological sprouting of adult nociceptors in chronic prostate cancer-induced bone pain. J Neurosci 30:14649-14656.

Jin HW, Ichikawa H, Fujita M, Yamaai T, Mukae K, Nomura K, Sugimoto T (2005) Involvement of caspase cascade in capsaicin-induced apoptosis of dorsal root ganglion neurons. Brain research 1056:139-144.

Johansen JP, Fields HL (2004) Glutamatergic activation of anterior cingulate cortex produces an aversive teaching signal. Nature neuroscience 7:398-403.

Jordt SE, Tominaga M, Julius D (2000) Acid potentiation of the capsaicin receptor determined by a key extracellular site. Proc Natl Acad Sci U S A 97:8134-8139.

Jow F, He L, Kramer A, Hinson J, Bowlby MR, Dunlop J, Wang K (2006) Validation of DRG-like F11 cells for evaluation of KCNQ/M-channel modulators. Assay Drug Dev Technol 4:49-56.

Julius D, Basbaum AI (2001) Molecular mechanisms of nociception. Nature 413:203-210.

Jung J, Shin JS, Lee SY, Hwang SW, Koo J, Cho H, Oh U (2004) Phosphorylation of vanilloid receptor 1 by Ca2+/calmodulin-dependent kinase II regulates its vanilloid binding. J Biol Chem 279:7048-7054.

Kashiba H, Senba E (1999) Up- and down-regulation of BDNF mRNA in distinct subgroups of rat sensory neurons after axotomy. Neuroreport 10:3561-3565.

Kedei N, Szabo T, Lile JD, Treanor JJ, Olah Z, Iadarola MJ, Blumberg PM (2001) Analysis of the native quaternary structure of vanilloid receptor 1. J Biol Chem 276:28613-28619.

Kessler W, Kirchhoff C, Reeh PW, Handwerker HO (1992) Excitation of cutaneous afferent nerve endings in vitro by a combination of inflammatory mediators and conditioning effect of substance P. Experimental brain research Experimentelle Hirnforschung Experimentation cerebrale 91:467-476.

Kidd BL, Urban LA (2001) Mechanisms of inflammatory pain. British journal of anaesthesia 87:3-11.

Kim S, Kang C, Shin CY, Hwang SW, Yang YD, Shim WS, Park MY, Kim E, Kim M, Kim BM, Cho H, Shin Y, Oh U (2006) TRPV1 recapitulates native capsaicin receptor in sensory neurons in association with Fas-associated factor 1. J Neurosci 26:2403-2412.

Kishimoto E, Naito Y, Handa O, Okada H, Mizushima K, Hirai Y, Nakabe N, Uchiyama K, Ishikawa T, Takagi T, Yagi N, Kokura S, Yoshida N, Yoshikawa T (2011) Oxidative stress-induced posttranslational modification of TRPV1 expressed in esophageal epithelial cells. American journal of physiology Gastrointestinal and liver physiology 301:G230-238.

Kitaguchi T, Swartz KJ (2005) An inhibitor of TRPV1 channels isolated from funnel Web spider venom. Biochemistry 44:15544-15549.

Klug S, Anderer P, Saletu-Zyhlarz G, Freidl M, Saletu B, Prause W, Aigner M (2011) Dysfunctional pain modulation in somatoform pain disorder patients. European archives of psychiatry and clinical neuroscience 261:267-275.

Knight ZA, Tan K, Birsoy K, Schmidt S, Garrison JL, Wysocki RW, Emiliano A, Ekstrand MI, Friedman JM (2012) Molecular profiling of activated neurons by phosphorylated ribosome capture. Cell 151:1126-1137.

Knoch D, Pascual-Leone A, Meyer K, Treyer V, Fehr E (2006) Diminishing reciprocal fairness by disrupting the right prefrontal cortex. Science 314:829-832.

Kobayashi K, Fukuoka T, Obata K, Yamanaka H, Dai Y, Tokunaga A, Noguchi K (2005) Distinct expression of TRPM8, TRPA1, and TRPV1 mRNAs in rat primary afferent neurons with adelta/c-fibers and colocalization with trk receptors. The Journal of comparative neurology 493:596-606.

Kubista M, Akerman B, Norden B (1987) Characterization of interaction between DNA and 4',6-diamidino-2-phenylindole by optical spectroscopy. Biochemistry 26:4545-4553.

Laird JM, Souslova V, Wood JN, Cervero F (2002) Deficits in visceral pain and referred hyperalgesia in Nav1.8 (SNS/PN3)-null mice. J Neurosci 22:8352-8356.

Latremoliere A, Woolf CJ (2009) Central sensitization: a generator of pain hypersensitivity by central neural plasticity. The journal of pain : official journal of the American Pain Society 10:895-926.

Lau SY, Procko E, Gaudet R (2012) Distinct properties of Ca2+-calmodulin binding to N- and C-terminal regulatory regions of the TRPV1 channel. The Journal of general physiology 140:541-555.

Lazic SE (2010) The problem of pseudoreplication in neuroscientific studies: is it affecting your analysis? BMC neuroscience 11:5.

Lev S, Katz B, Minke B (2012) The activity of the TRP-like channel depends on its expression system. Channels 6:86-93.

Lewin GR, Mendell LM (1993) Nerve growth factor and nociception. Trends in neurosciences 16:353-359.

Lewin GR, Moshourab R (2004) Mechanosensation and pain. Journal of neurobiology 61:30-44.

Lewin GR, Ritter AM, Mendell LM (1993) Nerve growth factor-induced hyperalgesia in the neonatal and adult rat. J Neurosci 13:2136-2148.

Li F, Obrosova IG, Abatan O, Tian D, Larkin D, Stuenkel EL, Stevens MJ (2005) Taurine replacement attenuates hyperalgesia and abnormal calcium signaling in sensory neurons of STZ-D rats. American journal of physiology Endocrinology and metabolism 288:E29-36.

Lin W, Margolskee R, Donnert G, Hell SW, Restrepo D (2007) Olfactory neurons expressing transient receptor potential channel M5 (TRPM5) are involved in sensing semiochemicals. Proc Natl Acad Sci U S A 104:2471-2476.

Liu J, Liu X, Duan K, Zhang Y, Guo SW (2012) The expression and functionality of transient receptor potential vanilloid 1 in ovarian endometriomas. Reproductive sciences 19:1110-1124.

Liu L, Shenoy M, Pasricha PJ (2011) Substance P and calcitonin gene related peptide mediate pain in chronic pancreatitis and their expression is driven by nerve growth factor. JOP : Journal of the pancreas 12:389-394.

Liu T, Ji RR (2013) New insights into the mechanisms of itch: are pain and itch controlled by distinct mechanisms? Pflugers Archiv : European journal of physiology.

Lizanecz E, Bagi Z, Pasztor ET, Papp Z, Edes I, Kedei N, Blumberg PM, Toth A (2006) Phosphorylation-dependent desensitization by anandamide of vanilloid receptor-1 (TRPV1) function in rat skeletal muscle arterioles and in Chinese hamster ovary cells expressing TRPV1. Molecular pharmacology 69:1015-1023.

Loeser JD, Treede RD (2008) The Kyoto protocol of IASP Basic Pain Terminology. Pain 137:473-477.

Macpherson LJ, Geierstanger BH, Viswanath V, Bandell M, Eid SR, Hwang S, Patapoutian A (2005) The pungency of garlic: activation of TRPA1 and TRPV1 in response to allicin. Current biology : CB 15:929-934.

Maggi CA, Meli A (1988) The sensory-efferent function of capsaicin-sensitive sensory neurons. General pharmacology 19:1-43.

Magrinelli F, Zanette G, Tamburin S (2013) Neuropathic pain: diagnosis and treatment. Practical neurology.

Manchikanti L, Singh V (2004) Managing phantom pain. Pain physician 7:365-375.

Mandadi S, Roufogalis BD (2008) ThermoTRP channels in nociceptors: taking a lead from capsaicin receptor TRPV1. Current neuropharmacology 6:21-38.

Mandadi S, Tominaga T, Numazaki M, Murayama N, Saito N, Armati PJ, Roufogalis BD, Tominaga M (2006) Increased sensitivity of desensitized TRPV1 by PMA occurs through PKCepsilon-mediated phosphorylation at S800. Pain 123:106-116.

McCoy ES, Taylor-Blake B, Street SE, Pribisko AL, Zheng J, Zylka MJ (2013) Peptidergic CGRPalpha primary sensory neurons encode heat and itch and tonically suppress sensitivity to cold. Neuron 78:138-151.

McNamara FN, Randall A, Gunthorpe MJ (2005) Effects of piperine, the pungent component of black pepper, at the human vanilloid receptor (TRPV1). British journal of pharmacology 144:781-790.

Meggio F, Donella Deana A, Ruzzene M, Brunati AM, Cesaro L, Guerra B, Meyer T, Mett H, Fabbro D, Furet P, et al. (1995) Different susceptibility of protein kinases to staurosporine inhibition. Kinetic studies and molecular bases for the resistance of protein kinase CK2. European journal of biochemistry / FEBS 234:317-322.

Melyan Z, Tarttelin EE, Bellingham J, Lucas RJ, Hankins MW (2005) Addition of human melanopsin renders mammalian cells photoresponsive. Nature 433:741-745.

Meng J, Ovsepian SV, Wang J, Pickering M, Sasse A, Aoki KR, Lawrence GW, Dolly JO (2009) Activation of TRPV1 mediates calcitonin gene-related peptide release, which excites trigeminal sensory neurons and is attenuated by a retargeted botulinum toxin with anti-nociceptive potential. J Neurosci 29:4981-4992.

Menozzi-Smarrito C, Riera CE, Munari C, Le Coutre J, Robert F (2009) Synthesis and evaluation of new alkylamides derived from alpha-hydroxysanshool, the pungent molecule in szechuan pepper. Journal of agricultural and food chemistry 57:1982-1989.

Michailov GV, Sereda MW, Brinkmann BG, Fischer TM, Haug B, Birchmeier C, Role L, Lai C, Schwab MH, Nave KA (2004) Axonal neuregulin-1 regulates myelin sheath thickness. Science 304:700-703.

Miller RJ (1991) The control of neuronal Ca2+ homeostasis. Progress in neurobiology 37:255-285.

Min JW, Liu WH, He XH, Peng BW (2013) Different types of toxins targeting TRPV1 in pain. Toxicon : official journal of the International Society on Toxinology 71:66-75.

Mohapatra DP, Nau C (2003) Desensitization of capsaicin-activated currents in the vanilloid receptor TRPV1 is decreased by the cyclic AMP-dependent protein kinase pathway. J Biol Chem 278:50080-50090.

Mohapatra DP, Nau C (2005) Regulation of Ca2+-dependent desensitization in the vanilloid receptor TRPV1 by calcineurin and cAMP-dependent protein kinase. J Biol Chem 280:13424-13432.

Nathan C (2002) Points of control in inflammation. Nature 420:846-852.

Neelands TR, Jarvis MF, Han P, Faltynek CR, Surowy CS (2005) Acidification of rat TRPV1 alters the kinetics of capsaicin responses. Molecular pain 1:28.

Nielsen CS, Stubhaug A, Price DD, Vassend O, Czajkowski N, Harris JR (2008) Individual differences in pain sensitivity: genetic and environmental contributions. Pain 136:21-29.

Nilius B, Talavera K, Owsianik G, Prenen J, Droogmans G, Voets T (2005) Gating of TRP channels: a voltage connection? The Journal of physiology 567:35-44.

Numazaki M, Tominaga M (2004) Nociception and TRP Channels. Current drug targets CNS and neurological disorders 3:479-485.

Numazaki M, Tominaga T, Toyooka H, Tominaga M (2002) Direct phosphorylation of capsaicin receptor VR1 by protein kinase Cepsilon and identification of two target serine residues. J Biol Chem 277:13375-13378.

Ohsawa M, Kamei J (1999) Role of intracellular calcium in thermal allodynia and hyperalgesia in diabetic mice. Brain research 833:278-281.

Opree A, Kress M (2000) Involvement of the proinflammatory cytokines tumor necrosis factor-alpha, IL-1 beta, and IL-6 but not IL-8 in the development of heat hyperalgesia: effects on heat-evoked calcitonin gene-related peptide release from rat skin. J Neurosci 20:6289-6293.

Orliac ML, Peroni RN, Abramoff T, Neuman I, Podesta EJ, Adler-Graschinsky E (2007) Increases in vanilloid TRPV1 receptor protein and CGRP content during endotoxemia in rats. European journal of pharmacology 566:145-152.

Osborne C (1983) Aristotle's De anima 3.2: how do we perceive that we see and hear? Classical quarterly 33:401-411.

Petrie CN, Smithson LJ, Crotty AM, Michalski B, Fahnestock M, Kawaja MD (2013) Overexpression of nerve growth factor by murine smooth muscle cells: role of the p75 neurotrophin receptor on sympathetic and sensory sprouting. The Journal of comparative neurology 521:2621-2643.

Petruska JC, Cooper BY, Gu JG, Rau KK, Johnson RD (2000) Distribution of P2X1, P2X2, and P2X3 receptor subunits in rat primary afferents: relation to population markers and specific cell types. Journal of chemical neuroanatomy 20:141-162.

Platika D, Boulos MH, Baizer L, Fishman MC (1985) Neuronal traits of clonal cell lines derived by fusion of dorsal root ganglia neurons with neuroblastoma cells. Proc Natl Acad Sci U S A 82:3499-3503.

Poli-Neto OB, Filho AA, Rosa e Silva JC, Barbosa Hde F, Candido Dos Reis FJ, Nogueira AA (2009) Increased capsaicin receptor TRPV1 in the peritoneum of women with chronic pelvic pain. The Clinical journal of pain 25:218-222.

Por ED, Samelson BK, Belugin S, Akopian AN, Scott JD, Jeske NA (2010) PP2B/calcineurin-mediated desensitization of TRPV1 does not require AKAP150. The Biochemical journal 432:549-556.

Prescott ED, Julius D (2003) A modular PIP2 binding site as a determinant of capsaicin receptor sensitivity. Science 300:1284-1288.

Price TJ, Flores CM (2007) Critical evaluation of the colocalization between calcitonin gene-related peptide, substance P, transient receptor potential vanilloid subfamily type 1 immunoreactivities, and isolectin B-4 binding in primary afferent neurons of the rat and mouse. Journal of Pain 8:263-272.

Puntambekar P, Van Buren J, Raisinghani M, Premkumar LS, Ramkumar V (2004) Direct interaction of adenosine with the TRPV1 channel protein. J Neurosci 24:3663-3671.

Rao CV, Wolf DM, Arkin AP (2002) Control, exploitation and tolerance of intracellular noise. Nature 420:231-237.

Riol-Blanco L, Ordovas-Montanes J, Perro M, Naval E, Thiriot A, Alvarez D, Paust S, Wood JN, von Andrian UH (2014) Nociceptive sensory neurons drive interleukin-23-mediated psoriasiform skin inflammation. Nature 510:157-161.

Romanovsky AA, Almeida MC, Garami A, Steiner AA, Norman MH, Morrison SF, Nakamura K, Burmeister JJ, Nucci TB (2009) The transient receptor potential vanilloid-1 channel in thermoregulation: a thermosensor it is not. Pharmacological reviews 61:228-261.

Rosenbaum T, Gordon-Shaag A, Munari M, Gordon SE (2004) Ca2+/calmodulin modulates TRPV1 activation by capsaicin. The Journal of general physiology 123:53-62.

Rush AM, Dib-Hajj SD, Liu S, Cummins TR, Black JA, Waxman SG (2006) A single sodium channel mutation produces hyper- or hypoexcitability in different types of neurons. Proc Natl Acad Sci U S A 103:8245-8250.

Ruth Isserlin GDB, Aled Edwards, Stephen Frye, Timothy Willson, Frank H. Yu (2011) The human genome and drug discovery after a decade. Roads (still) not taken. Nature (see arxive for extended online Version) 470.

Salazar H, Jara-Oseguera A, Hernandez-Garcia E, Llorente I, Arias O, II, Soriano-Garcia M, Islas LD, Rosenbaum T (2009) Structural determinants of gating in the TRPV1 channel. Nature structural & molecular biology 16:704-710.

Sanchez JF, Krause JE, Cortright DN (2001) The distribution and regulation of vanilloid receptor VR1 and VR1 5' splice variant RNA expression in rat. Neuroscience 107:373-381.

Sanz-Salvador L, Andres-Borderia A, Ferrer-Montiel A, Planells-Cases R (2012) Agonist- and Ca2+-dependent desensitization of TRPV1 channel targets the receptor to lysosomes for degradation. J Biol Chem 287:19462-19471.

Saria A, Martling CR, Theodorsson-Norheim E, Gamse R, Hua XY, Lundberg JM (1987) Coexisting peptides in capsaicin-sensitive sensory neurons: release and actions in the respiratory tract of the guinea-pig. Acta physiologica Hungarica 69:421-424.

Schnizler K, Shutov LP, Van Kanegan MJ, Merrill MA, Nichols B, McKnight GS, Strack S, Hell JW, Usachev YM (2008) Protein kinase A anchoring via AKAP150 is essential for TRPV1 modulation by forskolin and prostaglandin E2 in mouse sensory neurons. J Neurosci 28:4904-4917.

Sharif-Naeini R, Basbaum AI (2011) Targeting pain where it resides ... In the brain. Science translational medicine 3:65ps61.

Sharon N, Lis H (2004) History of lectins: from hemagglutinins to biological recognition molecules. Glycobiology 14:53R-62R.

Sherrington CS (1906) The integrative action of the nervous system. New York,: C. Scribner's sons.

Shmigol A, Verkhratsky A, Isenberg G (1995) Calcium-induced calcium release in rat sensory neurons. The Journal of physiology 489 (Pt 3):627-636.

Snider WD, McMahon SB (1998) Tackling pain at the source: new ideas about nociceptors. Neuron 20:629-632.

Song J, Lee JH, Lee SH, Park KA, Lee WT, Lee JE (2013) TRPV1 Activation in Primary Cortical Neurons Induces Calcium-Dependent Programmed Cell Death. Experimental neurobiology 22:51-57.

Starr CJ, Sawaki L, Wittenberg GF, Burdette JH, Oshiro Y, Quevedo AS, Coghill RC (2009) Roles of the insular cortex in the modulation of pain: insights from brain lesions. J Neurosci 29:2684-2694.

Staud R, Price DD, Janicke D, Andrade E, Hadjipanayis AG, Eaton WT, Kaplan L, Wallace MR (2011) Two novel mutations of SCN9A (Nav1.7) are associated with partial congenital insensitivity to pain. European journal of pain 15:223-230.

Staud R, Rodriguez ME (2006) Mechanisms of disease: pain in fibromyalgia syndrome. Nature clinical practice Rheumatology 2:90-98.

Steiner R, Steiner M (1938) Die zwölf sinne des menschen in ihrer beziehung zu imagination, inspiration und intuition. Dornach, 8. august 1920. Dornach, Schweiz,: Philosophisch-anthroposophischer verlag am Goetheanum.

Stenholm E, Bongenhielm U, Ahlquist M, Fried K (2002) VRl- and VRL-l-like immunoreactivity in normal and injured trigeminal dental primary sensory neurons of the rat. Acta odontologica Scandinavica 60:72-79.

Steuer R, Waldherr S, Sourjik V, Kollmann M (2011) Robust signal processing in living cells. PLoS computational biology 7:e1002218.

Storti B, Bizzarri R, Cardarelli F, Beltram F (2012) Intact microtubules preserve transient receptor potential vanilloid 1 (TRPV1) functionality through receptor binding. J Biol Chem 287:7803-7811.

Stucky CL, Lewin GR (1999) Isolectin B(4)-positive and -negative nociceptors are functionally distinct. J Neurosci 19:6497-6505.

Studer M, McNaughton PA (2010) Modulation of single-channel properties of TRPV1 by phosphorylation. The Journal of physiology 588:3743-3756.

Tee AR, Proud CG (2001) Staurosporine inhibits phosphorylation of translational regulators linked to mTOR. Cell death and differentiation 8:841-849.

Tominaga M (2008) [Capsaicin receptor TRPV1]. Brain and nerve = Shinkei kenkyu no shinpo 60:493-501.

Tominaga M, Caterina MJ, Malmberg AB, Rosen TA, Gilbert H, Skinner K, Raumann BE, Basbaum AI, Julius D (1998) The cloned capsaicin receptor integrates multiple pain-producing stimuli. Neuron 21:531-543.

Vaughn AH, Gold MS (2010) Ionic mechanisms underlying inflammatory mediator-induced sensitization of dural afferents. J Neurosci 30:7878-7888.

Veldhuis NA, Lew MJ, Abogadie FC, Poole DP, Jennings EA, Ivanusic JJ, Eilers H, Bunnett NW, McIntyre P (2012) N-glycosylation determines ionic permeability and desensitization of the TRPV1 capsaicin receptor. J Biol Chem 287:21765-21772.

Vellani V, Mapplebeck S, Moriondo A, Davis JB, McNaughton PA (2001) Protein kinase C activation potentiates gating of the vanilloid receptor VR1 by capsaicin, protons, heat and anandamide. The Journal of physiology 534:813-825.

Verderio C, Muzio L, Turola E, Bergami A, Novellino L, Ruffini F, Riganti L, Corradini I, Francolini M, Garzetti L, Maiorino C, Servida F, Vercelli A, Rocca M, Dalla Libera D, Martinelli V, Comi G, Martino G, Matteoli M, Furlan R (2012) Myeloid microvesicles are a marker and therapeutic target for neuroinflammation. Annals of neurology 72:610-624.

Voets T (2012) Quantifying and modeling the temperature-dependent gating of TRP channels. Reviews of physiology, biochemistry and pharmacology 162:91-119.

Voets T, Droogmans G, Wissenbach U, Janssens A, Flockerzi V, Nilius B (2004) The principle of temperature-dependent gating in cold- and heat-sensitive TRP channels. Nature 430:748-754.

Vriens J, Appendino G, Nilius B (2009) Pharmacology of vanilloid transient receptor potential cation channels. Molecular pharmacology 75:1262-1279.

Wang H, Wang DH, Galligan JJ (2010) P2Y2 receptors mediate ATP-induced resensitization of TRPV1 expressed by kidney projecting sensory neurons. American journal of physiology Regulatory, integrative and comparative physiology 298:R1634-1641.

Wang Y, Kedei N, Wang M, Wang QJ, Huppler AR, Toth A, Tran R, Blumberg PM (2004) Interaction between protein kinase Cmu and the vanilloid receptor type 1. J Biol Chem 279:53674-53682.

Ward NE, O'Brian CA (1992) Kinetic analysis of protein kinase C inhibition by staurosporine: evidence that inhibition entails inhibitor binding at a conserved region of the catalytic domain but not competition with substrates. Molecular pharmacology 41:387-392.

Winter J, Forbes CA, Sternberg J, Lindsay RM (1988) Nerve growth factor (NGF) regulates adult rat cultured dorsal root ganglion neuron responses to the excitotoxin capsaicin. Neuron 1:973-981.

Wood JN (2010) Nerve growth factor and pain. The New England journal of medicine 363:1572-1573.

Woolf CJ (2010) What is this thing called pain? The Journal of clinical investigation 120:3742-3744.

Yaksh TL, Farb DH, Leeman SE, Jessell TM (1979) Intrathecal capsaicin depletes substance P in the rat spinal cord and produces prolonged thermal analgesia. Science 206:481-483.

Yang JJ, Gawthrop A, Ye Y (2003) Obtaining site-specific calcium-binding affinities of calmodulin. Protein and peptide letters 10:331-345.

Yiangou Y, Birch R, Sangameswaran L, Eglen R, Anand P (2000) SNS/PN3 and SNS2/NaN sodium channel-like immunoreactivity in human adult and neonate injured sensory nerves. FEBS letters 467:249-252.

Zeilhofer HU, Kress M, Swandulla D (1997) Fractional Ca2+ currents through capsaicin- and proton-activated ion channels in rat dorsal root ganglion neurones. The Journal of physiology 503 (Pt 1):67-78.

Zhang X, Huang J, McNaughton PA (2005) NGF rapidly increases membrane expression of TRPV1 heat-gated ion channels. The EMBO journal 24:4211-4223.

Zhang X, Li L, McNaughton PA (2008) Proinflammatory mediators modulate the heat-activated ion channel TRPV1 via the scaffolding protein AKAP79/150. Neuron 59:450-461.

Zhou Y, Zhou ZS, Zhao ZQ (2001) PKC regulates capsaicin-induced currents of dorsal root ganglion neurons in rats. Neuropharmacology 41:601-608.

Zhu W, Oxford GS (2011) Differential gene expression of neonatal and adult DRG neurons correlates with the differential sensitization of TRPV1 responses to nerve growth factor. Neuroscience letters 500:192-196.

Zhu Y, Colak T, Shenoy M, Liu L, Pai R, Li C, Mehta K, Pasricha PJ (2011) Nerve growth factor modulates TRPV1 expression and function and mediates pain in chronic pancreatitis. Gastroenterology 141:370-377.

Zygmunt PM, Petersson J, Andersson DA, Chuang H, Sorgard M, Di Marzo V, Julius D, Hogestatt ED (1999) Vanilloid receptors on sensory nerves mediate the vasodilator action of anandamide. Nature 400:452-457.

8. Appendix

8.1 Trancriptome sequencing: Upregulated genes in TRPV1(+) DRG neurons

Rank	Symbol	Description	DMSO	RTX	FC	p-value
1	Cartpt	CART prepropeptide	702	78	8.94	3.72E-38
2	Iapp	islet amyloid polypeptide	449	60	7.54	4.64E-26
3	Crh	corticotropin releasing hormone	394	53	7.46	1.03E-23
4	Hal	histidine ammonia lyase	198	29	6.73	6.19E-13
5	Ptgdr	prostaglandin D receptor	291	59	4.98	1.98E-13
6	Ptgdrl	prostaglandin D receptor-like	396	81	4.87	2.73E-16
7	Nos1	nitric oxide synthase 1	677	147	4.61	3.28E-21
8	Slc16a12	solute carrier family 16, member 12	1269	275	4.61	7.39E-28
9	Mrgprd	MAS-related GPR, member D	2299	527	4.36	3.15E-31
10	Trpv1	transient receptor potential cation channel, subfamily V, member 1	14013	3446	4.07	1.40E-35
11	Mrgprx3	MAS-related GPR, member, X3	1919	499	3.84	1.65E-25
12	Lmx1a	LIM homeobox transcription factor 1 alpha	342	89	3.84	3.91E-11
13	Cldn16	claudin 16	80	21	3.77	4.14E-03
14	Gfra3	GDNF family receptor alpha 3	5060	1403	3.61	8.32E-28
15	Vom2r43	vomeronasal 2 receptor, 43; similar to putative pheromone receptor (Go-VN3); vomeronasal 2 receptor, 40; vomeronasal 2 receptor, 41; vomeronasal 2 receptor, 42	73	20	3.59	1.07E-02
16	Lpar3	lysophosphatidic acid receptor 3	1746	487	3.58	1.38E-22
17	Hprt1	hypoxanthine phosphoribosyltransferase 1	230	66	3.50	3.28E-07
18	Trpc4	transient receptor potential cation channel, subfamily C, member 4	210	62	3.37	2.07E-06
19	Pnmal1	paraneoplastic Ma antigen family-like 1	149	44	3.35	1.05E-04
20	Vwa5a	von Willebrand factor A domain containing 5A	920	280	3.29	1.01E-15
21	Tcf15	transcription factor 15	319	97	3.28	1.87E-08
22	Tac1	tachykinin 1	28731	8838	3.25	2.87E-26
23	Ewsr1	Ewing sarcoma breakpoint region 1	163	51	3.19	1.03E-04
24	Slc51a	solute carrier family 51, (orphan transporter)	789	247	3.19	4.98E-14
25	Zic5	Zic family member 5	1365	430	3.17	3.30E-17
26	Amdhd1	amidohydrolase domain containing 1; hypothetical protein LOC680706	432	142	3.04	3.34E-09
27	Nlrp4a	NLR family, pyrin domain containing 4	123	41	3.02	2.02E-03
28	LOC257642	rRNA promoter binding protein	6951	2320	3.00	3.62E-21
29	Vps37c	vacuolar protein sorting 37 homolog C (S. cerevisiae)	74	25	2.93	4.39E-02

30	Adcyap1	adenylate cyclase activating polypeptide 1 (pituitary)	2931	1011	2.90	4.68E-18
31	Slco1a5	solute carrier organic anion transporter family, member 1a5	75	26	2.89	4.52E-02
32	Kcnip1	Kv channel-interacting protein 1	3731	1305	2.86	2.85E-18
33	Rgs14	regulator of G-protein signaling 14	289	106	2.72	9.24E-06
34	Cd72	Cd72 molecule	292	108	2.72	8.52E-06
35	Ramp3	receptor (G protein-coupled) activity modifying protein 3	1826	673	2.71	2.79E-14
36	Aldh18a1	aldehyde dehydrogenase 18 damily member A1	131	49	2.69	6.17E-03
37	Rlim	ring finger protein, LIM domain interacting	137	53	2.57	8.45E-03
38	Chrna6	cholinergic receptor, nicotinic, alpha 6	4011	1567	2.56	7.43E-15
39	Kcnk2	potassium channel, subfamily K, member 2	1554	610	2.55	4.00E-12
40	Cpne5	copine V	528	210	2.52	2.50E-07
41	Tnni3k	TNNI3 interacting kinase	225	90	2.51	4.29E-04
42	Ipcef1	interactor protein for cytohesin exchange factors 1	183	74	2.47	2.29E-03
43	Kcnj5	potassium inwardly-rectifying channel, subfamily J, member 5	513	208	2.46	6.46E-07
44	Spata32	spermatogenesis associated 32	123	50	2.45	2.17E-02
45	Trpc3	transient receptor potential cation channel, subfamily C, member 3	2751	1139	2.42	2.37E-12
46	Rgs4	regulator of G-protein signaling 4	145775	60389	2.41	5.19E-15
47	Sepw1	selenoprotein W, 1	176	75	2.36	6.27E-03
48	Krt75	keratin 75	211	90	2.35	2.13E-03
49	Pfn2	profilin 2	315	134	2.35	1.44E-04
50	Foxs1	forkhead box S1	314	134	2.34	1.44E-04
51	Grik1	glutamate receptor, ionotropic, kainate 1	16513	7048	2.34	1.30E-13
52	Pfn2	profilin 2	289	126	2.30	4.47E-04
53	Rxfp1	relaxin/insulin-like family peptide receptor 1	175	77	2.29	9.41E-03
54	Impad1	inositol monophosphatase domain containing 1	424	187	2.27	3.91E-05
55	Acot4	acyl-CoA thioesterase 4	157	71	2.21	2.26E-02
56	Oprk1	opioid receptor, kappa 1	436	199	2.19	9.05E-05
57	Nnat	Neuronatin	5132	2348	2.19	1.47E-10
58	Gal	galanin prepropeptide	749	345	2.17	2.58E-06
59	C6	complement component 6	149	69	2.16	3.68E-02
60	Bex1	brain expressed gene 1	2100	973	2.16	8.79E-09
61	Fam70a	family with sequence similarity 70, member A	7838	3662	2.14	2.34E-10
62	Sstr1	somatostatin receptor 1	152	71	2.13	3.91E-02
63	Gnb4	guanine nucleotide binding protein	3399	1602	2.12	3.20E-09
64	Sh2d4a	SH2 domain containing 4A	490	231	2.12	9.86E-05

65	Kctd4	potassium channel tetramerisation domain containing 4	1027	485	2.12	8.78E-07
66	Xdh	xanthine dehydrogenase	2180	1033	2.11	2.42E-08
67	Pde9a	phosphodiesterase 9A	563	268	2.10	5.86E-05
68	Il7	interleukin 7	1188	570	2.09	8.51E-07
69	Clip3	CAP-GLY domain containing linker protein 3	380	183	2.08	7.86E-04
70	Kcnmb2	potassium large conductance calcium-activated channel, subfamily M, beta member 2	264	128	2.07	6.11E-03
71	Slc14a1	solute carrier family 14 (urea transporter), member 1	435	211	2.06	4.10E-04
72	Fam150b	family with sequence similarity 150, member B	307	149	2.05	3.07E-03
73	Hmx1	H6 family homeobox 1	781	385	2.03	2.48E-05
74	Mal2	mal, T-cell differentiation protein 2	1539	760	2.02	8.20E-07
75	Amigo2	adhesion molecule with Ig like domain 2	1853	920	2.01	5.11E-07
76	Dclk3	doublecortin-like kinase 3	230	115	2.01	1.60E-02
77	Ngb	Neuroglobin	656	328	2.00	1.01E-04
78	Armcx1	armadillo repeat containing, X-linked 1	264	133	1.99	1.21E-02
79	Cend1	cell cycle exit and neuronal differentiation 1	472	239	1.97	8.70E-04
80	Dpysl4	dihydropyrimidinase-like 4	14649	7455	1.97	2.44E-08
81	Ptpru	protein tyrosine phosphatase, receptor type, U	715	365	1.96	1.14E-04
82	Cd53	Cd53 molecule	2393	1233	1.94	1.01E-06
83	Kcna3	potassium voltage-gated channel, shaker-related subfamily, member 3	752	391	1.93	1.52E-04
84	Hnrnpab	heterogeneous nuclear ribonucleoprotein A/B	268	140	1.92	1.92E-02
85	Clic3	chloride intracellular channel 3	470	246	1.91	1.81E-03
86	Ptgir	prostaglandin I2 (prostacyclin) receptor	2799	1463	1.91	1.37E-06
87	Nt5e	5' nucleotidase, ecto	869	455	1.91	1.05E-04
88	P2rx3	purinergic receptor P2X, ligand-gated ion channel, 3	58261	30513	1.91	8.47E-08
89	Kcne3	potassium voltage-gated channel, Isk-related subfamily, gene 3	269	141	1.91	1.92E-02
90	Pcsk1n	proprotein convertase subtilisin/kexin type 1 inhibitor	3101	1639	1.89	2.06E-06
91	Npy5r	neuropeptide Y receptor Y5	454	241	1.88	3.07E-03
92	Drd2	dopamine receptor D2	1332	712	1.87	4.24E-05
93	Myl6l	myosin, light chain 6, alkali, smooth muscle and non-muscle; similar to Myosin light chain 1 slow a; myosin, light polypeptide 6, alkali, smooth muscle and non-muscle-like; myosin, light chain 6B, alkali, smooth muscle and non-muscle	259	139	1.87	3.01E-02
94	Vgf	VGF nerve growth factor inducible	7710	4138	1.86	8.71E-07

95	Lrrc55	leucine rich repeat containing 55	605	326	1.86	1.31E-03
96	Scml4	Sex comb on midleg-like protein 4	1712	931	1.84	3.75E-05
97	Ctxn3	cortexin 3	4000	2178	1.84	4.53E-06
98	Alk	anaplastic lymphoma kinase	3552	1950	1.82	8.52E-06
99	Plcxd3	phospholipase C, X domain containing 3	7510	4195	1.79	7.06E-06
100	Kcng1	potassium voltage-gated channel, subfamily G, member 1	797	446	1.79	1.16E-03
101	Hs6st2	heparan sulfate 6-O-sulfotransferase 2	3640	2060	1.77	3.44E-05
102	Ror2	receptor tyrosine kinase-like orphan receptor 2	411	233	1.77	1.62E-02
103	Galk1	galactokinase 1	2133	1208	1.77	1.01E-04
104	Cst12	cystatin 12	531	301	1.76	7.21E-03
105	Ccdc68	coiled-coil domain containing 68	1483	846	1.75	3.11E-04
106	Mycn	v-myc myelocytomatosis viral related oncogene, neuroblastoma derived (avian)	332	190	1.75	3.65E-02
107	Bfsp1	beaded filament structural protein 1, filensin	311	179	1.74	4.69E-02
108	Gpr68	G protein-coupled receptor 68	973	560	1.74	1.57E-03
109	Adcy5	adenylate cyclase 5	5116	2976	1.72	7.24E-05
110	Plcb3	phospholipase C, beta 3	26108	15207	1.72	2.95E-05
111	Ddah1	B-cell CLL/lymphoma 10; dimethylarginine dimethylaminohydrolase 1	1482	864	1.71	6.63E-04
112	Gfra2	GDNF family receptor alpha 2	7629	4492	1.70	8.52E-05
113	Kcnt1	potassium channel, subfamily T, member 1	5805	3420	1.70	1.03E-04
114	Rab27b	RAB27B, member RAS oncogene family	2330	1381	1.69	4.60E-04
115	Rab36	RAB36, member RAS oncogene family	750	445	1.69	7.29E-03
116	Klhl1	kelch-like 1	446	265	1.68	2.97E-02
117	Acpp	acid phosphatase	8049	4789	1.68	1.14E-04
118	Dgki	diacylglycerol kinase, iota	11870	7099	1.67	1.14E-04
119	Camk4	calcium/calmodulin-dependent protein kinase IV	1210	724	1.67	2.61E-03
120	Gna14	guanine nucleotide binding protein, alpha 14	17438	10457	1.67	1.14E-04
121	Ydjc	YdjC homolog (bacterial)	516	310	1.66	2.67E-02
122	Cbln4	cerebellin 4 precursor	1039	626	1.66	4.60E-03
123	Npy1r	neuropeptide Y receptor Y1	7289	4394	1.66	2.07E-04
124	Chrne	cholinergic receptor, nicotinic, epsilon	1538	930	1.65	2.07E-03
125	Fxyd2	FXYD domain-containing ion transport regulator 2	5659	3423	1.65	3.40E-04
126	Fam117a	family with sequence similarity 117, member A	782	474	1.65	1.10E-02
127	Calca	calcitonin/calcitonin-related polypeptide, alpha	71829	43554	1.65	1.45E-04
128	Rcan3	RCAN family member 3	864	525	1.64	9.51E-03
129	Celf6	Elav-like family member 6	3394	2066	1.64	6.91E-04

130	Slc5a7	solute carrier family 5 (orphan transporter), member 7	4960	3026	1.64	4.60E-04
131	Smim3	small integral membrane protein 3	1890	1154	1.64	2.01E-03
132	Fam89a	family with sequence similarity 89, member A	4278	2615	1.64	6.46E-04
133	Mt3	metallothionein 3	10422	6379	1.63	3.84E-04
134	Kcnc4	potassium voltage gated channel, Shaw-related subfamily, member 4	4873	2988	1.63	6.17E-04
135	Gpr35	G protein-coupled receptor 35	943	582	1.62	1.10E-02
136	Gpc5	glypican 5	2344	1447	1.62	1.98E-03
137	Tmeff1	transmembrane protein with EGF-like and two follistatin-like domains 1	3171	1958	1.62	1.29E-03
138	Slc7a4	solute carrier family 7 (orphan transporter), member 4	1068	661	1.62	9.03E-03
139	Fam43a	family with sequence similarity 43, member A	627	388	1.62	2.82E-02
140	Kcnf1	potassium voltage-gated channel, subfamily F, member 1	2390	1480	1.61	2.15E-03
141	Ina	internexin neuronal intermediate filament protein, alpha	6201	3849	1.61	8.39E-04
142	Synpr	Synaptoporin	33022	20508	1.61	4.47E-04
143	Kcnk18	potassium channel, subfamily K, member 18	1823	1133	1.61	3.67E-03
144	Lrrc3	leucine rich repeat containing 3	988	618	1.60	1.37E-02
145	Ptger3	prostaglandin E receptor 3 (subtype EP3)	853	534	1.60	1.92E-02
146	Paqr5	progestin and adipoQ receptor family member V	2824	1772	1.59	2.56E-03
147	S100a6	S100 calcium binding protein A6	15856	9973	1.59	9.24E-04
148	Lrrc2	leucine rich repeat containing 2	1309	824	1.59	9.87E-03
149	RGD1562284	predicted gene	695	438	1.59	3.15E-02
150	Pdxp	pyridoxal (pyridoxine, vitamin B6) phosphatase	4254	2688	1.58	2.15E-03
151	Slc37a1	solute carrier family 37 (glycerol-3-phosphate transporter), member 1	2243	1418	1.58	4.54E-03
152	Ssc5d	soluble scavenger receptor cysteine-rich domain-containing protein SSC5D precursor	919	583	1.58	2.17E-02
153	Gpr27	G protein-coupled receptor 27	1537	975	1.58	9.11E-03
154	Ldb2	LIM domain binding 2	9259	5898	1.57	1.81E-03
155	Slc39a3	solute carrier family 39 (zinc transporter), member 3	1243	793	1.57	1.47E-02
156	Mgat5b	mannosyl (alpha-1,6-)-glycoprotein beta-1,6-N-acetyl-glucosaminyltransferase, isozyme B	955	613	1.56	2.70E-02
157	Inpp5d	inositol polyphosphate-5-phosphatase D	3308	2131	1.55	5.26E-03
158	Dgkz	diacylglycerol kinase zeta	34884	22485	1.55	2.01E-03
159	Serpina11	serine (or cysteine) peptidase inhibitor, clade A (alpha-1 antiproteinase,	963	621	1.55	2.88E-02

		antitrypsin), member 9; serine (or cysteine) peptidase inhibitor, clade A (alpha-1 antiproteinase, antitrypsin), member 11; serine (or cysteine) peptidase inhibitor, clade A (alpha-1 antiproteinase, antitrypsin), member 12				
160	Adrbk2	adrenergic, beta, receptor kinase 2	1529	991	1.54	1.56E-02
161	Rspo2	R-spondin 2 homolog (Xenopus laevis)	1326	860	1.54	1.92E-02
162	Dusp26	dual specificity phosphatase 26 (putative)	7272	4726	1.54	4.12E-03
163	Nsg1	neuron specific gene family member 1	10593	6928	1.53	4.32E-03
164	Pkib	protein kinase (cAMP-dependent, catalytic) inhibitor beta	2060	1349	1.53	1.40E-02
165	Adam19	a disintegrin and metallopeptidase domain 19	23471	15368	1.53	3.75E-03
166	Ptprt	protein tyrosine phosphatase, receptor type, T	3009	1983	1.52	1.16E-02
167	Nqo1	NAD(P)H dehydrogenase, quinone 1	3864	2559	1.51	1.12E-02
168	Cacna1e	calcium channel, voltage-dependent, R type, alpha 1E subunit	1074	712	1.51	4.18E-02
169	Tspan8	tetraspanin 8	59688	39571	1.51	5.26E-03
170	Epha5	EphA5	7141	4737	1.51	8.07E-03
171	Kcnh6	potassium voltage-gated channel, subfamily H (eag-related), member 6	3243	2154	1.51	1.38E-02
172	Grik3	glutamate receptor, ionotropic, kainate 3	1188	789	1.51	3.75E-02
173	Cdh11	cadherin 11	21259	14140	1.50	6.57E-03
174	Celf4	Elav-like family member 4	3741	2492	1.50	1.33E-02
175	Eml5	echinoderm microtubule associated protein like 5	1121	749	1.50	4.69E-02
176	Pkig	protein kinase inhibitor, gamma	2721	1820	1.49	1.87E-02
177	Myt1	myelin transcription factor 1	4544	3041	1.49	1.34E-02
178	Tubb2b	tubulin, beta 2b	23000	15456	1.49	9.51E-03
179	Bdkrb2	bradykinin receptor B2	1556	1050	1.48	4.03E-02
180	Sytl3	synaptotagmin-like 3	1559	1053	1.48	4.07E-02
181	Nptx2	neuronal pentraxin 2	10848	7352	1.48	1.40E-02
182	Tmem164	transmembrane protein 164	8885	6027	1.47	1.47E-02
183	Serpinf1	serine (or cysteine) peptidase inhibitor, clade F, member 1	1863	1267	1.47	4.04E-02
184	Chn1	chimerin (chimaerin) 1	6203	4219	1.47	1.81E-02
185	Dync1i2	dynein cytoplasmic 1 intermediate chain 2	50050	34055	1.47	1.30E-02
186	Ppp1r2	rotein phosphatase 1, regulatory (inhibitor) subunit 2	114416	78009	1.47	1.31E-02
187	RGD1310110	predicted gene	8819	6016	1.47	1.74E-02
188	Dapk1	death associated protein kinase 1	8225	5611	1.47	1.80E-02
189	Syt5	synaptotagmin V	3009	2056	1.46	3.03E-02
190	Cib2	calcium and integrin binding family member 2	7892	5404	1.46	2.00E-02

191	Xylt2	xylosyltransferase II	5312	3643	1.46	2.43E-02
192	Ucp2	uncoupling protein 2 (mitochondrial, proton carrier)	4637	3181	1.46	2.60E-02
193	Gng2	guanine nucleotide binding protein	25095	17225	1.46	1.70E-02
194	Rgs10	regulator of G-protein signaling 10; Tia1 cytotoxic granule-associated RNA binding protein-like 1	10207	7010	1.46	2.01E-02
195	Fkbp1b	FK506 binding protein 1b	8318	5713	1.46	2.17E-02
196	Stk4	serine/threonine kinase 4	2120	1464	1.45	4.88E-02
197	Irf6	interferon regulatory factor 6	4365	3016	1.45	3.13E-02
198	Steap3	STEAP family member 3	5679	3924	1.45	2.88E-02
199	Lzts1	leucine zipper, putative tumor suppressor 1	3575	2474	1.45	3.70E-02
200	Anxa5	annexin A5	64634	44784	1.44	2.13E-02
201	Jup	junction plakoglobin	17363	12081	1.44	2.67E-02
202	Vstm5	V-set and transmembrane domain-containing protein 5	2774	1931	1.44	4.94E-02
203	Calcb	calcitonin-related polypeptide, beta	10342	7202	1.44	2.90E-02
204	Kcnd3	potassium voltage gated channel, Shal-related family, member 3	17914	12516	1.43	2.83E-02
205	Syt7	synaptotagmin VII	5988	4202	1.42	4.10E-02
206	Tmem45b	Transmembrane protein 45B	5750	4040	1.42	4.20E-02
207	Syt9	synaptotagmin IX	5110	3595	1.42	4.62E-02
208	Scn11a	sodium channel, voltage-gated, type XI, alpha	57106	40361	1.41	3.63E-02
209	Tmem151b	transmembrane protein 151B	8122	5743	1.41	4.52E-02
210	Ifi27	interferon, alpha-inducible protein 27	22082	15654	1.41	4.21E-02

Tab. 8.1.1. Up regulated genes in the TRPV1 positive subpopulation of rat dorsal root ganglia neurons Shown in the table are the enrichment rank, the gene name, a brief gene description, the average transcript read number from three technical replicates in the columns DMSO and RTX, a fold change (FC), and significance value calculated from single replicates. The data shown was generated in three independent technical experiments each based on 3 rats.

8.2 Tabular gene ontology results

Biological Process	Count	p-Value	Genes
negative regulation of bone resorption	4	8.6E-05	CALCA, IAPP, CARTPT, INPP5D
negative regulation of tissue remodeling	4	1.8E-04	CALCA, IAPP, CARTPT, INPP5D
regulation of bone resorption	4	5.3E-04	CALCA, IAPP, CARTPT, INPP5D
behavioral response to pain	3	8.4E-03	GRIK1, TRPV1, P2RX3
response to pain	5	1.9E-04	CALCA, GRIK1, TRPV1, P2RX3, TAC1
regulation of tissue remodeling	4	1.6E-03	CALCA, IAPP, CARTPT, INPP5D
negative regulation of homeostatic process	4	1.6E-03	CALCA, IAPP, CARTPT, INPP5D
positive regulation of amine transport	3	1.3E-02	GRIK1, DRD2, CARTPT
regulation of heart rate	4	3.0E-03	CALCA, DRD2, TAC1, FKBP1B
negative regulation of neurological system process	5	5.1E-04	CALCA, GRIK1, DRD2, GRIK3, NPY5R
negative regulation of ion transport	3	3.0E-02	CALCA, NOS1, DRD2
negative regulation of blood pressure	4	5.7E-03	CALCA, NOS1, DRD2, BDKRB2
multicellular organismal response to stress	6	2.4E-04	CALCA, NOS1, GRIK1, TRPV1, P2RX3, TAC1
feeding behavior	9	3.2E-06	CALCA, IAPP, DRD2, CRH, CARTPT, NPY1R, GAL, TCF15, NPY5R
Excretion	3	4.0E-02	PTGER3, TRPV1, DRD2
regulation of multicellular organism growth	6	1.3E-03	TRPV1, DRD2, NPY1R, PCSK1N, VGF, FOXS1
negative regulation of response to external stimulus	4	2.1E-02	SERPINF1, DRD2, CARTPT, NT5E
negative regulation of multicellular organ. Process	12	2.5E-06	CALCA, NOS1, GRIK1, IAPP, DRD2, GRIK3, TAC1, CARTPT, TSPAN8, INPP5D, ANXA5, NPY5R
muscle system process	7	9.9E-04	NOS1, TRPV1, DRD2, P2RX3, NPY1R, FKBP1B, MYL6L
regulation of homeostatic process	8	3.7E-04	CALCA, IAPP, DRD2, TAC1, CARTPT, INPP5D, DDAH1, FKBP1B
regulation of blood pressure	7	1.6E-03	CALCA, NOS1, DRD2, TAC1, CARTPT, BDKRB2, NPY1R
response to temperature stimulus	6	7.4E-03	CALCA, NOS1, TRPV1, P2RX3, PCSK1N, VGF
response to heat	4	4.8E-02	CALCA, NOS1, TRPV1, P2RX3
circulatory system process	8	2.4E-03	CALCA, CALCB, NOS1, DRD2, TAC1, CARTPT, BDKRB2, NPY1R
positive regulation of secretion	6	1.3E-02	GRIK1, DRD2, NNAT, CRH, TAC1, CARTPT
regulation of response to external stimulus	8	2.9E-03	CALCA, SERPINF1, DRD2, TAC1, CARTPT, TSPAN8, NT5E, NPY5R
negative regulation of response to stimulus	5	3.4E-02	SERPINF1, DRD2, CARTPT, INPP5D, NT5E

cellular chemical homeostasis	18	1.9E-06	PTGER3, GRIK1, DRD2, GRIK3, TAC1, LPAR3, NPY1R, BDKRB2, KCNIP1, FKBP1B, KCNMB2, CALCA, P2RX3, CARTPT, GNB4, CHRNA6, CHRNE, MT3
ion transport	30	7.1E-10	STEAP3, CLDN16, FXYD2, KCNC4, GRIK1, DRD2, TRPV1, GRIK3, KCNK18, KCNA3, FKBP1B, KCNIP1, KCNMB2, CHRNA6, SLC39A3, KCNE3, TRPC4, KCND3, PTGER3, TRPC3, KCNK2, SLCO1A5, KCNJ5, KCNT1, P2RX3, KCNH6, CACNA1E, SCN11A, SLC5A7, CHRNE
regulation of system process	14	9.9E-05	NOS1, LZTS1, GRIK1, DRD2, GRIK3, TAC1, NPY1R, VGF, FKBP1B, NPY5R, CALCA, P2RX3, CRH, CARTPT
negative regulation of cell communication	10	1.6E-03	RGS10, GRIK1, DRD2, GRIK3, RGS4, DGKZ, ADRBK2, INPP5D, RGS14, NPY5R
regulation of cellular localization	12	4.3E-04	NOS1, DRD2, PKIG, NNAT, CRH, SYT9, CARTPT, CHRNA6, SYT7, NPY1R, RAB27B, NPY5R
negative regulation of transport	6	2.5E-02	CALCA, NOS1, DRD2, PKIG, NPY1R, NPY5R
regulation of transport	19	7.4E-06	TRPC4, NOS1, GRIK1, DRD2, PKIG, NNAT, TAC1, SYT9, LPAR3, NPY1R, SYT7, FKBP1B, NPY5R, CALCA, CRH, CARTPT, CHRNA6, RAB27B, KCNE3
regulation of growth	11	2.8E-03	FXYD2, IL7, TRPV1, DRD2, CD53, NPY1R, LMX1A, PCSK1N, VGF, FOXS1, MT3
cell-cell adhesion	8	1.5E-02	JUP, CALCA, CLDN16, AMIGO2, ROR2, PTPRT, PTPRU, CDH11
positive regulation of multicellular organ. Process	9	9.3E-03	CALCA, NOS1, GRIK1, TRPV1, DRD2, TAC1, CARTPT, NPY1R, FOXS1
Secretion	9	1.4E-02	PTGER3, SYT5, TRPV1, DRD2, CARTPT, BDKRB2, SYTL3, VGF, FKBP1B
homeostatic process	24	9.4E-06	XDH, SEPW1, PTGER3, GRIK1, DRD2, IL7, TRPV1, GRIK3, LPAR3, TAC1, NPY1R, BDKRB2, VGF, KCNIP1, FKBP1B, KCNMB2, CALCA, P2RX3, CARTPT, GNB4, CACNA1E, CHRNA6, CHRNE, MT3
cell-cell signaling	11	5.7E-03	GRIK1, CAMK4, DRD2, GRIK3, P2RX3, TAC1, CARTPT, SLC5A7, VGF, FKBP1B, NPY5R
regulation of localization	20	1.3E-04	TRPC4, NOS1, GRIK1, DRD2, PKIG, NNAT, TAC1, SYT9, LPAR3, NPY1R, PTPRU, SYT7, FKBP1B, NPY5R, CALCA, CRH, CARTPT, CHRNA6, RAB27B, KCNE3
regulation of multicellular organismal process	28	2.9E-05	XDH, LZTS1, GRIK1, DRD2, TRPV1, GRIK3, BEX1, TAC1, TSPAN8, VGF, FKBP1B, FOXS1, CALCA, IAPP, INPP5D, DDAH1, MT3, NOS1, IL7, LMX1A, NPY1R, ANXA5, NPY5R, SERPINF1, P2RX3, CRH, CARTPT, PCSK1N
regulation of catalytic activity	19	1.1E-03	PTGER3, NOS1, RXFP1, DRD2, IL7, ADCY5, C6, PKIG, LPAR3, PKIB, DGKI, FKBP1B, ADCYAP1, CALCA, PPP1R2, DGKZ, CARTPT, GNB4, NQO1
regulation of cell communication	26	1.2E-04	LZTS1, GRIK1, DRD2, GRIK3, NNAT, ADRBK2, SYT9, TAC1, LPAR3, SYT7, VGF, RGS10, INPP5D, DDAH1, RAMP3, NOS1, DGKI, NPY1R, NPY5R, RGS14, PPP1R2, P2RX3, RGS4, CRH, CARTPT, DGKZ
regulation of response to stimulus	12	1.6E-02	CALCA, SERPINF1, DRD2, C6, TAC1, CARTPT, TSPAN8, INPP5D, GAL, DDAH1, NT5E, NPY5R
positive regulation of cell death	9	4.5E-02	STEAP3, C6, CRH, INPP5D, NQO1, GAL, DDAH1, STK4, DAPK1
response to wounding	11	2.8E-02	INA, CALCA, PTGER3, TRPV1, DRD2, C6, CRH, TAC1, SYT7, ANXA5, GAL
positive regulation of molecular function	13	1.7E-02	PTGER3, RXFP1, DRD2, C6, ADCY5, LPAR3, DGKI, ADCYAP1, CALCA, DGKZ, CARTPT, GNB4, DDAH1
signal transduction	40	6.3E-06	GNA14, DRD2, ADCY5, OPRK1, LPAR3, ADRBK2, BDKRB2,

			CALCA, PTGIR, PLCB3, GPR27, DCLK3, GNG2, INPP5D, RAB27B, DDAH1, PTGER3, RXFP1, PTGDRL, PKIG, MRGPRD, DGKI, NPY1R, RCAN3, STK4, RGS14, NPY5R, DAPK1, VOM2R43, GPR35, CAMK4, RAB36, SSTR1, PTGDR, KCNH6, CHN1, ROR2, CARTPT, DGKZ, GNB4, PDE9A
negative regulation of biological process	36	1.6E-04	HMX1, GRIK1, DRD2, GRIK3, BEX1, TAC1, ADRBK2, TSPAN8, BDKRB2, FKBP1B, ADCYAP1, CALCA, RGS10, IAPP, INPP5D, DDAH1, NT5E, MT3, HNRNPAB, NOS1, IL7, PKIG, PTPRU, LMX1A, NPY1R, ANXA5, GAL, RGS14, NPY5R, DAPK1, AMIGO2, SERPINF1, IRF6, RGS4, CARTPT, DGKZ
Transport	47	1.3E-05	STEAP3, CLDN16, FXYD2, KCNC4, GRIK1, TRPV1, SYT5, DRD2, GRIK3, KCNK18, KCNA3, SYT9, SYT7, BDKRB2, VGF, SLC7A4, FKBP1B, KCNIP1, MYL6L, KCNMB2, SYNPR, CHRNA6, RAB27B, SLC39A3, KCNE3, RAMP3, KCND3, TRPC4, TRPC3, PTGER3, SLCO1A5, KCNK2, KCNJ5, KCNT1, CAMK4, UCP2, RAB36, P2RX3, KCNH6, CARTPT, SCN11A, CACNA1E, NGB, SYTL3, SLC5A7, SLC14A1, CHRNE
regulation of cell proliferation	14	5.0E-02	FXYD2, DRD2, IL7, BEX1, TAC1, BDKRB2, PTPRU, GAL, NPY5R, MYCN, RGS10, SERPINF1, IRF6, INPP5D
negative regulation of cellular process	30	2.7E-03	HMX1, GRIK1, DRD2, GRIK3, BEX1, ADRBK2, BDKRB2, ADCYAP1, CALCA, RGS10, IAPP, INPP5D, DDAH1, HNRNPAB, MT3, NOS1, IL7, PKIG, PTPRU, LMX1A, NPY1R, GAL, RGS14, NPY5R, DAPK1, AMIGO2, SERPINF1, IRF6, RGS4, DGKZ
response to organic substance	19	2.5E-02	NOS1, DRD2, ADCY5, NNAT, TAC1, DGKI, NPY1R, PTPRU, GAL, VGF, HPRT1, ANXA5, FKBP1B, SERPINF1, UCP2, P2RX3, GNB4, GNG2, DDAH1
regulation of cellular process	83	4.2E-06	STEAP3, GNA14, S100A6, LZTS1, HMX1, GRIK1, GRIK3, ADCY5, SYT9, LPAR3, SYT7, VGF, FOXS1, PTGIR, PLCB3, IAPP, GNG2, CHRNA6, RAB27B, NQO1, DDAH1, MT3, RAMP3, PTGER3, RXFP1, PTGDRL, PKIG, MRGPRD, PKIB, PTPRU, GAL, STK4, MYCN, DAPK1, AMIGO2, CAMK4, SERPINF1, SSTR1, PTGDR, KCNH6, ROR2, CARTPT, GNB4, PDE9A, XDH, FXYD2, DRD2, C6, OPRK1, NNAT, BEX1, TAC1, ADRBK2, BDKRB2, MYT1, HPRT1, FKBP1B, ADCYAP1, CALCA, RGS10, PFN2, GPR27, DCLK3, INPP5D, HNRNPAB, SEPW1, NOS1, IL7, LMX1A, DGKI, NPY1R, RCAN3, RGS14, NPY5R, VOM2R43, GPR35, PPP1R2, RAB36, IRF6, RGS4, P2RX3, CRH, CHN1, DGKZ
system development	35	2.4E-02	XDH, LZTS1, GRIK1, DRD2, TRPV1, NNAT, BEX1, VGF, HPRT1, MYL6L, KLHL1, CALCA, DDAH1, MT3, HNRNPAB, INA, RXFP1, IL7, DPYSL4, PTPRU, LMX1A, ALK, GAL, SLCO1A5, MYCN, SERPINF1, IRF6, SSTR1, ZIC5, CRH, ROR2, PCSK1N, TCF15, GFRA2, GFRA3

Tab 8.2.1 DAVID gene annotation biological process The table illustrates significantly enriched genes, occurring in the TRPV1 positive population of rat DRG neurons. The grouping took place in accordance to the genes predicted appearance in biological processes.

Cellular Compartment	Count	p-Value	Genes
dendritic spine	6	9.7E-04	RGS10, LZTS1, NOS1, DRD2, P2RX3, ADRBK2
synaptic vesicle	7	3.2E-04	SYNPR, SYT5, DRD2, SYT9, SYT7, NPY1R, MT3
axon part	7	3.2E-04	CALCA, RGS10, GRIK1, DRD2, GRIK3, P2RX3, ADCYAP1
perikaryon	4	2.0E-02	DRD2, GRIK3, PDE9A, CACNA1E
ion channel complex	10	6.7E-05	KCNC4, KCND3, KCNA3, CACNA1E, SCN11A, CHRNA6, CHRNE, KCNK2, FKBP1B, KCNMB2

cell soma	16	2.7E-07	KCND3, GRIK1, SYT5, DRD2, CPNE5, GRIK3, TAC1, VGF, KCNIP1, KLHL1, CALCA, RGS10, IAPP, P2RX3, CACNA1E, PDE9A
neuron projection	19	3.4E-06	KCND3, LZTS1, NOS1, GRIK1, SYT5, DRD2, TRPV1, CPNE5, GRIK3, ADRBK2, TAC1, NPY1R, VGF, KCNIP1, KLHL1, ADCYAP1, CALCA, RGS10, P2RX3
cell projection part	11	8.2E-04	CALCA, RGS10, LZTS1, NOS1, GRIK1, DRD2, GRIK3, P2RX3, ADRBK2, SLCO1A5, ADCYAP1
cell projection	22	1.1E-04	KCND3, S100A6, LZTS1, NOS1, GRIK1, SYT5, CPNE5, DRD2, TRPV1, GRIK3, ADRBK2, TAC1, NPY1R, VGF, KCNIP1, SLCO1A5, KLHL1, ADCYAP1, CALCA, RGS10, P2RX3, GNB4
plasma membrane	62	2.9E-10	STEAP3, GNA14, KCNC4, LZTS1, GRIK1, TRPV1, SYT5, GRIK3, ADCY5, LPAR3, SYT9, KCNIP1, PTGIR, GNG2, CHRNA6, NT5E, DDAH1, KCND3, TMEFF1, PTGER3, RXFP1, PTGDRL, MRGPRD, PTPRT, PTPRU, JUP, AMIGO2, KCNT1, SSTR1, PTGDR, KCNH6, TNNI3K, SCN11A, GNB4, CLDN16, FXYD2, DRD2, C6, OPRK1, TAC1, KCNA3, BDKRB2, CD72, KCNMB2, SYNPR, GPR27, IPCEF1, INPP5D, TRPC4, NOS1, TRPC3, NPY1R, KCNK2, SLCO1A5, NPY5R, VOM2R43, KCNJ5, DGKZ, CACNA1E, SYTL3, SLC5A7, CHRNE, GFRA3
membrane-bounded vesicle	14	1.1E-02	NOS1, SYT5, DRD2, SYT9, NPY1R, SYT7, GAL, VGF, ACPP, SYNPR, IAPP, RAB27B, PCSK1N, MT3
plasma membrane part	33	8.4E-05	CLDN16, FXYD2, KCNC4, LZTS1, GRIK1, SYT5, DRD2, GRIK3, C6, KCNA3, SYT9, CD72, KCNMB2, SYNPR, GNG2, CHRNA6, DDAH1, TRPC4, KCND3, TRPC3, PTPRU, SLCO1A5, KCNK2, JUP, KCNJ5, AMIGO2, KCNH6, GNB4, CACNA1E, SCN11A, SYTL3, CHRNE, GFRA3
cytoplasmic vesicle	14	2.3E-02	NOS1, SYT5, DRD2, SYT9, NPY1R, SYT7, GAL, VGF, ACPP, SYNPR, IAPP, RAB27B, PCSK1N, MT3
intrinsic to membrane	75	1.8E-04	STEAP3, KCNC4, GRIK1, SYT5, TRPV1, GRIK3, ADCY5, KCNK18, SYT9, LPAR3, TSPAN8, CD53, SLC7A4, PTGIR, XYLT2, NSG1, LRRC55, CHRNA6, RAB27B, NT5E, DDAH1, RAMP3, LRRC3, TMEFF1, KCND3, PTGER3, RXFP1, PTGDRL, MRGPRD, ALK, AMIGO2, KCNT1, SSTR1, PTGDR, KCNH6, SCN11A, CLDN16, FXYD2, MAL2, DRD2, C6, OPRK1, CTXN3, KCNA3, BDKRB2, GPR68, CD72, FKBP1B, PAQR5, KCNMB2, SYNPR, GPR27, HS6ST2, ARMCX1, SLC39A3, KCNE3, TRPC4, TMEM45B, TRPC3, NPY1R, KCNK2, SLCO1A5, NPY5R, ACPP, VOM2R43, KCNJ5, EPHA5, GPR35, UCP2, P2RX3, CACNA1E, FAM70A, SLC5A7, SLC14A1, CEND1, CHRNE
membrane part	85	4.1E-04	STEAP3, KCNC4, LZTS1, GRIK1, SYT5, TRPV1, GRIK3, ADCY5, KCNK18, SYT9, LPAR3, TSPAN8, CD53, SLC7A4, KCNIP1, PTGIR, XYLT2, NSG1, GNG2, CHRNA6, LRRC55, RAB27B, NT5E, DDAH1, RAMP3, LRRC3, TMEFF1, KCND3, PTGER3, RXFP1, PTGDRL, MRGPRD, PTPRU, ALK, JUP, AMIGO2, KCNT1, SSTR1, PTGDR, KCNH6, GNB4, SCN11A, CLDN16, FXYD2, MAL2, DRD2, C6, OPRK1, CTXN3, KCNA3, BDKRB2, GPR68, CD72, FKBP1B, PAQR5, KCNMB2, SYNPR, GPR27, HS6ST2, INPP5D, ARMCX1, SLC39A3, KCNE3, TRPC4, TMEM45B, TRPC3, NOS1, NPY1R, KCNK2, SLCO1A5, NPY5R, ACPP, VOM2R43, KCNJ5, EPHA5, GPR35, UCP2, P2RX3, CACNA1E, FAM70A, SLC5A7, SYTL3,

			SLC14A1, CEND1, CHRNE, GFRA3
Membrane	98	8.6E-05	GNA14, KCNC4, GRIK1, SYT5, ADCY5, GRIK3, SYT9, LPAR3, TSPAN8, CD53, SYT7, SLC7A4, PTGIR, NSG1, GNG2, LRRC55, CHRNA6, RAB27B, DDAH1, LRRC3, TMEFF1, KCND3, PTGDRL, MRGPRD, PTPRT, PTPRU, JUP, KCNT1, SSTR1, FXYD2, DRD2, KCNA3, BDKRB2, CD72, KCNMB2, PAQR5, GPR27, TRPC4, TRPC3, BFSP1, KCNK2, NPY5R, ACPP, KCNJ5, EPHA5, GPR35, UCP2, P2RX3, CACNA1E, SYTL3, CEND1, CHRNE, STEAP3, LZTS1, TRPV1, KCNK18, VGF, KCNIP1, GPC5, PLCB3, XYLT2, NT5E, RAMP3, PTGER3, RXFP1, ALK, AMIGO2, PTGDR, KCNH6, TNNI3K, SCN11A, GNB4, CLDN16, MAL2, C6, OPRK1, CTXN3, TAC1, GPR68, FKBP1B, SYNPR, HS6ST2, IPCEF1, ARMCX1, INPP5D, SLC39A3, KCNE3, TMEM45B, NOS1, NPY1R, SLCO1A5, RGS14, VOM2R43, DGKZ, FAM70A, SLC5A7, SLC14A1, CDH11, GFRA3

Tab 8.2.2 DAVID gene annotation cellular compartment The table illustrates significantly enriched genes, occurring in the TRPV1 positive population of rat DRG neurons. The grouping was in accordance to the genes predicted cellular compartment appearance.

Molecular Function	Count	p-Value	Genes
neuropeptide binding	3	0.07	SSTR1, NPY1R, NPY5R
passive transmembrane transporter activity	22	0.00	FXYD2, TRPC4, KCND3, KCNC4, TRPC3, GRIK1, TRPV1, GRIK3, KCNK18, KCNA3, KCNIP1, KCNK2, KCNMB2, KCNJ5, KCNT1, P2RX3, KCNH6, CACNA1E, SCN11A, CHRNA6, CHRNE, KCNE3
neurotransmitter receptor activity	5	0.02	SSTR1, CHRNA6, NPY1R, CHRNE, NPY5R
peptide receptor activity	5	0.03	SSTR1, OPRK1, BDKRB2, NPY1R, NPY5R
substrate-specific transmembrane transporter activity	28	0.00	FXYD2, KCNC4, S100A6, GRIK1, TRPV1, GRIK3, KCNK18, KCNA3, SLC7A4, KCNIP1, KCNMB2, CHRNA6, SLC39A3, KCNE3, TRPC4, KCND3, TRPC3, KCNK2, SLCO1A5, KCNJ5, KCNT1, P2RX3, KCNH6, CACNA1E, SCN11A, SLC5A7, SLC14A1, CHRNE
receptor binding	17	0.01	RAMP3, DRD2, IL7, ADRBK2, TAC1, BDKRB2, ANXA5, GAL, VGF, FKBP1B, ADCYAP1, CALCA, CALCB, IAPP, NSG1, CRH, GNB4
cation binding	50	0.00	STEAP3, S100A6, KCNC4, TRPV1, SYT5, ADCY5, KCNK18, SYT9, SYT7, KCNIP1, PLCB3, CIB2, DDAH1, NT5E, MT3, KCND3, RXFP1, PDXP, STK4, KCNT1, CAMK4, KCNH6, TNNI3K, SCN11A, NGB, ADAM19, CLDN16, XDH, FXYD2, KCNA3, MYT1, HPRT1, MYL6L, NPTX2, SLC39A3, EWSR1, KCNE3, NOS1, TRPC3, LMX1A, ANXA5, ACPP, KCNJ5, CHN1, DGKZ, CACNA1E, SYTL3, SLC5A7, SLC14A1, CDH11

Tab 8.2.3 DAVID gene annotation cellular compartment The table illustrates significantly enriched genes, occurring in the TRPV1 positive population of rat DRG neurons. The grouping was performed in accordance to the genes molecular function.

8.3 Acknowledgements

Zu allererst danke ich meiner Gutachterin Frau Professor Petra Knaus, für die Zeit die Sie für meine Arbeit investiert hat, die erfrischenden, kurzweiligen Seminare und den finalen Impuls den sie mir gegeben hat diese Arbeit abzuschließen .

Ich möchte mich bei Professor Hilger Ropers bedanken, zum Einen weil er mir die Möglichkeit eröffnete in seiner Abteilung meine Fragen zu beantworten, zum Anderen für das Zusammenstellen eines so großartigen Teams aus WissenschaftlerInnen, OrganisatorInnen und TechnikerInnen, die fast jeden Arbeitstag zu einer Episode im Süßigkeitenwunderland werden ließen.

Vielen, vielen Dank an meinen direkten Betreuer Tim Hucho. Du warst großartig, witzig, anstrengend, verständnisvoll, gut getimed, empathisch, niederschmetternd, motivierend und tausend weitere Dinge ohne die diese Arbeit nicht hätte vollendet werden können. Mir wird der Begriff Doktorvater immer verständlicher.

Als nächstes möchte ich Jörg Isensee als meinen direkten Betreuer danken. Danke für das Vorleben strukturierten Arbeitens und die exzellente Betreuung an Bench, Schreibtisch und als Kopf der Karnevals-Polonäse. Für ihre freundschaftliche, kritische und offenherzige Kollegialität möchte ich mich bei Juliani Schreier und Vanessa Suckow bedanken.

Unzählige Diskussionen über verborgene Superkräfte, Definitionen vom Leben als auch die Beweise meiner eigenen Strukturiertheit kommen von euch Anibal Garca Carbajal und Chandan Goshwami, dank euch.

Zudem möchte ich mich bei Christine Andres und Julia Kuhn bedanken von denen ich lernen konnte, welchen Stellenwert die Politik in der Wissenschaft einnimmt.

Steffen Schüler, Josefine Pott und Sheila Hoffmann danke ich für ihre treuen Dienste während ihres Praktikums bei mir.

Steffen Waldherr danke ich für seine Geduld und seine Versuche mich in seine Denkwelten zu geleiten.

Für eine Zusammenarbeit die einfach nur Spaß gemacht hat, danke ich den Charite-Peopeln Marian Brackmann, Jessica Peters und Christian Casper.

Katson, Bruegg, Nico, Roland, Mina, Basti, Sarah, Alex, Anton, Kristin, Tine, Hagen, Stefan, Dejan, dem Frierock-Kollektiv und insbesondere meiner Familie danke ich für Kritik, Durchhalteparolen, psychosoziale Betreuung und einfach weil es euch gibt.

8.4 Abbreviations

*	$p < 0.05$
**	$p < 0.01$
***	$p < 0.001$
µg	Microgram
µl	Microliter
AC	Adenylyl Cyclase
Au	arbitary unit
CAM	Calmodulin
CAMKII	Ca2+ / calmodulin-dependent protein kinase II
cAMP	cyclic Adenosine Monophosphate
Cap	Capsaicin
CGRP	Calcitonin Gene Related Peptid
CREB	cAmp response element-binding protein
D	Day
DAPI	4,6-diamidino-2-phenylindole
Div	days in vitro
DMSO	Dimethyl Sulfoxide
DANN	Desoxyribonucleic acid
DRG	Dorsal Root Ganglia
e.g.	exempli gratia
EC50	half maximal Effective Concentration
ERK	Extracellular signal-regulated kinase
f.c.	final concentration
F11	cell line (clone)
FSK	Forskolin
G	Gram
h	Hour
HEK	Human Embryonic Kidney cells
IB4	isolectin B4

KCl	potassium chloride
kD	dissociation constant
M	molar mass
MEM	Modified Eagle Medium
mg	Miligram
min	Minute
ml	Millilitre
mM	milimolar
NaV1.8	voltage gated sodium channel
NGF	Nerve Growth Factor
Ns	not significant
P	p-value, probability value
p75	Low-Affinity Nerve Growth Factor Receptor
PBS	Phosphate Buffered Saline
PCR	Polymerase Chain Reaction
PKA	Protein Kinase A
PKC	Protein kinase C
PVDF	polyvinylidene difluoride
q-PCR	qantitative polymerase chain reaction
R	statistcal software
RNA	Ribonucleic Acid
RT	Room Temperature
RTX	Resiniferatoxin
S	Second
SD	Standard Deviation
SEM	Standard Error of Mean
Stauro	Staurosporine
TrkA	High affinity nerve growth factor receptor
TRP	Transient Receptor Family (protein family)
TRPV1	Transient Receptor Family subfamily Vanilloid 1
UCHL1	Ubiquitin Carboxy-Terminal Hydrolase L1

Xg	Fold gravity
P	Rho
Tab	table
Fig.	figure
GDNF	Glial cell-Derived Neurotrophic Factor
HCS	High Content Screening
MRGPRD	Mas-related G-protein coupled receptor member D
et al.	et alia: lat. and other